TECHNISCHE UNIVERSITÄT MÜNCHEN

Fakultät für Maschinenwesen

Lehrstuhl für Mikrotechnik und Medizingerätetechnik

Automated Design of Patient-Individual Catheters for the Minimally Invasive Closure of the Left Atrial Appendage

Eva Christina Graf

Vollständiger Abdruck der von der Fakultät für Maschinenwesen der Technischen Universität München zur Erlangung des akademischen Grades eines

Doktor-Ingenieurs (Dr.-Ing.)

genehmigten Dissertation.

Vorsitzender: Prof. Dr.-Ing. Michael W. Gee

Prüfer der Dissertation:

1. Prof. Dr. rer. nat. Tim C. Lüth
2. apl. Prof. Dr. med. Ralf Sodian

Die Dissertation wurde am 27.02.2018 bei der Technischen Universität München eingereicht und durch die Fakultät für Maschinenwesen am 29.11.2018 angenommen.

Abstract

The minimally invasive closure of the left atrial appendage is performed for stroke prevention in patients suffering from atrial fibrillation. To improve the accessibility of the left atrial appendage with the catheter, an interactive planning program was developed in this thesis, which works based on preoperative image data. The system calculates a patient-specific catheter shape and automatically generates a bending form. Furthermore, an anatomical model for the planning of the implant size and position is produced.

Kurzfassung

Der minimalinvasive Vorhofohrverschluss dient zur Schlaganfallprophylaxe bei Patienten mit Vorhofflimmern. Um die Erreichbarkeit des Vorhofohres mit dem Katheter zu verbessern, wurde in dieser Arbeit ein auf präoperativen Bilddaten beruhendes interaktives Planungsprogram entwickelt, mit dessen Hilfe eine patientenindividuelle Katheterform berechnet und automatisiert eine Biegeform erzeugt wird. Außerdem wird ein Anatomiemodell erstellt, mit dem Implantatgröße und -position geplant werden können.

Danksagung

Diese Arbeit entstand während meiner Tätigkeit als wissenschaftlicher Mitarbeiter am Lehrstuhl für Mikrotechnik und Medizingerätetechnik von Prof. Dr. rer. nat. Tim C. Lüth an der Technischen Universität München. Deshalb geht auch meiner erster Dank an meinen Doktorvater Herrn Prof. Dr. rer. nat Tim C. Lüth für die Betreuung der Arbeit. Besonders bedanken möchte ich mich für die vielfältigen Möglichkeiten, die mir als Mitarbeiter des Lehrstuhls geboten wurden.

Weiterhin danke ich herzlich Herrn Prof. Dr. med. Ralf Sodian für die Betreuung der Arbeit als Zweitgutachter und Herrn Prof. Dr.-Ing. Michael Gee für die Übernahme des Prüfungsvorsitzes.

Ich danke GE Global Research Europe und insbesondere Herrn Dr. Victor Samper für die Förderung des Projektes und die Kooperation.

Bei Frau Prof. Dr. med. Ilka Ott und Herrn Dr. med. Felix Bourier vom Deutschen Herzzentrum bedanke ich mich herzlich für die Zusammenarbeit. Ihnen und ihren Kollegen danke ich für die Evaluierung des Systems. Mein Dank geht auch an Herrn PD Dr. med. Klaus Tiemann für seine wertvollen Hinweise und seine Unterstützung.

Ein großer Dank gilt auch meinen ehemaligen Kollegen am Lehrstuhl für die vielen fachlichen und nicht fachlichen Diskussionen und den sehr guten kollegialen Zusammenhalt. Renate Heuser, Anke Harisch and Cornelia Härtling danke ich für ihre stetige Hilfsbereitschaft. Insbesondere möchte ich außerdem meine Kollegen aus der Arbeitsgruppe Medizinrobotik Johannes Coy, Konrad Entsfellner, Jan Gumprecht, Ismail Kuru und Daniel Roppenecker nennen. Den Kollegen Sandra Brecht, Suat Cömert, Christina Dietz, Christina Hein, Yannick Krieger und Simon Laudahn danke ich zudem für das Korrekturlesen. Ein besonderer Dank geht an Mattias Träger für die finale Durchsicht und Franziska Klein für die vielen interessanten Gespräche. Weiterhin bedanke ich mich bei an alle Studenten, die ich betreuen durfte, für ihre engagierte Arbeit, insbesondere bei Julian Praceus.

Ein herzlicher Dank gehört meinen Eltern und meinem Bruder für ihre bedingungslose Unterstützung während meiner gesamten Ausbildung und bei allen wichtigen Entscheidungen. Abschließend möchte ich mich ganz besonders bei meinem Freund Christoph, der mir stets mit Verständnis und viel Geduld zur Seite stand, bedanken.

Eva Graf, Januar 2018

Contents

1 Introduction

After the first cardiac catheterization in a living human by Forssmann in 1929 who introduced a catheter into the right atrium of his own heart (Forssmann, 1929), catheter-based cardiac procedures were developed for the treatment of a wide variety of indications and interventional cardiology was established as a new branch of cardiovascular medicine (Gaemperli & Lüscher, 2013, S. 3). Those procedures have the potential to substitute open-heart surgeries (which are a lot more invasive) or enable new treatment options. However, as all minimally invasive procedures, they suffer from a number of limitations compared to open surgery, as the physician does not have direct access to the area of the intervention. Rafii-Tari *et al.* (2014) mention the following clinical challenges of endovascular interventions: The conventional pre-shaped catheters, which are steered by a combination of insertion, retraction and rotation movements, only offer a limited range of motion. Due to the length of the instruments, the efficient delivery of torque to the tip of the catheter and the haptic feedback are limited. Additionally, there is no direct sight and the physician has to rely on image data that are often two-dimensional representations of the anatomy. Experience with the catheter dynamics and a three-dimensional understanding of the anatomy are necessary for successful catheter-based procedures.

One example of a minimally invasive procedure that was developed in recent years is the minimally invasive closure of the left atrial appendage (LAA). The procedure is performed to occlude the LAA, a pouch at the left atrium of the heart, in order to prevent the formation of thrombi in patients that suffer from atrial fibrillation (AF). During this procedure, a foldable implant is inserted into the left atrium of the heart and deployed in the LAA. The implant is delivered to the implantation site by a non-steerable curved catheter sheath under ultrasound and fluoroscopy imaging.

Among the challenges of this procedure are the correct sizing of the implant and the positioning of the catheter at the appropriate position inside the LAA. The correct positioning of the catheter can only be achieved by rotational and translational movement of the catheter and is restricted by the pathway of the catheter, which leads through a puncture site at the interatrial septum. In some cases, the anatomical conditions of the patient make this step rather challenging.

The goal of this project is to develop an interactive program that is designed to facilitate the planning of the intervention and the positioning of the catheter. To support the planning of the implant size a physical anatomical model of the LAA is produced and the implant is projected into the virtual image data. Furthermore, the suitability of the catheter for the respective patient's anatomy is evaluated and if it is not suited, a patient-individual catheter shape can be calculated and produced by using a bending form that is automatically constructed by the planning program. The planning program is designed as an interactive program that works based on preoperative three-dimensional image data of the patient.

1.1 Structure of the Thesis

The planning program and its functionalities are described in this dissertation, which is structured as follows. Following this introduction, the underlying medical problem and the possible treatment approaches are presented in the second chapter. As the project focuses on the minimally invasive closure of the LAA, the technical challenges that occur in this procedure are specified. In chapter three, the state of the art of the minimally invasive closure procedure and the devices that are used are presented. Additionally, an overview over the state of research concerning approaches to facilitate the positioning of the catheters in other cardiac procedures, planning programs for cardiac implantation procedures and the idea of automated construction is given. The following chapter describes the limitations of the state of the art, and in chapter five, the concept of the planning program to overcome these limitations is presented and the expected advantages are listed. In the following chapter, the features and calculations of the program are explained in detail. Those include the functionalities to support the implant planning, the evaluation of the standard catheter and the automated construction of the bending form. Three approaches for the calculation of a patient-individual catheter shape are presented. In addition, the heart models that are used for the evaluation experiments are described. In the subsequent experimental section, two experiments that compare the patient-specific catheters to the state of the art are presented and discussed.

Partial results of this work have been published in Graf *et al.* (2014), Graf *et al.* (2016) and Graf *et al.* (2018).

2 Stroke Prevention for Patients with Atrial Fibrillation

In this chapter, the medical background regarding the risk of stroke and approaches to prevent strokes in patients suffering from atrial fibrillation is presented.

2.1 Atrial Fibrillation

In healthy patients the heart beats 60 to 100 times per minute depending on the age and fitness level of the person (Laske *et al.*, 2015, p. 221). In doing so, the excitation starts at the sinoatrial node in the right atrium of the heart, which serves as a natural pacemaker (Laske *et al.*, 2015, p. 216). This is the reason why the normal heart rhythm is also called sinus rhythm. The depolarization spreads throughout the atrial before it is led over to the ventricles (Laske *et al.*, 2015, p. 217). Conditions with the cardiac rhythm differing from the normal sinus rhythm are called cardiac arrhythmias (Bayés de Luna, 2011, p. 3). The most common type of cardiac arrhythmia is atrial fibrillation (AF). AF is categorized as a supraventricular tachyarrhythmia, meaning that the heart rhythm of the atria is affected and that the frequency of the discharges is increased compared to normal rhythm (January *et al.*, 2014, p. e205). The atrial rate of patients with atrial fibrillation ranges between 350 and 500 beats per minute. If the atrial rate lies below 350 beats per minute, the arrhythmia is called atrial flutter (Silbernagl & Despopoulos, 2012, p. 3). In patients that suffer from atrial fibrillation, there are chaotic electrical impulses traveling in circles in the heart in the region of the atria, which leads to a quivering of the atria (Hoppe, 2009). The atrial activation is uncoordinated and as a consequence, the atrial contraction is inefficient (January *et al.*, 2014, p. e205).

Atrial fibrillation is a widespread disease especially in developed countries. In 2010, 33.5 million people worldwide (Chugh *et al.*, 2014) and 8.8 million in Europe (Krijthe *et al.*, 2013) suffered from atrial fibrillation. Current estimates suggest that 1.5-2% of the population in developed countries are affected (Camm *et al.*, 2012) and the lifetime risk to develop atrial fibrillation is over 20% for Europeans (Heeringa *et al.*, 2006). The prevalence of AF rises with age. Whereas the prevalence for men and women aged between 55 and 59 years is 1.3% and 1.7%, respectively, in the group aged above 85 years it rises to 24.2% for men and 16.1% for women. Due to this fact and in combination with the rising age of the population, the number of people with atrial fibrillation in Europe is expected to more than double by 2060 (Krijthe *et al.*, 2013). In the US, 2.7 to 6.1 million people were affected and the estimated annual costs for the treatment of atrial fibrillation were $26 billion in 2014 (January *et al.*, 2014).

While atrial fibrillation is often associated with fatigue, palpitations, dyspnea, hypotension, syncope or heart failure, it can also occur without any symptoms for the individual patient (January *et al.*, 2014, p. e205). However, worldwide, AF is considered as one of the major causes of stroke, heart failure, sudden death and cardiovascular morbidity (Kirchhof *et al.*, 2016). The risk for ischemic strokes is four- to fivefold increased for patients suffering from AF due to the facilitated formation of

thrombi caused by the altered blood flow during atrial fibrillation (Wolf *et al.*, 1991). The main but not only origin of the thrombi is the left atrial appendage (LAA) with 91% of the thrombi in patients with non-rheumatic AF and 57% in patients with rheumatic AF originating there (Blackshear & Odell, 1996).

2.2 Anatomy of the Heart

To understand the anatomy of the heart an overview over the chambers and the arteries and veins is given as described by Weinhaus (2015) before focusing on the left atrial appendage. Figure 1 shows a schematic representation of the anatomy of the heart.

2.2.1 Chambers

The heart is divided into two halves, the left and the right side of the heart. Their blood flow is physiologically completely separated and without interconnection, as the blood passes through them in different stages of the circulation: The left side of the heart pumps the oxygenated blood that comes from the lungs into the body's circulation system. After passing through the body, the blood flows back to the heart and the right side of the heart pumps it into the lungs where the carbon

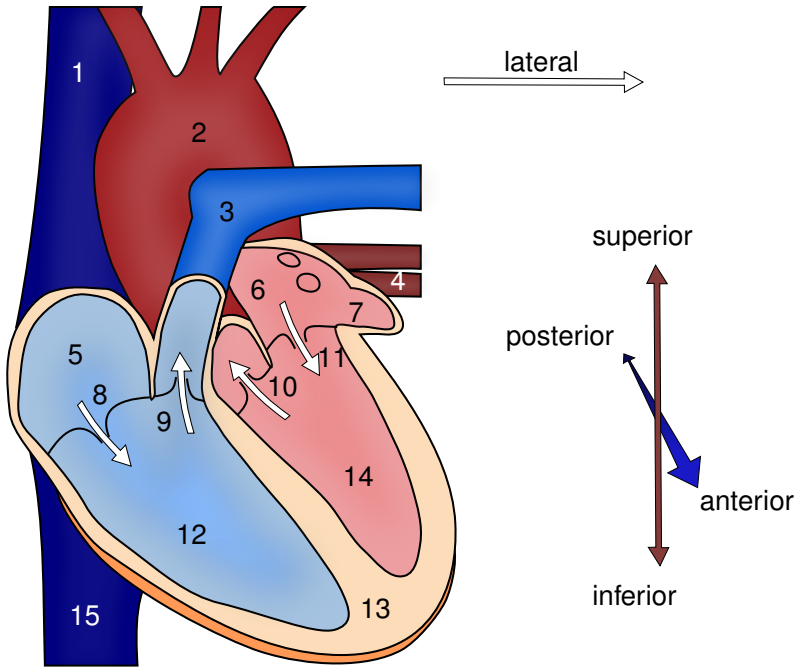

Figure 1 The heart consists of two ventricles (right ventricle (RV, 12), left ventricle (LV, 14)) and the corresponding atria (right atrium (RA, 5), left atrium (LA, 6)), which are separated by the interventricular septum (13) and the interatrial septum (not visible in the image, lies behind the aorta and the pulmonary trunk), respectively. The left atrial appendage (7) is a structure that is attached to the left atrium. The superior (1) and the inferior vena cava (15) deliver blood from the venous system into the right atrium of the heart whereas the pulmonary trunk (3) pumps it towards the lungs. The left heart receives blood through the pulmonary arteries (4, only two are visible in the image, the other two are situated behind the aorta) and the aorta (2) pumps the blood from the left ventricle into the body. The atria are separated from the ventricles by the tricuspid valve (8) and the mitral valve (11). The pulmonary valve (9) and the aortic valve (10) are situated at the base of the outlet vessels. The anatomical orientations inside the heart are referred to with the following expressions: lateral means towards the side of the body, superior and inferior stand for above and below and anterior and posterior describe the front and the backside.

dioxide in the blood is exchanged with oxygen.

Both sides of the heart consist of an atrium and a ventricle. The atrium serves as a reservoir to collect the blood and pump it into the ventricle. By contracting the ventricles, the pressure that is necessary to pump the blood into the body and the lungs is generated. Therefore, the muscular walls of the ventricles are much thicker than the atria.

The atrioventricular valves, which prevent regurgitation of the blood into the atria during the contraction of the ventricles (systole), separate atria and ventricles. The chordae tendineae, which are connected to the papillary muscles in the ventricles, prevent the eversion of the valves into the atria. The valve between atrium and ventricle it is called mitral valve in the left side of the heart and tricuspid valve in the right side.

The wall that is separating the left and the right ventricle is referred to as the interventricular septum. The atria are separated by the interatrial septum. In the fetal heart, the atria are interconnected by an opening in the wall, the so-called foramen ovale, as the lungs are not connected to the circulation and the blood has to bypass them. In the adult heart, this opening usually closes and the fossa ovalis, an oval shaped depression remains. However, in about one fifth of the population, the closure is incomplete and a small opening, which is called patent foramen ovale, remains (Hagen *et al.*, 1984).

2.2.2 Major Arteries and Veins

The general convention is that blood vessels leading to the heart are called veins and those carrying the blood away from the heart are arteries. The main artery of the human body is the aorta, which originates in the left ventricle and carries the blood from the heart into the systemic circulation. The right atrium receives the oxygen-depleted blood from the two major veins of the body, the superior and the inferior vena cava, which are collecting the blood from the upper and the lower part of the body. After passing through the right ventricle, the blood flows into the lungs through the pulmonary trunk. The blood is re-oxygenation in the lungs and subsequently enters the left atrium through the four pulmonary veins, which are arranged as two pairs on both sides of the left atrium.

Two heart valves, the aortic valve and the pulmonary valve, are situated between the ventricles and the arteries at the base of the aorta and the pulmonary trunk respectively to prevent regurgitation of the blood into the heart during the filling phase of the heart (diastole).

2.2.3 Left Atrial Appendage

Both atria have pouch-like extensions, the so-called atrial appendages or auricles. The left atrial appendage (LAA) is a muscular pouch situated at the left atrium (see Figure 2). Due to its embryological origin, the structure of the LAA differs from that of the rest of the left atrium. The atrium was part of the fetal pulmonary veins and therefore has a smooth surface whereas the LAA in contrast has pectinate walls, as it was part of the primitive right atrium, which is pectinate as well (Weinhaus, 2015, p. 73).

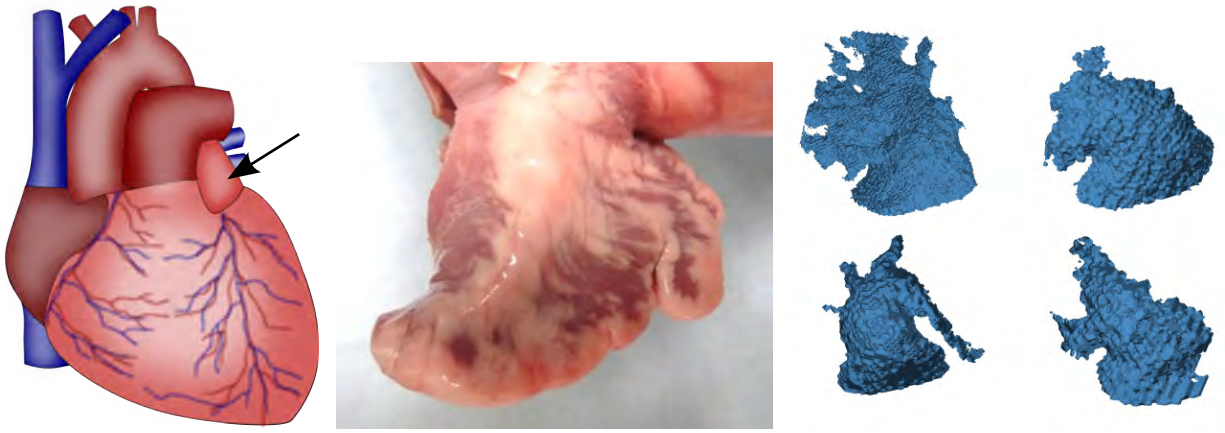

Figure 2 The LAA is a muscular pouch situated at the left atrium, which typically points anteriorly towards the right ventricular outflow track. The central image shows a porcine atrial appendage. The LAA is anatomically the most variable region of the left atrium. The images on the right show four exemplary different anatomies of the LAA.

As described by Don *et al.* (2015), the orifice of the LAA, which is called ostium, is situated anterior of the left pulmonary veins and superior to the mitral valve inside the left atrium. The narrow junction between the ostium and the lobar region of the LAA is referred to as neck of the LAA. Typically, the lobar region of the LAA points anteriorly towards the right ventricular outflow track. However, the size, shape and position of the LAA differs greatly between patients (Don *et al.*, 2015).

Generally, four different types of shapes of the left atrial appendage are distinguished according to Wang *et al.* (2010). The windsock type has one dominant lobe of sufficient length and the chicken wing type has a characteristic sharp bend in the main lobe. The overall length of the cauliflower type is limited and it has a complex internal structure whereas several secondary lobes extending from the main lobe characterize the cactus type. Wang *et al.* (2010) examined the LAA of 612 patients in CT data and found that the most frequent form was the windsock type with 47% of the patients. Depending on the study that is considered, the percentage of LAAs with multiple lobes ranged between 60% and 80% (Wang *et al.*, 2010; Veinot *et al.*, 1997). Di Biase *et al.* (2012) studied the risk of stroke for different LAA morphologies and found significant differences with the risk for stroke being highest in patients with a LAA of cauliflower type. Strokes were least likely in patients with chicken wing morphology.

The shape of the orifice was found to be mostly irregular and in more than 68% of the patients it could be described as oval with a mean diameter of 21.5 $\pm$ 5.3 mm in the long axis and 15.0 $\pm$ 4.8 mm in the short axis (Wang *et al.*, 2010). However, the diameter of the ostium changes during the cardiac cycle by 15% to 20% (Nakajima *et al.*, 2010). The mean distance of the orifice of the left atrial appendage to the interatrial septum was determined to 68.2 $\pm$ 13.4 mm (Wang *et al.*, 2010). The face of the interatrial septum has a lateral and posterior orientation and therefore points slightly away from the LAA (Don *et al.*, 2015, p. 48).

Unlike the left atrium, the LAA is trabeculated with visible largely parallel muscle bars (Al-Saady *et al.*, 1999). Su *et al.* (2008) measured the thickness of the wall of the left atrial appendage and

reported areas with extremely thin walls in 57.7% of the studied hearts. Pits or troughs were found in these hearts with a remaining wall thickness ranging from 0.4 to 1.5 mm.

2.3 Stroke Prevention in Patients Suffering from AF

Risk scores are used to assess the patient's individual risk for strokes. The European Society for Cardiology recommends the use of the CHA_2-DS_2-VASc score (Kirchhof *et al.*, 2016). This risk score considers other diseases such as congestive heart failure, hypertension, diabetes mellitus and vascular diseases in addition to the risk factors previous strokes, sex and age of the patient. If the calculated patient's risk factor exceeds a boundary value, stroke prevention should be considered.

2.3.1 Medication Treatment

The standard way of stroke prevention is oral anticoagulation (OAC), which can prevent the majority of the strokes (Kirchhof *et al.*, 2016). Anticoagulants are given to the patient, which reduce the coagulation and therefore prevents the formation of thrombi and subsequent strokes. The description of the anticoagulants is based on Cairns (2015) and Ageno *et al.* (2012).

Warfarin and other vitamin K antagonists (VKA) were the first medication that was used for stroke prevention. The anticoagulant effect of VKAs is based on the decrease in the regeneration of reduced vitamin K, which is necessary for the hepatic synthesis of several coagulation protein factors. Thus, the medication intervenes in a complex series of steps and is therefore difficult to control (Cairns, 2015, p. 20). Studies showed a reduction in the rate of strokes by approximately 60% due to the use of Warfarin (Hart *et al.*, 2007).

Later, so-called New Oral Anticoagulants (NOAC), which are also called Non Vitamin K Antagonist Oral Anticoagulants, such as Rivaroxaban, Dabigatran or Apixaban were developed to overcome some of the limitations of Warfarin. These medications affect the coagulation process much more directly by inhibiting coagulation factors. Therefore, compared to Warfarin their starting dose is less variable, the absorption is not influenced by diet and most drugs and coagulation monitoring is not required (Cairns, 2015, p. 25-26).

Limitations. The use of anticoagulation cannot be recommended for all patients, as patients with high risk of bleeding have contraindications against coagulation. The risk of bleeding can be assessed with bleeding risk scores such as the HAS-BLED, ORBIT or ABC. Several of the risk factors of strokes are also risk factors of bleeding (Kirchhof *et al.*, 2016). Other limitations of the oral anticoagulation are the restricted therapeutic window and the fact that the anticoagulation treatment may need to be interrupted for surgeries or diagnostic tests and the medication has to be taken every day over years, wahat is challenging for the patients (Whitlock *et al.*, 2014).

2.3.2 Surgical LAA Closure

Being the main source of thrombi in patients with atrial fibrillation, the idea of mechanical removal of the left atrial appendage has already been studied in the 1940s (Madden, 1949). Nowadays, several

techniques are performed with the intention of excluding the left atrial appendage from the circulation or completely excising the left atrial appendage concomitant to other open-heart surgeries (Hanif & Whitlock, 2015).

Hanif & Whitlock (2015) describe the techniques to exclude the LAA, which are ligation of the LAA neck using a vascular clamp, closing the LAA via a purse-string suture, suturing the LAA endocardially from within the left atrium or invaginating the LAA into the left atrium and subsequently closing it with two sutures, one in the invaginated state and one after pulling the LAA outwards again. Alternatively an appendectomy can be performed which means complete amputation of the LAA and sewing the neck closed. Excision or exclusion of the LAA can also be performed using a surgical stapler to close the LAA. (Hanif & Whitlock, 2015) In the recent years two new devices for the surgical closure of the LAA were approved for use under direct vision and concomitant to other open-heart procedures: the Atriclip (Atricure Inc., Westchester, OH, USA) and the TigerPaw (Maquet, Rastatt, Germany), which has been recalled in 2015 (Ventosa-Fernandez *et al.*, 2015) due to safety concerns. Both devices are implantable clips that close the left atrial appendage at its base from the outside of the heart (Ailawadi *et al.*, 2011; Slater *et al.*, 2012).

Limitations. The surgical closure of the LAA may only be considered for patients that are undergoing cardiac surgery (January *et al.*, 2014, p. 221). Furthermore, Kanderian *et al.* (2008, S. 926) found out that only 40% of the surgical closure procedures were successful. Among the studied techniques, excisions were the most successful technique with a success rate of 73% but there was a likelihood that a residual stamp would remain after the procedure, which could pose a risk for thrombi. They identified persistent flow into the LAA as a major problem of patients that underwent suture exclusion of the LAA, which affected 60% of the patients. The biggest problem of the stapler exclusion was a persistent LAA stump, which occurred in 59% of the cases.

2.3.3 Minimally Invasive Closure of the LAA

As an alternative to the surgical closure of the LAA, percutaneous procedures were developed. Two basic approaches are available: an endovascular and an extravascular approach.

- **Extravascular Approach**
  In the extravascular approach, as described by Kanmanthareddy *et al.* (2015), the LARIAT system (SentreHEART, Palo Alto, CA) leaves an epicardially placed suture around the left atrial appendage to occlude it. Therefore, an endocardial balloon is inflated temporarily in the LAA to serve as a guide while a suture is tightened epicardially around the LAA with the help of a pericardially inserted snare. In order to position the endocardial and the epicardial devices relative to each other, guidewires with magnetic tips are used on either side of the LAA wall (Kanmanthareddy *et al.*, 2015).

- **Endovascular Approach**
  In the endovascular approaches, implants are introduced into the heart and placed in the left atrial appendage to occlude its orifice. The first procedure that was performed in humans was the closure of the LAA with the PLAATO device in 2001 (Sievert, 2002). Since then several

closure devices got clinical approval. The available implants and the implantation procedure will be discussed in detail in the following chapter. The number of interventions increased in the recent years. While 2128 interventions were performed in Germany in 2013 (Statistisches Bundesamt, 2014) in 2015 the number has increased to 4961 (Statistisches Bundesamt, 2016). The majority of the patients were aged between 75 and 80 years. In a randomized study, the non-inferiority of the closure procedure compared to medical anticoagulation treatment for stroke prevention was proved (Holmes *et al.*, 2009). According to a study, 10 years after the intervention the procedure was more cost efficient than all other alternative therapies for stroke prevention (Panikker *et al.*, 2016).

2.4 Technical Challenges of the Minimally Invasive Closure

In order to successfully implant the device in the left atrial appendage, a suitable device has to be **chosen**, the implant's landing zone has to be **reached** and the implant has to be **positioned** and **anchored** in the LAA. The following technical challenges are faced to fulfill these tasks.

- **Limited Diameter of the Instruments**
  As the access to the implantation site is gained via the vascular system of the patient, the available outer diameter of the instruments that are used is limited. Bigger instruments may lead to increased trauma and complication risks (Gafoor *et al.*, 2015b).
- **Distance between Access Point and Operation Site**
  The access point of the catheter into the body of the patient is situated at his groin and lies in a significant distance to implantation site. Therefore, long instruments are necessary to access the implantation site. Thus, the force transmission to the tip of the catheter but also the force feedback are limited (Rafii-Tari *et al.*, 2014). Additionally, the maneuverability of the instruments is constrained.
- **Limited Sight**
  In contrast to open surgery, the physicians have no direct sight onto the implantation site but have to rely on the available information that are provided by imaging systems. The correct interpretation of these images requires adequate display as well as visual thinking and experience in the interpretation of the physician.
- **Safety of the Procedure**
  The trauma of the procedure should be minimized. In order to ensure the safety of the procedure, the instruments have to be hemocompatible and sterile and mechanical damaging of the heart walls have to be avoided. Additionally, it has to be ensured that the implant is seated properly to avoid dislocations or incomplete closure.
- **Integration into the Clinical Workflow**
  The minimally invasive closure procedure is performed in the cardiac catheterization laboratory and has to be compatible with the clinical workflow and the equipment that is available in most catheter laboratories.

3 State of the Art

This thesis focuses on the endovascular approach for the minimally invasive closure of the left atrial appendage. In the following, the state of the art is presented. Additionally, approaches to facilitate the positioning of the catheter in other catheter-based cardiac procedures are described and the approach of automated construction is introduced, as it is a useful tool for the development of patient-specific support systems.

3.1 Minimally Invasive Closure of the LAA

During the minimally invasive closure of the LAA, a foldable implant is introduced into the LAA through a hollow catheter sheath, the so-called delivery sheath. To do so, the implant is mounted on the tip of a smaller catheter, the delivery catheter, and pushed through the delivery sheath. The implantation process including the imaging procedures, the available devices and the state of the research to facilitate the procedure are presented.

3.1.1 Implantation Process

Independent of the device type that is used, the general steps of the implantation procedure are similar for all of the devices and described in an expert consensus statement by Meier *et al.* (2014).

Preoperative Inspection. Prior to the intervention, the existence of a thrombus in the left atrial appendage has to be ruled out. Furthermore, the anatomy of the LAA has to be examined to choose the appropriate device type and check for contraindications.

Access to the Heart. The patient's circulation is accessed through the venous system. A catheter is introduced into the right femoral vein of the patient, a vein at the thigh of the patient. Subsequently, the catheter is advanced into the inferior vena cava, which leads to the right atrium of the heart as shown in Figure 3.

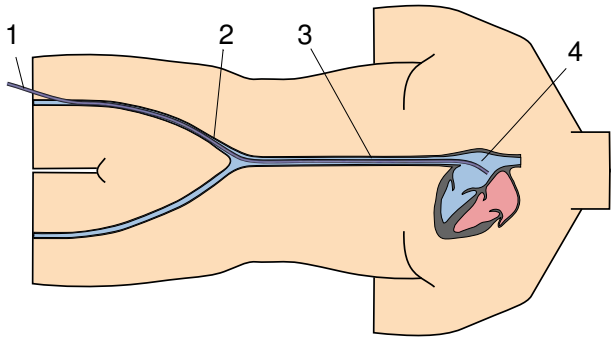

Figure 3 The catheter (1) is introduced into the circulation system at the right femoral vein (2). Due to the venous access, the catheter enters the heart at the right atrium (4) through the inferior vena cava (3).

Transseptal Puncture. Due to the access through the venous system, the catheter enters the heart in the right atrium. To reach the left atrial appendage, which is situated in the left atrium, the interatrial septum has to be crossed with the catheter. Puncturing the interatrial septum is a standard procedure in several minimally invasive cardiac procedures and the transseptal puncture for LAA occlusion is performed with standard equipment (Bergmann *et al.*, 2017, p. 59). Positioning the transseptal puncture correctly is crucial, as the location of the puncture influences the feasibility of coaxial alignment of the catheter with the axis of the LAA. Saw (2015, p. 186) recommends an inferioposterior location at the fossa ovalis. It is not advisable to use a patent foramen ovale for the access to the left atrium, as the resulting angle of the catheter is generally geometrically not favorable (Saw, 2015, p. 186).

Positioning of the Catheter. After the puncture, the hollow catheter sheath through which the implant is introduced into the LAA has to be positioned at the implantation site. To minimize the risk of injuries, the use of a pigtail catheter is recommended for the first introduction of instruments into the LAA due to its soft, atraumatic tip, which is curled (Phillips & Kar, 2015, p. 157). It is exchanged for the delivery sheath by introducing a guidewire, which is a thin flexible wire, through the pigtail catheter to lead the delivery sheath to the target position after removal of the pigtail catheter. According to the expert consensus, two options are available for the positioning of the delivery catheter in the LAA. Either a pigtail catheter is directly introduced into the LAA and later replaced by the delivery sheath over a stiff guidewire (see Figure 4) or in a first step, a catheter or guidewire is positioned in the left upper pulmonary vein and exchanged for the delivery sheath over a guidewire. In this case, a pigtail catheter is introduced through the delivery sheath into the LAA and the delivery sheath is advanced over the pigtail catheter into the LAA. To avoid damages to the heart walls and to facilitate the introduction into the left atrium through the transseptal puncture, a dilator with a conical tip is placed inside the delivery sheath during the insertion. In order to achieve

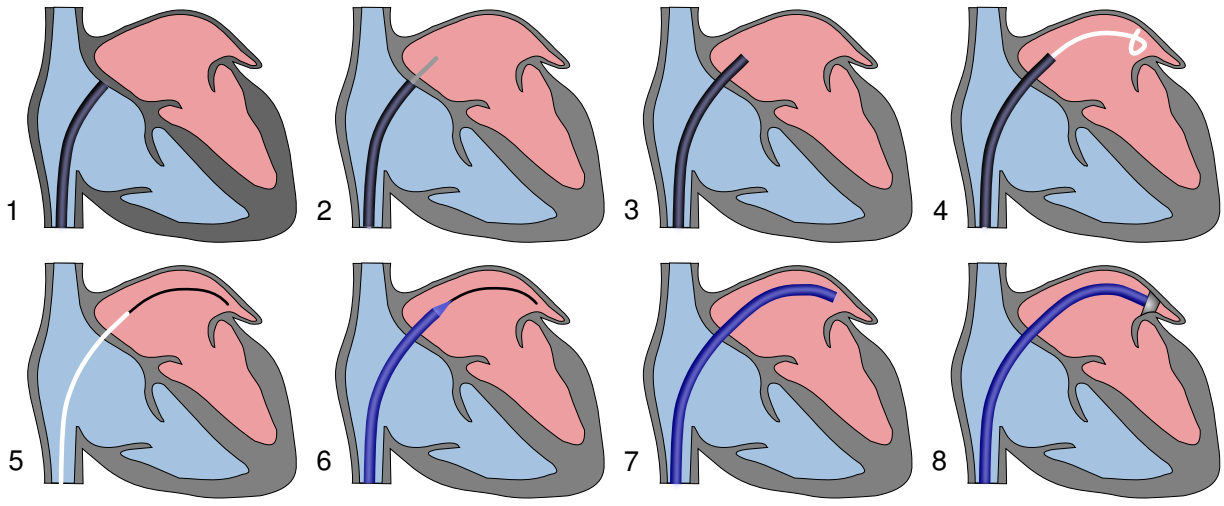

Figure 4 The implantation process according to one possibility described by Meier *et al.* (2014) consists of several stages: the introduction of the transseptal sheath into the right atrium (1), the puncture of the interatrial septum (2), the insertion of the transseptal sheath into the left atrium and the retraction of the puncture needle (3), the placement of a pigtail catheter in the left atrial appendage (4), the introduction of a guidewire through the pigtail catheter (5), the insertion of the delivery sheath with a dilator over the guidewire (6), the placement of the delivery sheath in the left atrial appendage (7) and the insertion of the implant through the delivery sheath and its placement in the LAA (8).

coaxial positioning of the catheter sheath and the LAA, a counterclockwise rotation of the catheter is often necessary (Saw, 2015, p. 188).

Choice of the Implant Size. The dimensions of the implant's landing zone have to be measured properly in order to be able to choose the correct implant size and the implant type. The standard implants have to be oversized compared to the maximum diameter of the LAA ostium in order to achieve a stable device position (Meier *et al.*, 2014, p. 6). Differing from the common practice that refers to the maximum LAA dimensions, Bergmann *et al.* (2017, p. 39) suggest the use of a mean LAA landing zone diameter.

Implantation of the device. After correct positioning of the delivery sheath, the pigtail catheter or guidewire is retracted and air is removed from the delivery sheath. The device is prepared and flushed outside of the patient's body and inserted into the sheath by mounting it onto the tip of the delivery catheter, a wire that is used to push the device into the delivery sheath. The device is advanced until the tip of the delivery sheath. When the delivery sheath is pulled back, it allows the device to unfold. The correct position of the device is checked in the image data and its tight fit is checked with a tug test. If the position is satisfactory, the device is released and the catheters are removed from the patient's body. If not, the device can be retracted into the catheter sheath, the sheath is repositioned and the implant is deployed again.

Postoperative follow-up. Follow-up imaging after four to six months is recommended to verify the outcome of the procedure and to decide on further anticoagulation treatment. Furthermore, there is a risk for the formation of thrombi on the device and for residual flow, which has to be assessed (Meier *et al.*, 2014, p. 16).

3.1.2 Available Implants and Catheters

Different devices were developed for the minimally invasive closure of the LAA for stroke prevention (see Figure 5). According to Caliskan *et al.* (2017), in August 2017, apart from the PLAATO device, which is no longer commercially available, the endocardial devices of seven manufacturers have received CE mark. Those implants are presented in detail below. In 2015, two of these implants were mainly used in the clinical practice: the Amplatzer Cardiac Plug (St. Jude Medical, St. Paul, MN, USA) and the WATCHMAN device (Boston Scientific, Maple Grove, MN, USA) (Pison *et al.*, 2015, S. 643). Additionally, six other devices are described based on Gafoor *et al.* (2015a) and Caliskan *et al.* (2017). The devices are sold with a customized delivery system for the implant. The delivery system usually consists of a delivery sheath through which the implant is brought to the implantation site and a delivery catheter with the implant mounted on its tip, which is used to insert the implant through the sheath and to release the device. For safe crossing of the transseptal puncture, a dilator can be inserted into the delivery sheath.

- **PLAATO device**
  The first device that was developed for the minimally invasive closure of the left atrial appendage and successfully implanted in humans, the PLAATO device, is no longer available on the market

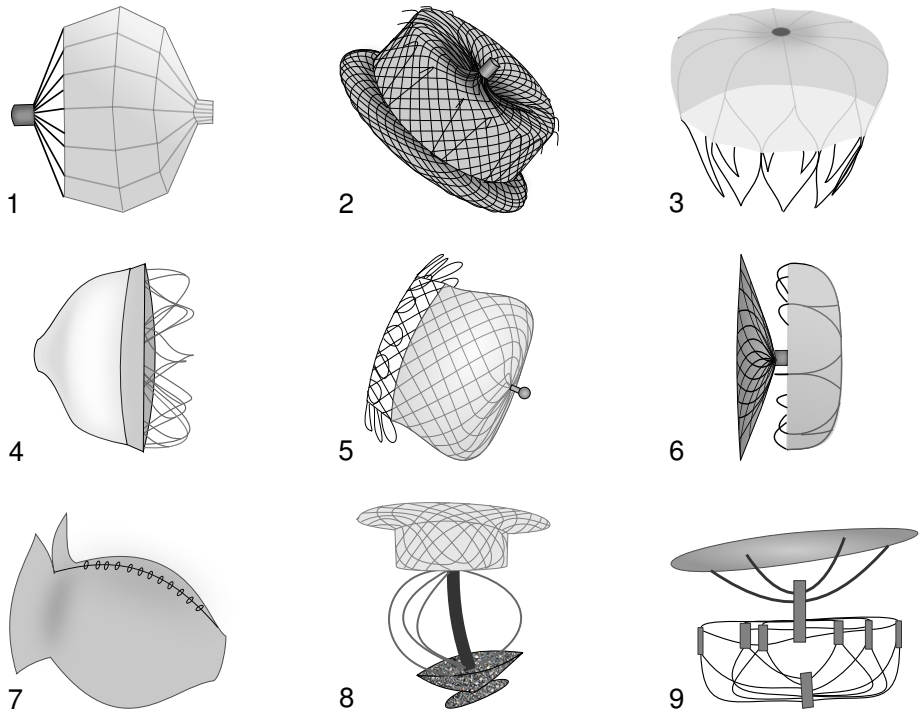

Figure 5 There are different devices available for the minimally invasive closure of the LAA. The PLAATO device (1) was the first device but is no longer available. The Amplatzer implants (2) and the WATCHMAN device (3) are the devices that are mostly used in the clinic. Further devices are the Wavecrest device (4), the Occlutech Occluder (5), the LAmbre LAA Occluder (6), the Trancatheter Patch (7), the pfm LAA Occluder (8) and the Cardia Ultrasept LAA Occluder (9) (based on Caliskan *et al.*, 2017).

for economic reasons (Lee, 2015, p. 141). The PLAATO (Percutaneous Left Atrial Appendage Transcatheter Occlusion, Appriva Medical, Sunnyvale, CA, USA) device was a self-expanding nitinol metal cage, which was covered with a PTFE membrane (Lee, 2015, p. 136).

- **Amplatzer Cardiac Plug**
  Based on their atrial septal occluders, which were also used for LAA closure in selected patients (Meier *et al.*, 2003), St. Jude Medical developed specialized occlusion devices for the left atrial appendage. The implants and the corresponding delivery system is described based on Saw (2015, p. 182-184). The Amplatzer Cardiac Plug (ACP) or its next development stage, the Amplatzer Amulet, are devices that consist of two circular bodies, a thin disc and a thicker lobe with smaller diameter. A thin neck connects the two parts. The implants consist of a nitinol mesh with a sewn-in polyester layer and they are self-expanding. Nitinol has superelastic properties and the implant can be compressed into the catheter for insertion into the heart. When it leaves the catheter, the lobe expands in the orifice of the LAA and anchors with the help of six to ten pairs of anchoring wires, which are located at the distal part of the lobe. The disc lies outside the left atrial appendage in the left atrium and should cover the LAA orifice completely. The devices are available in different sizes ranging from a diameter of the lobe from 16 mm to 34 mm with the diameter of the disc being up to 7 mm larger than the lobe. The lobe has a thickness of 6.5 to 10 mm whereas the disc is very thin. The Amplatzer implants are upsized 3 to 5 mm for the Amplatzer cardiac plug and 2 to 4 mm for the Amulet device compared to the maximum diameter

of the LAA orifice (Saw, 2015, p. 188). The Amplatzer cardiac plug and the Amplatzer Amulet received CE mark in 2008 and 2013, respectively.

Catheter sheaths with diameters between 9 and 14 French (Fr, 3 Fr = 1 mm) are used for the delivery of the Amplatzer implants. The catheter sheaths have an inner diameter of 3.1 to 4.8 mm and an outer diameter of 3.8 to 5.5 mm, resulting in a wall thickness of about 0.4 mm. The TorqueVue 45x45 delivery sheath with 100 cm length is manufactured for the implantation of the ACP and Amulet. It has a three-dimensional distal tip with two bends with bending angles of 45°, which enable an anterior and superior angulation. Other sheath shapes were manufactured in the past but they are no longer sold, as they were not adopted by the operators (Saw, 2015, p. 184). The catheter sheath is made of polymer that is reinforced with a stainless-steel braid and it has a PTFE lining to reduce friction (Gafoor *et al.*, 2015b). The catheter sheath is torsional stiff and is therefore able to transmit rotational movements at the proximal end of the sheath to the tip of the catheter.

The implant is introduced into the catheter sheath and unfolded in the heart on the tip of a delivery catheter. The delivery catheter is a wire with a flexible tip and a thread on its tip. The implant can be mounted on the delivery catheter by screwing. For this purpose, the implant as well has a thread fixed to it.

- **WATCHMAN Device**
  The WATCHMAN Device was developed by Atritech Inc. (Plymouth, MN, USA) and later acquired by Boston Scientific (Natick, MA, USA). After the first implantation in humans in 2002, it received CE Mark in 2005 and FDA Approval in 2015 (Saw *et al.*, 2015a). Phillips & Kar (2015) present the device and the corresponding delivery system. The implant is formed like an umbrella and it consists of a self-expanding nitinol frame, which is covered by a PET membrane cap. The device has ten fixation anchors at its distal end for the fixation in the left atrial appendage. Different diameters of the implant ranging from 21 to 33 mm are available to match the patient's anatomy. The implant is chosen about two to four millimeter larger than the maximum LAA dimensions for the WATCHMAN device (Phillips & Kar, 2015, pp. 153-155).

  The device is introduced into the heart on the tip of a 12 French (Fr, 3 Fr = 1 mm) delivery catheter, which is introduced through a delivery sheath. The delivery sheath has an outer diameter of 14 Fr and an inner diameter of 12 Fr. Three types of catheter sheaths are available, a single bended catheter sheath with a 90° bend and double bended catheter sheaths with a secondary superior or anterior bend (Phillips & Kar, 2015, p. 151).

- **WaveCrest Device**
  Coherex (Salt Lake City, UT, USA), which was acquired by Johnson & Johnson (New Brunswick, NJ, USA), developed the WaveCrest LAA Occlusion system. The occluder has an umbrella shape covered with a PTFE membrane (Caliskan *et al.*, 2017, p. 8). It is exceptional that the positioning and the anchoring of the implant can be operated separately with the anchors rolled out after positioning of the device (Bergmann & Landmesser, 2014). The first implantation of the device was performed in 2012 and the system received CE mark in 2013 (Gafoor *et al.*, 2015a, p. 236).

- **Occlutech Occluder**
  The Occlutech (Jena, Germany) occluder received CE mark in June 2016 but the devices were recalled in September Dave & Valderrábano (2017) and the commercialization was stopped. The device is a self-expanding nitinol wire mesh with distal closed loops for anchoring (Gafoor *et al.*, 2015a, S. 236). A steerable sheath that can be rotated in an angulation of 180° is used for the implantation of the device, which facilitates device positioning (Bellmann *et al.*, 2017).

- **LAmbre LAA Occluder**
  The LifeTech LAmbra LAA occluder is a self-expanding, nitinol-based system by Lifetech Scientific (Shenzhen, China), which consists of an hook-embedded umbrella and a cover, which are connected by a short central waist. The umbrella is anchored in the walls of the LAA and the cover drapes the LAA orifice. During the design of the umbrella, the manufacturer in particular tried to improve recapture and repositioning capabilities. The implant comes with a delivery system consisting of sheath, dilator, delivery cable, loader and vise. A first registry in Asia was completed in 2013 (Lam, 2013) and the implant received CE approval in 2016.

- **Transcatheter Patch**
  The Transcatheter Patch was developed by Custom Medical Device (Athens, Greece). Differing from all other devices, it does not have a metal frame. A tailored polyurethane foam patch is delivered to the heart through a catheter and a latex balloon is inflated to stretch the device to the LAA. It is then fixated by activating a surgical adhesive. A standard catheter sheath is used for the introduction. The results of the trial in the first patients were reported in 2011 (Toumanides *et al.*, 2011).

- **pfm LAA Occluder**
  There is little information available about the pfm LAA Occluder (pfm Medical, Cologne, Germany), which is made of nitinol. It consists of an occluder disc, which is connected to an anchor by a variable length connector (Caliskan *et al.*, 2017, p. 9). According to Caliskan *et al.* (2017), it has already received CE mark.

- **Cardia Ultrasept LAA Occluder**
  The Cardia Ultrasept LAA Occluder (Cardia Inc., Eagan, MN, USA), which is sometimes also referred to as Ultraseal, consists of two parts, a distal cylindrical bulb with 12 hooks, which provide the anchoring in the LAA, and a sail, which unfolds over the ostium and occludes it. Both parts are connected by an articulating joint, which allows relative movement of the two parts. The device is made of nitinol with a polyvinyl acetate foam (PVA) covering the sail. The delivery system of the device consists of a delivery forceps, which has jaws to hold and release the device, an introducer and a delivery sheath and dilator, which is available in a single curved or a double curved version. Regueiro *et al.* (2016) presented a study with successful implantation of the device in 12 patients. However, according to Caliskan *et al.* (2017), the device has not received CE mark until mid of 2017.

3.1.3 Imaging

Available Imaging Modalities. The heart including the left atrial appendage can be visualized with different imaging modalities. Radiography, ultrasound or magnetic resonance imaging might be applicable depending on the intended use. Figure 6 shows the LAA in different imaging modalities.

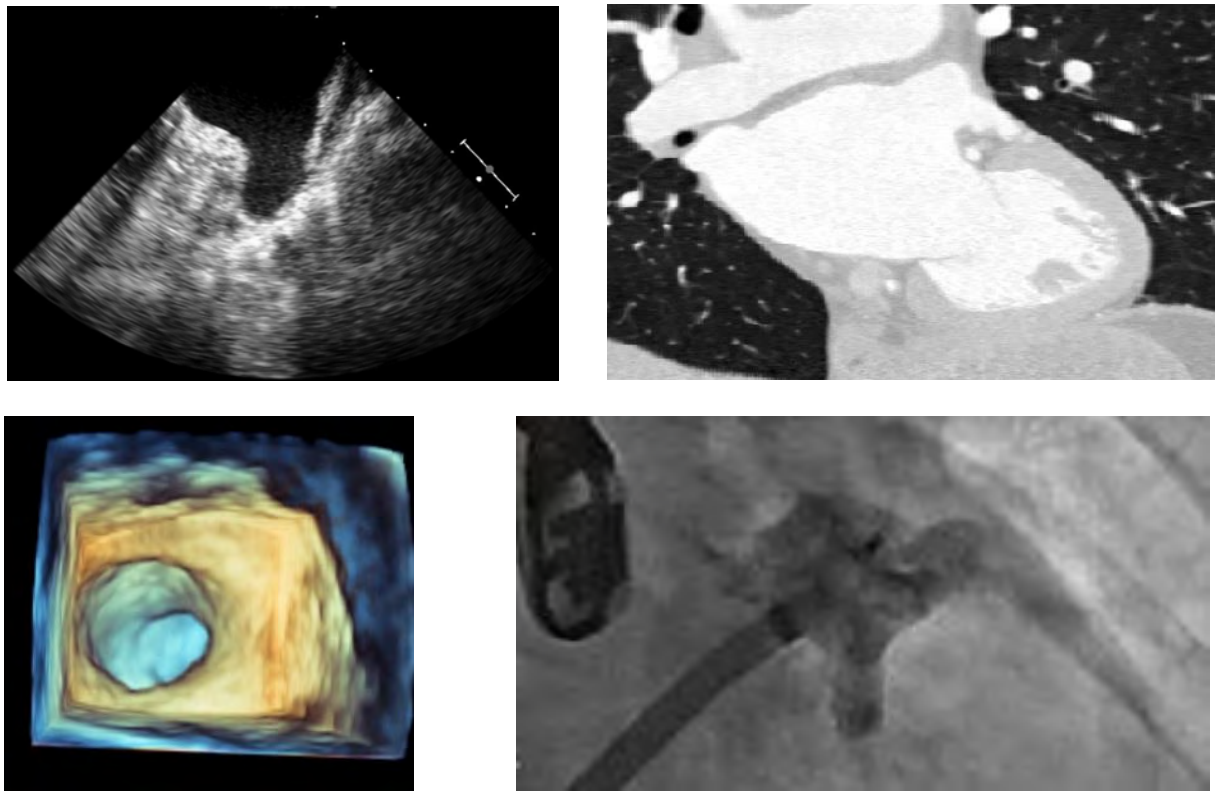

Figure 6 Different imaging modalities can be used to support the implantation process of the left atrial appendage closure. 2D (top left) and 3D (bottom left, taken from Graf *et al.* (2014), ©IEEE 2014) TEE images show the anatomy and the device, preoperative CT images (top right) can also be used to assess the anatomy and fluoroscopy images (bottom right, taken from Saw (2015), with permission of Springer, ©Springer 2015) are used during the operation.

- **Radiography**
  In radiography, X-rays are used to capture images of the human body. It is well suited for structures with inhomogeneous densities. When images of the circulation of the cavities of the heart are captured what is called angiography, the injection of iodine-based contrast medium is necessary, as the natural contrast between the structures would not be sufficient. Two-dimensional as well as three-dimensional radiographic images are used for the minimally invasive closure of the LAA. During the use of fluoroscopy, a series of two-dimensional images is taken with a C-arm and they are displayed on a screen as real-time moving images. Alternatively, three-dimensional images that are taken with multidetector computerized tomography (MDCT or CT) can be used to assess the heart (Bergmann *et al.*, 2017, p. 42). As it serves for the visualization of the cardiac structures, the term cardiac computed tomography angiography (CCTA) can be used (Saw *et al.*, 2015b). The CT images offer good spatial resolution and the ability to freely choose image planes. The image data can be displayed in multiplanar reconstructions (MPR) or maximum-intensity projection (MIP) or three-dimensional volume rendering can be used (Saw *et al.*, 2015b).

- **Ultrasound**
  Ultrasound imaging is based on the sound echoes of ultrasound waves that occur at the interfaces between tissues with different acoustic impedance. Based on the position of the transducer during the imaging, different techniques can be distinguished. During transthoracic echocardiography (TTE), the transducer is placed on the chest of the patient and it can be used to assess the LAA dimensions, volumes and function (Bergmann *et al.*, 2017, p. 30). However, transesophageal echocardiography (TEE) or intracardiac echocardiography (ICE) are regarded as the better alternatives for the assessment of the LAA anatomy. In transesophageal echocardiography, an ultrasound probe is introduced into the esophagus of the patient and advanced until it is positioned at the backside of the heart. The LAA is then the furthest structure from the TEE probe (Humphries, 2015, p. 83). Periprocedural imaging with TEE is mentioned as the gold standard for guiding LAA occlusion procedures (Meier *et al.*, 2014). Using TEE, the short axis as well as the long axis of the LAA are visible in the image planes. 3D TEE imaging platforms provide not only 3D views of the LAA, but 2D dual plane imaging is also possible (Humphries, 2015). In ICE, the transducer is integrated into a catheter that is introduced into the heart. By using ICE, general anesthesia, which is required for TEE, is not necessary (Berti *et al.*, 2015). However, the limitations compared to TEE are the lack of multiplanar imaging and the need of an interventionalist who is experienced with ICE and who is able to maneuver the catheter effectively (Bergmann *et al.*, 2017, p. 45).

- **Magnetic Resonance Imaging**
  For magnetic resonance imaging (MRI), the different nuclear magnetic resonance behavior of tissues in an external magnetic field is used. Due to its three-dimensional properties, MRI is interesting for assessing the left atrial appendage (Bergmann *et al.*, 2017, p. 44). An advantage compared to CT images is, that it does not require radiation or iodinated contrast agents. However, the spatial resolution is poorer, the patients have to hold the breath for adequate time and they may not have any devices implanted that are not compatible with MRI (Bergmann *et al.*, 2017, p. 44).

Preprocedural Imaging. Prior to the intervention, the existence of thrombi in the LAA, which is a contraindication for the procedure, has to be ruled out. TEE and CT are suitable imaging techniques for this task (Meier *et al.*, 2014).

Furthermore, the dimensions of the LAA have to be measured and the shape and the number or lobes of the LAA have to be examined in order to choose the appropriate implant type and size for the patient. Prior to the intervention, the physician has to have information on the roundness of the orifice, the number of lobes, any shapes or configurations that make the closure more challenging and the sizes of the LAA. Furthermore, the orientation of the LAA has to be known to be able to choose an appropriate puncture location and device delivery system (Humphries, 2015, p. 86). The imaging modalities that are generally used for the examination of the LAA are TTE and TEE and occasionally CT or MRI (Bergmann *et al.*, 2017, p. 30). Meier *et al.* (2014) recommend the use of three-dimensional representations for shape examinations, which are available with 3D TEE, MRI and CT. Rajwani *et al.* (2016) consider the use of CT data advisable, as they found out that sizes

predicted by TEE and CT differed in more than half of the cases and the outcome of sizing with CT data was excellent.

To use the full potential of the three-dimensional image data and support the device size planning and the determination of the best angiographic angle during implantation, the preoperative CT data sets can be processed with dedicated software such as 3mensio Medical Imaging (Pie Medical Imaging BV, Maastricht, Netherlands). This software offers segmentation and cropping of the image data, the use of sizing tools and an overlay of defined measurements on a fluoroscopic image (Bergmann *et al.*, 2017, p. 42).

Periprocedural Imaging. The standard setting for periprocedural imaging is 2D TEE in combination with fluoroscopy. Although some groups use solely fluoroscopy, the use of 3D TEE is recommended, as it is able to deliver real-time full view of the LAA and its ostium (Meier *et al.*, 2014). ICE is a potential alternative to TEE. 2D X-plane and 3D TEE support the optimal positioning of the transseptal puncture and TEE and fluoroscopy are used during the crossing of the septum and the positioning of the delivery sheath (Bergmann *et al.*, 2017, p. 45-48). A typical setup in the catheter laboratory using TEE and fluoroscopy is displayed in Figure 7.

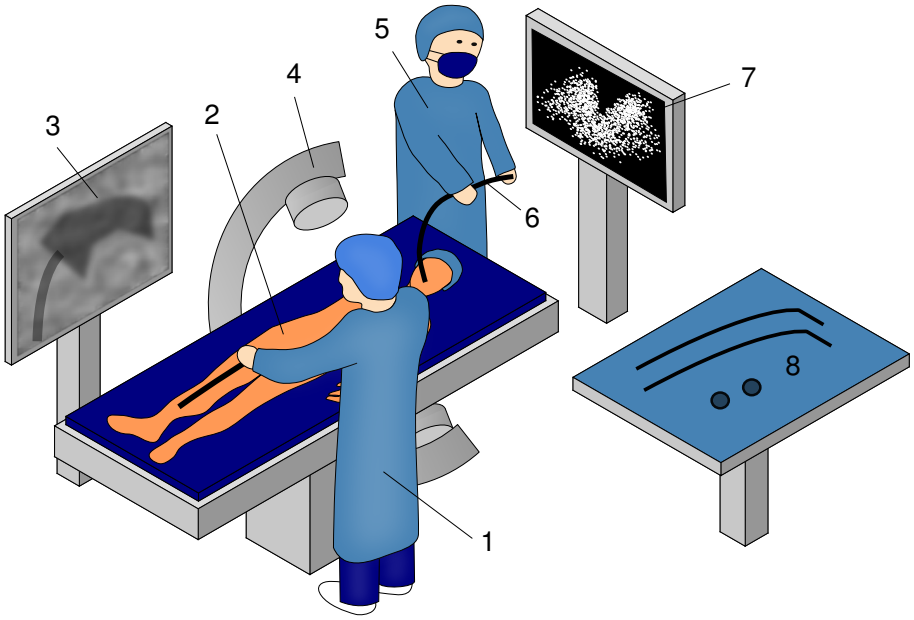

Figure 7 Typical setup in the cardiac catheterization laboratory: The interventionalist (1) performs the intervention standing near the bedside of the patient (2). In his viewing area is a screen that displays the fluoroscopy images (3) taken by a C-arm (4). A second cardiologist (5) takes the ultrasound images with the TEE probe (6), which are displayed on his own screen (7). A table (8) at the side serves for the preparation of the catheters and the implant.

To facilitate the orientation and to transfer the planning data, the information of CT images and especially the planning information that was achieved with the 3mensio software can be fused with the intraoperative fluoroscopy data. For this purpose, the Valve ASSIST 2 system (GE Healthcare, Chalfont St Giles, UK) can be used, which enables the display of planning data during the operation (Roy *et al.*, 2017).

Assessment of the Results. After deployment of the implant, apart from checking the appropriate device positioning, the complete closure of the LAA can be assessed under fluoroscopy by using contrast agent and residual flow can be detected using color-flow Doppler imaging (Bergmann *et al.*, 2017, p. 49).

For long-term follow up, TEE is recommended as the method of choice (Meier *et al.*, 2014, p. 16).

3.1.4 State of the Research

Manual Shaping of the Catheter. In the expert consensus of Meier *et al.* (2014, S. 5) the option of custom shaping of the catheter with or without the use of a hot air gun is mentioned in case that the alignment of the delivery sheath with the LAA is suboptimal.

Gafoor *et al.* (2015b) describe a method for patient-specific shaping of the catheter sheaths (see Figure 8). They perform the shaping of the catheter when the patient is already on the operating room table and the guidewire has been inserted into the heart and through the transseptal puncture. The guidewire is placed in the left atrial appendage and therefore its shape corresponds to an appropriate shape to reach the left atrial appendage. The catheter sheath that is used for the implant delivery is placed on the patient's breast while X-ray images are taken with the C-arm. Those images show the catheter sheath and the guidewire and their shapes can be compared. The catheter sheath is manually deformed to match the shape of the guidewire and the result is controlled in a new X-ray image. These steps are repeated iteratively until the shape of the catheter sheath corresponds to that of the guidewire.

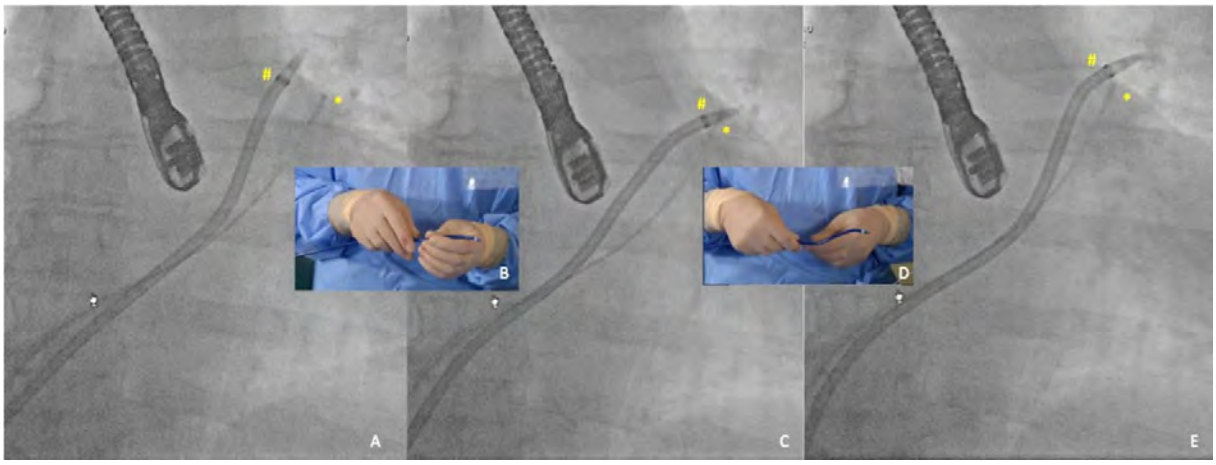

Figure 8 Gafoor *et al.* (2015b) present the 'shape-the-sheath'-method to find patient-individual optimized catheter sheath shapes. The catheter is iteratively deformed using a guidewire that is placed in the left atrial appendage and while the catheter sheath is lying on the patient's breast (taken form (Gafoor *et al.*, 2015b), with permission of John Wiley and Sons, ©John Wiley and Sons 2015)

Additive Manufacturing of LAA Planning Models. Different groups used three-dimensional additively manufactured models of the left atrial appendage for planning purposes in minimally invasive closure of the left atrial appendage (Fan *et al.*, 2016; Otton *et al.*, 2015; Pellegrino *et al.*, 2016). Several cases are described where the additive manufacturing of models were used to support the choice of the appropriate implant and the planning of an optimal device position. The models were

generated based on 3D TEE or CT data. The groups used Mimics, a 3D medical image processing software by Materialise Software (Leuven, Belgium) or the devices were made by Caretronik (Prato, Italy), a company that produces additively manufactured anatomical models.

3D Visualization of the LAA. In a patent originally entered by the GE Medical Systems Global Technology Company a system was proposed to support the planning of the implant size for LAA occlusion (Okerlund *et al.*, 2010). It describes a virtual 3D model of the LAA based on preoperative image data that should be generated and visualized intraoperatively by registration of landmarks with images from the interventional imaging system.

Use of Steerable Catheters. Regularly, no steerable catheters are available for the use in minimally invasive closure of the left atrial appendage. However, in 2016 Lange *et al.* (2016) successfully used a steerable catheter sheath for the implantation of an Amplatzer Amulet device, as they could not succeed with the standard equipment. They proved that the use of steerable catheters is possible for minimally invasive closure of the LAA and may be useful in difficult anatomical conditions.

3.2 Catheter Positioning in Other Cardiac Procedures

Positioning of the catheter is a challenging step in the minimally invasive closure of the left atrial appendage. Since the occlusion procedure is still relatively new, there is not much literature available that addresses this problem. However, in other catheter-based procedures that are targeting towards the left atrium and therefore require transseptal puncture such as catheter ablation or mitral clipping, this is a well-known problem, which has already been addressed.

3.2.1 Steerable Catheters

Only non-steerable catheter sheaths are available for the Amplatzer Devices or the Watchman device, but steerable catheters are the standard equipment in other cardiac procedures (Fu *et al.*, 2009). Examples for the use of steerable catheters in other transseptal implantation procedure are the steerable guide catheters that are used for mitral clipping (Feldman *et al.*, 2005) or the steerable catheter sheaths that are used for atrial fibrillation ablation (Rajappan *et al.*, 2009).

For catheter ablation in the left atrium the steerable sheath were compared to non-steerable sheaths in randomized trials with different outputs. While some studies showed better results with the use of the steerable sheaths (Piorkowski *et al.*, 2011), others could not find better outcomes (Rajappan *et al.*, 2009). However, they reported that there is a significant learning curve and the use of steerable sheaths could be very important for patients with difficult anatomy.

Ali *et al.* (2016) provide an overview of catheters that are mechanically actuated. The steerable catheters are mainly moved by stainless steel cables that run from the handle to the tip of the catheter, which can be deflected by push/pull movement of the cables. The catheters allow either actuation of one or multiple segments and the bending motion can be realized in one plane or multiple planes by the selection of the number of cables and the arrangement of the cables and compliant or stiff

segments in the catheter. Thereby, different bending radii can be realized and by actuating multiple segments, S-shapes can be achieved. By combining multiple concentric segments, a great flexibility and independent steering of the segments can be achieved. However, the increase in possible degrees of freedom of movement (DOF), adds to the complexity of the use and the steering of the catheter as well. Furthermore, the number of cables increases what leads to challenges such as friction, buckling and wedging of cables (Ali *et al.*, 2016).

3.2.2 Robotic Catheters

Robotic catheters were developed mainly for the catheter ablation. They are used to enhance the maneuverability but also to protect the physicians from radiation by remote control of the catheter. Two catheter systems are currently available for clinical use: The Sensei Robotic Catheter System (Hansen Medical, Mountain View, CA, USA), which works with a pull-wire driven catheter, and the magnetically steered Niobe system (Stereotaxis, St. Louis, MO, USA).

The Sensei Robotic Catheter System is used with the Artisan catheter, a sterile single use catheter, which consists of an inner and an outer part that can be steered independently by actuation of pull-wires (Kanagaratnam *et al.*, 2008). The outer sheath can be moved in one plane whereas the inner sheath can be actuated in two directions. Conventional catheters can be inserted through the guides and the system is remote controlled by a three-dimensional hand-operated joystick (Kanagaratnam *et al.*, 2008).

The Niobe system as described by Ernst *et al.* (2004) is an external catheter navigation system, which moves the catheters magnetically inside the body. Two permanent magnets, which are positioned on either side of the patient table, generate a magnetic field that forces the tip of the catheter, which is equipped with a permanent magnet at its tip, to align with the magnetic field inside the body. The orientation of the external magnets can be changed to deflect the catheter. The catheter is advanced by a computer-controlled catheter advancer system, the Cardiodrive unit. The user interface can be either a joystick or a mouse.

Riga *et al.* (2011) compared the positioning skills of novices in cardiology using endovascular non-steerable, manually steerable and robotically steerable catheters in a phantom of the aorta and found that the advanced catheters offer better positional control.

Robotically steering catheters is an active field of research. Different actuation principles are investigated including electric, thermal, magnetic, hydraulic and mechanic cable actuation (Ali *et al.*, 2016). Regarding mechanical cable actuation and magnetic actuation, there are commercially available products as described above. The other principles are still in the research stage, mainly due to manufacturing and safety issues (Ali *et al.*, 2016). A lot of research has been carried out in this field and only a short overview of the actuation principles based on the classification by Ali *et al.* (2016) and some examples are mentioned here. For a full review of work on active and robotic catheters see Ali *et al.* (2016), Rafii-Tari *et al.* (2014) and Fu *et al.* (2009).

- **Electrical Actuation**
  Electrical actuation can either be realized by direct or indirect actuation. Direct electrical actuation uses materials that respond to electrical currents by a bending motion such as piezoelectric actuators (Rogers, 2012). If the actuation is based on the interaction between electrically responsive material and the surrounding medium as for example in ionic polymer-metal composites (Guo *et al.*, 1995; Fang *et al.*, 2007), the principle is called indirect electrical actuation (Ali *et al.*, 2016).

- **Thermal Actuation**
  Shape memory alloys (SMAs) can be used to actuate catheters thermally (Haga *et al.*, 2000; Ayvali *et al.*, 2012). By the change of the temperature, which is usually evoked by electrical current, the actuator changes between a high-temperature and a low-temperature phase, which both have a specific memorized shape, and as a consequence, the actuator changes between these two shapes (Ali *et al.*, 2016).

- **Hydraulic Actuation**
  For hydraulic chamber actuation, fluid pressure is used to bend the device in a specific direction (Ikuta *et al.*, 2012; Suzumori *et al.*, 1991). The bending direction can be realized and controlled by the integration of several bellows or by nonuniform distribution of the stiffness of the walls. The fluid chambers can have either a static or a dynamic size and location.

- **Concentric Tubes**
  Another approach to enable steering of the catheter tip is the telescoping of flexible precurved concentric tubes (Webster *et al.*, 2006; Sears & Dupont, 2006). By changing their relative position translationally and rotationally, the position and orientation of the tip of the device can be controlled.

3.2.3 Planning Programs

Li *et al.* (2001) developed a program for interactive planning of the catheter shape for radiology catheters used in the aortic root, as this is an anatomically variable region and the choice of a well-suited catheter is crucial for the success of the procedure. In the program, the user could build up its own catheter shape by a combination of a number of different catheter segments and could visualize the resulting catheter. The planned catheter shape was subsequently used in an interventional radiology simulation system that the group had developed earlier.

Jayender *et al.* (2011) addressed the problem of the limited maneuverability in catheter ablation in the left atrium by calculating an optimized transseptal puncture location. Their program was targeted towards the use of a robotic catheter. They modeled the catheter to determine the point in the interatrial septum that will allow maximum maneuverability of the catheter.

In the program developed by Rahman *et al.* (2011) a virtual evaluation of different available catheters for the angiography of the right coronary artery based on preoperative image data is performed. After the segmentation of the anatomical structures, angles and distances between the aorta and the coronary arteries are calculated and compared to the parameters of the available catheters to find the one that is best suited.

Several planning programs are available for the planning of catheter-based aortic valve implantation. The planning programs focus on the implant placement and measurements, as the choice of the correct implant size and a suitable implant position are crucial for the success of the procedure. Gessat *et al.* (2009) describe a planning program for a transapical catheter-based aortic valve implantation. The aortic root is segmented semiautomatically and the geometrical constraints for the size and the position of the implant are calculated based on user selected anatomical landmarks. The implants can then be inserted virtually into the segmented aortic root. Other planning systems for aortic valve planning are available such as the image post processing software of CIRCLE Cardiovascular Imaging (Calgary, Alberta, Canada), which among others can be used for assessment of the prosthetic orifice area (von Knobelsdorff-Brenkenhoff *et al.*, 2011), and the FEops (Gent, Belgium) software, which allows simulation of the transcatheter aortic valve implantation (TAVI) procedure and the implant deployment (de Jaegere *et al.*, 2016). Furthermore, with the Philips HeartNavigator (Philips, Amsterdam, Netherlands) and GE ValveAssist (General Electric, Boston, MA, USA) there are two systems that allow the planning of the procedure and the periprocedural imaging of the planning results for aortic valve implantation (Agarwal *et al.*, 2015).

3.3 Automated Construction

At the Institute of Micro Technology and Medical Device Technology at the Technical University of Munich, the approach of automated construction is implemented in MATLAB (The MathWorks, Inc., Natick, MA, USA). The basic idea of automated construction is that the design of systems is adapted automatically to requirements or restrictions. This goes beyond parametrized construction and alters the construction more fundamentally. The idea was designed for the automated construction of task based mechanisms (Lüth, 2015) and is also applied to medical robots that are adapted to the patient, the intervention or the physician (Krieger *et al.*, 2017) and the automated construction of gear wheels (Träger *et al.*, 2015). The manufacturing of these individualized components is realized by additive manufacturing methods. Additive manufacturing methods allow the efficient production of small sample sizes and easy alterations of the geometry of the parts. As standard construction programs for the CAD design like CATIA, SolidWorks or ProEngineer are targeted primarily towards machining technologies, the SG-Library, a MATLAB toolbox, was developed, which supports the automated design. The approach is described in detail in the publications (Lüth & Irlinger, 2013) and (Lüth, 2015) and based on these articles this chapter only offers a short overview over the functionalities that are important for the planning program.

The standard file format for additive manufacturing is STL. STL stands for 'Stereolithography' or 'Standard Tessellation Language'. In these files, the parts are described by defining their surfaces as a net of multiple flat triangles what is referred to as triangulation. This kind of representation is called Boundary Representation (BREP). The three-dimensional part is described by a list of points (vertex) and a list describing which three points belong to one flat surface (facet). The order of the points in the facet list defines the orientation of the triangle. MATLAB uses boundary representation for three-dimensional visualization with the command 'patch'. Furthermore, it enables the triangulation of binary voxel data sets and the generation of vertex and facets lists using the 'isosurface' command.

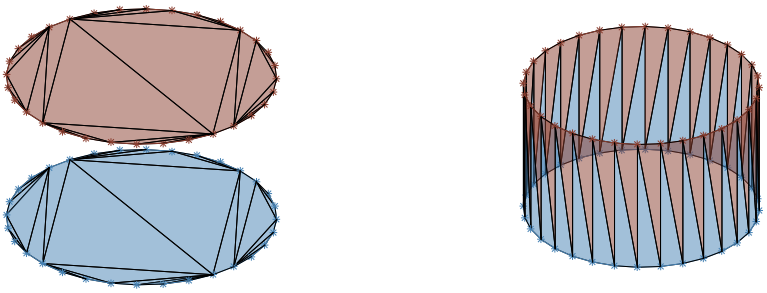

Figure 9 Extruded parts, which are based on a stack of cross-sections, are constructed by Delaunay triangulations of flat surfaces (left) and connection of the sidewalls between the cross-sections by triangles (right).

If a part can be described by extrusion and is therefore based on a stack of cross-sections, the main two tasks are the triangulation of the end surfaces and the construction of the sidewalls. The triangulation of the flat surfaces at the end is based on the Delaunay triangulation (Lüth & Irlinger, 2013). In order to build the sidewalls, the cross-sections are connected. Therefore, two triangles are added between two pairs of points on the neighboring cross-section. Figure 9 shows these two principles.

4 Limitations of the State of the Art

The minimally invasive closure of the LAA is described as challenging by experts and there is a learning curve, which is not steep (Meier *et al.*, 2014, p. 11). The following three points are challenging steps especially for unexperienced physicians, which can be facilitated to enhance the risk-benefit analysis.

- **Danger of Damaging the Heart Walls**
  With over 90%, most of the complications of the minimally invasive closure of the left atrial appendage are procedure-related complications that occur in a short period after the intervention (Reddy *et al.*, 2011). There is a danger of injuring the heart walls during the procedure that can lead to pericardial effusion, the most frequent major complication for LAA closure (Reddy *et al.*, 2011; Park *et al.*, 2011). This complication occurs especially at repeated placements of the device (Lewalter *et al.*, 2013, p. 655) but also during the transseptal puncture and due to movements of the catheter inside the left atrial appendage (Reddy *et al.*, 2011, p. 6). A careful movement of the instruments is particularly necessary, as the walls of the heart are extremely thin and they can contain pits or troughs where the catheters can become lodged (Su *et al.*, 2008, p. 1169). Therefore, movements of the instruments inside the LAA should be minimized.

- **Challenging Positioning of the Catheter**
  The anatomy of the left atrial appendage differs widely between patients (Don *et al.*, 2015). The position as well as the orientation of the orifice is different for each patient. However, the variability of available catheter sheath shapes for the positioning of the catheters is limited. Joy *et al.* (2017) state that the curvature of the tip of the catheter should correspond to the angulation of the appendage. By minimizing sheath manipulation and device recapture maneuvers due to a well-fitting catheter shape, the risk for perforations could be reduced.

  In order to unfold and orientate the device correctly, the coaxial alignment of the catheter and the LAA is important (Meier *et al.*, 2014, p. 2; Saw, 2015, p. 186; Saw *et al.*, 2015b, p. 127). The choice of a suitable puncture location is very important, as an inconvenient puncture location makes the coaxial alignment harder and with an optimized puncture location, the manipulation of the catheter sheath can be reduced (Saw *et al.*, 2015b, p. 127). This is particularly true for an inconvenient orientation of the left atrial appendage (López-Mínguez *et al.*, 2014; Phillips & Kar, 2015, p. 153). Many variables such as the distance and angle between the fossa ovalis and the LAA and between the fossa ovalis and the inferior vena cava but also the tortuosity of the venous system influence the alignment options. These factors are difficult to control and no software supporting the physician during the planning is available up to now (Saw *et al.*, 2015b, p. 127). During the procedure, in order to reduce the risk for device-associated thrombi, the time that the device remains inside the catheter sheath should be minimized (Meier *et al.*, 2014, p. 5).

- **Choice of the Implant Size as a Challenge**
  The choice of the implant size is not always clear. Especially for LAA orifices with non-circular cross section, there is a risk of dramatically oversizing the implant, which could lead to the extrusion of the lobe of the Amplatzer implant out of the LAA (Saw, 2015, p. 188; Saw *et al.*, 2015b, p. 126). According to a study, in 17% of the cases a second implant with a different size than the previously planned had to be used during the operation (Park *et al.*, 2011, p. 703). Wrong choice of the implant size can lead to extrusion of the implant or damages to the heart walls. Only since recently, with the 3mension system, a system supporting the physician during the choice of the implant size by offering additional views, measurements and 3D visualization is available (Bergmann *et al.*, 2017, p. 42).

In order to overcome these limitations, the concept of a preoperative planning system that supports the physician during the planning of the intervention and that helps to facilitate the positioning of the catheter and the implant is developed.

5 Concept of a Preoperative Planning System for the LAA Occlusion

In order to support the physician during the planning of the procedure and to facilitate the implant placement, a preoperative planning system was developed and the concept of the planning program is presented hereafter.

5.1 Aim of the Project

To solve the limitations that are presented in the previous chapter, a planning system for the minimally invasive closure of the left atrial appendage was developed. The planning system supports the physician during the planning of the procedure and particularly during the selection of the appropriate implant size and the subsequent positioning of the catheter in the left atrial appendage. There are three major goals of the planning system. However, not all of them may be relevant for every patient.

- **Planning of the Implant Size**
  The planning system should support the planning of the implant size based on the image data of the patient. The anatomical conditions and the expected implant position should be presented intuitively, easy to access and without the need for external software.
- **Evaluation of the Standard Catheter Sheath**
  With the high variability of the anatomical conditions of the left atrial appendage, a preoperative evaluation of the suitability of the standard catheter sheath for the given anatomy can predict the level of difficulty of the procedure for the individual patient. Therefore, the suitability of the given catheter should be tested based on the patient's image data.
- **Support the Accessibility of the Target Position with the Catheter Sheath**
  Especially for patients where the standard catheter sheath seems not to be suitable, a solution to facilitate the positioning of the catheter sheath is necessary. The solution should allow the adaptation to the given anatomical conditions of the patient, which include the position and orientation of the left atrial appendage in relation to the puncture location and the route of the access pathway to the heart.

5.2 Concept of the Planning System

The previously described aims can be achieved by a planning system that is based on preoperative image data of the patient. The planning system has the following major functionalities, which are illustrated in Figure 10.

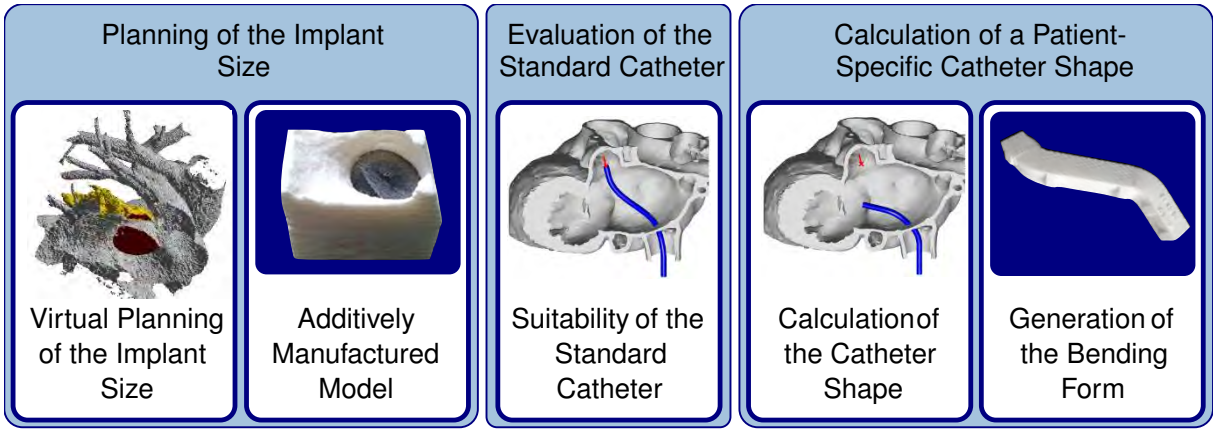

Figure 10 The three main goals of the planning program are the support of the physician during the selection of the appropriate implant size by a virtual display of the implant and the anatomy and the generation of an additively manufactured model, the evaluation of the suitability of the standard catheter and the calculation of a patient-specific catheter shape, which can be realized with the help of a bending form that is generated by the program.

- **Planning Model for the Visualization and Choice of the Implant Size**
  The planning of the implant size and shape is supported by the system through the display of the anatomy of the left atrial appendage and the virtually inserted implant of different sizes. The planned implant position and size can thus be evaluated. Furthermore, the compression that the chosen implant receives at the planned position is estimated. Additively manufactured models of the left atrial appendage can assist the physician during the planning of the implant size and position. The planning program offers an interface for the generation of the necessary virtual surface model of the left atrial appendage. The additively manufactured model can be used to insert and test implants of different sizes in order to choose the one that is fitting best.

- **Suitability Evaluation of the Standard Catheter Sheath**
  For the evaluation of the suitability of the standard catheter sheath for the given anatomy, the shape of the standard catheter is projected into the image data of the patient's anatomy. To do this, the boundary points of the procedure need to be planned and an evaluation of the accessibility of the planned implant position with the given standard catheter sheath is performed. For that reason, the distance and the deviation of the tip of the virtually inserted catheter to the planned implant position is calculated and the catheter sheath is displayed in relation to the patient's image data.

- **Patient-Individual Catheter Shape**
  Especially for patients where the standard catheter sheath seems not to be suitable, the positioning of the catheter sheath has to be supported. The solution that is presented in this project is not to use a steerable catheter or even a robotic catheter, as these include the use of new equipment, which is more complex and more expensive and would change the implantation procedure and the usage by the physician. This would force the physician to learn new processes and might add new challenges to the procedure. Instead, the positioning of the catheter is facilitated by calculating a patient-individual catheter shape that is adapted to the patient's anatomy. The calculated shape is displayed relative to the image data to be approved by the physician.

- **Shaping the Catheter Sheath**
  After the calculation of the patient-specific catheter shape, the catheter sheath has to be shaped into the calculated form. To keep the planning system and its use as simple as possible, no bending machine is used, but the catheter is shaped with the help of a customized additively manufactured bending form. The catheter is inserted into the bending form that resembles the desired catheter shape and the new form is stabilized by heating and subsequent cooling of the catheter.

5.3 Unique Features and Expected Advantages

The presented system differs from the known approaches that were described in the state of the art by the following features.

- **Preoperative Evaluation of the Access to the Implantation Site**
  The program allows a preoperative computer-assisted evaluation of the suitability of the catheter for the given anatomy for implantation procedures inside the heart. Most planning programs for minimally invasive implantation of cardiac devices solely focus on the implants and their shapes and sizes. This program however, offers the possibility to identify potential difficult anatomical conditions. In the state of the art, this evaluation relies on the experience and the imagination of the user and no support is offered.
- **Preoperative Computer-Assisted Planning of the Catheter Shape**
  The manual shaping methods described in the state of the art are purely based on the experience of the physician without any guidance system to support him. The approach that Gafoor *et al.* (2015a) present gives a guideline on how to shape the catheter, but as the shaping is an iterative process that is performed during the operation, it consumes a lot of time in the operation room, which leads to additional strain for the patient and increased procedure times and costs. The proposed system is the first system for minimally invasive cardiac implantation procedures that supports the physician by preoperatively calculating an optimized and patient-specific catheter shape.
- **Bending Form for the Support of the Catheter Shaping**
  To realize the planned catheter shape, the planning program generates bending forms that are produced by additive manufacturing. This is the first program that offers bending forms for the shaping of patient-specific cardiac catheters. No forms for the assistance of catheter bending are known up to now.
- **Integration of Virtual Implantation Planning and Generation of an Anatomical Model**
  In the state of the art, there are cases that report the additive manufacturing of anatomical models based on preoperative image data of the patient. Furthermore, there are programs for the planning of the position and the shape of cardiac implants. However, this is the first program that combines the virtual planning with the generation of additively manufactured models to offer the physicians complete support depending on the complexity of the respective anatomy.

5.3.1 Expected Advantages

Due to the virtual insertion of the standard catheter and the patient-individual shaping of the catheter, it is expected that it is easier for the physician to assess the challenge of reaching the target position with the standard catheter and that the positioning of the catheter in cases of difficult anatomies is facilitated. As the catheter shape is adapted to the anatomical conditions of the patient, the accessibility of the left atrial appendage is ensured and the necessary movements of the catheter in the left atrium are reduced. The manipulation with non-fitting catheters, which might only be inserted into the LAA with application of high torque, is prevented. Therefore, another expected advantage of this new approach over the existing standard procedure is that the procedure is not only faster but also safer at the same time, as increased catheter sheath movement increases the risk of injuries of the heart walls and therefore pericardial effusions.

The risk of complications can be further reduced by the assisted choice of the implant size. The necessity to try different implant sizes can be avoided by controlling the implant size beforehand on the additively manufactured anatomical model. Furthermore, the planning model for the anatomy of the left atrial appendage does not only support the choice of the implant size and type but the best implant position can also be tested and evaluated by the physician.

5.4 Integration of the Planning System in the Clinical Workflow

The new planning system has to be integrated into the clinical workflow. As it is a preoperative planning system, the main part of its use is taking place before the operation and outside the catheterization laboratory but some steps have to be performed inside the catheterization laboratory. The process flow for the use of all functionalities of the program is described below and shown in Figure 11.

Outside the Catheterization Laboratory. The proposed planning program is used preoperatively. As additive manufacturing of parts is required, the planning needs to be done well in advance to allow enough time for the manufacturing process.

In a first step, the physician acquires three-dimensional image data of the patient and loads the image data into the planning system. In the planning program, he plans the boundary points of the intervention, tests the suitability of the standard catheter and if necessary calculates a patient-specific catheter shape. During the planning of the intervention with the planning program, two STL files are generated and saved in a user-defined folder: an anatomical model of the left atrial appendage and a bending form to shape the catheter sheath. Those files are transferred to a suitable additive manufacturing machine and produced.

The anatomical model of the left atrial appendage can be used to check the suitable implant size by physically inserting implants of the appropriate size into the model. Furthermore, the planned implant position can be checked for feasibility and the physical model may help the imagination of the physician, as it is more vivid than displayed images.

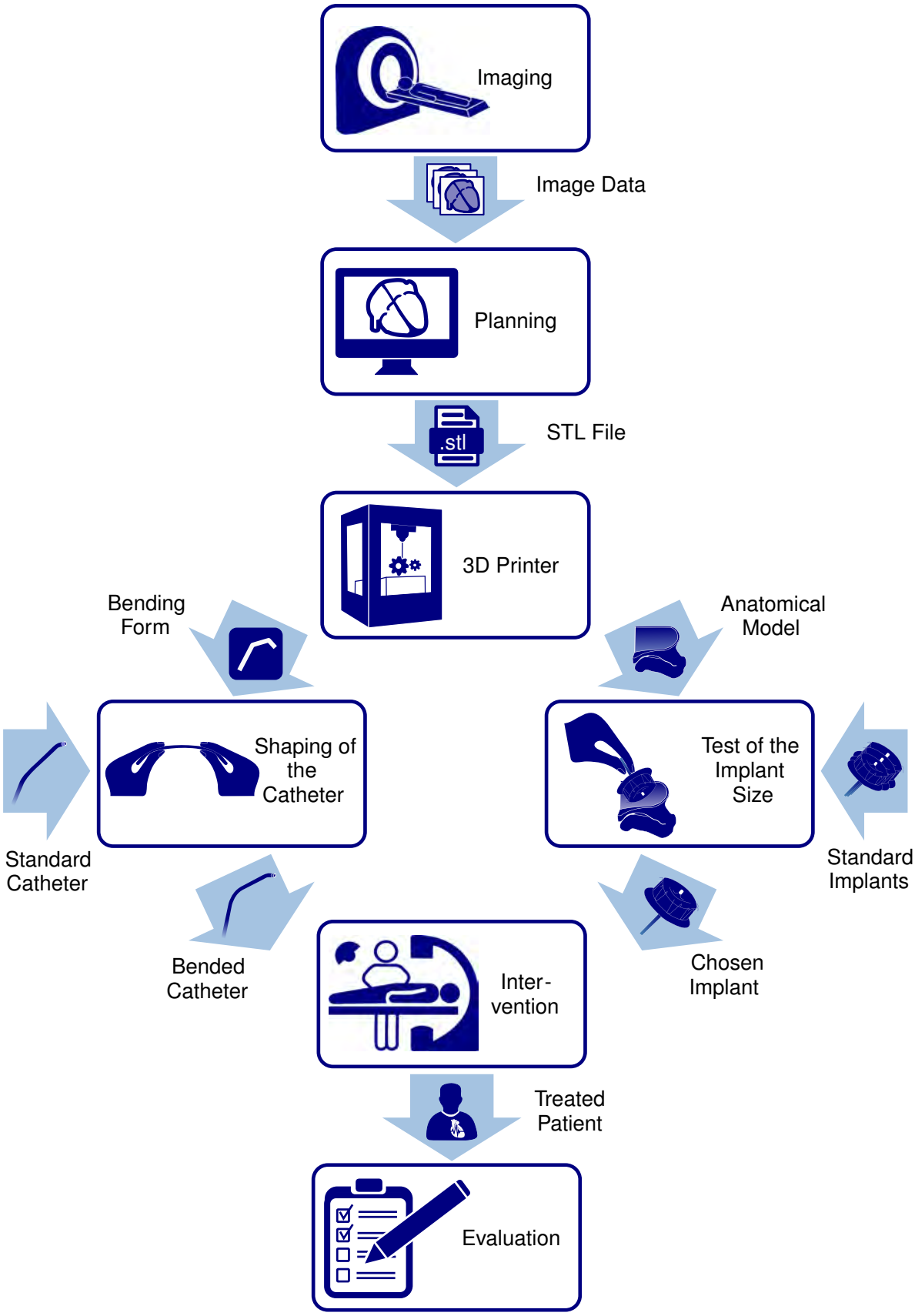

Figure 11 The planning system works based on preoperative image data of the patient. The physician plans the intervention with the proposed program. He tests the implant size in a physical anatomical model and shapes the catheter according to the planning if the standard catheter is not well suited for the patient. The planning program automatically generates the necessary STL files of the anatomical model and the bending form and the parts are produced by additive manufacturing.

Inside the Catheterization Laboratory. The bending form is used to bring the sterile standard catheter into the desired shape. In order to provide the safety of the procedure, adequate sterilization and preparation of the bending form has to be ensured. The catheter is manually deformed to fit into the bending form. The bending process is supported and the new shape is secured by placing the catheter inside the bending form in hot water or steam and cooling it down afterwards. Prolonged dwell time in the bending form will improve the shape.

The subsequent intervention and follow-up is performed as described in the state of the art. While doing the transseptal puncture, the physician has to keep in mind that the puncture location was previously planned and deviations from the location might lead to accessibility problems. He should therefore try to meet the puncture position as close as possible. After the procedure, the results and the difficulties encountered are evaluated.

5.5 Structure of the Planning System

In this section, the principal components of the planning system as shown in Figure 11 are described.

5.5.1 Image Data

The program works based on three-dimensional preoperative image data of the patient. For the planning of the implant size, only the region of the left atrial appendage needs to be visible in the image data. Therefore, the necessary information can be found in three-dimensional ultrasound data as well as in CT data (see Figure 12). However, to enable the planning of the catheter shape, additionally the pathway of the inferior vena cava and the interatrial wall have to be part of the image data. Therefore, CT data are used for the catheter shape planning.

The ultrasound images show the cardiac tissue and the interfaces to the cavities. The gray scale values of the voxels range between values of 0 (= black) and 255 (= white) with tissue having higher values than cavities. The CT images are acquired with the help of a contrast agent to gain contrast in the cavities. The blood-filled cavities are clearly visible and can be distinguished from cavities outside the heart as long as the amount of contrast agent in the cavity was sufficient during the

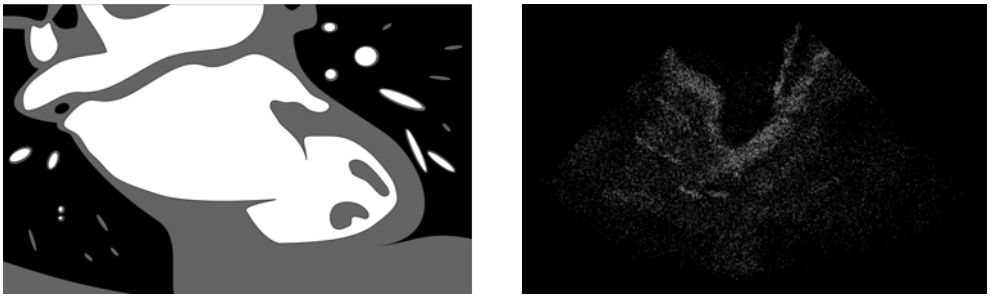

Figure 12 The LAA is visible in ultrasound and in CT data. In CT data, the contrast enhanced blood pools are displayed in white, muscle or fat tissue in gray and air in black (left). The ultrasound images display the reflection of the ultrasound waves especially at boundary layers of different tissues (right).

acquisition of the images. CT images have a gray scale value range that contains 4096 gray scale values. These gray scale values are converted to Hounsfield units (HU) in the range -1024 HU to 3071 HU. Air has the lowest Hounsfield value ($\sim$ -1000 HU), tissue is ranging in the medium segment (fat: -100 HU to -40 HU) and the Hounsfield value of blood pools with contrast agent is higher than the ones of these other two materials (300 HU - 500 HU) (Budoff, 2016, p. 4).

The image data are available in the DICOM format, a standard file format for medical images. The three-dimensional image data set is available as a stack of image slices with information about the spacing of the pixel in the image slices and the distances of the slices to each other. Furthermore, in the header of the files, further information about the imaging modality and the patient are available.

5.5.2 Planning Program

The planning program can be executed on standard computers with no special requirements except the installation of a suitable MATLAB version. The planning program is available as a MATLAB library, which can be installed and executed in the MATLAB program.

The program has a graphical user interface, which guides the user through the program. The user can interact with the program with a standard mouse and keyboard.

The program consists of several phases for the planning of the intervention: the planning of the implant size, the calculation and display of a catheter shape and the calculation and display of a corresponding bending form. The input of the planning program are the image data of the patient and it exports the anatomy of the left atrial appendage and the bending form.

5.5.3 Files in STL Format

The program exports the model of the anatomy of the left atrial appendage as well as the constructed bending form in files in STL format. These files are normal data files that can be transferred to other data media. STL files describe the surface of geometric bodies. The surface is triangulated and described by a list of points and a second list that describes the connection of the points to triangles. By using this file format, the parts can generally be manufactured on any available additive manufacturing machine that fulfill the requirements of the components concerning accuracy of the dimensions and the material properties.

5.5.4 Anatomical Model

The additively manufactured anatomical model is used for the visualization of the anatomy and for testing implants of different sizes. The models display the boundary layer between the cardiac tissue and the cavity of the left atrial appendage as it is depicted in the image data. An area of interest around the planned implant position is displayed in the model. The size of this area of interest might depend on the anatomical conditions of the patient. As a minimum wall thickness is required for the additive manufacturing, the boundary layers are thickened in direction of the heart walls away from the cavities. The necessary minimum wall thickness depends on the properties of the additive manufacturing technique that is used. The anatomical model can be used to insert and deploy

implants. As the additive manufacturing method can be chosen freely, the model can also be made of flexible material. The attainable resolution of the anatomical model depends on the resolution of the applied image data.

5.5.5 Bending Form

The bending form is calculated in the planning program based on the desired patient-specific catheter shape. It is used to shape the catheter by forcing it into its new shape. The catheter is clamped into the bending form and plastic deformation that makes the shape permanent is evoked by placing the catheter inside the bending form in hot water or steam and cooling it subsequently. Therefore, the bending form has to replicate the desired catheter shape and completely enclose the catheter in its desired shape. The bending form is a negative of the desired patient-individual catheter shape and in order to allow the insertion of the catheter, the bending form can be opened. It consists of a continuous bottom part and a lid, which is separated into multiple parts for easier insertion of the catheter into the bending form. The lids are connected to the bottom part by hinges and can be closed by snap-in hooks. Therefore, the bending form can be produced monolithically. The position and number of the lid segments and the hinges are adapted to the shape of the bending form. In order to avoid confusion, the bending form can be automatically labeled with the patient's name and the date.

5.6 Boundaries of the Project

Some of the components that are shown in Figure 11 were not newly developed in the project but standard equipment was used. The components that were not developed as part of the project are listed below.

- **Imaging Systems**
  The planning system works based on preoperative image data. Standard imaging systems were used for their acquisition. For the planning procedure, three-dimensional CT data or ultrasound image data acquired with a transesophageal ultrasound probe were used.
- **Catheters**
  The component that is referred to as 'catheter' in the following chapters is the delivery sheath, which is used for the introduction and positioning of the devices. The planning system only focuses on the calculation of the shape of the catheter sheath. The development and production of catheters was not part of the project. The planning system was tested with the AMPLATZER TorqVue 45x45 Catheter (St. Jude Medical, St. Paul, MN, USA) as the standard catheter sheath used for the Amplatzer devices. It was possible to bend the catheter in hot water or steam though it is not intended for this use. Its original shape was measured to allow the evaluation of the standard catheter. However, the evaluation of the catheter with the planning system is not restricted to this catheter, as different double bended catheter shapes could be used by entering the description of the lengths of their segments and the bending angles between the segments.

- **Implants**
  The system is designed to be used for the implantation of standard occlusion devices. In the system that is presented, the shapes of the Amplatzer Cardiac Plug devices and the Amplatzer Amulet devices are recorded. However, in general the system can be adapted for any rotational symmetric occlusion device by adding the dimensions of the implant into a look-up table.

- **Additive Manufacturing Systems**
  To make use of the full potential of the planning system, additive manufacturing of parts of the system is required. Several additive manufacturing methods were tested for the production of the model. The main requirement for the additive manufacturing method is that it replicates the sizes exactly. The construction of the bending form was targeted towards the production by selective laser sintering with an EOS Formiga (EOS, Krailling, Germany), as each additive manufacturing method has certain inherent requirements concerning minimal wall thicknesses or minimal gap widths between parts that should not merge during the manufacturing process.

5.7 Process Description of the Planning Program

The planning program itself is structured in four stages: In the first stage, the import stage, the image data is loaded. The second stage serves for the planning of the intervention. After that, three different branches can be chosen in the calculation stage: the planning of the implant size, the planning of a patient-individual catheter shape or the evaluation of the suitability of the standard catheter. In the export stage, the model of the left atrial appendage anatomy or the bending form are exported in STL format. At any point during the process, the user can go back to a previous step to change the settings if necessary.

Figure 13 describes the major process steps of the program. The three functionalities 'Planning of the implant size', 'Calculation of a patient-individual catheter shape' and 'Evaluation of the suitability of the standard catheter' are realized by particular functions. However, there are also some shared functions that are required by more than one functionality and that are used to control the execution of the program.

5.7.1 Interactive Planning of Boundary Points

The planning of the procedure takes place after loading the appropriate image data into the program. The planning step includes the planning of the position and orientation of the implant and of additional structures in the heart that are relevant for the procedure. These are the pathway and the position of the inferior vena cava and the location of the fossa ovalis, where the transseptal puncture is going to be performed. However, if only the implant size is of importance for the user and the catheter pathway is not considered, these additional structures do not have to be planned. For the determination of the correct implant size and the generation of the anatomical model, the planning of only the implant position is sufficient. The planned structures serve as boundary points for the following calculations. The process description of the interactive planning is shown in Figure 14.

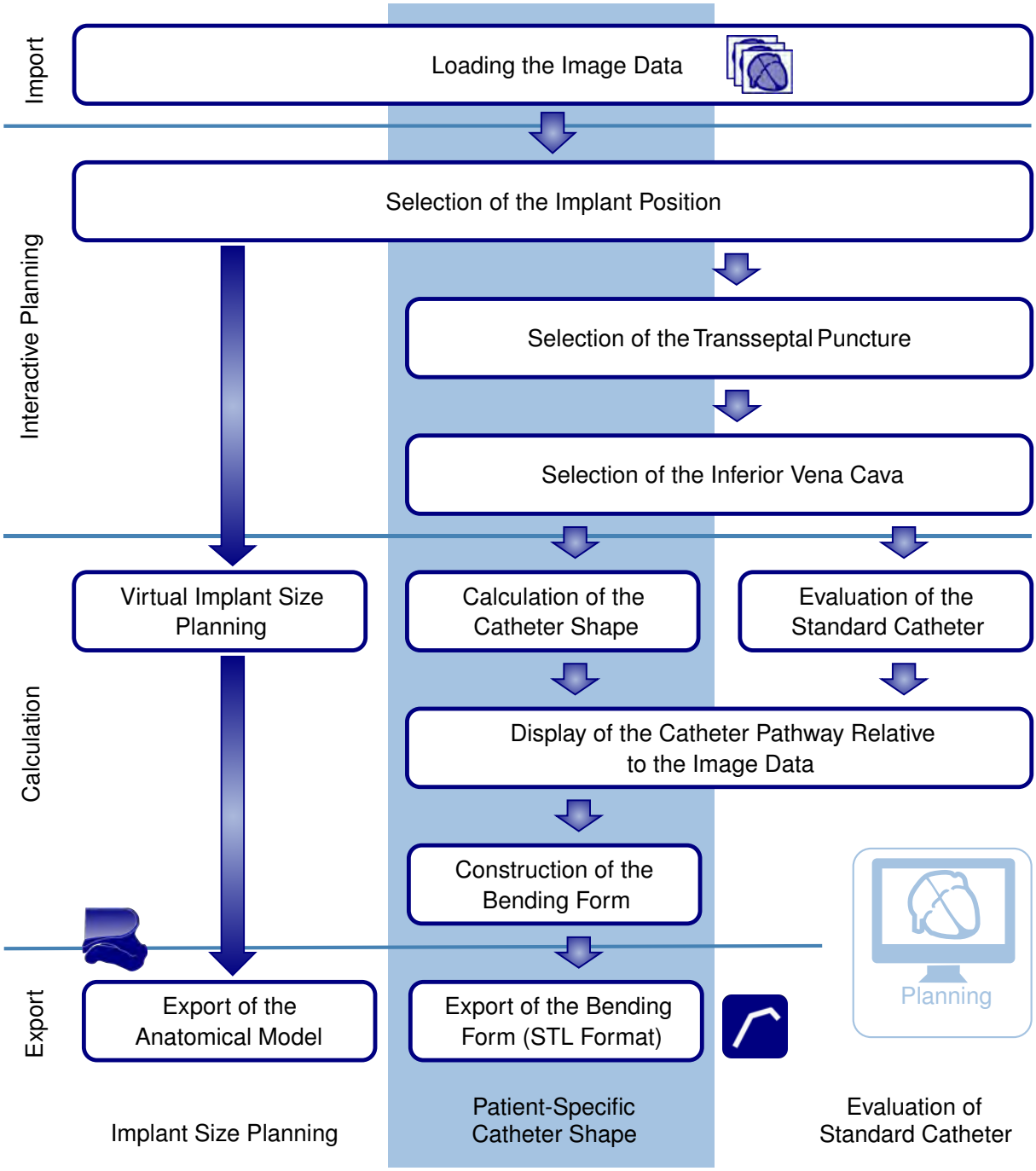

Figure 13 The process of the planning system is divided into four stages: the import stage, the interactive planning section, the calculation section and the export stage. To realize the three major functionalities 'Planning of the implant size', 'Calculation of a patient-specific catheter shape' and 'Evaluation of the suitability of the standard catheter' both shared and specific functions are used.

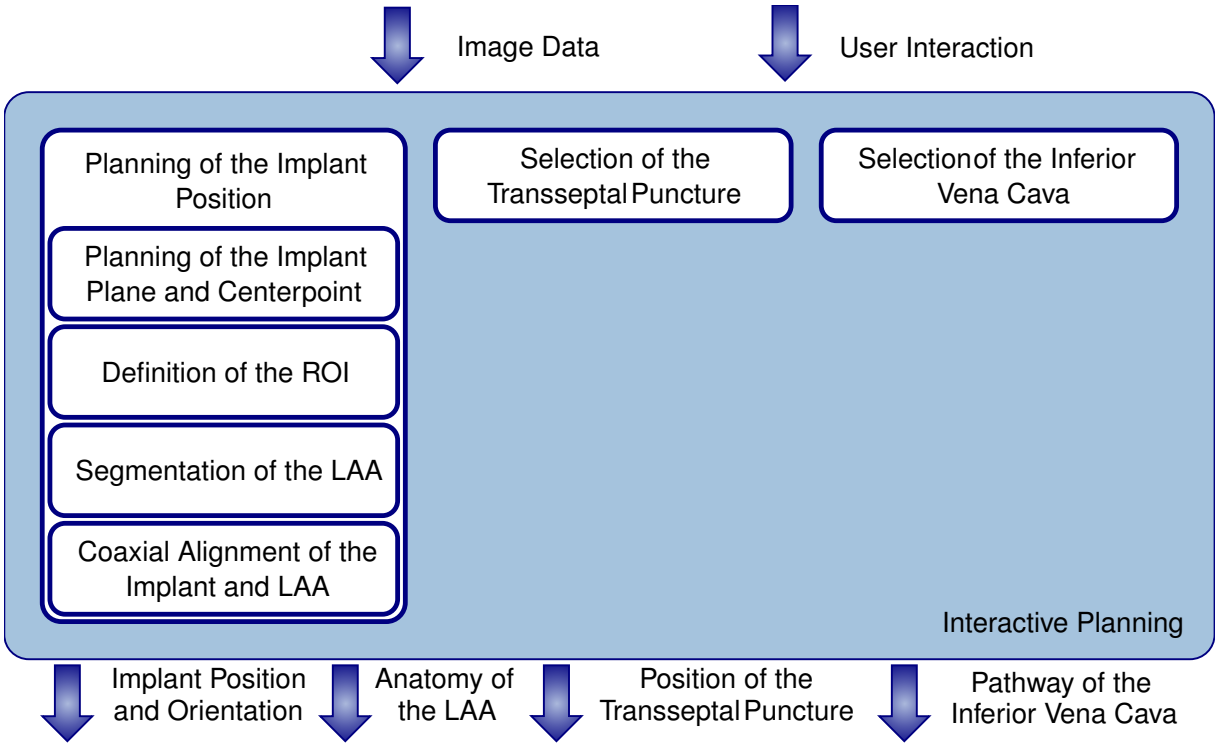

Figure 14 Process description of the interactive planning phase: the implant position, the location of the transseptal puncture and the pathway of the inferior vena cava are planned. Optionally, the LAA can be segmented in a region of interest around the implant position and the implant position can be aligned coaxially with the LAA.

The planning process works based on user interaction. The user marks different points in various two-dimensional image slices of the patient's heart in order to plan the implant position and to mark the anatomical features. No automatic detection of structures is used, as this requires a uniform image quality, which is not necessarily guaranteed. The planning of the three components can be performed in arbitrary order.

After planning the implant position and orientation, a region of interest (ROI) surrounding the implant position and containing the LAA is defined. In this ROI, the boundary layer of the left atrial appendage is segmented to obtain information about the anatomy of the left atrial appendage. These steps are necessary for the planning of the implant size. The position of the implant can be further adapted by performing an automatic coaxial alignment of the implant position and the anatomy of the left atrial appendage.

5.7.2 Planning of the Implant Size and Generation of an Anatomical Model

To support the physician in the choice of an optimal implant size, three different approaches are used as illustrated in Figure 15. The geometry of the implant is inserted virtually into the segmented anatomy of the left atrial appendage and displayed in two-dimensional and three-dimensional representations. Furthermore, a rough estimation of the compression that the implant experiences at the planned implant size is performed. Different implant sizes can be chosen and compared. Additionally, an anatomical model of the implant can be generated and additively manufactured. The model is based on the segmented anatomy of the left atrial appendage and exported as an STL file.

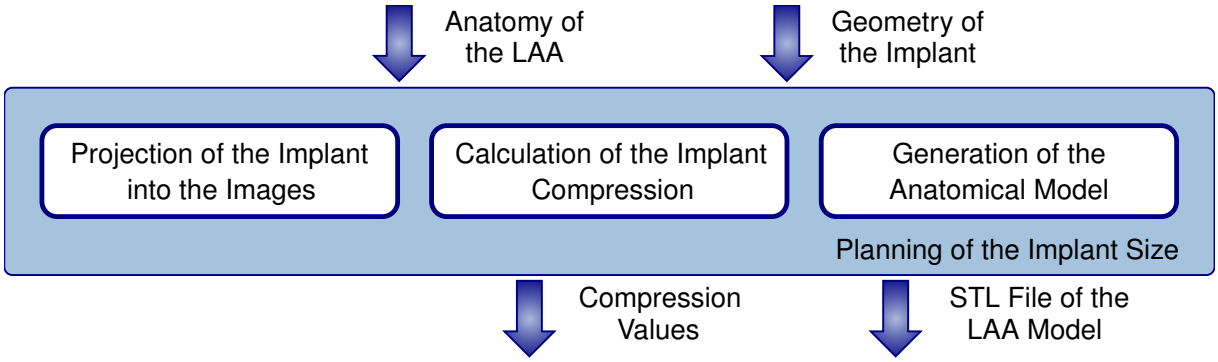

Figure 15 Three approaches are implemented to support the planning of the appropriate implant size: the geometry of the implant is projected into the anatomy of the LAA, the compression of the implant is estimated and an anatomical model of the LAA is generated, which can be additively manufactured. They work independent of each other and can be executed in arbitrary order.

5.7.3 Evaluation of the Standard Catheter

The planning program allows an evaluation of the suitability of the standard catheter for the given anatomy and the planned boundary points (see Figure 16). Therefore, the shape of the standard catheter is inserted virtually into the boundary points that were defined in the planning stage. The resulting catheter pathway is visualized and the distance of the catheter tip to the planned implant position and the angle between the planned implant axis and the direction vector of the tip segment of the inserted standard catheter are calculated. These values can support the user in the decision whether the procedure can be performed with the standard catheter or a patient-individual catheter should be calculated to facilitate the procedure.

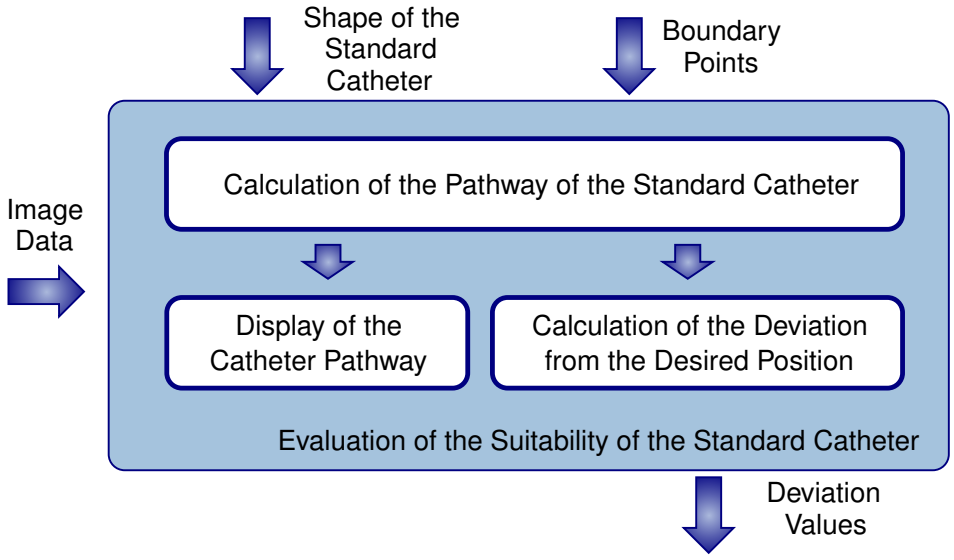

Figure 16 The shape of the standard catheter is inserted into the virtual boundary points. Subsequently, the pathway is displayed relative to the image data and the deviation of the calculated position of the tip to the planned implant position is determined.

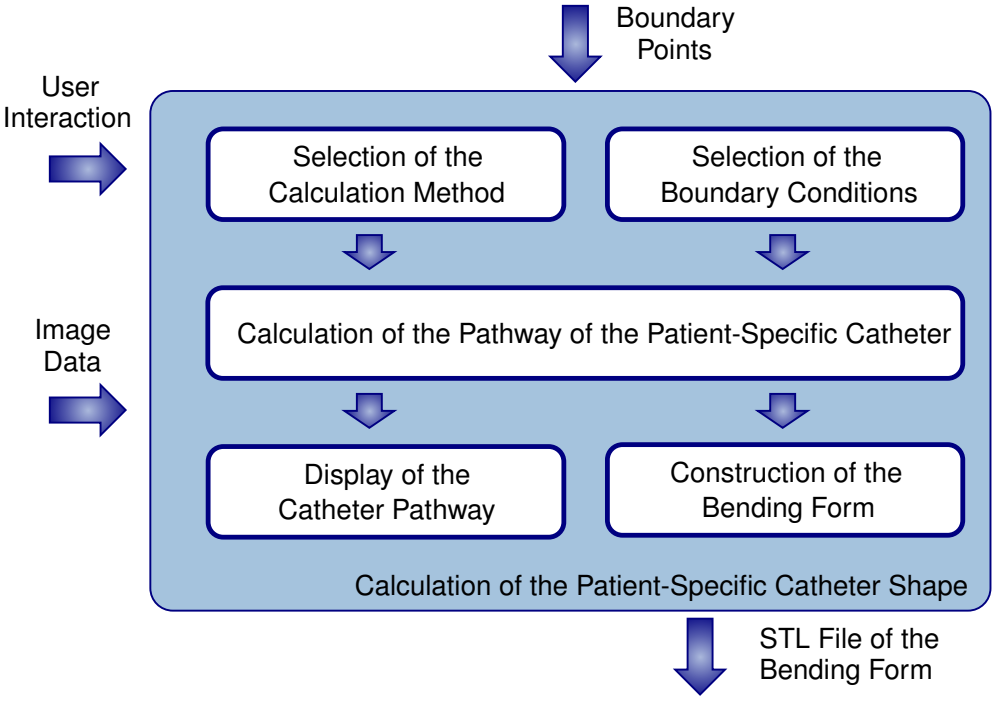

Figure 17 Different calculations methods are available for the calculation of the patient-specific catheter shape. The calculated catheter pathway is displayed relative to the image data and a bending form is generated.

5.7.4 Calculation of a Catheter Shape and Construction of the Bending Form

Based on the planning of the intervention, a patient-individual catheter shape can be calculated and displayed and a customized bending form is calculated (see Figure 17). Three different calculation methods are implemented in the planning program and available for the calculation of a patient-individual catheter shape. Either a double bended catheter, a catheter with four bends and maximized bending radii or a catheter with varying curvature can be calculated. The user can choose which calculation method he wants to use, compare the results and adjust the constraints and boundary conditions for the calculation of the catheter shape.

After the calculation of the catheter shape, it is described by the points on the catheter centerline and by a transformation matrix at every point. Furthermore, information about the beginning and end of the straight and curved segments is available. The following steps that are the display of the catheter and the calculation of the bending form work based on only this information. Therefore, the calculation method can be easily exchanged without changing the other functionalities of the planning program.

The calculation of the catheter shape works purely based on the geometric points defined in the planning and no segmentation is applied. In order to detect intersections with the heart walls or unwanted behavior, the catheter shape is displayed in relation to the image data and checked by the user. The constraints for the calculation have to be adjusted until the resulting shape is satisfactory.

A bending form that allows the shaping of the catheter into the calculated patient-specific shape is generated based on the calculation of the catheter shape. The bending form is calculated automatically without interaction of the user and it is adapted to the calculated catheter shape. The user controls the bending form and minor changes can be made to ensure its functionality.

6 Realization of the Interactive Planning Program

In this chapter, the functionalities and calculations of the planning program are described in detail. Additionally, the graphical user interface and its use are presented followed by heart models that serve for the evaluation of the program.

6.1 Fundamentals of the Interactive Program

The planning program was written in MATLAB R2014b. The SG-Library Toolbox in the version 2.7, developed at the Institute of Micro Technology and Medical Device Technology, Technical University of Munich by Prof. Lüth was used (Lüth, 2015). The planning program was summarized in a MATLAB library, which requires an installed MATLAB version 2014b or higher. For the development of the graphical user interface, the development environment for graphical user interfaces of MATLAB, GUIDE, was used. The following sections describe the realization of the previously described functionalities in an interactive planning program.

6.1.1 Overall Structure of the Program

The planning program is structured into eight different phases that describe the different steps of the program usage. These phases are

- Loading the image data
- Planning of the implant position
- Display of the LAA and the implant
- Planning of the puncture location
- Marking the pathway of the inferior vena cava
- Choosing the catheter calculation method and boundaries
- Display of the calculated catheter shape
- Display of the bending form

Each of these eight phases has a distinct user interface. Moreover, some comprehensive functions are implemented that control the use of the program or have some general functionality and that are used in several different phases. Examples are the display of orthogonal images and corresponding lines, functions to center the orthogonal images on one point and the function to write STL files. The particular functions of the eight phases can be classified into initialization functions, functions for the display in the graphical user interface, functions to process user interactions and calculation functions.

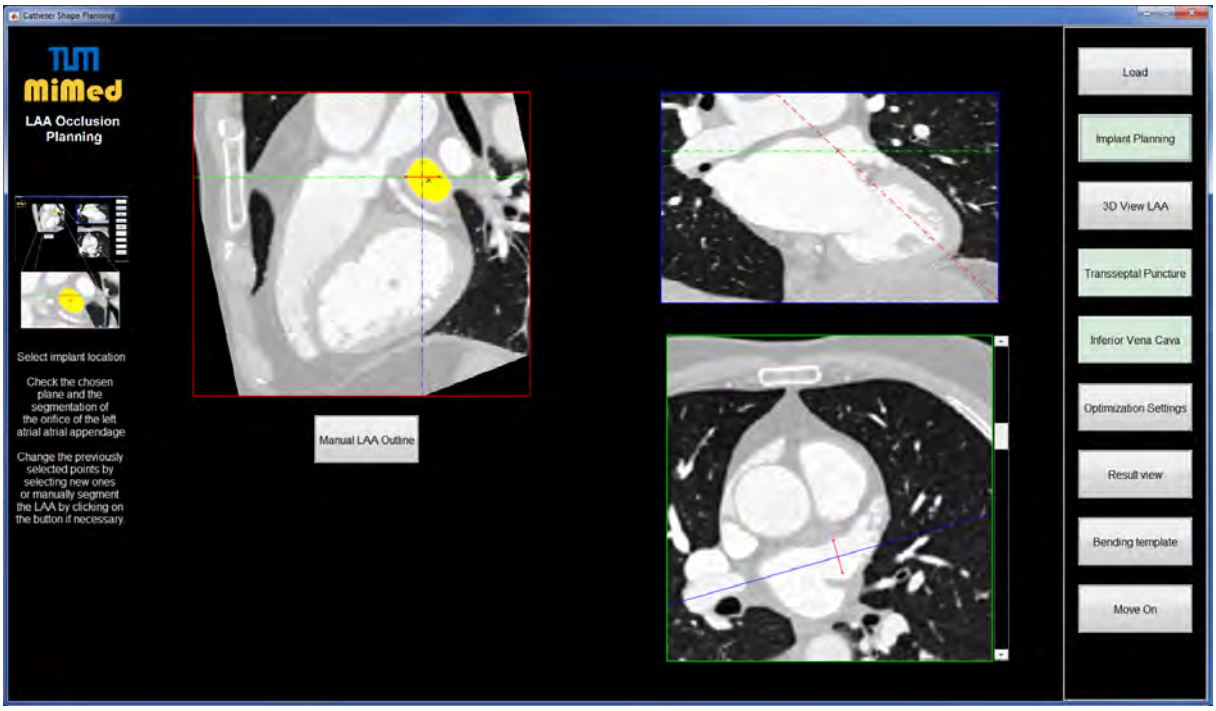

Figure 18 The graphical user interface of the program is divided into three parts. On the left side of the window, a help menu leads the user through the program. On the right side, there are buttons to change the active phase. Depending on the phase, different elements are displayed in the central part of the program window.

The graphical user interface of the planning program is structured in three parts as shown in Figure 18. The main frame showing the phase dependent display is situated in the center of the window. On the left side, a help menu that guides the user through the program with explaining texts and images is integrated. On the right, there is a menu with buttons that allow the user to change the phase and navigate through the program. The phases can be generally executed repeatedly and in arbitrary order. However, some phases depend on input information that is generated in other phases. Their selection is disabled as long as the information is not available. Particularly, if ultrasound images are loaded, only the planning of the implant position and the display of the LAA and implant are enabled, as the other phases require image data that contain the puncture location and the pathway of the inferior vena cava.

6.1.2 Principal Calculation Processes

The features of the program are based on the image data of the patient and different visualization approaches are used as for example the display of two-dimensional image slices or three-dimensional representations. The principal calculations that are necessary for the display of the image slices and the selection of points in these images, which are applied in different phases of the program, are presented in this chapter. At first, the basics of coordinate transformations using transformation matrices, the conversion of image slices to voxel data and the display of orthogonal image slices are described based on Lüth (2014) and Lüth (2017). Furthermore, the calculation of oblique images planes and the extrusion of cross-sectional shapes are presented.

Transformation of Coordinates. In order to display images from different perspectives and to describe virtual parts in three-dimensional space, transformations between different coordinate systems using homogenous transformation matrices are applied as described by Lüth (2014). Each coordinate systems is defined by its origin p_0 and three orthogonal unit vectors $\mathbf{x}$, $\mathbf{y}$ and $\mathbf{z}$. The following transformation matrix ${}^{2}\mathbf{T}_{1}$ converts coordinates from system 1 (index bottom right) to system 2 (index top left). It is a $4x4$ matrix that consists of a rotational and a translational part. The rotational part ${}^{2}\mathbf{R}_{1}$ is a $3x3$ matrix and the translational part ${}^{2}\mathbf{t}_{1}$ is a $3x1$ matrix. The fourth row of the matrix consists of three zeros and a one.

$$ {}^{2}\mathbf{T}_{1} = \begin{pmatrix} {}^{2}\mathbf{R}_{1} & {}^{2}\mathbf{t}_{1} \\ \mathbf{0} & 1 \end{pmatrix} \tag{6.1} $$

The rotational part is assembled by the three basis unit vectors of the coordinate system 1 that are described in the coordinate system 2.

$$ {}^{2}\mathbf{R}_{1} = \begin{pmatrix} {}^{2}\mathbf{x}_{1} & {}^{2}\mathbf{y}_{1} & {}^{2}\mathbf{z}_{1} \end{pmatrix} \tag{6.2} $$

Analogously, the translational part ${}^{2}\mathbf{t}_{1}$ describes the position of the origin of the coordinate system 1 in the coordinates of system 2.

$$ {}^{2}\mathbf{t}_{1} = {}^{2}\mathbf{p}_{0_1} \tag{6.3} $$

The transformation from coordinate system 1 to system 2 is applied to $3x1$ matrices such as points by adding an additional dimension with a value of one and multiplying the matrix with the transformation matrix ${}^{2}\mathbf{T}_{1}$. To convert a point from coordinate system 2 to system 1, a multiplication with the inverse matrix ${}^{2}\mathbf{T}_{1}^{-1}$ is performed.

$$ \begin{aligned} \begin{pmatrix} {}^{2}\mathbf{p} \\ 1 \end{pmatrix} &= {}^{2}\mathbf{T}_{1} \cdot \begin{pmatrix} {}^{1}\mathbf{p} \\ 1 \end{pmatrix} \\ \begin{pmatrix} {}^{1}\mathbf{p} \\ 1 \end{pmatrix} &= {}^{2}\mathbf{T}_{1}^{-1} \cdot \begin{pmatrix} {}^{2}\mathbf{p} \\ 1 \end{pmatrix} \end{aligned} \tag{6.4} $$

Three-Dimensional Voxel Data Sets. Three-dimensional CT images are recorded as a set of image slices with each image slice being a raster image. That means that for every point in the rectangular image grid, the so-called pixel, a gray scale intensity value is defined, which is stored in a two-dimensional matrix $\mathbf{I}(r, s)$. The pixels of the image are addressed by their position in the data structure that is identical to the indices r and s in the matrix (Lüth, 2017).

To enable further computing, the slices have to be converted to a three-dimensional voxel data set $\mathbf{V}$ as shown in Figure 19. Therefore, the two-dimensional matrices of the image slices are combined to a three-dimensional matrix. The elements of this matrix are called voxels and their positions are described by their indices u, v and w (Lüth, 2017). Some ultrasound devices also allow the direct export of three-dimensional data as voxel data sets in Cartesian coordinates.

Generally, the voxel sizes are anisotropic in both CT and ultrasound data, as the slice distance is not equal to the spacing of the pixels within the slice. The size of each voxel is described by the

parameters b_x, b_y and b_z. Especially for calculations with formulas containing angles, the voxel positions in the image data set have to be converted to an equally spaced Cartesian coordinate system at first. As the coordinate system describes a virtual model of the patient, it is denoted as mod in the following. The position of a voxel $\mathbf{v}$ that is initially described by its indices u, v and w in the voxel data set $\mathbf{V}$ is converted to coordinate in a millimeter unit by multiplying each component with the corresponding voxel size (Lüth, 2017). The resulting point ${}^{mod}\mathbf{p}$ is defined by the coordinates x, y and z. In Lüth (2017), the origin of the coordinate system lies in the center point of the voxel with the indices one. However, as in the planning program only relative distances and positions in the image data are of interest, the calculation is facilitated by placing the origin of the voxel coordinate system and the coordinate system mod at the same position, which is at the top, left backside of the patient. The position ${}^{mod}\mathbf{p}$ of a voxel $\mathbf{v} = [u\ v\ w]^T$ in the coordinate system mod can thus be calculated by

$$ {}^{mod}\mathbf{p} = \begin{pmatrix} x \\ y \\ z \end{pmatrix} = \begin{pmatrix} b_x \cdot u \\ b_y \cdot v \\ b_z \cdot w \end{pmatrix} . \tag{6.5} $$

The resulting voxel position ${}^{mod}\mathbf{p}$ in the coordinate system mod describes the distance of the voxel from the origin of the coordinate system in the three dimensions in millimeters. Unless otherwise designated, all calculations that are described in the following chapters are based on this coordinate system mod with unit vectors of equal lengths. The lengths of the unit vectors is set to 1 mm.

$$ |{}^{mod}\mathbf{x}_{mod}| = |{}^{mod}\mathbf{y}_{mod}| = |{}^{mod}\mathbf{z}_{mod}| = 1mm \tag{6.6} $$

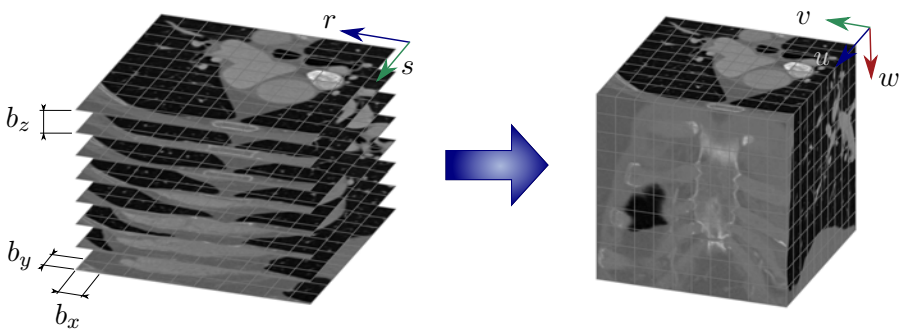

Figure 19 The image data slices that are read from the DICOM file are converted to a voxel data set. The different spacing of the voxels has to be taken into account, as the voxels are generally anisotropic.

Display of the Principal Image Planes. A commonly used approach for the visualization of three-dimensional image data, which is described in Lüth (2017) and which is applied in the planning program, is the display of images slices that are orientated normal to one of the principal axes of the coordinate system. All pixels of these image slices lie in a single layer of the voxel data set in one of the three principal orientations and they can be easily extracted by selecting all voxel with the corresponding coordinate u_p, v_p or z_p, which is defined by the orientation of the slice and the selected slice number. The two axes r and s of the image are oriented along the other two free dimensions with r being displayed horizontally and s vertically.

The resulting grid is the raster image and the resolution of the image is defined by the voxel size of the image data set. Depending on the orientation of the slice relative to the body, it is named axial ($\mathbf{I}_{w_p}$), coronal ($\mathbf{I}_{u_p}$) or sagittal ($\mathbf{I}_{u_p}$) plane as shown in Figure 20. These three planes intersect in one point whereas a pair of planes has an intersection line in common. If a point (r_p, s_p) is selected in one of the image planes that show the intensity matrices of the images, its position ${}^{mod}\mathbf{p}_{r_p,s_p}$ in the coordinate system mod can be calculated as follows:

- Coronal: $\mathbf{I}_{u_p}(r,s) = \mathbf{I}_{u_p}(v,w) = \mathbf{V}(u_p, v, w),\ {}^{mod}\mathbf{p}_{r_p,s_p} = \begin{pmatrix} b_x \cdot u_p \\ b_y \cdot r_p \\ b_z \cdot s_p \end{pmatrix}$
- Sagittal: $\mathbf{I}_{v_p}(r,s) = \mathbf{I}_{v_p}(u,w) = \mathbf{V}(u, v_p, w),\ {}^{mod}\mathbf{p}_{r_p,s_p} = \begin{pmatrix} b_x \cdot r_p \\ b_y \cdot v_p \\ b_z \cdot s_p \end{pmatrix}$
- Axial: $\mathbf{I}_{w_p}(r,s) = \mathbf{I}_{w_p}(v,u) = \mathbf{V}(u, v, w_p),\ {}^{mod}\mathbf{p}_{r_p,s_p} = \begin{pmatrix} b_x \cdot s_p \\ b_y \cdot r_p \\ b_z \cdot w_p \end{pmatrix}$

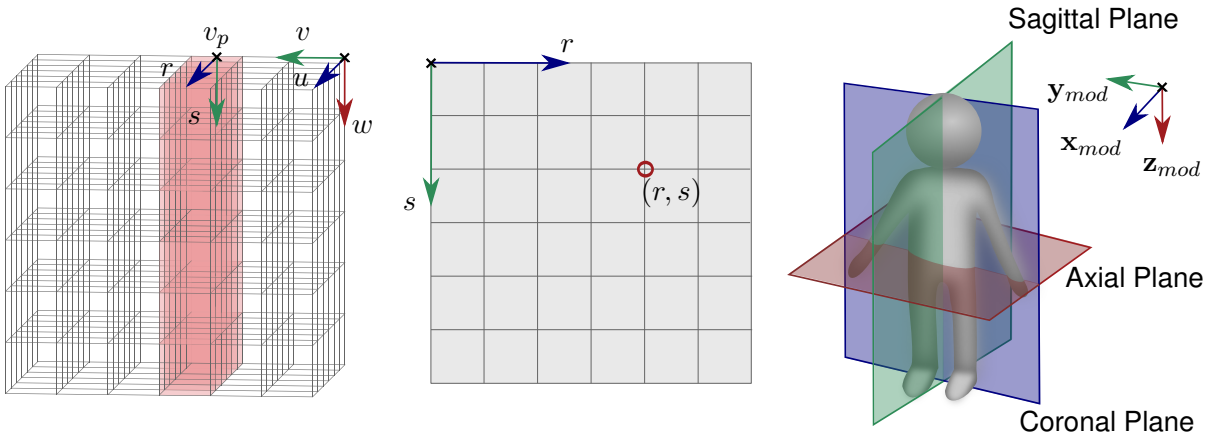

Figure 20 Image slices normal to one of the principal axes are realized by extracting one slice from the matrix of the voxel data (left). The displayed images are raster images with the coordinates r and s (middle). The planes are named axial, coronal and sagittal planes depending on their position relative to the body of the patient (right).

Oblique Planes. While images orthogonal to the principal axes use the raster grid of the voxel data set, a separate raster has to be defined for oblique planes and the positions of the grid points relative to the voxel data set have to be calculated. Therefore, a coordinate system for the image img is defined. The image slice that is displayed is a two-dimensional pixel grid with the two vectors r and s aligned with the two basis vectors $\mathbf{x}_{img}$ and $\mathbf{y}_{img}$ of the coordinate system img of the image plane (see Figure 21, right). The origin of the coordinate system defines the upper left edge of the image. In oblique planes in a cubic voxel data set, the intersection area of the plane with the data volume will generally not be a rectangular plane (see Figure 21, left, blue plane). The dimensions and borders of the image have to be chosen so that it shows all interesting structures. It may happen, that parts of the image plane lie outside the volume of the voxel data set. Starting from a point of interest, the four intersection points $\mathbf{p}_{q,x_1}$, $\mathbf{p}_{q,x_2}$, $\mathbf{p}_{q,y_1}$ and $\mathbf{p}_{q,y_2}$ of the two vectors $\mathbf{x}_{img}$ and $\mathbf{y}_{img}$ with the borders of the voxel data set are calculated. Those four points define the outline of the rectangular image grid (red plane in Figure 21).

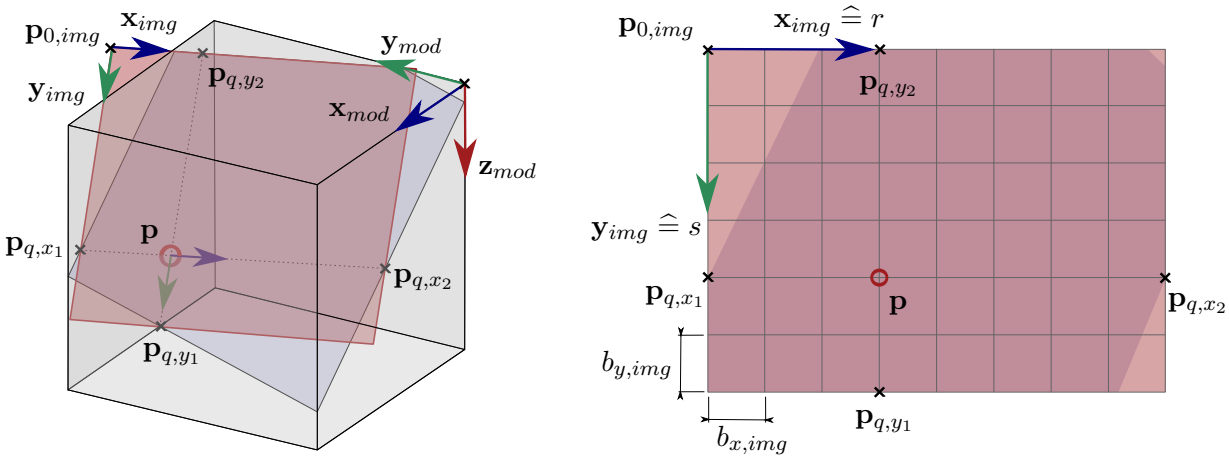

Figure 21 The position of an image slice that is oriented obliquely in the voxel data set is defined by a coordinate system img with the origin $\mathbf{p}_{0,img}$ and the vectors $\mathbf{x}_{img}$ and $\mathbf{y}_{img}$ (left). As the intersection area is usually not rectangular, an appropriate image size and origin has to be chosen. The direction vectors of the coordinate system build the borderlines of the image grid with the origin of the coordinate system in the upper left corner (right).

The resolution of the grid in the two directions can be chosen freely. However, it is reasonable that it is in the same order of magnitude as the resolution of the image data. The pixel sizes are defined as $b_{x,img}$ and $b_{y,img}$. The position in the coordinate system mod of a point with indices r, s in the image grid can be determined using the transformation matrix ${}^{mod}\mathbf{T}_{img}$.

$$
\begin{aligned}
{}^{mod}\mathbf{T}_{img} &= \begin{pmatrix} {}^{mod}\mathbf{x}_{img} & {}^{mod}\mathbf{y}_{img} & ({}^{mod}\mathbf{x}_{img} \times {}^{mod}\mathbf{y}_{img}) & {}^{mod}\mathbf{p}_{0,img} \\ 0 & 0 & 0 & 1 \end{pmatrix} \\
\begin{pmatrix} {}^{mod}\mathbf{p} \\ 1 \end{pmatrix} &= {}^{mod}\mathbf{T}_{img} \cdot \begin{pmatrix} b_{x,img} \cdot r \\ b_{y,img} \cdot s \\ 0 \\ 1 \end{pmatrix} = {}^{mod}\mathbf{T}_{img} \cdot \begin{pmatrix} {}^{img}\mathbf{p} \\ 1 \end{pmatrix}
\end{aligned}
\tag{6.7}
$$

In this way, the position of every pixel in the coordinate system mod is calculated. In order to define the gray value at every pixel, the three-dimensional position $\mathbf{v}$ in the voxel data set has to be determined what is done by division of every component through the corresponding voxel size.

$$
\mathbf{v} = \begin{pmatrix} u \\ v \\ w \end{pmatrix} = \begin{pmatrix} x/b_x \\ y/b_y \\ z/b_z \end{pmatrix} = {}^{mod}\mathbf{p} \tag{6.8}
$$

The resulting value is usually not an integer. To find the corresponding voxel for the determination of the gray value, a nearest neighbor interpolation is used that finds the voxel with least distance to the calculated position.

The calculation can also be used for the definition of a three-dimensional region of interest (ROI) with an oblique position compared to the original voxel data set. In order to do so, an appropriate value for the thickness $b_{z,img}$ has to be chosen additionally and instead of a two-dimensional pixel grid, a three-dimensional voxel grid has to be defined.

Extrusion of Cross-Sectional Shapes. The definition of coordinate systems and matrix transformations is also used for the extrusion of cross-sectional shapes along a curve. To do so, several points $\mathbf{p}_{c_k}$ on a central line are defined and at every point, a transformation matrix ${}^{mod}\mathbf{T}_{c_k}$ into the coordinate system c_k is built with the $\mathbf{z}_{c_k}$-vectors pointing along the central line. The two-dimensional cross-sectional shape is defined by the points ${}^{c_k}\mathbf{p}_j$ in the $\mathbf{x}_{c_k}\mathbf{y}_{c_k}$-plane that lies normal to the $\mathbf{z}_{c_k}$-vector. This cross-sectional shape is identical in the coordinate systems of every point. The three-dimensional shape is realized by transformation of the cross-sections from the coordinate systems c_k of each centerline point into the system mod as shown in Figure 22.

$$
\begin{aligned}
{}^{mod}\mathbf{T}_{c_k} &= \begin{pmatrix} {}^{mod}\mathbf{x}_{c_k} & {}^{mod}\mathbf{y}_{c_k} & {}^{mod}\mathbf{z}_{c_k} & {}^{mod}\mathbf{p}_{c_k} \\ 0 & 0 & 0 & 1 \end{pmatrix} \\
\begin{pmatrix} {}^{mod}\mathbf{p}_j \\ 1 \end{pmatrix} &= {}^{mod}\mathbf{T}_{c_k} \cdot \begin{pmatrix} {}^{c_k}\mathbf{p}_j \\ 1 \end{pmatrix}.
\end{aligned}
\tag{6.9}
$$

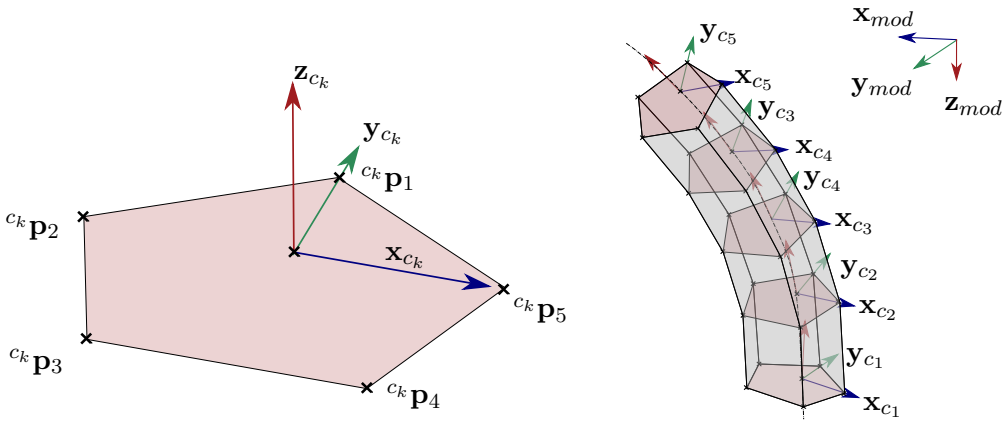

Figure 22 The extrusion of cross-sectional shapes is realized by defining several transformation matrices along a central line with the $\mathbf{z}_{c_k}$-vectors pointing along this curve. The cross-sections are defined in the $\mathbf{x}_{c_k}\mathbf{y}_{c_k}$-planes of the coordinate systems of the points and they are identical for every point. By transformation of the points of the cross-sections into the coordinate system mod, the three-dimensional shape is realized.

6.2 Loading the Image Data

The program works based on preoperative three-dimensional image data that are available as DICOM files, which contain information about the type of image data. Three-dimensional CT images as well as three-dimensional ultrasound images can be processed with the planning program. The image data are selected by choosing the appropriate folder that contains the image data slices.

Interactive Control of the Orientation of the Image Data. Especially for the CT data, which allow the planning of the catheter shape, the correct orientation of the image is of importance, as positional relation information is used for the catheter calculation. Therefore, the correct orientation of the image data has to be ensured by the user before the calculation can be started. A sagittal and a coronal image slice is displayed relative to labels that describe the desired orientation of the images (see Figure 23). If necessary, the image data can be flipped along one of the axes by clicking on the corresponding button.

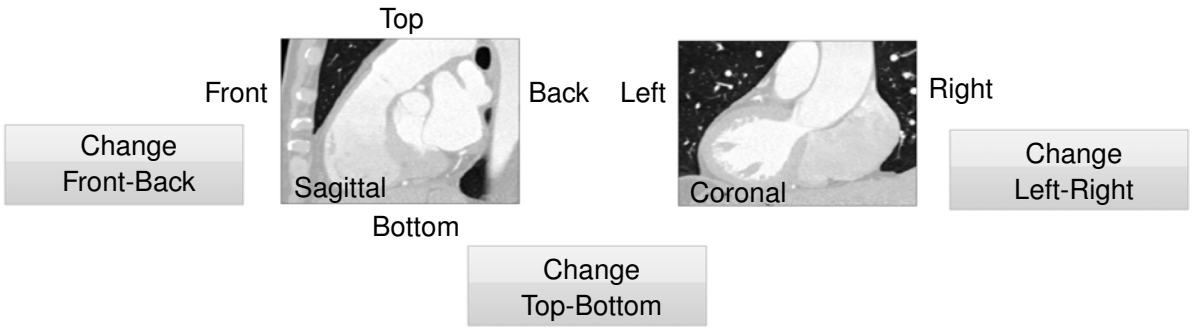

Figure 23 After loading the image data, image slices are displayed with hints how they should be oriented. The user checks the orientation and flips the image data if necessary by clicking on the respective button.

6.3 Planning of the Implant Position

The planning of the implant position defines the target position of the catheter tip inside the heart. Furthermore, it describes the position of the LAA orifice in the image data. After interactive planning of the implant position, the anatomy of the LAA can be segmented and the implant axis can be aligned coaxially to the axis of the LAA in the landing zone.

6.3.1 Interactive Planning of the Implant Plane and Position

The Amplatzer implants as well as the WATCHMAN devices are rotational symmetric and therefore their position can be described by the location of one point on the implant axis $\mathbf{p}_i$ and the direction vector of the implant axis $\mathbf{v}_i$. For the Amplatzer implants, the point where the lobe of the implant transitions into the neck is defined as the implant position as shown in Figure 24. For correct placement of the implant, its axis should be aligned coaxially to the left atrial appendage at the landing zone. Thus, if placed correctly, its direction vector is a normal vector on a cross-sectional plane of the left atrial appendage and it is defined to point into the LAA. As the implant is self-centering, its axis is situated in the center of the left atrial appendage in the landing zone. The plane that contains the implant center and lies normal to the implant axis is called the implant plane hereafter.

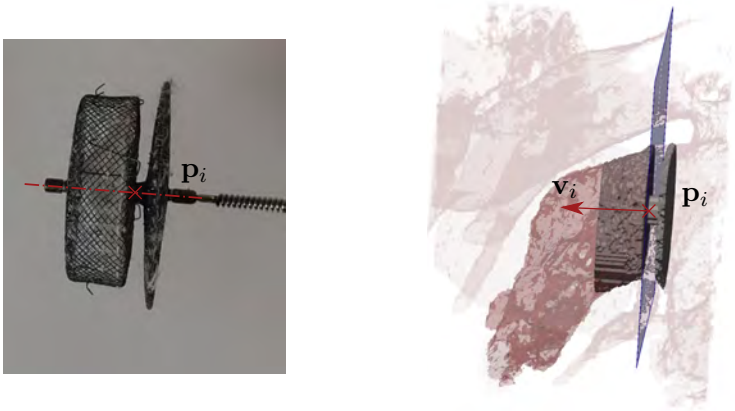

Figure 24 The position and orientation of the rotational symmetric implant can be defined by one point $\mathbf{p}_i$ on its rotational axis and the direction vector $\mathbf{v}_i$ of the axis. The point on the implant axis that lies on the top of the lobe at the transition to the implant neck is defined as the position of the implant. The implant vector points along the implant axis into the LAA.

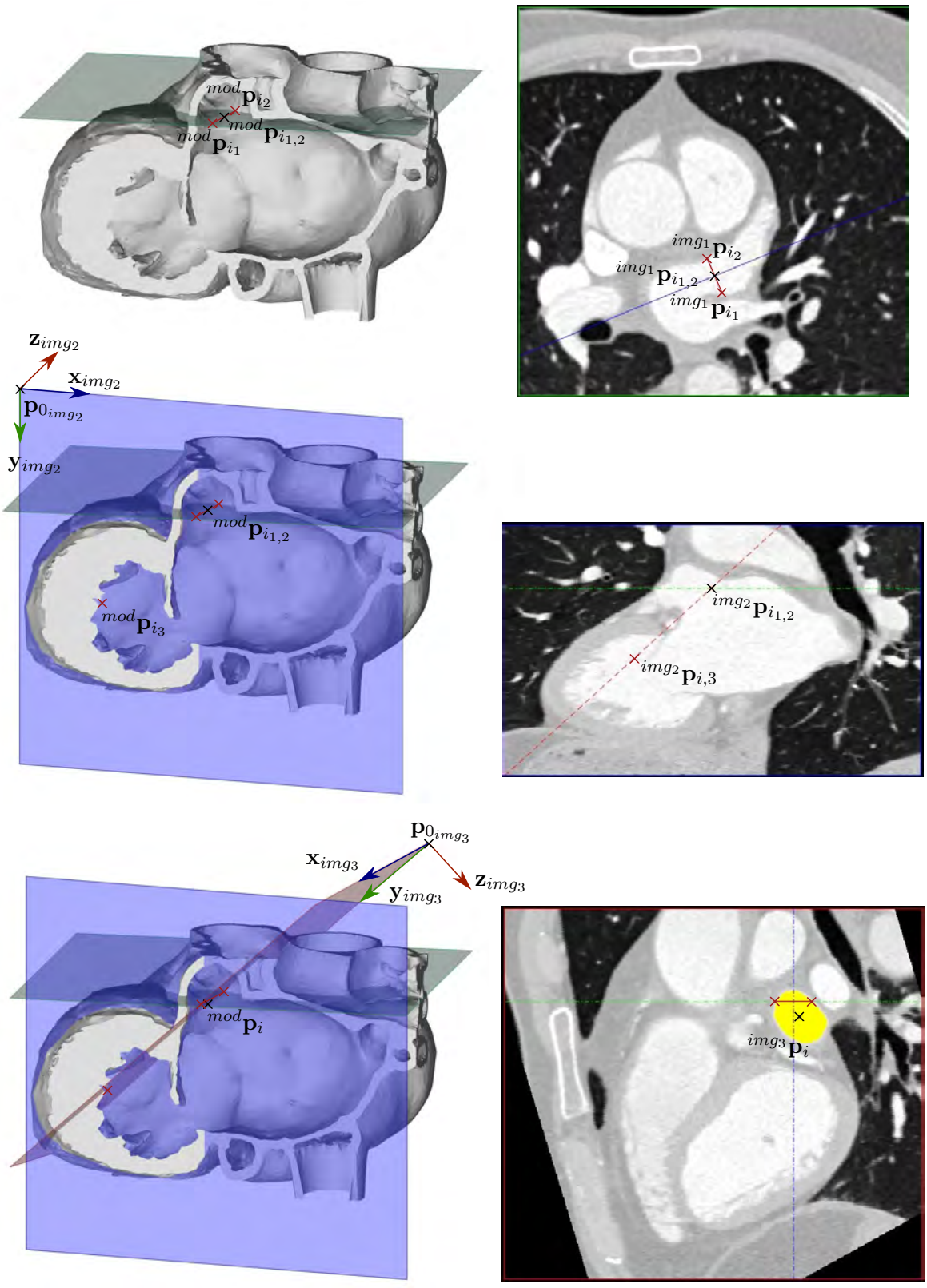

Figure 25 The implant plane that lies perpendicular to the implant axis is defined by three points. The first two points $^{img_1}\mathbf{p}_{i_1}$ and $^{img_1}\mathbf{p}_{i_2}$ mark a cross-section of the LAA in an axial plane. The third point $^{img_2}\mathbf{p}_{i,3}$ describes the inclination of the implant in an image plane that lies perpendicular to the connecting line of the first two points. The plane that contains these three points is defined as the implant plane.

In the planning program, the position and orientation of the implant plane is described by three points as shown in Figure 25. The first two points $\mathbf{p}_{i_1}$ and $\mathbf{p}_{i_2}$ mark a cross-section of the left atrial appendage at the planned implant position in an axial plane. The point that is lying in the middle of the connecting line of these two points is defined as $\mathbf{p}_{i_{1,2}}$.

$$^{mod}\mathbf{p}_{i_{1,2}} = \frac{^{mod}\mathbf{p}_{i_1} + ^{mod}\mathbf{p}_{i_2}}{2} \tag{6.10}$$

To define the third point, the vertical plane in the image volume that is orientated normal to the connecting line of these first two points and that comprises $\mathbf{p}_{i_{1,2}}$ is determined. The plane is displayed in blue in Figure 25. The coordinate system img_2 of the plane is defined by the selected first two points $\mathbf{p}_{i_1}$ and $\mathbf{p}_{i_2}$. As the plane is oriented normal to the connecting line of the first two points, the vector $\mathbf{z}_{img_2}$ is aligned with the vector between these two points. To ensure the vertical orientation of the plane, the vector $\mathbf{y}_{img_2}$ points in the direction of the $\mathbf{z}_{mod}$-vector and $\mathbf{x}_{img_2}$ lies normal to the other two basis vectors.

$$\begin{aligned}
^{mod}\mathbf{z}_{img_2} &= \frac{^{mod}\mathbf{p}_{i_1} - ^{mod}\mathbf{p}_{i_2}}{|^{mod}\mathbf{p}_{i_1} - ^{mod}\mathbf{p}_{i_2}|} \\
^{mod}\mathbf{y}_{img_2} &= ^{mod}\mathbf{z}_{mod} = \begin{pmatrix} 0 & 0 & 1 \end{pmatrix}^T \\
^{mod}\mathbf{x}_{img_2} &= ^{mod}\mathbf{y}_{img_2} \times ^{mod}\mathbf{z}_{img_2}.
\end{aligned} \tag{6.11}$$

Starting form the point $\mathbf{p}_{i_{1,2}}$, which is defined to lie in the image plane, the origin $\mathbf{p}_{0_{img_2}}$ of the coordinate system is determined as the intersection point with the borders of the voxel data set and the transformation matrix is defined to

$$^{mod}\mathbf{T}_{img_2} = \begin{pmatrix} ^{mod}\mathbf{x}_{img_2} & ^{mod}\mathbf{y}_{img_2} & ^{mod}\mathbf{z}_{img_2} & ^{mod}\mathbf{p}_{0_{img_2}} \\ 0 & 0 & 0 & 1 \end{pmatrix}. \tag{6.12}$$

The center point of the connecting line is visible in the new image at the position $^{img_2}\mathbf{p}_{i_{1,2}}$ that is calculated by the transformation

$$\begin{pmatrix} ^{img_2}\mathbf{p}_{i_{1,2}} \\ 1 \end{pmatrix} = ^{mod}\mathbf{T}_{img_2}{}^{-1} \begin{pmatrix} ^{mod}\mathbf{p}_{i_{1,2}} \\ 1 \end{pmatrix}. \tag{6.13}$$

This vertical plane shows a longitudinal view of the left atrial appendage. The inclination of the implant is defined in this view by a third point $^{img_2}\mathbf{p}_{i,3}$ and its connecting line to $^{img_2}\mathbf{p}_{i_{1,2}}$. The position of $\mathbf{p}_{i,3}$ is transferred into the basis coordinate system by

$$\begin{pmatrix} ^{mod}\mathbf{p}_{i_3} \\ 1 \end{pmatrix} = ^{mod}\mathbf{T}_{img_2} \begin{pmatrix} ^{img_2}\mathbf{p}_{i,3} \\ 1 \end{pmatrix}. \tag{6.14}$$

Based on these three points, the implant plane (red plane in Figure 25) is calculated. The position of the plane in the image volume is generally oblique. Another transformation matrix $^{mod}\mathbf{T}_{img_3}$ is defined to calculate the position of the grid points of the plane in the coordinate system mod. The transformation matrix is based on the three marked points and the intersection point $\mathbf{p}_{0_{img_3}}$ of the plane and the borders of the image data set. The $\mathbf{x}_{img_3}$-vector is identical to the $\mathbf{z}_{img_2}$-vector of the

vertical plane and the vector $\mathbf{y}_{img_3}$ is aligned with the connecting line between the central point on their connecting line $\mathbf{p}_{i_{1,2}}$ and the third point $\mathbf{p}_{i,3}$. An appropriate origin $\mathbf{p}_{0_{img_3}}$ is defined starting from the point $\mathbf{p}_{i_{1,2}}$.

$$
\begin{aligned}
{}^{mod}\mathbf{x}_{img_3} &= \frac{{}^{mod}\mathbf{p}_{i_1} - {}^{mod}\mathbf{p}_{i_2}}{|\,{}^{mod}\mathbf{p}_{i_1} - {}^{mod}\mathbf{p}_{i_2}|} = {}^{mod}\mathbf{z}_{img_2} \\
{}^{mod}\mathbf{y}_{img_3} &= \frac{{}^{mod}\mathbf{p}_{i_{1,2}} - {}^{mod}\mathbf{p}_{i_3}}{|\,{}^{mod}\mathbf{p}_{i_{1,2}} - {}^{mod}\mathbf{p}_{i_3}|} \\
{}^{mod}\mathbf{z}_{img_3} &= {}^{mod}\mathbf{x}_{img_3} \times {}^{mod}\mathbf{y}_{img_3} \\
{}^{mod}\mathbf{T}_{img_3} &= \begin{pmatrix} {}^{mod}\mathbf{x}_{img_3} & {}^{mod}\mathbf{y}_{img_3} & {}^{mod}\mathbf{z}_{img_3} & {}^{mod}\mathbf{p}_{0_{img_3}} \\ 0 & 0 & 0 & 1 \end{pmatrix}.
\end{aligned}
\tag{6.15}
$$

The implant plane shows a cross-sectional plane of the implant and the orifice of the left atrial appendage in this plane is specified. Either the user marks an outline of the left atrial appendage or all pixels that lie inside the orifice are determined by gray value based segmentation as described in section 6.3.3. Independent of the chosen method, the center point of the implant is defined as the centroid $\mathbf{p}_i$ of the selected n_{laa} points $\mathbf{p}_{laa}$. Those points are either the list of points on the outline of the orifice that were marked by the user or the center points of the segmented pixels of the LAA (see Figure 26). The position of the centroid in the implant plane is the mean value of these n_{laa} points ${}^{img_3}\mathbf{p}_{laa}$ and can be calculated by

$$
{}^{img_3}\mathbf{p}_i = \frac{1}{n_{laa}} \sum_{m=1}^{n_{laa}} {}^{img_3}\mathbf{p}_{laa}. \tag{6.16}
$$

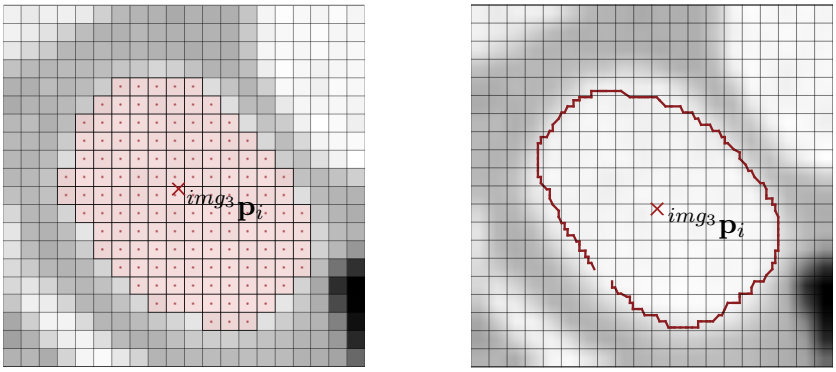

Figure 26 The implant position is calculated as the central point of the orifice of the left atrial appendage in the implant plane. This point is defined as the centroid of the position of all pixels that are part of the segmented left atrial appendage in the implant plane (left) or as the centroid of the points on the outline of the orifice (right).

This point ${}^{img_3}\mathbf{p}_i$ is defined as the center point of the implant in the coordinate system img_3 of the implant plane and its position can be transformed into the basis coordinate system to get the implant

position ${}^{mod}\mathbf{p}_i$.

$$\begin{pmatrix} {}^{mod}\mathbf{p}_i \\ 1 \end{pmatrix} = {}^{mod}\mathbf{T}_{img_3} \begin{pmatrix} {}^{img_3}\mathbf{p}_i \\ 1 \end{pmatrix}. \tag{6.17}$$

The vector $\mathbf{v}_i$ along the axis of the implant pointing into the LAA is defined as the normal vector $\mathbf{z}_{img_3}$ on the implant plane.

Realization of the Planning in the Interactive Program. For the planning of the implant position, three images need to be displayed in the graphical user interface: the axial image, the image orthogonal to the connecting line of the first two points and the implant plane. The images that are displayed in the graphical user interface are shown in Figure 25 on the right. In the beginning, only the axial image is visible. A suitable slice to mark the cross-section of the LAA is selected with the slider next to the image or by scrolling the mouse wheel. The two points $\mathbf{p}_{i_1}$ and $\mathbf{p}_{i_2}$ are marked in the image by clicks. If the slice number was changed during the selection of the two points and thus they do not lie in the same slice, the first point is erased. The intersection line between the selected points is displayed and the position of the points can be adjusted by selecting further points. In this case, the additional point replaces the closest one of the old points. The position of the connecting line in the image can be shifted by clicking on the line and moving the mouse. Both of the end points are shifted equally so that the orientation of the line is kept constant. Additionally, the line orthogonal to the connecting line through its central point $\mathbf{p}_{i_{1,2}}$ is displayed. This line represents the position of the second image.

When the two points are selected, the orthogonal image is displayed and the central point $\mathbf{p}_{i_{1,2}}$ of the connecting line between the points $\mathbf{p}_{i_1}$ and $\mathbf{p}_{i_2}$ is displayed in this image as a fixed point. The position of the axial slice that is currently displayed is marked in the orthogonal image for better orientation. The inclination is determined by selecting one point $\mathbf{p}_{i,3}$. The position of this point can be adjusted by selecting a new point that overwrites the old one. The connecting line between the fix point $\mathbf{p}_{i_{1,2}}$ and the selected point $\mathbf{p}_{i,3}$ is marked. The position of the line can be adapted by clicking on it and moving it. When doing so, also the position of the first two axial points is altered based on the new position of the point $\mathbf{p}_{i,3}$.

In a third image, the selected implant plane is displayed. Due to the oblique position of the image plane, parts of the rectangular image may lie outside the region of the image data set. These pixels are displayed in black. The positions of the previously selected first two points $\mathbf{p}_{i_1}$ and $\mathbf{p}_{i_2}$ in the image are displayed. By default, automatic segmentation of the left atrial appendage is performed and the resulting segmented area and its central point are marked.

The user may choose to mark the outline of the left atrial appendage manually instead of the automatic segmentation. A button is available to select manual segmentation. If the automatic segmentation fails, manual marking of the outline is automatically chosen.

6.3.2 Definition of a Region of Interest at the Implant Position

A region of interest (ROI) around the implant position that contains the LAA entirely is defined. The ROI is specified as a cubic region that is aligned with the implant plane and a voxel data set in the ROI is defined so that the image slices in the ROI are showing cross-sections of the LAA.

A transformation matrix ${}^{mod}\mathbf{T}_{roi}$ for the conversion into the coordinate system roi of the ROI is defined by its basis vectors. The vector $\mathbf{z}_{roi}$ is aligned with the implant axis $\mathbf{v}_i$. Thereby, the alignment with the implant plane is ensured and the vectors $\mathbf{x}_{roi}$ and $\mathbf{y}_{roi}$ can be defined freely. The convention is that the vector $\mathbf{x}_{roi}$ is defined to not have any component in $\mathbf{z}_{mod}$-direction as shown in Figure 27. A resolution b_{roi} for the image, which is identical in all three dimensions in space, is defined. The resolution is set to the mean value of the resolutions b_x and b_y of the original voxel data set in the axial plane.

$$b_{roi} = b_{x,roi} = b_{y,roi} = b_{z,roi} = \frac{b_x + b_y}{2} \tag{6.18}$$

The size of the ROI is defined to 40 mm in every dimension and an appropriate origin for the coordinate system is chosen.

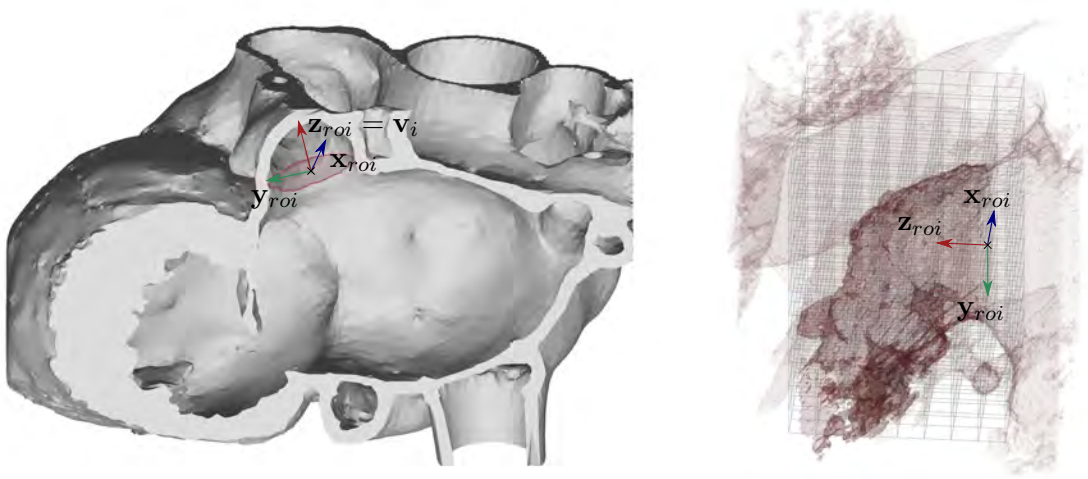

Figure 27 A coordinate system roi with the vector $\mathbf{z}_{roi}$ normal to the implant plane defines a the region of interest around the left atrial appendage (left). The voxel values in the region of interest are calculated by nearest neighbor interpolation (right).

6.3.3 Segmentation of the Left Atrial Appendage

The implant position can be planned in both three-dimensional ultrasound data and CT data. The previously described steps for the planning of the implant position work based on user-selected points and are identical for ultrasound and CT data. However, for the automatic detection of the orifice in the implant plane or the three-dimensional display of the left atrial appendage, segmentation of the image data has to be performed. A threshold-based segmentation of the gray scale values is applied either to a three-dimensional ROI or to a two-dimensional plane in the image data. Therefore, the program calculates an initial threshold, which can be adapted interactively by the user. The segmentation step distinguishes between the data types in the determination of the initial threshold and in the choice of the selected segment. The initial threshold value is a gray level intensity between the value of the orifice and the surrounding tissue.

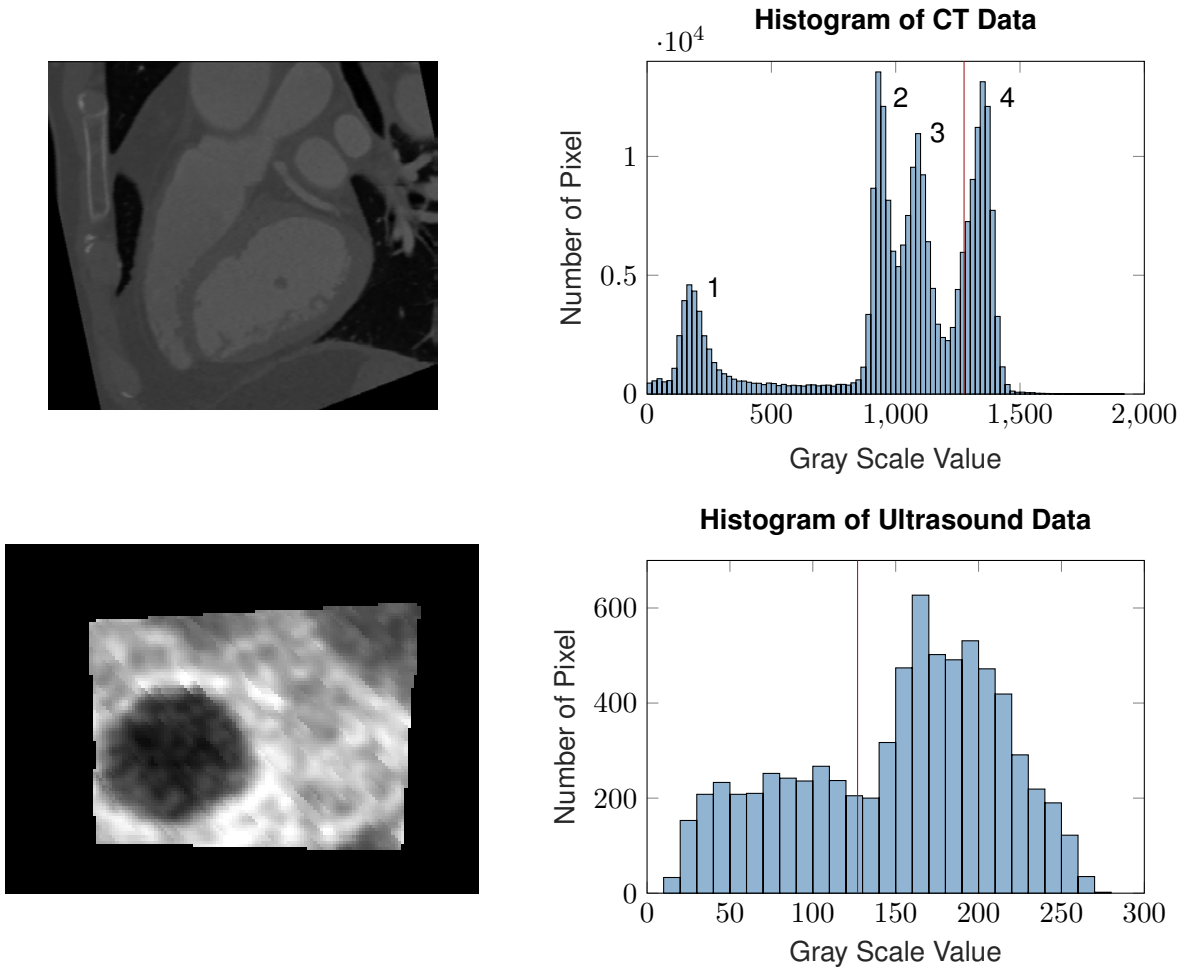

Figure 28 The histogram of CT images (top) usually shows two to four peaks: these are the air filled regions in the heart (1), the fat (2) and muscle (3) tissue of the heart and the blood filled cavities of the heart (4), which are visualized using contrast agent. In contrast, in the ultrasound images only the tissue of the heart is visible (bottom). The red lines mark the initial threshold values for the segmentation.

In the CT data set, a histogram of the gray scale values of an image in the area surrounding the left atrial appendage usually shows two to four peaks (see Figure 28). The peak with the highest intensity (= white) represents the voxels of the orifices of the heart, as contrast agent is used for the recording of the CT images. The central peaks represent the different types of tissue of the heart walls and the peak with least intensity represents the air-filled lungs surrounding the heart. If only two peaks are visible, these are the orifices and the tissue of the heart and no air is visible in the ROI. In some data sets, the peaks of the cardiac tissue consisting of muscle tissue and fat tissue cannot be clearly distinguished. The segmentation threshold is set to the mean value between the peak representing the orifices and the minimum value between the two peaks representing orifices and muscle tissue. The threshold can be controlled, as CT values are normalized gray values ranging between -1024 HU and 3071 HU. Therefore, the threshold has to lie between the Hounsfield values of 0 HU and 300 HU, the values for water and contrast agent (Budoff, 2016, p. 4).

Before determining the initial threshold for the ultrasound images, a mean filter is applied to the images. The gray level intensity of the orifice is approximated based on the points surrounding its

center point, which is user selected. The mean value between the maximum occurring value in the image and this calculated value of the orifice is used as an initial threshold for the ultrasound images.

Threshold-based segmentation is applied to the image data (see Figure 29). In the CT data set, the voxels with higher gray value than the threshold are selected, in the ultrasound images, the values below the threshold are selected as part of the LAA. Connected components are identified and all segmented voxels that are not connected to the main component that contains the position of the implant are erased. The connectivity can be checked either in two or three dimensions meaning that only the orifice or the entire connected region of the left side of the heart is selected.

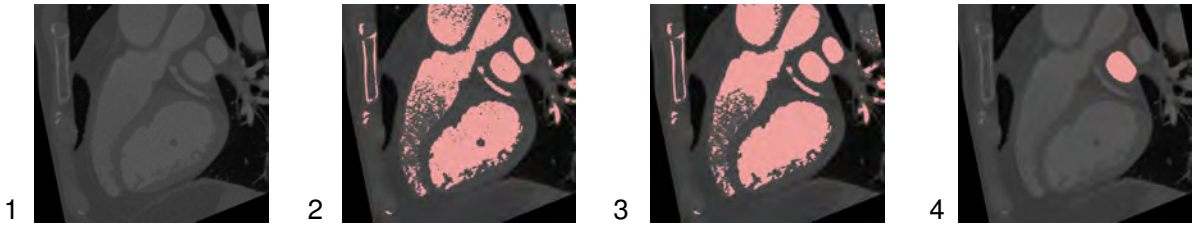

Figure 29 The segmentation of the LAA in two and in three dimensions is achieved in three steps: in a first step, all voxels with gray values above the threshold value are defined in CT data (2). Then the holes in the segmented regions are closed (3) and only the segmented regions that are connected to the area around the implant position are chosen (4).

6.3.4 Coaxial Alignment of Implant and Left Atrial Appendage

The information about the anatomy of the left atrial appendage in the ROI around the planned implant position, which is obtained by the segmentation, can be used to adapt the planned position of the implant in the left atrial appendage in order to ensure the coaxial positioning of the planned implant position relative to the LAA. Therefore, in an iterative process, an adapted implant position $\mathbf{p}_{i,j+1}$ and orientation $\mathbf{v}_{i,j+1}$ is automatically calculated in the coordinate system roi based on the anatomy of the LAA and the planned position $\mathbf{p}_{i,j}$ and orientation $\mathbf{v}_{i,j}$ of the implant. In the first iteration, these are determined by the user through the selection of the three points $\mathbf{p}_{i_1}$, $\mathbf{p}_{i_2}$ and $\mathbf{p}_{i,3}$.

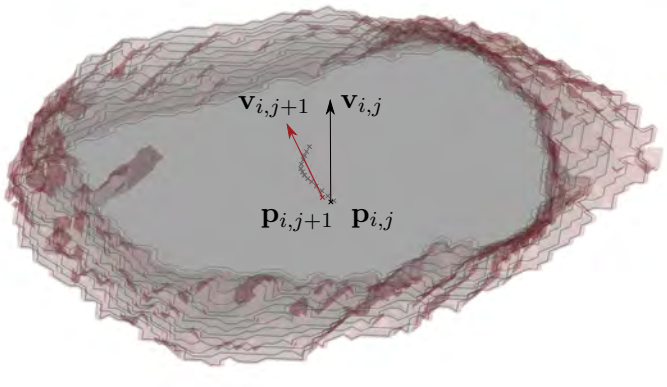

Figure 30 To align the planned implant position with the axis of the LAA, the centroids of the segmented areas of the LAA, which are visible in the image slices in the relevant ROI, are calculated and the new direction vector is determined by principal component analysis.

For the alignment, the centerline of the left atrial appendage in the landing zone has to be determined. Therefore, in the currently defined and segmented ROI that is aligned with the planned implant axis $\mathbf{v}_{i,j}$, the image slices that lie in the relevant area of the landing zone are extracted. In every slice, the centroid of the cross-section of the left atrial appendage is calculated. A linear regression calculated by principal component analysis (PCA) is used to find the line with least deviation from these centroids (see Figure 30). The PCA delivers three orthogonal vectors. The vector that has the smallest angle to the original vector is defined as the new adapted implant axis ${}^{roi}\mathbf{v}_{i,j+1}$ and the plane that lies perpendicular to the adapted implant vector ${}^{roi}\mathbf{v}_{i,j+1}$ and that contains the original implant position ${}^{roi}\mathbf{p}_{i,j}$ is defined as the new implant plane. The intersection point of this implant plane with the adapted implant vector is defined as the new implant position ${}^{roi}\mathbf{p}_{i,j+1}$. Furthermore, based on the new implant axis ${}^{mod}\mathbf{v}_{i,j+1}$ and position ${}^{mod}\mathbf{p}_{i,j+1}$ in the coordinate system mod, the ROI in the left atrial appendage is defined and recalculated.

As the segmented left atrial appendage in the ROI is analyzed layer by layer, the resulting vector depends on the orientation of the ROI. Therefore, iteration may be necessary to find the perfect location, as the ROI changes with the newly calculated vector. Therefore, the calculation is repeated iteratively until the angle δ_j between the vectors that are calculated in two consecutive iterations no longer differ more than $\delta_{j,min} = 5°$.

6.4 Planning the Implant Size

Three approaches are offered in parallel to support the planning of the implant size. The implant can be projected into the image data and the segmented anatomy of the left atrial appendage, the compression that the implant receives can be estimated and a model of the left atrial appendage, which can be additively manufactured for physical testing of different implants, can be generated.

6.4.1 Projection of the Implant into the Left Atrial Appendage

To support the physician during the choice of the implant size and to visualize the planned implant position, the geometry of the implant is virtually projected into two-dimensional or three-dimensional images of the left atrial appendage. In order to project the implant into the model, a three-dimensional data set of the implant has to be available.

As the ROI is aligned with the implant axis, the implant lies centric in the data set of the ROI. The Amplatzer implants are described by the radii and lengths of their three components lobe, neck and disc. An empty voxel data set with the size of the ROI around the implant position is defined and for every voxel the information whether it is part of the implant is determined. For each slice parallel to the implant plane, the distance to the implant plane is calculated and based on this information it is defined which of the three components of the implant lies in the slice or if the slice does not contain any part of the implant (see Figure 31). Subsequently, the distance of every voxel in the image slice to the implant axis, which runs through the central point of the slice, is calculated. If the distance of the respective voxel to the implant axis is smaller than the radius of the component of the implant that is corresponding to the slice, the voxel is considered to be part of the implant.

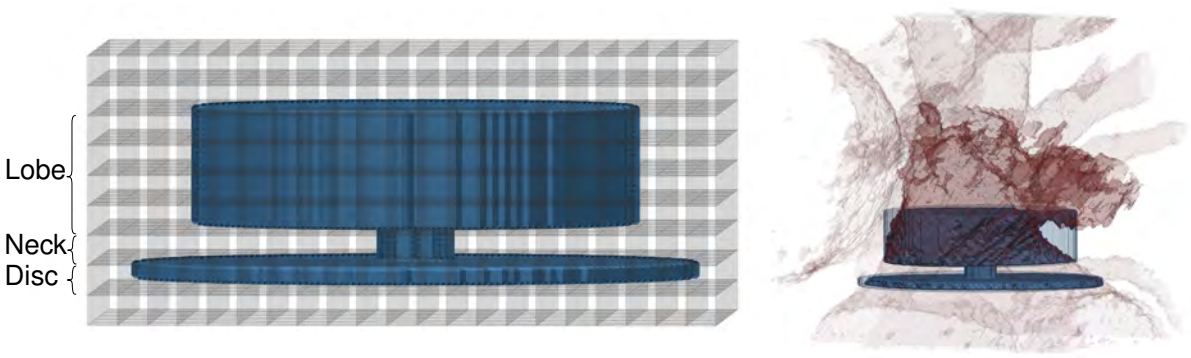

Figure 31 In the voxel data set of the ROI around the implant position, the implant is defined by the comparison of the distance of every voxel to the center point in every layer with the radius of the implant parts lobe, neck and disc. The voxels are considered part of the implant if they lie in a slice that contains a component of the implant and the distance is less than the radius of the respective component (left). The implant can be projected into the segmented left atrial appendage and parts that lie outside the area of the LAA are identified (right).

As for every voxel in the ROI it is know whether the implant lies in these respective voxels, the geometry of the implant can be projected into two-dimensional orthogonal CT images by coloring the voxels containing the implant (Figure 32, right). Additionally, the maximum and minimum diameter of the orifice of the LAA in the respective slice that lies parallel to the implant plane is shown.

The surface of the left atrial appendage and the implant can be triangulated using the 'isosurface' command in MATLAB. By using the 'patch' command, these surfaces models can be displayed in three dimensions (Figure 32, left).

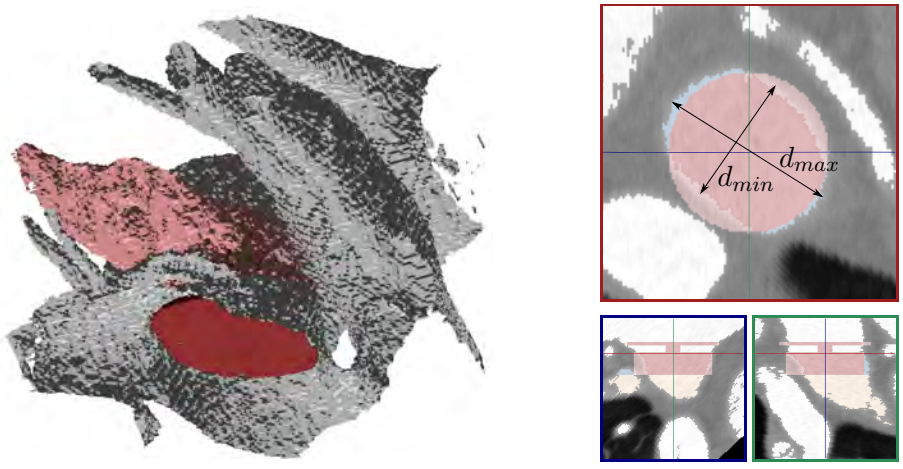

Figure 32 The implant is projected into two-dimensional and three-dimensional images of the LAA to support the choice of the optimal implant size. In the three-dimensional image on the left, the implant (red) is projected into the LAA (light red) and the surrounding tissue (gray). In two-dimensional orthogonal image slices, cross-sections of the implant (red) and the maximum and minimum diameter of the orifice in the slice are shown (right). Voxels that lie in the segmented area of the LAA in the image slices of the lobe but that are not covered by the implant are marked in blue.

6.4.2 Estimation of the Compression of the Implant

The overall compression of the implant and the compression that the implant experiences in every image slice is estimated based on the voxel data sets of the segmented left atrial appendage and the implant. A Boolean 'AND' operation is performed to find all voxels that are segmented in the voxel

data sets of the implant and the orifice of the left atrial appendage. Those voxels are considered part of the compressed implant.

By comparing the number of marked voxels in the uncompressed implant data set n_{uncomp} to the number of marked voxels in the compressed implant data set n_{comp}, the compression c in percentage is estimated.

$$c = \left(1 - \frac{n_{comp}}{n_{uncomp}}\right) \cdot 100\% \tag{6.19}$$

As only the lobe of the implant is relevant for the jamming of the implant, only the slices that are part of the lobe are taken into consideration. This estimation does not consider the elongation of the implant, which results from the radial compression. However, it allows a first estimation of the suitability of the implant.

Analogously, the voxels that are part of the segmented left atrial appendage in the slices containing the lobe but that are not part of the implant itself are determined. Those voxels are potential positions of leakages and show that the implant may not be big enough or that it is positioned incorrectly. These regions are marked in the orthogonal images (see blue area in Figure 32, right).

In order to mark the planned implant position in the anatomical model, a groove in the wall of the left atrial appendage can be added in the implant plane as shown in Figure 35 by erasing the voxels of the segmented area in the proximity of the previously identified boundary voxels in the slice of the implant plane.

6.4.3 Anatomical Model of the LAA

Based on the segmented image data set of the left atrial appendage, which is necessary for the three-dimensional display of the left atrial appendage, an anatomical model of the left atrial appendage can be exported as a file in STL format, which allows the additive manufacturing of the model. The model represents the surface of the cavity of the left atrial appendage.

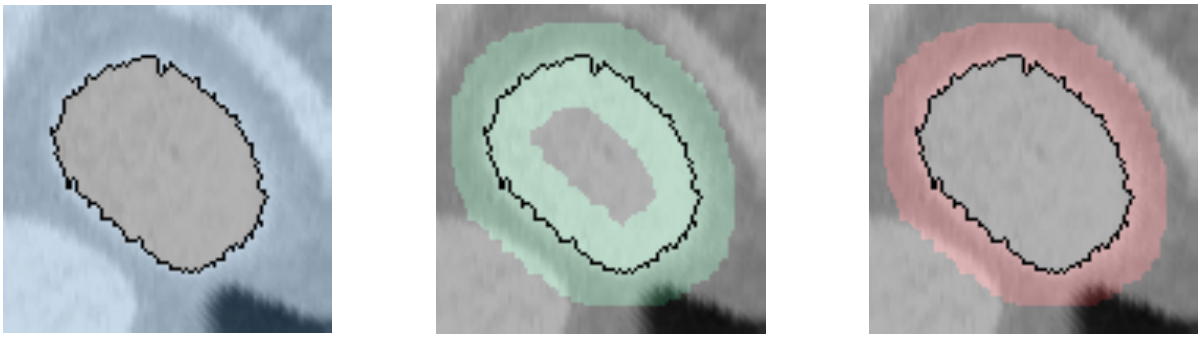

Figure 33 The anatomical model of the LAA that is additively manufactured cannot display the infinitesimally thin boundary layer between tissue and cavity, but needs a wall thickness. Therefore, the boundary layer (black) is identified and thickened. All voxels that are situated near the boundary layer (green) and at the same time lying outside of the cavity of the LAA (blue) are forming the basis for the anatomical model (red) (based on Graf *et al.*, 2016).

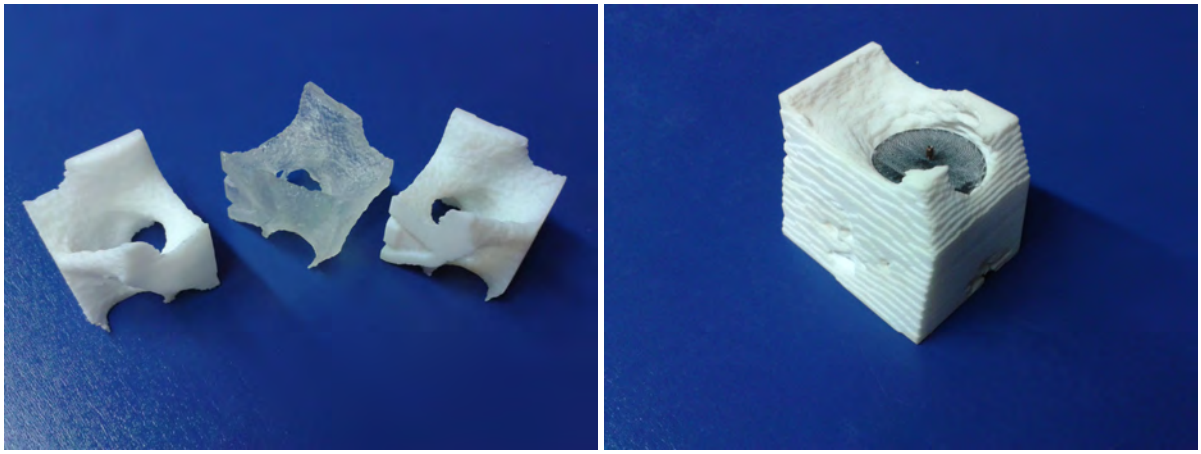

Figure 34 Additively manufactured models of the LAA based on CT data by fused deposition modelling, stereolithography and polyjet technology (image on the left, from left to right) and ultrasound data (right).

In contrast to the three-dimensional representation that only displays the infinitesimally thin boundary layer between the tissue and the blood-filled cavity, walls with a defined thickness are necessary for the additive manufacturing of the model. Therefore, a wall thickness of d_{wall} is added in the voxel data before converting the data to a surface model by triangulation. In the segmented binary images, the boundary voxels that lie between the segmented and not segmented regions are identified in every slice. Subsequently, the voxels that have a distance of less than d_{wall} to any boundary voxel are identified. A Boolean operation is applied to find all voxels that lie in the proximity of the boundary voxels and that are part of the walls of the heart and not of the left atrial appendage as shown in Figure 33. Triangulation is applied on this binary data set to get the surface model of the anatomy, which is saved in an STL file.

Additive Manufacturing of the Anatomical Model of the LAA. The anatomical model can be generated with any available generative manufacturing method. The most important requirement for the model production is dimensional accuracy. Test boxes with defined side length can be added to the manufactured part in order to check the dimensions (see Figure 35). As the left atrial appendage is concave in the landing zone, which is of interest for the planning of the implant size, support

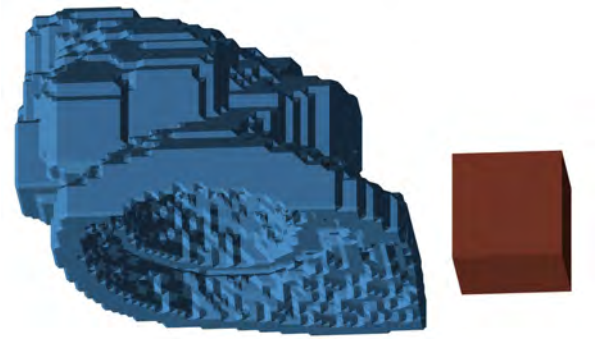

Figure 35 A groove marking the planned implant position can be added to the model (left, blue). In order to check the dimensional accuracy of the additive manufacturing process, the program automatically generates test boxes with defined side lengths, which are printed with the models (right, red).

structures that are necessary for some manufacturing methods do not adversely affect the suitability of the method as they lie on the backside of the model. A minimum wall thickness of d_{wall} = 5 mm showed good results with various manufacturing methods (see Figure 34).

6.5 Planning of the Puncture Location

The planned puncture location is determined by the selection of one point $\mathbf{p}_p$ in the image data set. The point is located on the interatrial septum between left and right atrium.

At the puncture location, the normal vector to the interatrial septum is estimated. Therefore, a segmentation of the left atrium in proximity to the puncture location as described in chapter 6.3.3 is necessary. The boundary wall of this segmented area can be triangulated and the normal vector for every triangle is calculated. To minimize the influence of roughness of the segmented wall, the normal vector at the transseptal puncture location is approximated as the mean value of the normal vectors of the interatrial septum in the close surroundings (see Figure 36). The direction of the normal vector is defined to point from the right atrium towards the left atrium. Due to the curvature of the left atrium, this means that the direction vector typically has to be oriented upwards.

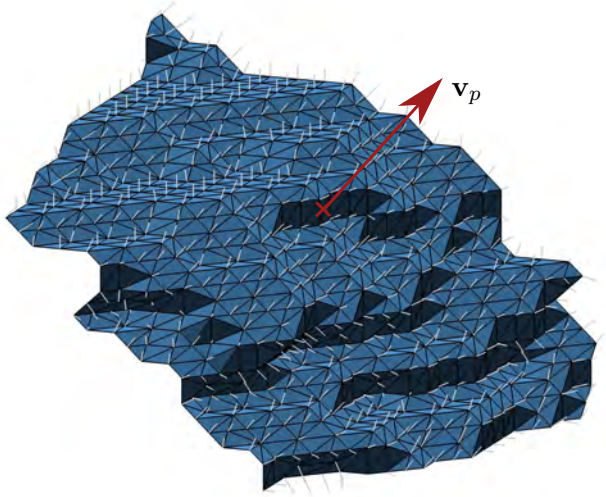

Figure 36 For the calculation of the normal vector at the transseptal puncture location $\mathbf{v}_p$, the normal vectors on the triangulated surface of the left atrium (blue) in the surrounding area are calculated and averaged.

Realization in the Interactive Program. Three orthogonal planes of the image data are displayed for the selection of the puncture position: a sagittal, a coronal and a transversal plane. Intersection lines mark the relative position of the images. The slice position for each of the lines can be changed by sliders or scrolling the mouse wheel.

The puncture location is planned by a click into one of the three images as shown in Figure 37 and the marked position is selected as the puncture location. All three orthogonal images are adjusted to show the slice that contains the selected point and its position is marked in each of them. The

position can be adjusted by selecting a new point that replaces the old one. If the definition of the direction vector at the puncture location is required, the segmented image in the proximity of the puncture point and a three-dimensional representation of the surface of the left atrium as well as the resulting vector are displayed and the segmentation threshold can be interactively adapted.

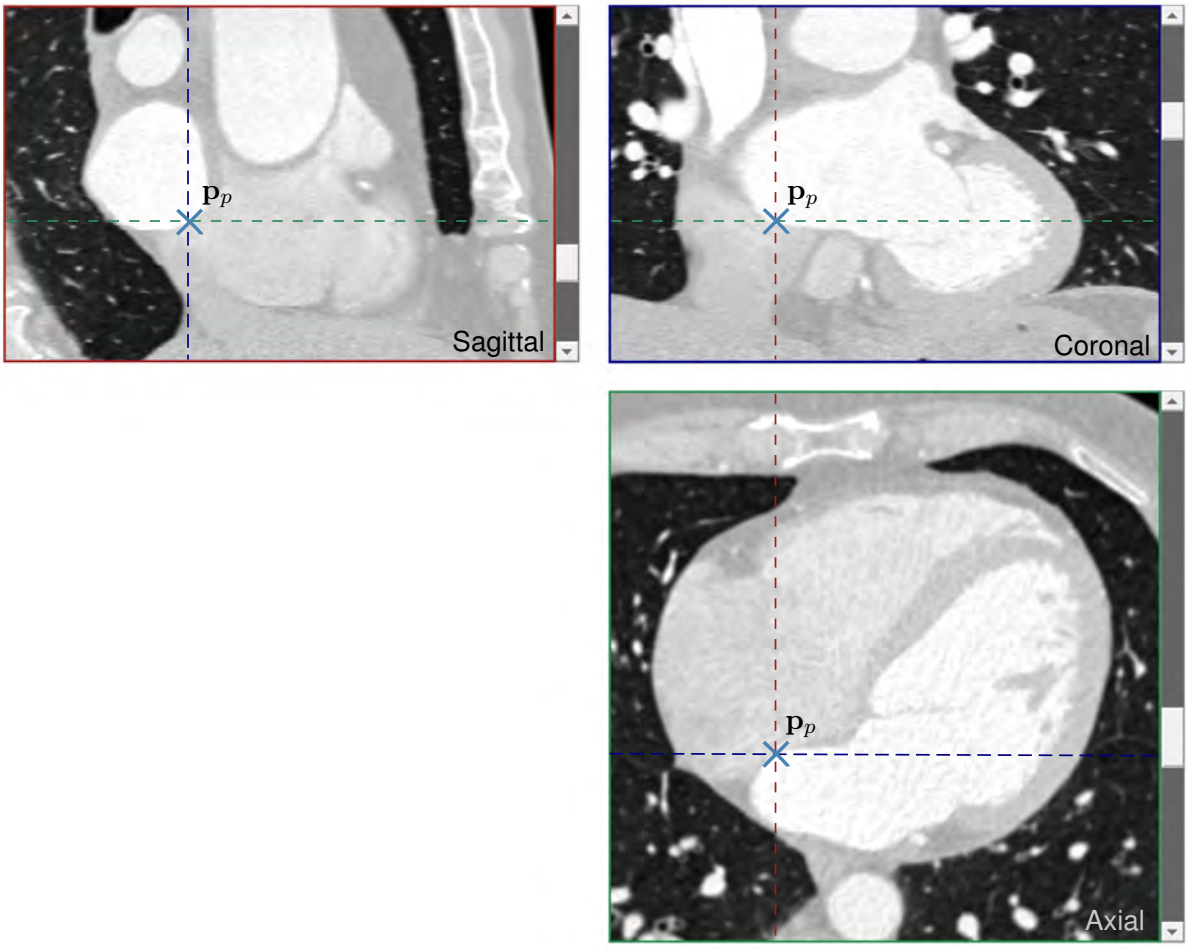

Figure 37 The position of the planned puncture $\mathbf{p}_p$ in the interatrial septum is defined by selecting one point in one of the three orthogonal image slices.

6.6 Selection of the Inferior Vena Cava

To achieve information about the pathway of the catheter entering the right atrium, the position and orientation of the inferior vena cava have to be known. For this purpose, the inferior vena cava is approximated by a line. Therefore, two outlines of the inferior vena cava in two axial image slices with maximum distance to each other are marked. The centroid of each outline is defined as the center point of the inferior vena cava in the respective slice. The center point that is closer to the heart is defined as the end point of the inferior cava and the point where the catheter enters into the right atrium. The direction vector of the inferior vena cava is defined as the connecting line between the two centroids of the outlines pointing upwards into the heart.

Realization in the Interactive Program. Similar to the selection of the transseptal puncture location, three orthogonal planes are displayed for the planning of the pathway of the inferior vena cava as shown in Figure 38. Two outlines of the inferior vena cava are marked in two axial slices, which are selected by the user by drawing a line around the vena. The center point of the outline contour points is calculated and displayed. One plane is selected as close as possible to the entry point of the vena into the right atrium. In order to minimize the effect of deviations, the second plane should have maximum distance to the first plane. The marked direction of the inferior vena cava is projected into the sagittal and coronal images.

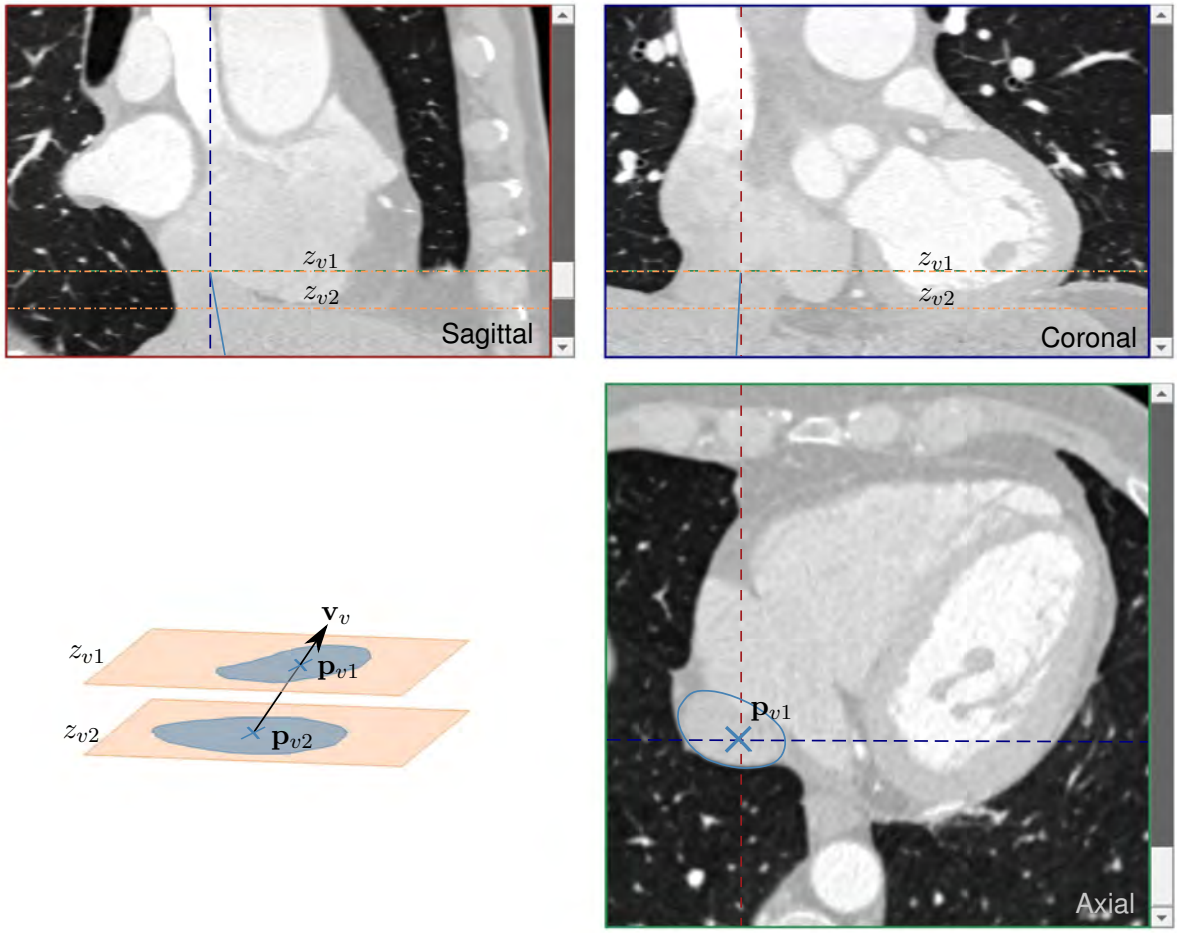

Figure 38 The pathway of the inferior vena cava is defined by the selection of two outlines of the vena cava in two image slices. The line through the center points of the cross-sections is defined as the direction vector of the inferior vena cava $\mathbf{v}_v$ (light blue). The position of the two axial slices that were used for the selection of the outlines are marked in the coronal and sagittal images (orange).

6.7 Evaluation of the Suitability of the Standard Catheter

The suitability of the double bended standard catheter is evaluated for the specific patient based on the planned boundary points and the shape of the standard catheter. All calculations are done in the coordinate system mod.

6.7.1 Description of a Double Bended Catheter

The standard catheter that is used with the Amplatzer implants is a double bended catheter. That means it has two bends with constant bending radii, which connect three straight segments. The centerlines of the straight segments can be described as lines by the unit vectors $\mathbf{v}_1$, $\mathbf{v}_2$ and $\mathbf{v}_3$ and one point on each line ($\mathbf{p}_1$, $\mathbf{p}_2$ and $\mathbf{p}_3$, see Figure 39). All direction vectors have a length of 1 mm and point towards the distal end of the catheter, which is referred to as the tip. The segments are numbered starting from the tip. If the lines are extended into the curved segments, they intersect at the points $\mathbf{p}_{b_1}$ and $\mathbf{p}_{b_2}$. Those points are called the bend points. $\mathbf{p}_{b_1}$ is located in the left atrium and $\mathbf{p}_{b_2}$ in the right atrium of the heart.

The shape of a double bended catheter independent of its position in the heart can be uniquely described by six variables: the two bending angles α_1 and α_2, the lengths l_1 from the tip of the catheter to the first bending point and l_2 between the two bending points, the rotation angle β between the bending planes of the two bends and the bending radius r_b.

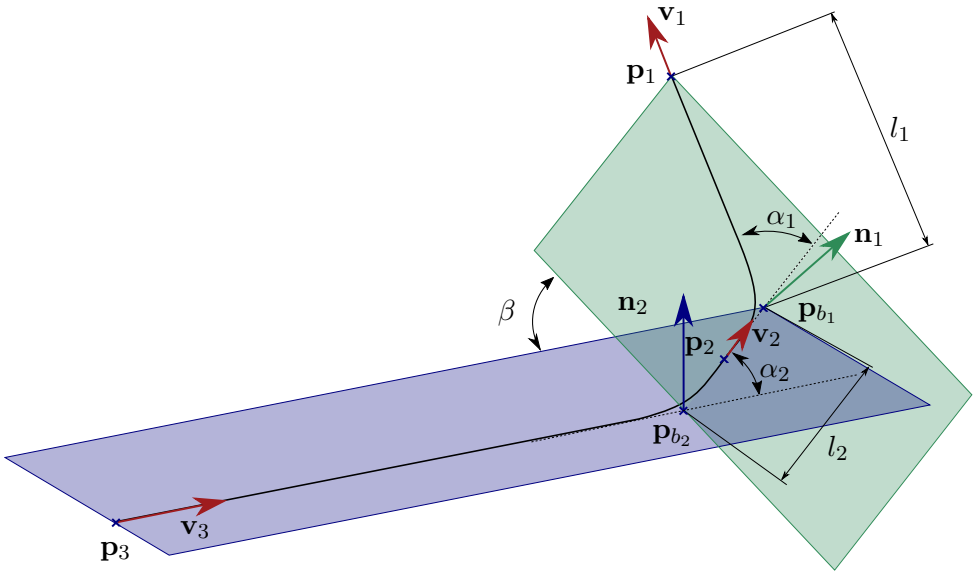

Figure 39 The double bended catheter can be described by the two bending angles α_1 and α_2, the lengths of the first two segments l_1 and l_2, the bending radius r_b of the bends and the rotation angle between the two bending planes β. The rotation angle is defined in a range from -180° to 180° to describe the shape of the catheter uniquely. The sign of the rotation angle depends on the orientation of the normal vector of the second bending plane and the vector of the first segment relative to each other.

The bending angles describe the deviation from a straight line and they are defined by the direction vectors of the adjacent lines, which are unit vectors. They can be calculated as

$$\begin{aligned} \alpha_1 &= \arccos(\mathbf{v}_1 \cdot \mathbf{v}_2) \\ \alpha_2 &= \arccos(\mathbf{v}_2 \cdot \mathbf{v}_3). \end{aligned} \tag{6.20}$$

The resulting values range in an interval between 0° and 180°.

The two lines at each bending point span the bending plane of the respective bend. The absolute

value of the rotation angle β between the bending planes is equal to the angle that the two normal vectors $\mathbf{n}_1$ and $\mathbf{n}_2$ of the bending planes form. The normal vectors are calculated as the cross product of the direction vectors of the two corresponding lines.

$$|\beta| = \arccos(\mathbf{n}_1 \cdot \mathbf{n}_2) = \arccos((\mathbf{v}_1 \times \mathbf{v}_2) \cdot (\mathbf{v}_2 \times \mathbf{v}_3)) \tag{6.21}$$

The calculation using the dot product and the arc cosine function provides values ranging from 0° to 180°. A value between 0° and 90° means that the normal vectors of both bending planes point into the same direction and the resulting catheter shape is of a 'C'-type as shown in Figure 40. In contrast, an 'S'-type shape exists if the normal vectors point into opposite directions and their angle is bigger than 90°. As the catheter tip can be situated at both sides of the bending plane of the second bend, further information regarding the direction of the rotation between the bending planes, which is defined by the sign of β, is needed to describe the catheter shape uniquely. The sign of β is determined by the angle between the third catheter segment and the normal vector of the first bending plane. If these vectors point into the same direction and thus the angle β_2 between the vectors is smaller than 90°, a positive sign is chosen for β and vice versa.

$$\begin{aligned} \beta_2 &= \arccos(\mathbf{v}_3 \cdot \mathbf{n}_1) \\ \beta &= \begin{cases} \beta \text{ if } \beta_2 \leq 90 \\ -\beta \text{ if } \beta_2 > 90 \end{cases} \end{aligned} \tag{6.22}$$

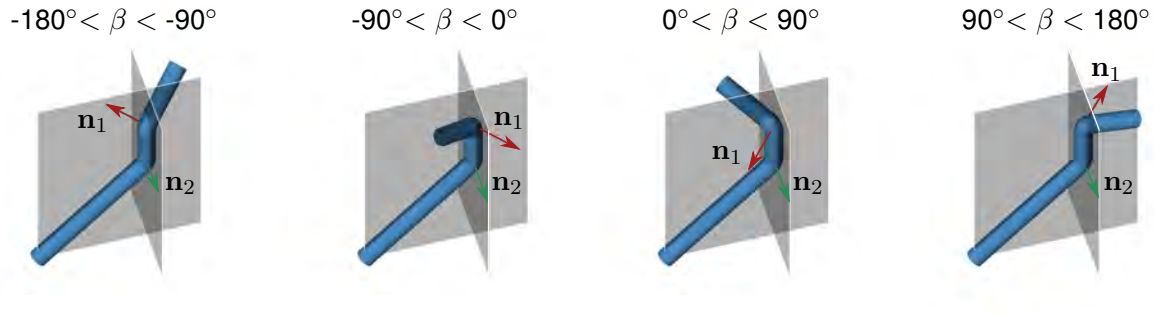

Figure 40 The rotation angle between the two bending planes is defined in a range from -180° to 180° to uniquely describe the shape of the catheter. The sign of the rotation angle depends on the orientation of the normal vector of the second bending plane and the vector of the first segment relative to each other. Depending on the value of the angle β between the bending planes, the shape of the catheter differs.

6.7.2 Projection of the Standard Double Bended Catheter into the Anatomy

To evaluate the suitability of the standard catheter for the given anatomy and the planned procedure, the geometry of the standard catheter is projected into the image data of the heart passing through the boundary points, which were defined in the planning stage as illustrated in Figure 41. The deviation of the position and orientation of the tip of the virtual catheter to the planned implant position and the direction of the implant axis is calculated. The standard catheter is a double bended catheter, which is defined by the six parameters α_1, α_2, l_1, l_2, β and r_b. However, the bending radius r_b does not influence the position of the catheter tip.

The third segment of the catheter is aligned with the previously defined line through the inferior vena

cava. Therefore, the direction vector $\mathbf{v}_3$ and one point $\mathbf{p}_3$ on the segment are defined by the planning of the inferior vena cava. The second segment runs through the puncture point, so that the point $\mathbf{p}_2$ is known. The line of the third segment and the puncture point uniquely define the second bending plane and its normal vector $\mathbf{n}_2$.

$$\mathbf{n}_2 = \frac{(\mathbf{p}_2 - \mathbf{p}_3) \times \mathbf{v}_3}{|(\mathbf{p}_2 - \mathbf{p}_3) \times \mathbf{v}_3|} \tag{6.23}$$

The second segment lies in the bending plane of the second bend and is thus perpendicular to the normal vector $\mathbf{n}_2$ of the bending plane. This means that the scalar product of the normal vector and $\mathbf{v}_2$ is zero. The unit vectors of the two line segments $\mathbf{v}_2$ and $\mathbf{v}_3$ form the angle α_2. The direction vector is a unit vector, which can therefore be calculated with the following three equations:

$$\begin{aligned} \mathbf{v}_2 \cdot \mathbf{v}_3 &= \cos(\alpha_2) \\ \mathbf{n}_2 \cdot \mathbf{v}_2 &= 0 \\ |\mathbf{v}_2| &= 1 \end{aligned} \tag{6.24}$$

Solving this equation system provides the direction vector $\mathbf{v}_2$. The second bending point $\mathbf{p}_{b_2}$ in the right atrium is the intersection point between the line segments two and three.

$$\mathbf{p}_{b_2} = \mathbf{p}_2 - l_{2,2} \cdot \mathbf{v}_2 = \mathbf{p}_3 + l_3 \cdot \mathbf{v}_3 \tag{6.25}$$

$l_{2,2}$ and l_3 describe the distances between the given points and the bending point.

The first bend point $\mathbf{p}_{b_1}$ is on the second line segment and has a distance of l_2 from the second bending point.

$$\mathbf{p}_{b_1} = \mathbf{p}_{b_2} + l_2 \cdot \mathbf{v}_2 \tag{6.26}$$

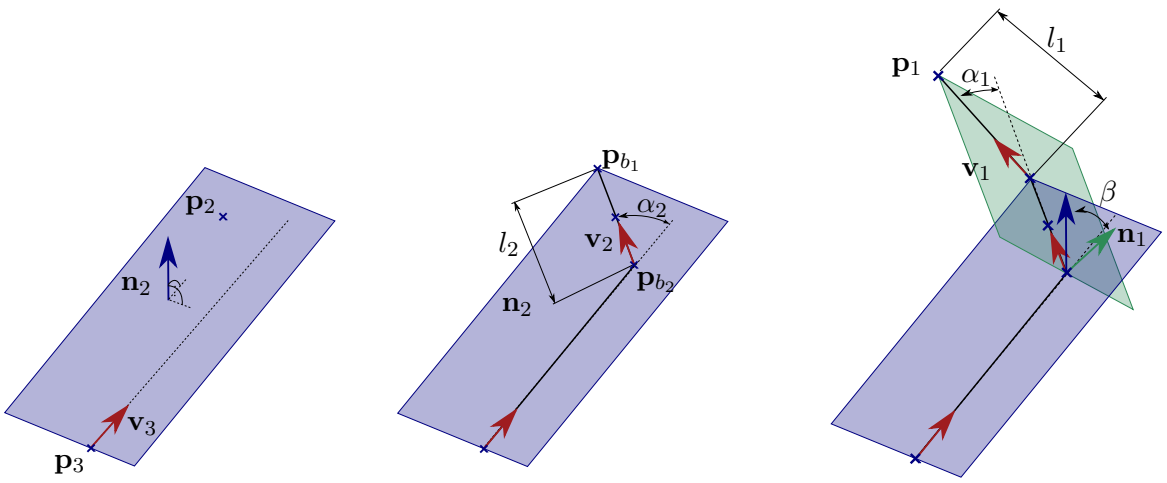

Figure 41 The standard catheter is inserted into the planned boundary points based on position and orientation of the inferior vena cava ($\mathbf{p}_3$ and $\mathbf{v}_3$) and the position of the puncture location $\mathbf{p}_2$ (left). The position of the two bending points $\mathbf{p}_{b_1}$ and $\mathbf{p}_{b_2}$ and the orientation of the second segment $\mathbf{v}_2$ are calculated based on the position of the bending plane with the normal vector $\mathbf{n}_2$, the bending angle of the second bend α_2 and the length of the second segment l_2 (middle). The position $\mathbf{p}_1$ and the orientation $\mathbf{v}_1$ of the tip of the catheter are calculated using the information about the bending angle of the first bend α_1, the rotation angle β between the bending planes and therefore the normal vector of the first bending plane $\mathbf{n}_1$ and the length l_1 of the first segment (right).

To ensure that the bending points are located in the two atria and therefore on different sides of the puncture point on the line segment, the distance between $\mathbf{p}_{b_2}$ and $\mathbf{p}_2$ must not exceed l_2. If it does so, the standard catheter cannot be virtually inserted into the planning points, which is a hint for a badly suited standard catheter.

The first segment of the catheter forms an angle of α_1 with the second segment and the bending planes of the first and second bend enclose the rotation angle β. Therefore, their normal vectors $\mathbf{n}_1$ and $\mathbf{n}_2$ also form an angle of β. The normal vector of the first bending plane is calculated by the cross product of the unit vectors of the first two segments. The direction vector of the first segment $\mathbf{v}_1$, which is a unit vector, can be calculated by solving the following equation system.

$$\begin{aligned} \mathbf{v}_1 \cdot \mathbf{v}_2 &= \cos(\alpha_1) \\ \mathbf{n}_1 \cdot \mathbf{n}_2 = \mathbf{n}_1 \cdot \frac{\mathbf{v}_1 \times \mathbf{v}_2}{|\mathbf{v}_1 \times \mathbf{v}_2|} &= \cos(\beta) \\ |\mathbf{v}_1| &= 1 \end{aligned} \tag{6.27}$$

The position of the tip $\mathbf{p}_1$ is determined using the information about the length of the first segment l_1.

$$\mathbf{p}_1 = \mathbf{p}_{b_1} + l_1 \cdot \mathbf{v}_1 \tag{6.28}$$

The deviation from the planned implant position is described by the distance of the tip of the calculated standard catheter from the implant position and the angle that the first segment builds with the direction vector of the implant axis $\mathbf{v}_i$ (see Figure 42).

$$\begin{aligned} d_{std} &= |\mathbf{p}_i - \mathbf{p}_1| \\ \delta_{std} &= \arccos(\mathbf{v}_1 \cdot \mathbf{v}_i) \end{aligned} \tag{6.29}$$

The standard catheter is displayed relative to the patient's image data as described in chapter 6.9.

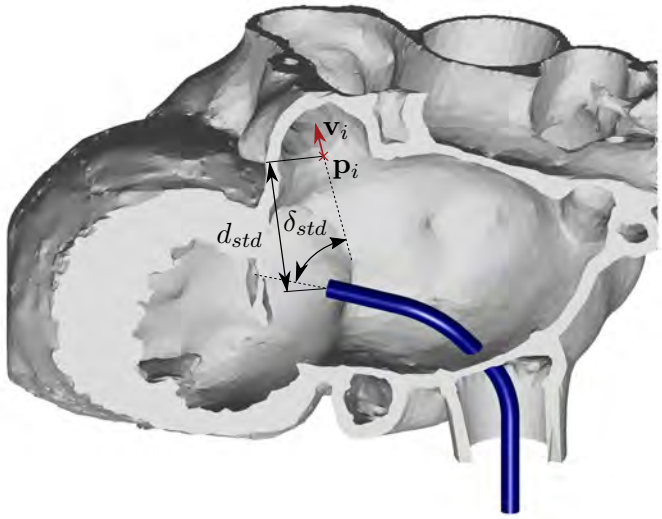

Figure 42 The shape of the standard catheter is projected into the planned boundary points and the distance of the tip of the catheter to the planned implant position d_{std} as well as the deviation of the direction vectors of implant and tip δ_{std} are calculated to determine the suitability of the catheter for the given anatomy.

6.7.3 Description of the Catheter

Centerline and Transformation Matrices. The catheter shape of the standard catheter or the patient-individually calculated catheter is the basis for the display of the catheter and the construction of the bending form. In order to be able to process different catheter shapes and to allow easy exchange of the calculation methods for the patient-individual catheter shape, a general interface is necessary to avoid the need for adaptations in the algorithms for the visualization of the catheter shape and the calculation of the bending form. Therefore, the catheter shape is described by the centerline points $\mathbf{p}_{c_k}$ of the catheter and the corresponding normal vectors $\mathbf{n}_{c_k}$ on the catheter cross-section at each point of the centerline. Based on the normal vectors, three basis vectors for a transformation matrix into the coordinate system of the particular centerline point c_k are defined (see Figure 43). The component in $\mathbf{y}_{mod}$-direction of the first vector is defined as zero to define the position of the vector ${}^{mod}\mathbf{x}_{c_k}$ in a horizontal plane in the coordinate system mod. All unit vectors are perpendicular to each other and by using this information, the vectors ${}^{mod}\mathbf{x}_{c_k}$ and ${}^{mod}\mathbf{y}_{c_k}$ can be calculated as follows:

$$
\begin{aligned}
{}^{mod}\mathbf{x}_{c_k} &= \begin{pmatrix} {}^{mod}\mathbf{n}_{c_k}(3) \\ 0 \\ -{}^{mod}\mathbf{n}_{c_k}(1) \end{pmatrix} \frac{1}{\sqrt{{}^{mod}\mathbf{n}_{c_k}(1)^2 + {}^{mod}\mathbf{n}_{c_k}(3)^2}} \\
{}^{mod}\mathbf{y}_{c_k} &= -{}^{mod}\mathbf{x}_{c_k} \times {}^{mod}\mathbf{z}_{c_k} \\
{}^{mod}\mathbf{z}_{c_k} &= \frac{{}^{mod}\mathbf{n}_{c_k}}{|{}^{mod}\mathbf{n}_{c_k}|}
\end{aligned}
\tag{6.30}
$$

If the normal vector $\mathbf{n}_{c_k}$ points only into y-direction and does not have any component in x- and z-direction, the vector $\mathbf{x}_{c_k}$ has to be defined separately, as the previously presented calculation with

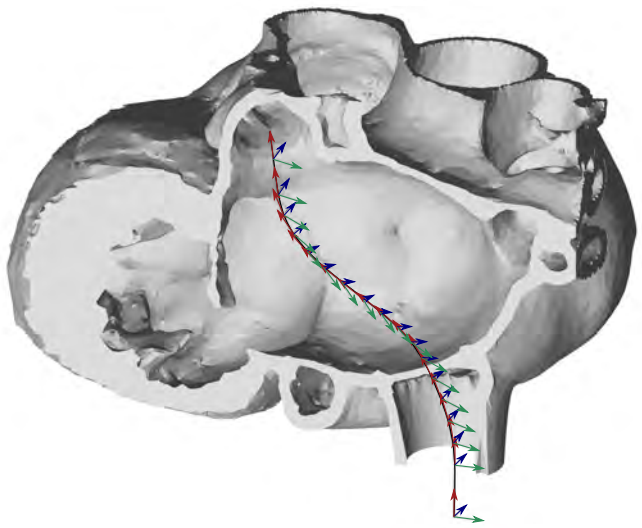

Figure 43 The centerline of the catheter is described by the points $\mathbf{p}_{c_k}$ on the centerline, the normal vectors $\mathbf{n}_{c_k}$ (red) on the catheter cross-section along the centerline and the corresponding two basis vectors $\mathbf{x}_{c_k}$ (blue) and $\mathbf{y}_{c_k}$ (green) in the cross-sectional plane of the catheter.

the fixed definition of y-component of $\mathbf{x}_{c_k}$ will lead to problems. In this case, the $\mathbf{x}_{c_k}$ vectors of the neighboring two points are interpolated. If the point has only one neighbor, as it is an endpoint of the centerline, the $\mathbf{x}_{c_k}$ vector of the neighboring point is adopted.

Due to the definition of $\mathbf{x}_{c_k}$ by the components of the normal vector, the vectors $\mathbf{x}_{c_k}$ and $\mathbf{y}_{c_k}$ change direction if the x- or z-components of $\mathbf{n}_{c_k}$ change their sign. This leads to restrictions in the display of the catheter and problems in the calculation of the bending form as displayed in Figure 44. To avoid this, the angles between neighboring $\mathbf{x}_{c_k}$ and $\mathbf{y}_{c_k}$ vectors along the centerline are calculated. In case, the angle exceeds 90° at some point, the direction of the vector and all following $\mathbf{x}_{c_k}$ respectively $\mathbf{y}_{c_k}$ vectors are inverted.

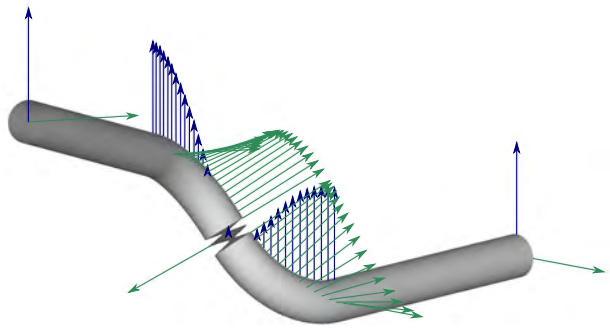

Figure 44 Without the testing and correction of the orientation of the basis vectors $\mathbf{x}_{c_k}$ (blue) and $\mathbf{y}_{c_k}$ (green), twisting of the catheter shape can occur when the angles between neighboring basis vectors exceed 90°. In this case, the orientations of the cross-sections at this point differ what leads to problems with the connection of the cross-sections and with the display of the catheter shape.

The transformation matrix for every point on the centerline is defined as a linear combination of these basis vectors and the location of the centerline point.

$$ {}^{mod}\mathbf{T}_{c_k} = \begin{pmatrix} {}^{mod}\mathbf{x}_{c_k} & {}^{mod}\mathbf{y}_{c_k} & {}^{mod}\mathbf{z}_{c_k} & {}^{mod}\mathbf{p}_{c_k} \\ 0 & 0 & 0 & 1 \end{pmatrix} \tag{6.31} $$

Intersection Points and Radii. The bends of the catheters are specified as the intersection points of two straight lines with the direction vectors $\mathbf{v}_1$ and $\mathbf{v}_2$. If the lines lie in one plane and are not parallel, they have an intersection point $\mathbf{p}_{b_1}$, which is determined by solving the equation

$$ \mathbf{p}_{b_1} = \mathbf{p}_1 + l_1 \cdot \mathbf{v}_1 = \mathbf{p}_2 + l_2 \cdot \mathbf{v}_2. \tag{6.32} $$

The normal vector on the bending plane can be calculated as the cross product of the two lines. To determine the bending angle α_1 between the two lines, the scalar product is used as described in Equation 6.20.

To calculate the centerline of catheters with constant bending radii in their bends, the bends, which are described by the intersection points and the direction vectors of the intersecting lines, have to be rounded off as illustrated in Figure 45. Therefore, at every bending point a circle segment with

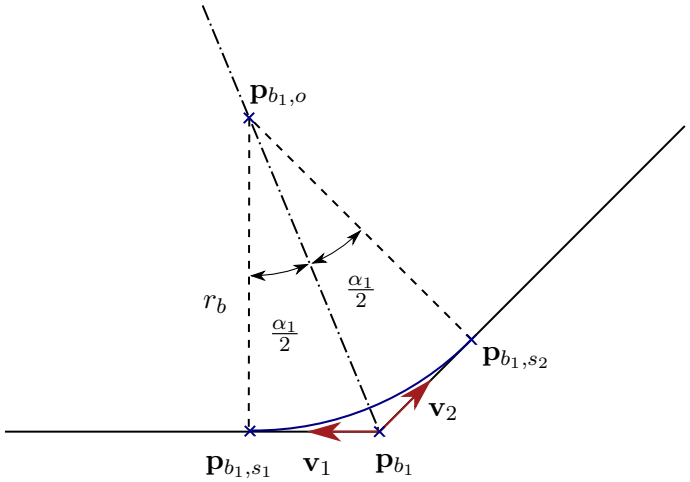

Figure 45 Based on the position of the intersection point $\mathbf{p}_{b_1}$ and the two adjacent direction vectors $\mathbf{v}_1$ and $\mathbf{v}_2$ as well as the bending radius r_b, the curvature at the intersections of two lines in space are calculated.

the given bending radius is added. The input parameters for the calculation of the circle segment are the bending radius r_b and the desired distance between the points in the circle segment d_b apart from the intersection point $\mathbf{p}_{b_1}$ and the direction vectors of the two lines $\mathbf{v}_1$ and $\mathbf{v}_2$. The points $\mathbf{p}_{b_1,s_1}$ and $\mathbf{p}_{b_1,s_2}$ that mark the transition between the straight segments and the bends are calculated as

$$\begin{aligned} \mathbf{p}_{b_1,s_1} &= \mathbf{p}_{b_1} + \frac{r_b}{\tan(\frac{\pi-\alpha_1}{2})} \cdot \mathbf{v}_1 \\ \mathbf{p}_{b_1,s_2} &= \mathbf{p}_{b_1} - \frac{r_b}{\tan(\frac{\pi-\alpha_1}{2})} \cdot \mathbf{v}_2. \end{aligned} \tag{6.33}$$

The center point $\mathbf{p}_{b_1,o}$ of the circle segment for the first bend point is calculated using the same information.

$$\mathbf{p}_{b_1,o} = \mathbf{p}_{b_1} + \frac{r_b}{\sin(\frac{\pi-\alpha_1}{2})} \cdot \frac{\mathbf{v}_1 + \mathbf{v}_2}{|\mathbf{v}_1 + \mathbf{v}_2|} \tag{6.34}$$

With these points the two vectors $\mathbf{u}_{b_1}$ and $\mathbf{v}_{b_1}$ that lie in the bending plane can be calculated. The vector $\mathbf{u}_{b_1}$ points from the center point $\mathbf{p}_{b_1,o}$ of the circle segment to the transition point $\mathbf{p}_{b_1,s_1}$. $\mathbf{v}_{b_1}$ is oriented normal to $\mathbf{u}_{b_1}$.

$$\begin{aligned} \mathbf{u}_{b_1} &= \frac{\mathbf{p}_{b_1,s_1} - \mathbf{p}_{b_1,o}}{|\mathbf{p}_{b_1,s_1} - \mathbf{p}_{b_1,o}|} \\ \mathbf{v}_{b_1} &= \frac{\mathbf{u}_{b_1} \times (\mathbf{v}_1 \times \mathbf{v}_2)}{|\mathbf{u}_{b_1} \times (\mathbf{v}_1 \times \mathbf{v}_2)|} \end{aligned} \tag{6.35}$$

The necessary number of points $n_{b_1,j}$ to smoothly describe the curve depends on the radius r_b, the desired distance d_b and the bending angle α_1.

$$n_{b_1,j} = \text{round}\left(\frac{\alpha_1}{2 \cdot \arcsin(d_b/2/r_b)}\right) \tag{6.36}$$

The points $\mathbf{p}_{b_1,j}$ in the curved segment and the normal vectors $\mathbf{n}_{b_1,j}$ on the bend are determined by

$$
\begin{aligned}
a_{b_1,j} &= \frac{j\alpha_1}{n_{b_1,j}}, \quad j \in [1, n_{b_1,j}] \\
\mathbf{p}_{b_1,j} &= \mathbf{p}_{b_1,o} + r_b \cdot \mathbf{u}_{b_1} \cdot \cos(a_{b_1,j}) + r_b \cdot \mathbf{v}_{b_1} \cdot \sin(a_{b_1,j}) \\
\mathbf{n}_{b_1,j} &= \mathbf{u}_{b_1} \cdot \sin(a_{b_1,j}) - \mathbf{v}_{b_1} \cdot \cos(a_{b_1,j}).
\end{aligned}
\tag{6.37}
$$

This calculation is performed analogously for the curvature at the second bend.

The number of centerline points that are positioned on the straight segments depends on the intended use of the centerline and can be altered easily. Furthermore, for the construction of the bending form, it is necessary to know which points belong to the straight and which to the curved segments. Therefore, the indices of the first points of the respective segments are noted.

6.8 Calculation of the Catheter Shape

Based on the planning of the implant position and the transseptal puncture and the position of the inferior vena cava, a patient-specific catheter shape is calculated that fits into these boundary conditions, which are shown in Figure 46. The coordinate system mod is used for the following calculations.

Three exemplary approaches for the calculation of the catheter with their corresponding advantages and disadvantages are subsequently described. All of these approaches have in common, that they work based on the final position of the catheter before unfolding the implant. That means the catheter is already inserted into the left atrial appendage and the catheter is aligned at the implant position. The insertion process is not taken into account, as the catheter is guided during this phase by a guide wire that is previously inserted into the LAA and that makes the patient-specific shaping redundant for that process step.

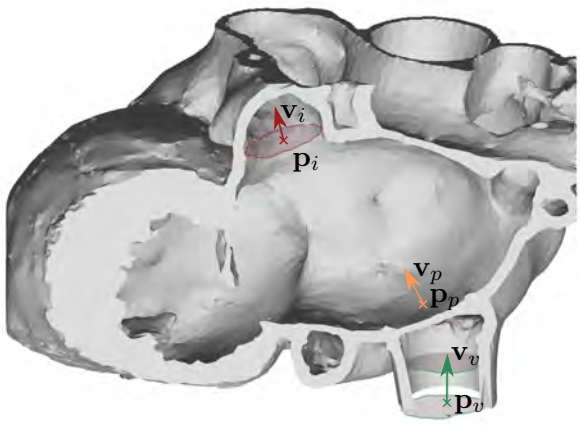

Figure 46 The boundary conditions for the calculation of the catheter shape are the points and direction vectors at the implant position and the vena. At the puncture location, the position is defined and the direction vector perpendicular to the interatrial septum can be set as an additional boundary condition.

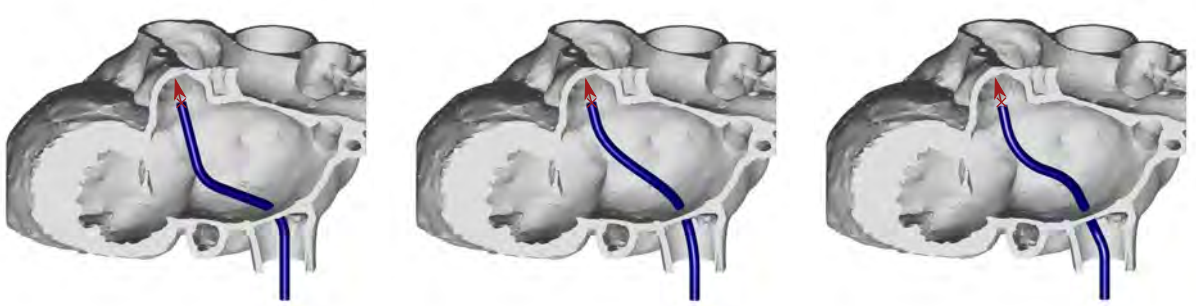

Figure 47 Three calculation approaches are presented: the calculation of a double bended catheter (left), a catheter with varying curvature in the atria (middle) and a catheter with four bends and maximized bending radii (right).

The approaches that are presented are a double bended catheter either passing exactly through the boundary points or with a deviation at one of the boundaries, a catheter with varying curvature in the atria that is described by a smooth spline interpolation between the boundary points and a catheter with four bends that has maximized bending radii at every bend (see Figure 47). All of the calculation approaches assume that the tip of the catheter is located at the planned implant location and that the vector pointing along the catheter axis at its tip is equal to the normal vector of the implant plane and thus the implant axis. The catheter runs through the puncture location at some point. For the calculation approaches with the spline line and the four times bent catheter, also the normal vector at the puncture location is considered. The entry point of the catheter into the heart is determined by the previously defined position of the inferior vena cava and the catheter is aligned with the axis of the inferior vena cava. In order to offer sufficient space for the transition between the defined direction vectors at the entry point and the puncture location, the lower one of the two selected points of the vena is chosen as the boundary point for the catheter with four bends and the catheter with variable curvature. The upper point is selected for the double bended catheter, as the direction vector at the puncture location is not predefined in this case. Apart from these boundary conditions at the boundary points, further constraints have to be regarded as for example minimum distances between the bending points, minimum distances of curved segments from the boundary points or maximum bending angles.

User Interaction During the Calculation of the Catheter Shape. Buttons are available for the user to choose the desired calculation method for the catheter shape and in a table, the parameters for the calculation can be adapted interactively. The available parameters depend on the calculation method that is used. For the double bended catheter, three options to allow a tolerance at different boundary points are available if no exact solution can be calculated. The resulting catheter shape is displayed in a three-dimensional representation for a first evaluation of the results.

6.8.1 Double Bended Catheter

The calculation approach for the double bended catheter is inspired by the shape of the standard catheter with one bend in the left and one in the right atrium, both with constant bending radius throughout the bended segment as displayed in Figure 48.

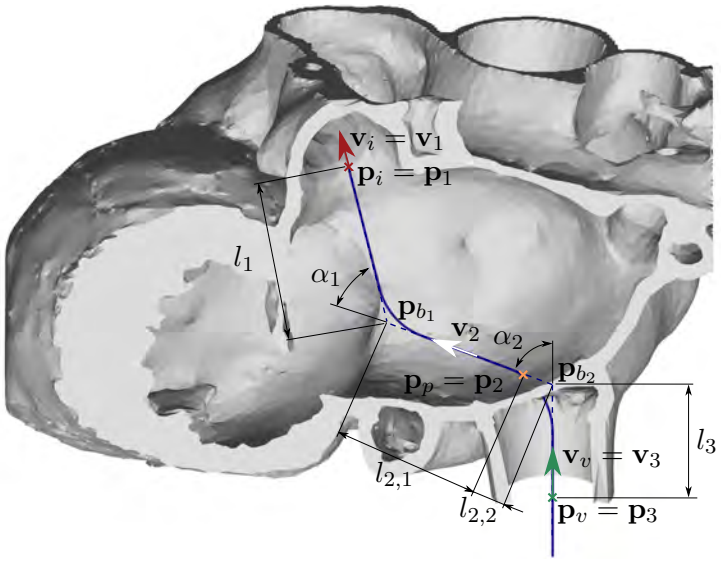

Figure 48 The double bended catheter that exactly meets all boundary points is defined by the points and vectors at the planned implant position ($\mathbf{p}_i$ and $\mathbf{v}_i$) and the inferior vena cava ($\mathbf{p}_v$ and $\mathbf{v}_v$) as well as by the location of the puncture point ($\mathbf{p}_p$). The catheter is described as three straight segments that intersect at the points $\mathbf{p}_{b_1}$ and $\mathbf{p}_{b_2}$.

To calculate the pathway of a patient-specific double bended catheter through the heart that is adapted to the anatomical structures and the implant position, it is assumed that the tip of the catheter $\mathbf{p}_1$ is identical to the planned implant location $\mathbf{p}_i$ and the direction vector of the first segment $\mathbf{v}_1$ is aligned with the normal vector of the implant plane $\mathbf{v}_i$. Therefore, the position as well as the direction vector of the first segment is known. In the left atrium, the catheter has a bending point $\mathbf{p}_{b_1}$ between the implant position and the puncture location. The second segment of the catheter passes through the puncture point $\mathbf{p}_p$. The direction vector of the second segment $\mathbf{v}_2$ is not explicitly determined by the boundary points, but it intersects with the other two lines at the bending points. In the right atrium, the catheter has another bending point $\mathbf{p}_{b_2}$ before leaving the heart through the inferior vena cava. With the knowledge of the pathway of the inferior vena cava ($\mathbf{p}_v$ and $\mathbf{v}_v$) the direction vector of the third segment $\mathbf{v}_3$ as well as one point on the line $\mathbf{p}_3$ are known. A catheter that meets all of these conditions is defined exactly, as the equations for the calculation of the bending points and the definition of the direction vectors as unit vectors build a system of equations with one solution. The three components of the direction vector of the second segment $\mathbf{v}_2$ and the distances between the boundary points and the bending points l_1, $l_{2,1}$, $l_{2,2}$ and l_3 can be calculated by solving this equation system.

$$\begin{aligned} \mathbf{p}_{b_1} &= \mathbf{p}_1 - l_1 \cdot \mathbf{v}_1 = \mathbf{p}_2 + l_{2,1} \cdot \mathbf{v}_2 \\ \mathbf{p}_{b_2} &= \mathbf{p}_2 - l_{2,2} \cdot \mathbf{v}_2 = \mathbf{p}_3 + l_3 \cdot \mathbf{v}_3 \\ |\mathbf{v}_1| &= |\mathbf{v}_2| = |\mathbf{v}_3| = 1 \end{aligned} \tag{6.38}$$

In order to solve the equation system the following approach is used. The bending planes of the two bends can be described by their normal vector $\mathbf{n}_1$ and $\mathbf{n}_2$. The normal vector $\mathbf{n}_1$ is the normalized cross product of the direction vector of segment one and the vector from the implant point to the puncture point. Analogously, $\mathbf{n}_2$ is determined based on the direction vector of segment two and the

vector from a point on the inferior vena cava to the puncture point.

$$\begin{aligned} \mathbf{n}_1 &= \frac{\mathbf{v}_1 \times (\mathbf{p}_p - \mathbf{p}_i)}{|\mathbf{v}_1 \times (\mathbf{p}_p - \mathbf{p}_i)|} \\ \mathbf{n}_2 &= \frac{\mathbf{v}_2 \times (\mathbf{p}_p - \mathbf{p}_v)}{|\mathbf{v}_2 \times (\mathbf{p}_p - \mathbf{p}_v)|} \end{aligned} \tag{6.39}$$

As the second segment is part of the two bends, it has to lie in both bending planes. Therefore, the direction vector of the second segment is perpendicular to both normal vectors of the bending planes and can be calculated as their cross product.

$$\mathbf{v}_2 = \frac{\mathbf{n}_1 \times \mathbf{n}_2}{|\mathbf{n}_1 \times \mathbf{n}_2|} \tag{6.40}$$

The position of the bending points can be calculated as the intersection points of the two intersecting segment lines. They are described by the variable parameters l_1, $l_{2,1}$, $l_{2,2}$ and l_3 of the line equations.

$$\begin{aligned} \mathbf{p}_{b_1} &= \mathbf{p}_i - l_1 \cdot \mathbf{v}_i = \mathbf{p}_p + l_{2,1} \cdot \mathbf{v}_2 \\ \mathbf{p}_{b_2} &= \mathbf{p}_p - l_{2,2} \cdot \mathbf{v}_2 = \mathbf{p}_v + l_3 \cdot \mathbf{v}_v \end{aligned} \tag{6.41}$$

However, this calculation does not ensure that the bending points lie in the left respectively the right atrium. This is true if the points lie between the puncture point and the implant point respectively the puncture point and the vena point. To ensure this all of the variable parameter l_1, $l_{2,1}$, $l_{2,2}$ and l_3 have to be positive values. If $l_{2,1}$ and $l_{2,2}$ both are negative, the direction of $\mathbf{v}_2$ has to be inverted to get a valid solution.

The addition of further restrictions might be necessary to identify suitable catheter shapes. These can be minimum or maximum values for the variable parameters, which ensure minimum or maximum distances between the boundary points and the bending points. Furthermore, limits for the bending angles can be added. The calculated shape can be tested for these constraints and if they are not met, tolerances need to be added at one of the three segments to allow deviations from the boundary points and the shape can be approximated.

6.8.2 Optimized Calculation of the Double Bended Catheter Shape

If the previously described intersection problem does not have a valid solution, deviations can be added at each of the three boundary points: the implant position, the puncture location and the inferior vena cava. At the implant and the vena, a deviation of the segment's direction vector to the direction vector of the implant or the vena, respectively, is allowed whereas the positions of the boundary points are met exactly. If the tolerance is added at the puncture site, a deviation from the exact puncture location is allowed while the other boundary points are met exactly in position and direction. In any of the three cases, the catheter shape can be described by two independent variables k_1 and k_2 that define the bending points, the direction vectors and the positions of all three segments. Those variables can be optimized to achieve a catheter shape that complies with all of the boundary conditions and constraints but has minimal deviation from the planned boundaries.

Tolerance at the Implant Position. If a tolerance is added at the direction vector of the implant, the system is defined by the direction vector and position of the inferior vena cava, the position of the puncture point and the position of the implant point as well as two variable parameters k_1 and k_2 that determine the position of the intersection points between the line segments. Figure 49 displays the pathway of the catheter with tolerance at the implant position.

The first parameter k_1 defines the distance of the second bending point to the entry point of the inferior vena cava into the heart.

$$\mathbf{p}_{b_2} = \mathbf{p}_v + k_1 \cdot \mathbf{v}_v \tag{6.42}$$

With the knowledge of the second bending point $\mathbf{p}_{b_2}$, the direction vector of the second segment can be calculated as the vector between the puncture point and the bending point.

$$\mathbf{v}_2 = \frac{\mathbf{p}_p - \mathbf{p}_{b_2}}{|\mathbf{p}_p - \mathbf{p}_{b_2}|} \tag{6.43}$$

The second parameter k_2 describes the distance of the first bending point $\mathbf{p}_{b_1}$ to the puncture location $\mathbf{p}_p$ and thus defines the position of the first bending point.

$$\mathbf{p}_{b_1} = \mathbf{p}_p + k_2 \cdot \mathbf{v}_2 \tag{6.44}$$

The direction vector of the first segment $\mathbf{p}_p$ is the vector from the implant position to the first bending point.

$$\mathbf{p}_p = \frac{\mathbf{p}_i - \mathbf{p}_{b_1}}{|\mathbf{p}_i - \mathbf{p}_{b_1}|} \tag{6.45}$$

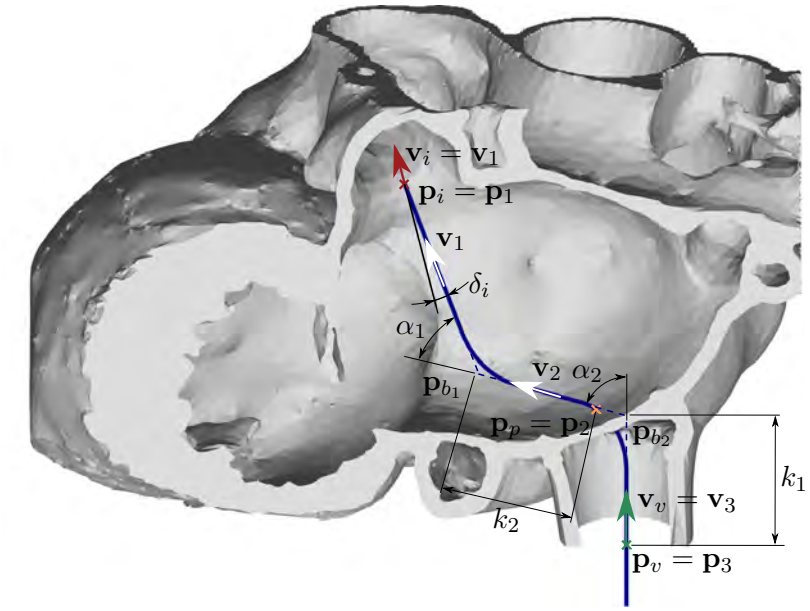

Figure 49 The catheter shape with tolerance at the implant position is defined by the position and direction vector at the inferior vena cava ($\mathbf{p}_v$ and $\mathbf{v}_v$), the position of the puncture point $\mathbf{p}_p$ and the planned implant position $\mathbf{p}_i$ as well as the distances of the bending points to the entry point of the inferior vena cava k_1 and to the puncture point k_2. The deviation angle δ_i of the tip segment of the catheter to the planned implant axis $\mathbf{v}_i$ is minimized.

The deviation δ_i of the first segment to the implant vector can be calculated as

$$\delta_i = \arccos(\mathbf{v}_i \cdot \mathbf{v}_1). \tag{6.46}$$

Tolerance at the Puncture Location. The second possibility is to allow the second segment of the catheter to not meet the puncture location exactly (see Figure 50). The system is defined by the location and direction vectors at the implant and the inferior vena cava and the two variable parameters k_1 and k_2 describing the distance of the bending points $\mathbf{p}_{b_1}$ and $\mathbf{p}_{b_2}$ from the implant position and the entry point of the inferior vena cava.

$$\begin{aligned} \mathbf{p}_{b_1} &= \mathbf{p}_i - k_1 \cdot \mathbf{v}_i \\ \mathbf{p}_{b_2} &= \mathbf{p}_v + k_2 \cdot \mathbf{v}_v \end{aligned} \tag{6.47}$$

Thus, the position of the bending points is defined and the second segment is the connecting line between the two bending points.

$$\mathbf{v}_2 = \frac{\mathbf{p}_{b_1} - \mathbf{p}_{b_2}}{|\mathbf{p}_{b_1} - \mathbf{p}_{b_2}|} \tag{6.48}$$

To evaluate the deviation from the planned puncture location, the point $\mathbf{p}_f$ on the second line segment with least distance to the puncture location is calculated and the deviation d_p is determined.

$$\begin{aligned} \mathbf{p}_f &= \mathbf{p}_{b_1} + \frac{\mathbf{v}_2 \cdot (\mathbf{p}_p - \mathbf{p}_{b_1})}{|\mathbf{v}_2|^2} \cdot \mathbf{v}_2 \\ d_p &= |\mathbf{p}_p - \mathbf{p}_f| \end{aligned} \tag{6.49}$$

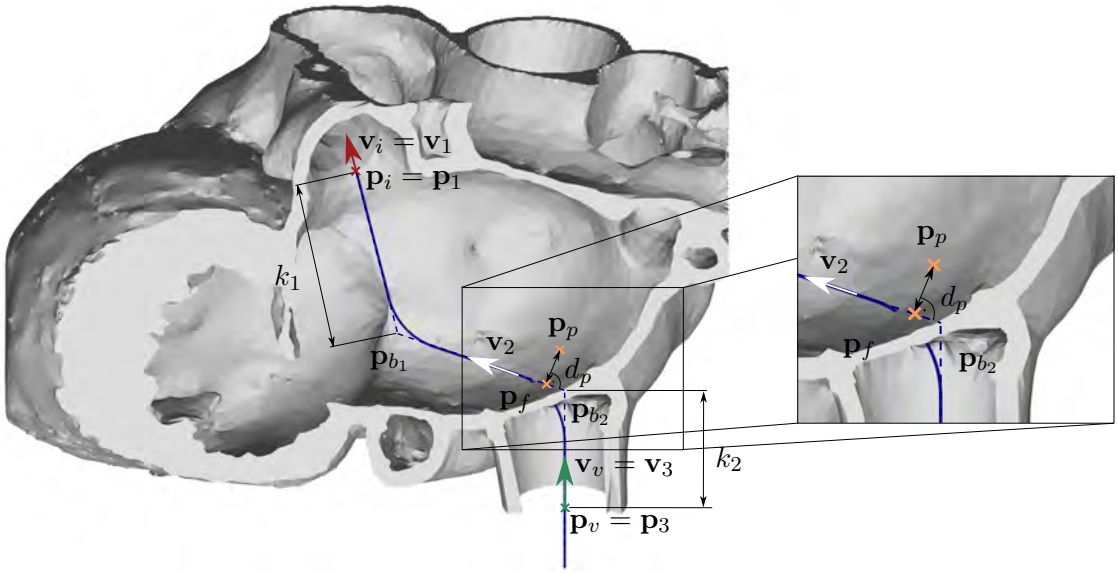

Figure 50 The catheter shape with tolerance at the puncture location is defined by the position and orientation of the boundary points and vectors at the planned implant position ($\mathbf{p}_i$ and $\mathbf{v}_i$) and the inferior vena cava ($\mathbf{p}_v$ and $\mathbf{v}_v$) and the distances k_1 and k_2 of the bending points $\mathbf{p}_{b_1}$ and $\mathbf{p}_{b_2}$ to the defined points at the position of the implant and the inferior vena cava. The second segment does not pass the interatrial septum at the planned puncture location but in a distance d_p to it that is minimized.

Tolerance at the Inferior Vena Cava. A tolerance can also be added at the inferior vena cava, allowing a deviation of the direction vector of the third segment of the catheter shape from the direction vector of the inferior vena cava as illustrated in Figure 51. The implant position and the direction vector of the implant define the first segment. The first variable parameter k_1 determines the distance of the first bending point to the implant position and therefore describes the position of the first bending point $\mathbf{p}_{b_1}$.

$$\mathbf{p}_{b_1} = \mathbf{p}_i - k_1 \cdot \mathbf{v}_i = \mathbf{p}_1 - k_1 \cdot \mathbf{v}_1 \tag{6.50}$$

The line connecting the bending point $\mathbf{p}_{b_1}$ and the puncture location $\mathbf{p}_p$ is the direction vector of the second segment $\mathbf{v}_2$, which ends at the second bending point $\mathbf{p}_{b_2}$. The position of $\mathbf{p}_{b_2}$ is defined by the second variable parameter k_2 describing the distance between the puncture location and the second bending point.

$$\mathbf{p}_{b_2} = \mathbf{p}_p - k_2 \cdot \frac{(\mathbf{p}_{b_1} - \mathbf{p}_p)}{|\mathbf{p}_{b_1} - \mathbf{p}_p|} = \mathbf{p}_p - k_2 \cdot \mathbf{v}_2 \tag{6.51}$$

The direction vector of the third segment $\mathbf{v}_3$ is equal to the connecting line between the second bending point and the point on the inferior vena cava $\mathbf{p}_v$.

$$\mathbf{v}_3 = \frac{\mathbf{p}_{b_2} - \mathbf{p}_v}{|\mathbf{p}_{b_2} - \mathbf{p}_v|} \tag{6.52}$$

Therefore, the deviation δ_v of the third segment of the catheter shape to the direction vector $\mathbf{v}_v$ of the inferior vena cava is

$$\delta_v = \arccos(\mathbf{v}_v \cdot \mathbf{v}_3) \tag{6.53}$$

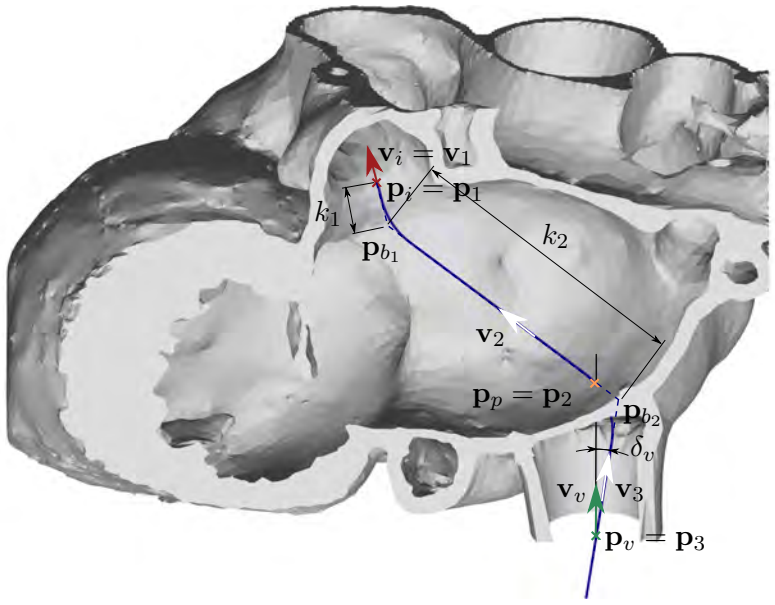

Figure 51 The catheter shape with tolerance at the inferior vena cava is defined by the position and direction vector at the planned implant position ($\mathbf{p}_i$ and $\mathbf{v}_i$), the location of the puncture point $\mathbf{p}_p$ and the inferior vena cava $\mathbf{p}_v$ as well as the distances k_1 and k_2 from the bending points $\mathbf{p}_{b_1}$ and $\mathbf{p}_{b_2}$ to the implant position and to the puncture location. The angular deviation δ_v between the third segment of the catheter $\mathbf{v}_3$ and the orientation of the inferior vena cava $\mathbf{v}_v$ is minimized.

Optimization of the Catheter Shape with Two Bends. A gradient-based optimization process is applied to find the best-suited values for the two independent variable parameters k_1 and k_2 for the calculation of the catheter shape. The target of the optimization is a minimization of the absolute value of the deviation from the planned boundary points and directions. The calculation formulas for the deviation of the different optimization approaches are mentioned in the paragraphs before (see equations 6.46,6.49 and 6.53). The minimum achievable value for the deviation is zero. The maximum value depends on the type of deviation. For angular deviations, the maximum value is π whereas the value for the deviation of the position is theoretically unlimited. However, values above 100 mm are not considered reasonable.

Penalty Functions. Minimization of the deviation alone is not sufficient, as it has to be ensured that the additional constraints like maximum or minimum angle values or distances between points are met. Penalty functions are added to the target function to describe the constraints and make sure that the solution is inside the boundaries. Those penalty functions are applied to maximum and minimum values of the two bending angles and the distances between the bending points and the boundary points and to a maximum value for the tolerance. The following equations show the calculation of the penalty function using the example of α_1. The penalty function must show a behavior similar to a step function with high values in the area outside the boundaries and values of approximately zero inside the boundaries. However, the target function for a gradient-based approach has to be continuous and differentiable in the relevant area. Therefore, the arc tangent function is used as a penalty function, as it is a continuous and differentiable function. Arc tangent functions are applied to all of the boundary values and penalize exceeding the maximum value or coming below the minimal value. If the parameter lies inside the boundaries, the penalty function has a value of approximately zero and if it is outside the boundary it is scaled to h. h is chosen well above the range that is reasonably reachable by the calculation of the deviation with a value of 10 for deviations of the angle and 1000 mm for deviations of the position. The arc tangent function has to be shifted so that its step is located at the boundary maximum value $\alpha_{1,max}$ or the minimal value $\alpha_{1,min}$ (see Figure 52). Furthermore, the step should be as sharp as possible. The steepness of

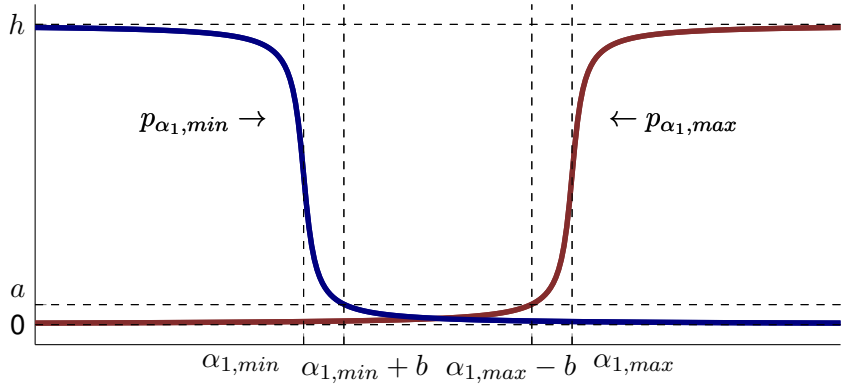

Figure 52 The arc tangent function is used as a penalty function that penalizes exceeding the maximum or minimum boundary values. The penalty function for the angle α_1 is shown as an example. The function is a combination of the two functions $p_{\alpha_1,max}$ and $p_{\alpha_1,min}$. The functions have a value of houtside the limits and almost zero if the limits are respected. The shape of the function in the region of the transition is defined by the value a in a distance of b from the boundary value.

the step is adapted by the parameter g. The penalty function for each variable is a composition of the functions for exceeding the maximum and falling below the minimum value if applicable.

$$\begin{aligned} p_{\alpha_1,max} &= \left(\arctan\left((\alpha_1 - \alpha_{1,max}) \cdot g\right) + \frac{\pi}{2}\right) \cdot \frac{h}{\pi} \\ p_{\alpha_1,min} &= \left(\arctan\left((\alpha_{1,min} - \alpha_1) \cdot g\right) + \frac{\pi}{2}\right) \cdot \frac{h}{\pi} \\ p_{\alpha_1} &= p_{\alpha_1,max} + p_{\alpha_1,min}. \end{aligned} \tag{6.54}$$

The parameter g is adapted so that the penalty function has a value of b at a distance of a from the boundary point inside the boundaries.

$$\begin{aligned} p_{\alpha_1,max}(\alpha_{1,min} + a) = p_{\alpha_1,max}(\alpha_{1,max} - a) &= b \\ g &= \frac{\tan((0.5 - \frac{b}{h}) \cdot \pi)}{a} \end{aligned} \tag{6.55}$$

The target functions f_i, f_p and f_v of the optimization approaches with tolerances at the implant, the puncture and the inferior vena cava respectively are composed of the square value of the deviation value and the sum of the values of the penalty functions.

$$\begin{aligned} f_i &= \delta_i^2 + p_{\alpha_1} + p_{\alpha_2} + p_{l_{11}} + p_{l_{12}} + p_{l_{21}} + p_{l_{22}} + p_{\delta_i} \\ f_p &= d_p^2 + p_{\alpha_1} + p_{\alpha_2} + p_{l_{11}} + p_{l_{12}} + p_{l_{21}} + p_{l_{22}} + p_{d_p} \\ f_v &= \delta_v^2 + p_{\alpha_1} + p_{\alpha_2} + p_{l_{11}} + p_{l_{12}} + p_{l_{21}} + p_{l_{22}} + p_{\delta_v} \end{aligned} \tag{6.56}$$

Newton-Raphson-Method. The minimum values of a function can be found by identifying the critical points where the components of the gradient of the function are zero. This means the nonlinear system

$$\nabla f = 0 \tag{6.57}$$

has to be solved. A damped Newton-Raphson-Method is applied to find the parameters for a vanishing gradient of the target function. The parameters that are optimized are combined to the variable $\mathbf{k} = [k_1 \quad k_2]^T$ and in an iterative process the value is calculated by

$$\mathbf{k}^{j+1} = \mathbf{k}^j - w_f^j [\mathbf{H}_f(\mathbf{k}^j)]^{-1} \nabla f(\mathbf{k}^j) \tag{6.58}$$

where w_f is a damping parameter, $[\mathbf{H}_f(\mathbf{k})]^{-1}$ is the inverse of the Hessian matrix and $\nabla f(\mathbf{k})$ the gradient of the target function. The iteration is stopped when the absolute values of the components of the gradient $\nabla f(\mathbf{k})$ and the absolute difference of the values of the parameters between two iteration steps $\mathbf{k}^{j+1}$ and $\mathbf{k}^j$ are below certain limits ϵ_g and ϵ_v (see Figure 53).

$$\begin{aligned} \left| \left. \frac{\partial f}{\partial k_m} \right|_{\mathbf{k}^{j+1}} \right| &< \epsilon_g = 10^{-6} \\ \left| \mathbf{k}^{j+1} - \mathbf{k}^j \right| &< \epsilon_v = 10^{-5} \end{aligned} \tag{6.59}$$

Herein k_m are the components of the vector $\mathbf{k}$.

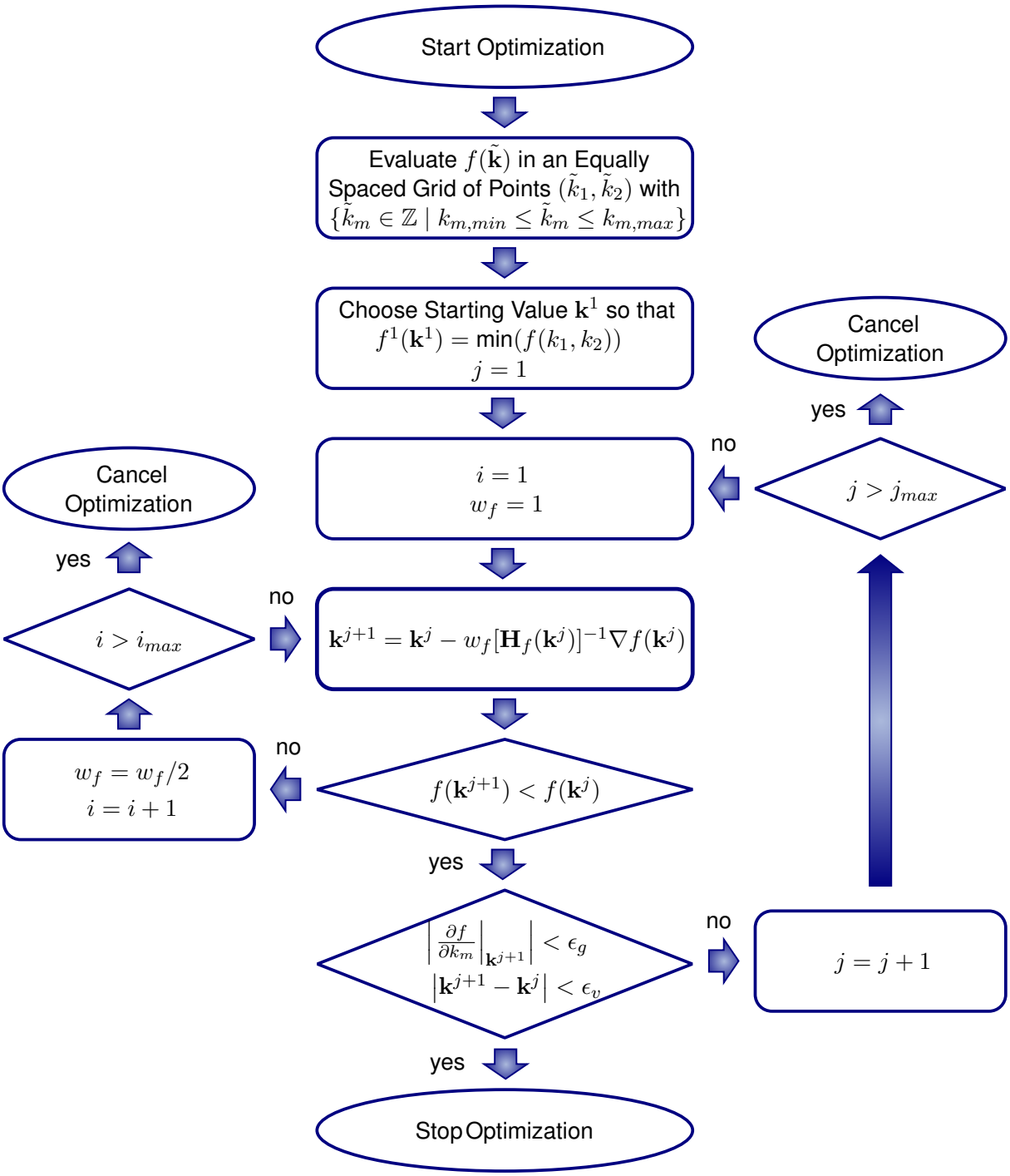

Figure 53 An iterative process is applied to find the optimized parameters for the double bended catheter. The starting value is calculated by gridding the data and determination of the minimal value. Two iteration loops are used to adapt the parameters. The calculation is stopped when the certain limits are reached and it is aborted when the number of iterations exceeds a maximum number.

The damping parameter w_f lies between zero and one and is determined by a line search. Starting with the value one, the new parameters $\mathbf{k}^{j+1}$ and the corresponding value of the target function is calculated. The damping parameter is halved as long as the value of the target function resulting from the new variable parameters $f(\mathbf{k}^{j+1})$ is bigger than the value calculated with the old parameters $f(\mathbf{k}^j)$.

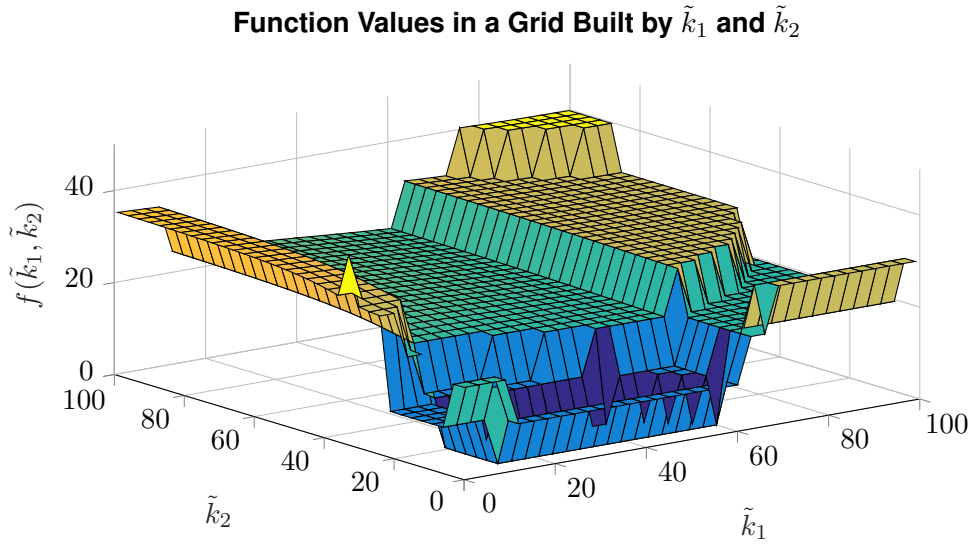

Figure 54 The target function is evaluated in a grid that is built by the equally spaced parameters $\tilde{k}_1$ and $\tilde{k}_2$. Their starting values for the optimization are chosen by the location of the minimum function value in this grid.

As the success of the Newton-Raphson-Method is highly dependent on the starting value and it is only possible to find a local, not a global minimum, the starting value has to be chosen carefully. The target function is evaluated in an equally spaced grid of points $(\tilde{k}_1, \tilde{k}_2)$. To do so, the integer values $\tilde{k}_m$ of the parameters k_m between their boundary values are considered.

$$\{\tilde{k}_m \in \mathbb{Z} \quad | \quad k_{m,min} \leq \tilde{k}_m \leq k_{m,max}\}, \quad m = 1, 2 \tag{6.60}$$

The value of the target function is calculated using every possible combination of the two parameters $\tilde{k}_1$ and $\tilde{k}_2$. These values can be visualized by a surface plot as shown in Figure 54. The starting value $\mathbf{k}^1 = [k_1^1, k_2^1]^T$ that has the minimum value for the target function in the grid is chosen as the starting point for the optimization. If there is no combination of the two parameters that meets all of the boundary conditions, the calculation is aborted and the boundary values or boundary points have to be adapted to find a valid solution.

The number of iterations j and i for every loop is recorded. If any of the two iteration loops exceeds a boundary number of iterations i_{max} or j_{max}, which are set to 100, the calculation is aborted and considered as not successful.

6.8.3 Catheter with Variable Curvature

As the shaping process with the use of the bending forms does not have any constraints concerning the configuration of the catheter shape, even complex shapes can be processed that cannot be produced by standard bending machines. Therefore, a varying curvature can be allowed in the curved segments, connecting the boundary points with a smooth curve. This is achieved by describing the curved segments using splines. This calculation approach allows the definition of further boundary conditions and the control of the direction vector at each boundary point including the direction vector at the puncture location $\mathbf{v}_p$. No optimization is required, as the boundary points are met exactly.

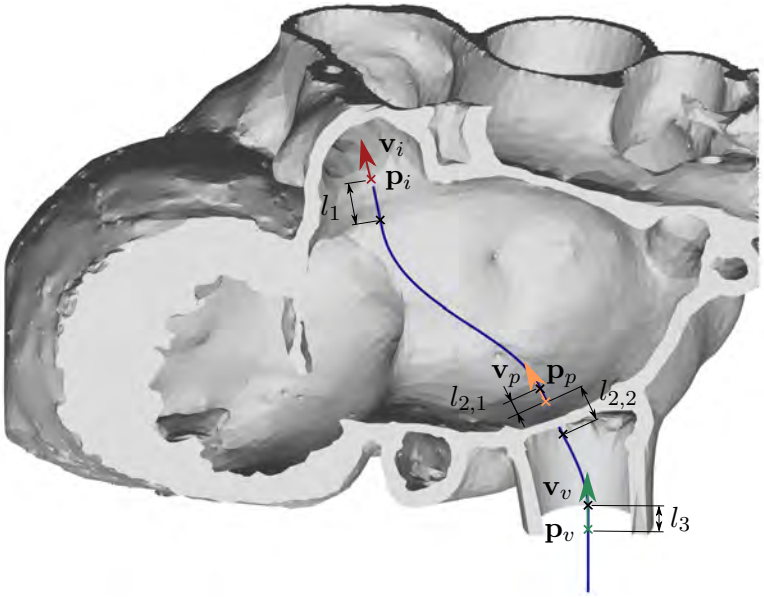

Figure 55 The catheter shape with varying curvature is described by a spline interpolation that is evaluated separately for the segments in the left and right atrium. Straight segments with lengths l_1 to l_3 can be added at the boundary points.

To ensure that the connections between straight and curved segments is smooth and the direction vector at the boundary points can be controlled, a cubic Hermite spline is used to describe the catheter shape. Cubic Hermite splines allow the control of the direction vector as well as the position at every knot. The spline is calculated for each of the three directions in space and the two curved segments separately. A cubic Hermite spline segment between two points $\mathbf{p}_{s0}$ and $\mathbf{p}_{s1}$ with the direction vectors $\mathbf{v}_{s0}$ and $\mathbf{v}_{s1}$ is calculated as

$$\mathbf{p}(t) = \begin{bmatrix} t^3 & t^2 & t & 1 \end{bmatrix} \cdot \begin{bmatrix} 2 & -2 & 1 & 1 \\ -3 & 3 & -2 & -1 \\ 0 & 0 & 1 & 0 \\ 1 & 0 & 0 & 0 \end{bmatrix} \cdot \begin{bmatrix} \mathbf{p}_{s0} \\ \mathbf{p}_{s1} \\ \mathbf{v}_{s0} \\ \mathbf{v}_{s1} \end{bmatrix} \quad , \; t \in [0,1] \tag{6.61}$$

with the parameter t ranging from zero to one.

If straight segments are required at the tip of the catheter or the puncture location, the boundary points for the calculation of the spline segments can be moved along the direction vector at the boundary point. The lengths of the straight segments are defined as l_1, $l_{2,1}$, $l_{2,2}$ and l_3. The resulting catheter shape is a combination of straight and curved segments as shown in Figure 55.

The calculation with the presented spline description has the characteristic that the length of the vectors control the appearance of the curve including the curvature of the line. The curvature is a critical parameter for the calculation, as catheter shapes with strong curvatures are difficult to produce without damaging the catheter. If the vector length is too short, the curvature is very sharp and the bend appears like a kink. For vectors that are too long, the line starts to loop as shown in

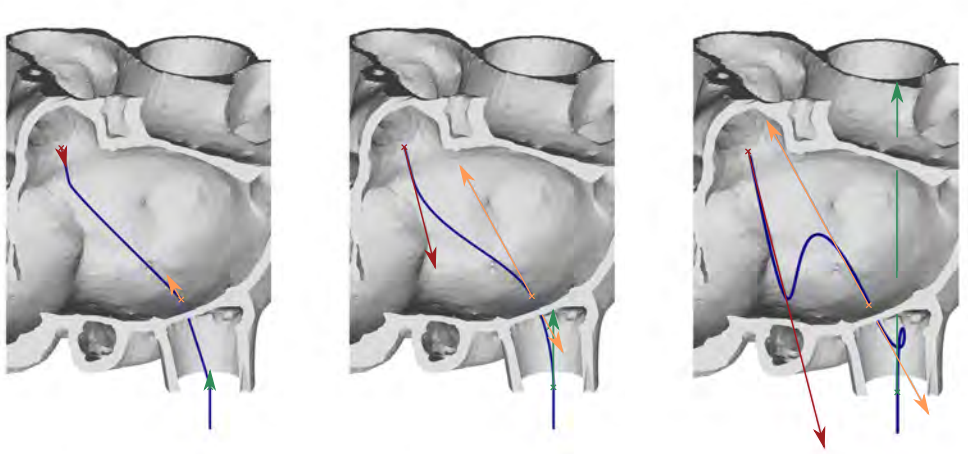

Figure 56 The length of the vectors at the boundary points determine the curvature of the spline. A standard value is to use the vectors of the same length as the distances between the points (middle). The image on the left shows vectors with a fifth of the length and on the right, the vectors are five times the length of the distance. If the vectors are too short, the spline appears like a kinked line with strong curvature (left). If they are too long, the line tends to loop (right).

Figure 56. The curvature of a three-dimensional line in space is calculated as

$$\kappa = \frac{|\mathbf{p}'(t) \times \mathbf{p}''(t)|}{|\mathbf{p}'(t)|^3}. \tag{6.62}$$

The resulting term is complex and non-linear. A standard value for the length that showed good resulting curvatures is equal to the distance of the two knots at the ends of the line. Table 1 shows the values for the calculation of the two spline segments.

Table 1 Variables for the spline calculation.

	$\mathbf{p}_{s0}$	$\mathbf{p}_{s1}$	$\mathbf{v}_{s0}$	$\mathbf{v}_{s1}$
Left Atrium	$\mathbf{p}_i - l_1 \cdot \mathbf{v}_i$	$\mathbf{p}_p + l_{2,1} \cdot \mathbf{v}_p$	$\mathbf{v}_i \cdot \lvert\mathbf{p}_i - \mathbf{p}_p\rvert$	$\mathbf{v}_p \cdot \lvert\mathbf{p}_i - \mathbf{p}_p\rvert$
Right Atrium	$\mathbf{p}_p - l_{2,2} \cdot \mathbf{v}_p$	$\mathbf{p}_v + l_3 \cdot \mathbf{v}_v$	$\mathbf{v}_p \cdot \lvert\mathbf{p}_p - \mathbf{p}_v\rvert$	$\mathbf{v}_v \cdot \lvert\mathbf{p}_p - \mathbf{p}_v\rvert$

6.8.4 Catheter Shape with Four Bends

The double bended catheter does not make use of the full potential that the patient-individual calculation of a catheter shape and especially the bending process offers. It is possible to produce more complex catheter shapes and this calculation method does not allow the control of the direction vector at the transseptal puncture location. Additionally, the compliance with the boundary conditions cannot be guaranteed. In contrast, the curvature of the spline catheter is difficult to control. Therefore, a catheter shape that combines the advantages of the two approaches is defined. This approach is based on Graf *et al.* (2018).

Instead of the spline segment, two circular bends are allowed in every atrium (see Figure 57). By defining two bends per atrium, a free choice of the bend points and their direction vectors is possible with compliance to the boundary points and vectors. To facilitate the shaping of the catheter, the

position of the bends is adapted to maximize the bending radii. The catheter pathway runs through the puncture location. Its direction vector $\mathbf{v}_{p,\delta}$ at that point is affected by the normal vector on the left atrium, but a certain deviation is allowed.

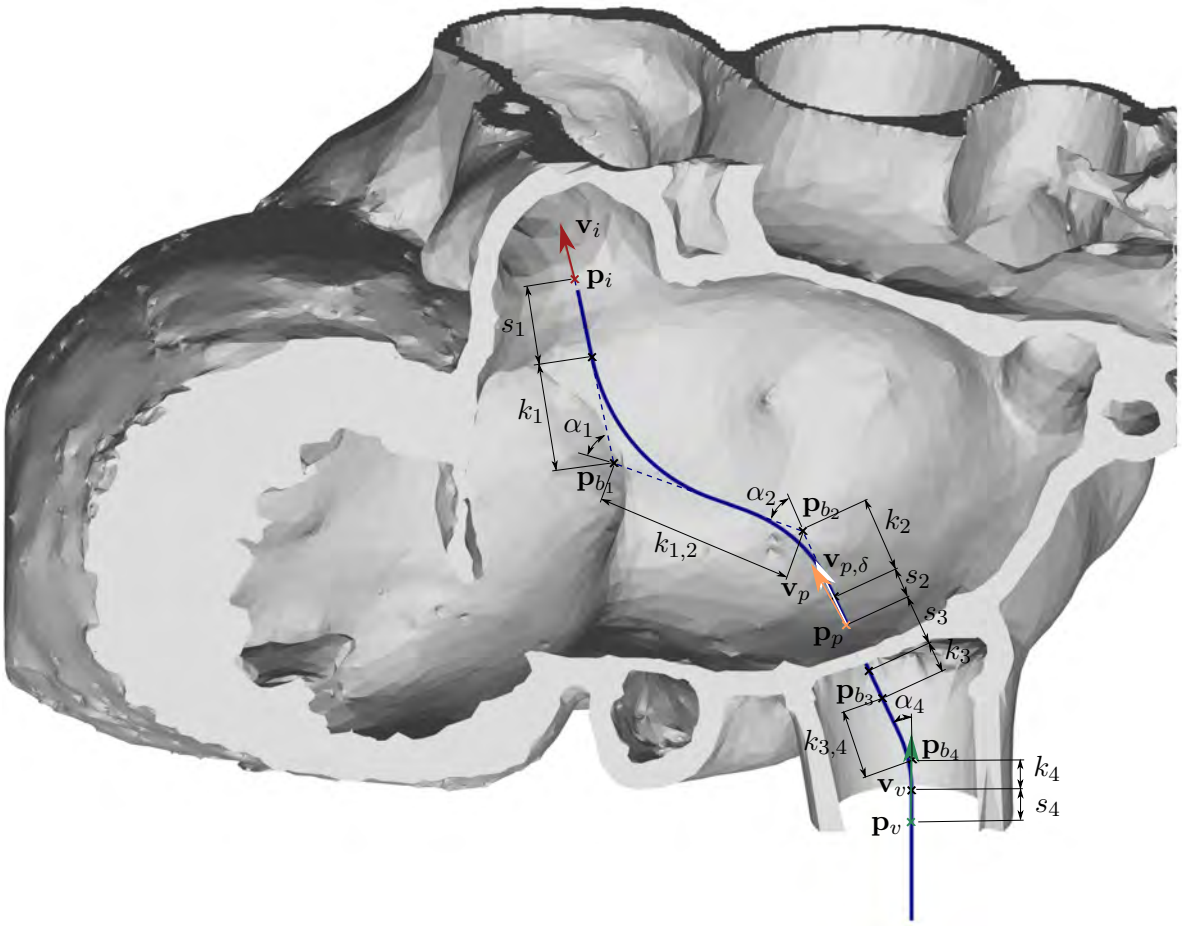

Figure 57 A catheter with two bends per atrium is defined (bending points $\mathbf{p}_{b_1}$ to $\mathbf{p}_{b_4}$). The catheter passes through the puncture location but a deviation from the planned vector at that point is allowed. The catheter shape with the four bends is calculated by an optimization approach that maximizes the bending radii. At every boundary point, straight segments with lengths s_1 to s_4 can be defined. The variables that can be altered are the direction vector through the puncture point $\mathbf{v}_{p,\delta}$ and the distances k_1 to k_4 of the bends to the adjacent boundary points.

The calculation of the catheter shape with four bends is performed by an optimization process. In a first step, the segments of the catheter are modeled as straight lines with the bending points being the intersection points of the lines. The parameters that are optimized are the positions of the four bending points, which are described by their distances k_1, k_2, k_3 and k_4 from the adjacent boundary points, and the two angles γ_1 and γ_2 that describe the deviation of the vector through the puncture site from the normal vector on the left atrium.

The orientation of the vector through the puncture point $\mathbf{v}_{p,\delta}$ is described by its deviation from the planned puncture vector $\mathbf{v}_p$, which is normal to the surface of the left atrium. The new vector is calculated by two rotations around the basis axes of the coordinate system. γ_1 describes the rotation angle around the ${}^{mod}\mathbf{x}_{mod}$-axis and γ_2 around the ${}^{mod}\mathbf{y}_{mod}$-axis (see Figure 58). With these two angles, the total angular deviation δ_{v_p} of the unit vector $\mathbf{v}_{p,\delta}$ from $\mathbf{v}_p$ can be determined. This description of the vector will not work if the original vector lies in the ${}^{mod}\mathbf{x}_{mod}\,{}^{mod}\mathbf{y}_{mod}$-plane.

However, this is very unlikely due to the typical shape of the left atrium in the region of the fossa ovalis.

$$\mathbf{R}_x(\gamma_1) = \begin{pmatrix} 1 & 0 & 0 \\ 0 & \cos(\gamma_1) & -\sin(\gamma_1) \\ 0 & \sin(\gamma_1) & \cos(\gamma_1) \end{pmatrix}, \quad \mathbf{R}_y(\gamma_2) = \begin{pmatrix} \cos(\gamma_2) & 0 & \sin(\gamma_2) \\ 0 & 1 & 0 \\ -\sin(\gamma_2) & 0 & \cos(\gamma_2) \end{pmatrix}$$
$$\mathbf{v}_{p,\delta} = \mathbf{R}_y(\gamma_2) \cdot \mathbf{R}_x(\gamma_1) \cdot \mathbf{v}_p \tag{6.63}$$
$$\delta_{v_p} = \arccos\left(\mathbf{v}_{p,\delta} \cdot \mathbf{v}_p\right)$$

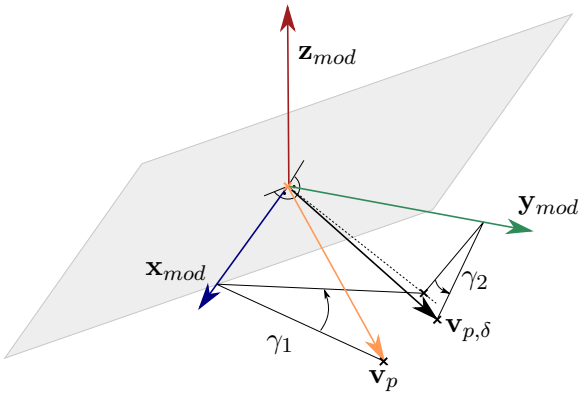

Figure 58 The orientation of the vector through the puncture location is described by the deviation from the planned puncture vector $\mathbf{v}_p$, which is perpendicular to the surface of the left atrium. The new vector $\mathbf{v}_{p,\delta}$ is calculated by a rotation by the angle γ_1 about the ${}^{mod}\mathbf{x}_{mod}$-axis and by γ_2 about the ${}^{mod}\mathbf{y}_{mod}$-axis.

At each boundary point, a straight segment can be added before the curvature may start. Therefore, the lengths s_1 to s_4 of the straight segments are added to the variable parameters k_1 to k_4 before calculating the positions of the four bending points.

$$\begin{aligned} \mathbf{p}_{b_1} &= \mathbf{p}_i - (k_1 + s_1) \cdot \mathbf{v}_i \\ \mathbf{p}_{b_2} &= \mathbf{p}_p + (k_2 + s_2) \cdot \mathbf{v}_{p,\delta} \\ \mathbf{p}_{b_3} &= \mathbf{p}_p - (k_3 + s_3) \cdot \mathbf{v}_{p,\delta} \\ \mathbf{p}_{b_4} &= \mathbf{p}_v + (k_4 + s_4) \cdot \mathbf{v}_v \end{aligned} \tag{6.64}$$

Using these points, the distances $k_{1,2}$ and $k_{3,4}$ between the two bending points in every atrium can be calculated.

$$\begin{aligned} k_{1,2} &= |\mathbf{p}_{b_2} - \mathbf{p}_{b_1}| \\ k_{3,4} &= |\mathbf{p}_{b_4} - \mathbf{p}_{b_3}| \end{aligned} \tag{6.65}$$

The bending angles are calculated using the dot product of the adjacent lines. Each of them depends on the two variable parameters of the respective atrium and the rotation angles γ_1 and γ_2 of the vector through the puncture point.

The bending radius at every bend point is limited by three factors: the distance between the boundary point and the respective bend point, the distance to the second bending point in the atrium and the bending angle at the bending point. For every atrium, three bending radii are calculated that are limited by the lengths of the segments in the atrium as illustrated in Figure 59. In the left atrium, r_1 and r_3 are defined by the bending angles, the distances of the bending points to the implant position and the puncture point, respectively, and the lengths of straight segments that are added at the boundary points. For the calculation of r_2 that is limited by the distance between the bending points it is assumed that the bending radius is similar for both bends and that the entire straight segment between the bending points is part of the two radii. Therefore, the radii of the two bends intersect at one point on the line.

$$\begin{aligned} r_1 &= \frac{k_1}{\tan(0.5 \cdot (\pi - \alpha_1))} = \frac{k_1}{\tan(\frac{\alpha_1}{2})} \\ r_2 &= \frac{k_{1,2}}{\tan(0.5 \cdot (\pi - \alpha_1)) + \tan(0.5 * (\pi - \alpha_2))} = \frac{k_{1,2}}{\tan(\frac{\alpha_1}{2}) + \tan(\frac{\alpha_2}{2})} \\ r_3 &= \frac{k_2}{\tan(0.5 \cdot (\pi - \alpha_2))} = \frac{k_2}{\tan(\frac{\alpha_2}{2})} \end{aligned} \tag{6.66}$$

The calculated bending radii depend on the variable parameters k_1 and k_2 and the angles γ_1 and γ_2. For every bend, the minimum value of the two respective bending radii is determining the maximum bending radius that can be achieved and that is chosen for the catheter shape.

$$\begin{aligned} r_{b1}(k_1, k_2, \gamma_1, \gamma_2) &= \mathsf{min}(r_1, r_2) \\ r_{b2}(k_1, k_2, \gamma_1, \gamma_2) &= \mathsf{min}(r_2, r_3) \end{aligned} \tag{6.67}$$

The calculation for the bending radii r_3 to r_6 in the right atrium, which depend on the parameters k_3, k_4, γ_1 and γ_2, is done analogously.

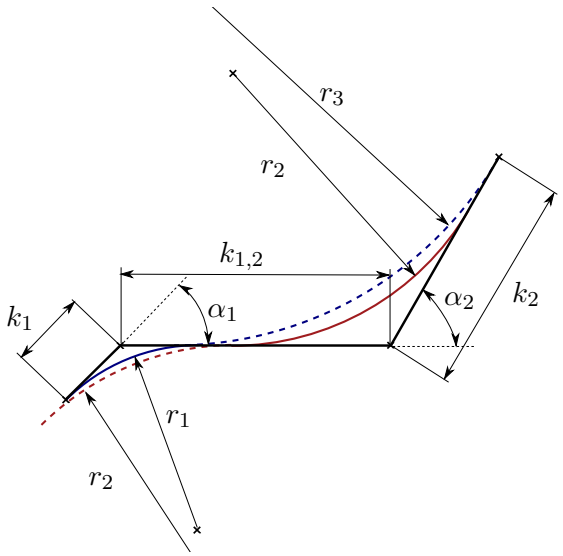

Figure 59 The possible bending radii are limited by the bending angles and distances between the boundary points and the bend points (blue) or the distances between the bending points (red). For every bend, the smaller one of the two applicable values is determining.

The goal of the optimization is to avoid small bending radii. The minimal value of the calculated bending radii r_1 to r_6 should be as big as possible which means a maximization of the minimum radius is performed. In the calculation, the curvature of the bends is used that is defined as the inverse value of the bending radius. Therefore, a minimization problem of the maximum curvature value κ_{max} is solved. To obtain a continuous and differentiable function, the maximum function is approximated by a function of the form

$$f(x) = \sqrt[n_r]{\sum_{i=1}^{I} x_i^{n_r}}. \tag{6.68}$$

For high values of n_r, this function approaches the maximum of the values x_i. A value of n_r = 10 was used for the calculation.

The maximum of the curvature values is calculated by using the inverse values of the radii.

$$\kappa_{max} = \sqrt[n_r]{\frac{1}{r_1^{n_r}} + \frac{1}{r_2^{n_r}} + \frac{1}{r_3^{n_r}} + \frac{1}{r_4^{n_r}} + \frac{1}{r_5^{n_r}} + \frac{1}{r_6^{n_r}}} \tag{6.69}$$

The target function of the optimization is composed of the maximum curvature κ_{max}, the deviation from the vector normal to the wall of the left atrium at the puncture location δ_{v_p} and penalty functions that penalize the violation of the boundary conditions.

$$f(k_1, k_2, k_3, k_4, \gamma_1, \gamma_2) = \kappa_{max} + m_f \cdot \delta_{v_p} + p \tag{6.70}$$

m_f is a factor to weight the influence of the deviation from the puncture vector in relation to the curvature. The higher the value, the smaller is the resulting deviation from the puncture vector. The initial value of m_f is 0.1, which means a bending radius of 10 mm has the same weight in the target function as a deviation of 57° from the puncture vector.

The penalty functions are arc tangent functions similar to those presented in chapter 6.8.2 for the calculation of the double bended catheter. They are evaluated separately for each of the atria and then combined to an overall penalty function. The boundary conditions that are controlled by the penalty functions are upper and lower values for the lengths of the segments k_1, k_2, k_3 and k_4 and the four bending angles α_1 to α_4 as well as an upper limit for the deviation δ_{v_p} from the puncture vector.

$$\begin{aligned} p_{left} &= p_{\alpha_1} + p_{\alpha_2} + p_{k_1} + p_{k_2} \\ p_{right} &= p_{\alpha_3} + p_{\alpha_4} + p_{k_3} + p_{k_4} \\ p &= p_{left} + p_{right} + p_{\delta_{v_p}} \end{aligned} \tag{6.71}$$

The Newton-Raphson-Method is applied to find the set of the six parameters k_1, k_2, k_3, k_4, γ_1 and γ_2 that result in a vanishing gradient ∇f of the target function. For the calculation, the parameters are combined to the vector $\mathbf{k} = [k_1, k_2, k_3, k_4, \gamma_1, \gamma_2]^T$ and the six components of the vector are named k_m.

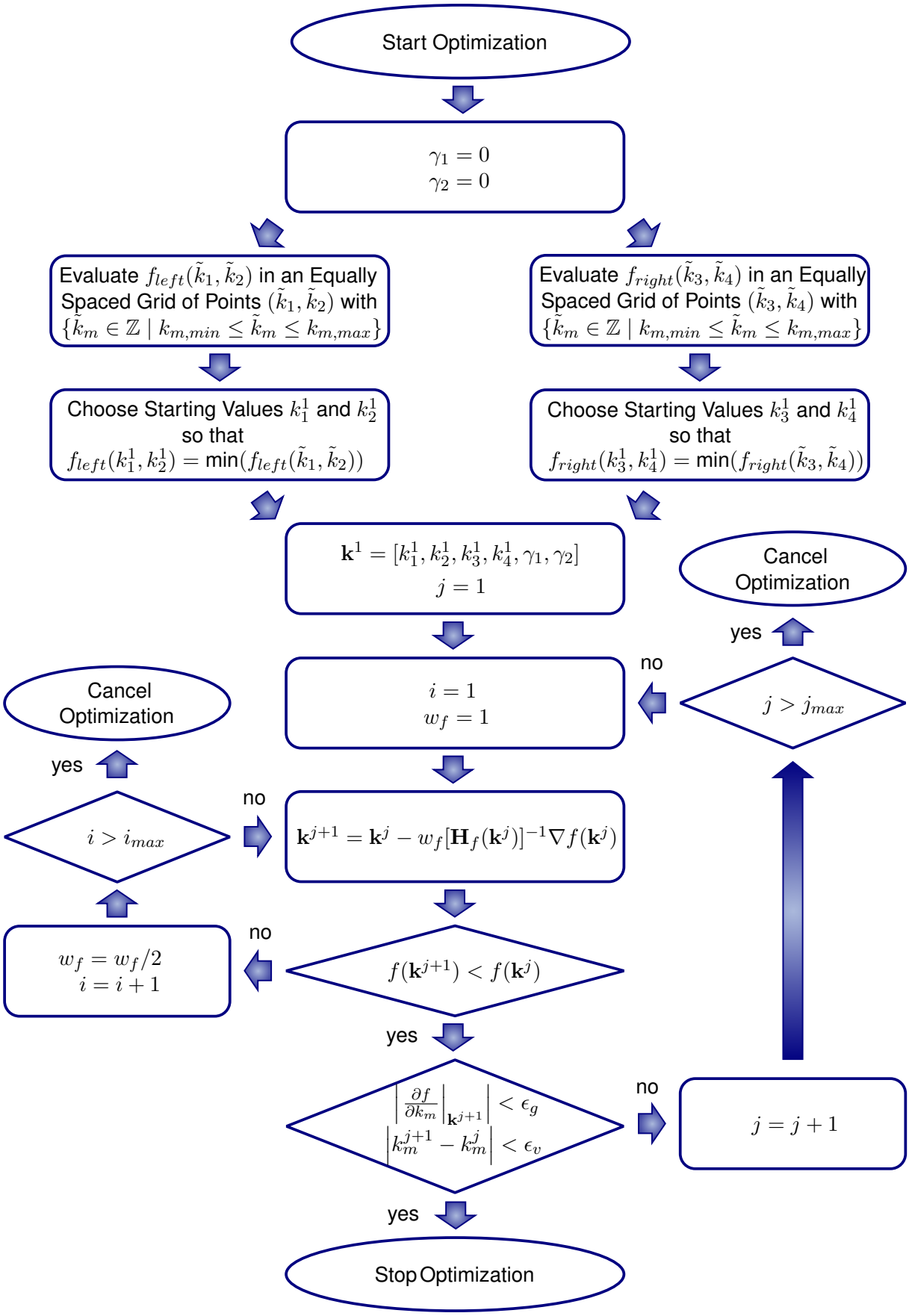

Figure 60 The parameters for the description of the catheter shape with four bends are determined in an optimization process. A damped Newton-Raphson-Method is applied in an iterative process to find the parameters $\mathbf{k}$ for a vanishing gradient of the target function.

As a starting point, the deviation of the vector through the puncture position from the planned vector is set to zero. The functions f_{left} and f_{right} that find the minimum curvature for each atrium separately are evaluated with the defined values $\gamma_1 = 0$ and $\gamma_2 = 0$.

$$\begin{aligned} \gamma_1 = 0, \quad \gamma_2 = 0 \\ f_{left}(k_1, k_2) = \sqrt[n_r]{\frac{1}{r_1^{n_r}} + \frac{1}{r_2^{n_r}} + \frac{1}{r_3^{n_r}}} + p_{left} \\ f_{right}(k_3, k_4) = \sqrt[n_r]{\frac{1}{r_4^{n_r}} + \frac{1}{r_5^{n_r}} + \frac{1}{r_6^{n_r}}} + p_{right} \end{aligned} \tag{6.72}$$

With this precondition, both functions depend on only two variables and they are evaluated in a grid of points that is built by these equally spaced variables. To do so, only the integer values of the parameters that lie between the boundary values are considered.

$$\{\tilde{k}_m \in \mathbb{Z} \quad | \quad k_{m,min} \leq \tilde{k}_m \leq k_{m,max}\}, \quad m = 1, 2, 3, 4 \tag{6.73}$$

For both atria the combination of the two variables $(\tilde{k}_1, \tilde{k}_2)$ and $(\tilde{k}_3, \tilde{k}_4)$ that cause minimal curvatures of the segments while complying with the boundary conditions are selected as starting values for the optimization.

As for the optimization of the double bended catheter, a damped optimization with the damping parameter w_f is performed, which is stopped when the absolute difference of the parameter values between two iterations k_m^{j+1} and k_m^j for all parameters and the absolute values of the components of the gradient ∇f fall below the boundary values ϵ_v and ϵ_g (see Figure 60).

$$\begin{aligned} \left| \left. \frac{\partial f}{\partial k_m} \right|_{\mathbf{k}^{j+1}} \right| < \epsilon_g = 10^{-6} \\ \left| k_m^{j+1} - k_m^j \right| < \epsilon_v = 10^{-5} \end{aligned} \tag{6.74}$$

The optimization is also canceled if the number of iterations exceeds the limiting values j_{max} and i_{max}, which are both set to 100.

An alternative possibility to avoid sharp bends would be to include the bending angles into the target function so that the bending angles are also minimized. However, bends in the catheter are necessary to be able to steer the catheter by rotation. If the bending angles are included into the target function, depending on the weighting, the bending angles are reduced and the shape of the catheter is straighter what might complicate the steering.

6.9 Visualization of the Calculated Catheter Shape

After the calculation of a patient-individual catheter shape or the virtual insertion of the standard catheter into the boundaries, the calculated catheter shape is visualized in a three-dimensional representation as well as projected into the orthogonal image data slices to evaluate its position

relative to the anatomy of the patient. Furthermore, a stack of image slices orthogonal to the catheter axis is calculated. As no segmentation of the heart is performed, the display of the calculated shape is necessary to allow manual inspection of the calculated catheter shape by the physician to detect unwanted intersections of the catheter pathway with heart walls or unwanted behavior of the catheter shape. The catheter shape is visualized based on the centerline of the catheter with the transformation matrices for every centerline point and therefore it is independent of the used calculation method.

Display in the Planning Program. The pathway of the catheter is displayed in three orthogonal image slices and a fourth image is provided that shows the image slice that lies orthogonal to the catheter axis. For each of the four displayed images, a stack of images is available and one slice is chosen for the display. Using a slider, the user can select the appropriate slice. The position of the chosen slice is marked by a line in the other images and by a frame in the three-dimensional representation of the catheter.

6.9.1 Three-Dimensional Representation of the Catheter

A three-dimensional representation of the catheter as shown in Figure 61 provides an overall impression of the resulting catheter shape and allows easy detection of any mistakes in the calculation. It can be realized by a description of the outer surface of the catheter by faces and vertices. Therefore, a circle with the diameter of the catheter is described by a number of points in the $\mathbf{x}_{c_k}\mathbf{y}_{c_k}$-plane. The circle is transformed to every point on the centerline of the catheter shape with the normal vector on the circle pointing along the catheter axis. The sidewalls are described by triangles that result from the interconnection of the points of the various cross-sections on top of each other. For the three-dimensional representation of the catheter, in the straight segments of the catheter center line only points at the beginning and end are necessary. Thus, the catheter shape can be described by the points in the curved segments and one start and end point of the catheter.

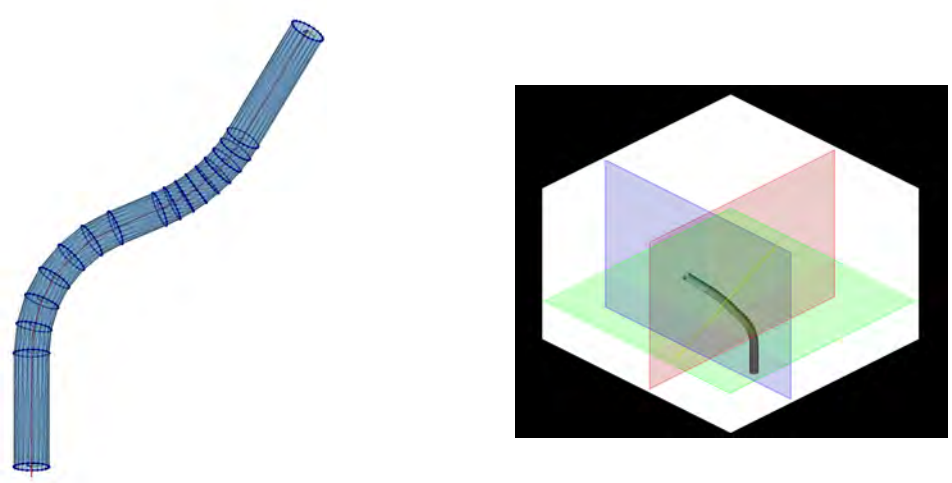

Figure 61 A three-dimensional representation gives and overall impression of the resulting catheter shape. It is produced by transforming the points of a circle with the catheter diameter into every point on the catheter centerline. The three-dimensional representation is displayed together with frames that offer information about the position of the other displayed image slices with the projected catheter as shown in Figure 62.

6.9.2 Projection of the Catheter into the Orthogonal Images

The shape of the catheter can be projected into the orthogonal images of the patient as illustrated in Figure 62. It is overlaid on the image slices to check the relative position of the catheter to the anatomical structures. In order to project the catheter shape into the image data, the information whether it is part of the catheter shape or not has to be available for every voxel of the image. Therefore, a binary matrix with the same size as the image matrix that contains this information is defined.

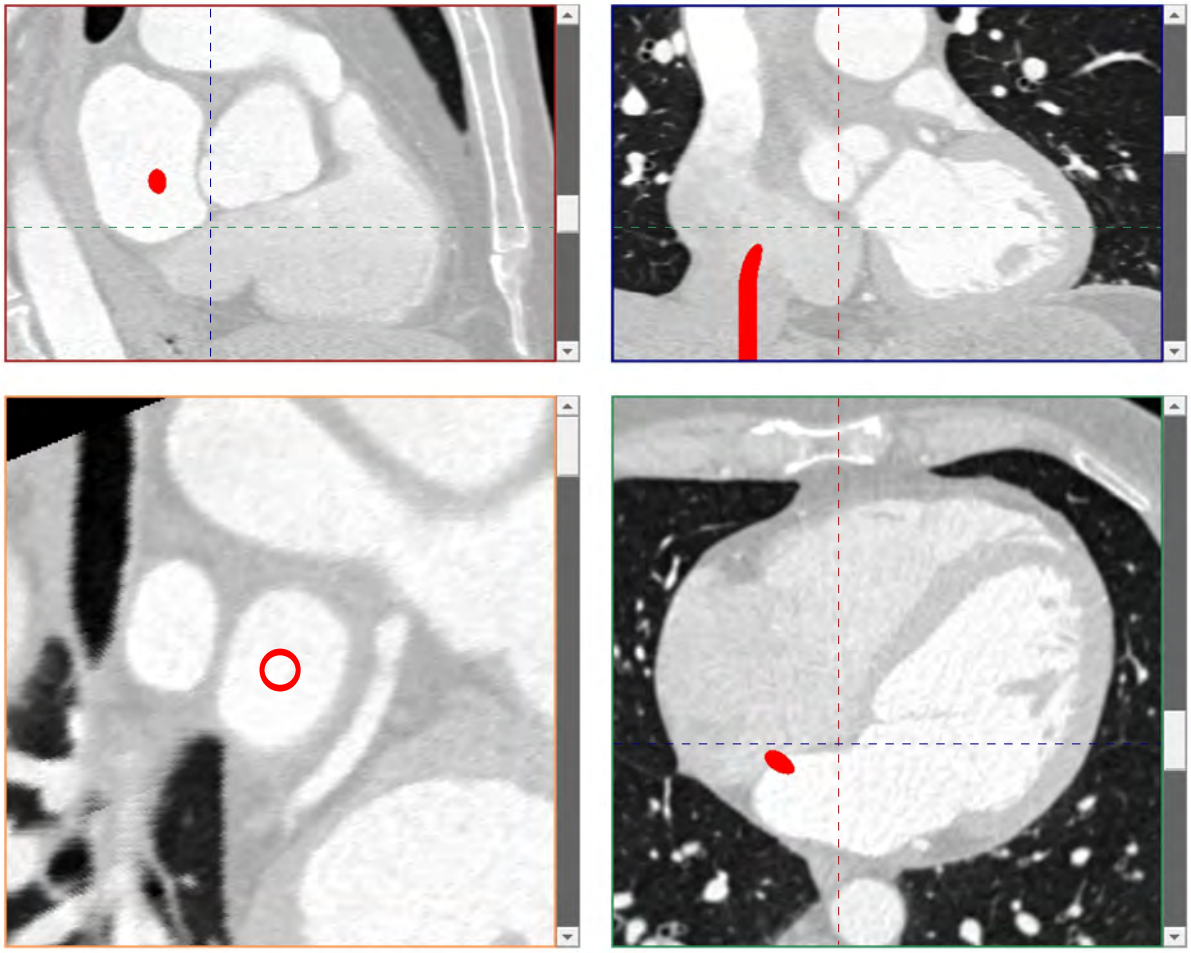

Figure 62 The catheter is projected into the image data and overlaid on the three orthogonal image slices. Furthermore, an image stack perpendicular to the catheter axis is calculated and displayed (bottom left).

To determine if a voxel is part of the catheter, the distance between the voxel and the catheter centerline is calculated. All voxels with a distance of less than the catheter radius are considered part of the catheter. However, the centerline is described by points and not by a formula. Therefore, the distances have to be evaluated point by point on the centerline. To get good results and enable a smooth display of the catheter shape, the distance between the points on the catheter centerline has to be smaller than the catheter radius not only in the curved but also in the straight segment.

Around every point on the centerline, a cubic ROI with a side length of at least the catheter radius is defined, whereby the point on the centerline does not necessarily lie in the center of a voxel. For every voxel in this ROI, the distance to the centerline point is evaluated and if it is smaller than the

catheter radius, the value of the voxel is set to one. The ROI is evaluated for every point on the centerline (see Figure 63).

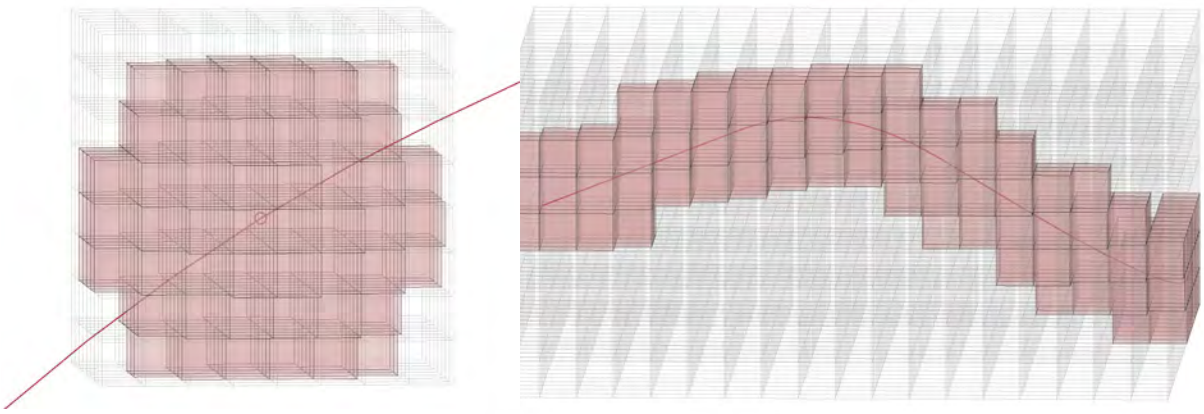

Figure 63 To show the catheter in the orthogonal image data, a voxel data set indicating if the voxel is part of the catheter or not has to be calculated. Voxels with a distance of less than the catheter radius to the points on the catheter centerline are considered part of the catheter. The distances are evaluated at a ROI around every point on the centerline.

6.9.3 Image Planes Orthogonal to the Catheter Axis

In addition to the projection of the catheter into the orthogonal image slices, image planes perpendicular to the catheter axis are displayed to enable an easier assessment whether the catheter touches or penetrates any wall of the heart. The cross-sectional image plane at a point on the centerline is defined by the two basis vectors $\mathbf{x}_{c_k}$ and $\mathbf{y}_{c_k}$ of the transformation matrix ${}^{mod}\mathbf{T}_{c_k}$. A grid with defined length and spacing is spanned along these two vectors around the centerline point and the position of each pixel on this grid is calculated. For every pixel in the plane, the nearest voxel of the image data set is identified and the gray scale value of this voxel is adopted. The cross-section of the catheter in the images is a circle with the catheter diameter. By calculating the image plane

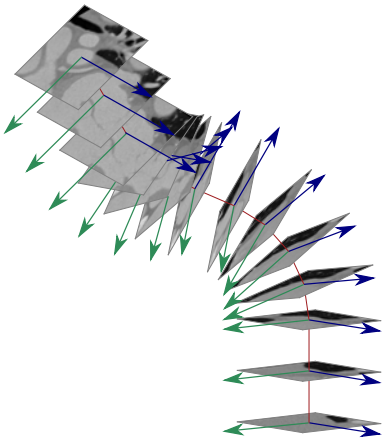

Figure 64 Several image planes orthogonal to the catheter axis are calculated. They allow the verification, if the catheter shape touches any heart wall. The image planes are defined by the two basis vectors $\mathbf{x}_{c_k}$ (green) and $\mathbf{y}_{c_k}$ (blue) of the transformation matrices at the respective equally spaced centerline points and the gray values are determined by nearest neighbor interpolation.

for every point on the centerline, an image stack along the catheter shape is defined as shown in Figure 64. The points on the centerline need to be equally spaced to gain a consistent display of the pathway of the catheter.

6.10 Calculation of the Bending Form

A bending form that covers the patient-individually shaped tip of the catheter is automatically constructed based on the previously calculated catheter centerline. This means that it is generated without any input of the user and the construction is automatically adapted to the properties of the catheter shape. The user adjusts only minor settings. Depending on the calculation method used, the catheter shapes can have different complex shapes in three dimensions and therefore the calculation of the bending form is designed to work independent of the calculation method.

6.10.1 Basic Structure of the Bending Form

Cross-Section of the Bending Form and Extrusion. In the closed state, the bending form has a rectangular cross-section with a hole in the middle, which is oversized in relation to the diameter of the catheter to enable the insertion of the catheter as shown in Figure 65. The bending form consists of a bottom part and a lid and the parting line between them divides the hole into two half circles. Therefore, the cross-sections of both bottom part and lid have a rectangular shape with a semicircle at the surface line facing each other. After extrusion along the catheter centerline, these semicircles form a nut running along the bending form, which represents a negative form of the desired catheter shape.

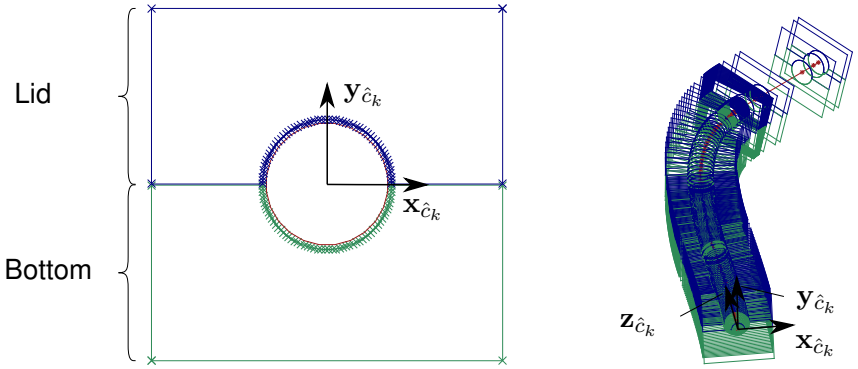

Figure 65 The bending form has a rectangular cross-section with a hole surrounding the catheter in the center, which is separated into a bottom part and a lid (left). The cross-section is extruded along the catheter centerline to get a negative form of the catheter (right).

To ensure a suitable orientation of the cross-sections, a coordinate system $form$ is defined for the extrusion and the coordinate systems $\hat{c}_k$ at the centerline points are adapted. Thereby, the positions $\mathbf{p}_{\hat{c}_k}$ of the points and the orientation of the vectors along the catheter centerline $\mathbf{z}_{\hat{c}_k}$ are unchanged

and determined by a transformation between the coordinate systems mod and $form$.

$$\begin{pmatrix} {}^{form}\mathbf{p}_{\hat{c}_k} \\ 1 \end{pmatrix} = \begin{pmatrix} {}^{form}\mathbf{p}_{c_k} \\ 1 \end{pmatrix} = {}^{mod}\mathbf{T}_{form} \cdot \begin{pmatrix} {}^{mod}\mathbf{p}_{c_k} \\ 1 \end{pmatrix}$$
$$\begin{pmatrix} {}^{form}\mathbf{z}_{\hat{c}_k} \\ 1 \end{pmatrix} = \begin{pmatrix} {}^{form}\mathbf{z}_{c_k} \\ 1 \end{pmatrix} = {}^{mod}\mathbf{T}_{form} \cdot \begin{pmatrix} {}^{mod}\mathbf{z}_{c_k} \\ 1 \end{pmatrix} \tag{6.75}$$

However, the orientations of the vectors $\mathbf{x}_{\hat{c}_k}$ and $\mathbf{y}_{\hat{c}_k}$ differ from those of the vectors $\mathbf{x}_{c_k}$ and $\mathbf{y}_{c_k}$. They are recalculated based on the coordinate system $form$ using the same rules as for the calculation of the vectors $\mathbf{x}_{c_k}$ and $\mathbf{y}_{c_k}$ as described in chapter 6.7.3.

$${}^{form}\mathbf{x}_{\hat{c}_k} = \begin{pmatrix} {}^{form}\mathbf{z}_{\hat{c}_k}(3) \\ 0 \\ -{}^{form}\mathbf{z}_{\hat{c}_k}(1) \end{pmatrix} \frac{1}{\sqrt{{}^{form}\mathbf{z}_{\hat{c}_k}(1)^2 + {}^{form}\mathbf{z}_{\hat{c}_k}(3)^2}}$$
$${}^{form}\mathbf{y}_{\hat{c}_k} = -{}^{form}\mathbf{x}_{\hat{c}_k} \times {}^{form}\mathbf{z}_{\hat{c}_k} \tag{6.76}$$

Based on these vectors a transformation matrix ${}^{form}\mathbf{T}_{\hat{c}_k}$ is defined at every point of the centerline. The two-dimensional cross-sections of the bottom part and the lid are described by a point list in the $\mathbf{x}_{\hat{c}_k}\mathbf{y}_{\hat{c}_k}$-plane in the coordinate system of the points $\hat{c}_k$. Thereby, the $\mathbf{x}_{\hat{c}_k}$-vectors of the transformation matrices point along the separation line of bottom part and lid and the $\mathbf{y}_{\hat{c}_k}$-vectors lie normal to it. The three-dimensional shape is realized by a transformation of the cross-sections from the coordinate system $\hat{c}_k$ into the coordinate system $form$ as shown in Figure 65. After the extrusion, the surface separating bottom part and lid is perpendicular to all $\mathbf{y}_{\hat{c}_k}$-vectors of the transformation matrices. The surfaces of the bending form are described by triangulation of the cross-sections at the endpoints and by connecting the cross-section along the centerline.

Definition of the Coordinate System for the Construction of the Bending Form. For easy opening of the lids, the surface that is separating the bottom part and the lid of the bending form should be as flat as possible (see Figure 66). The orientation of the parting surface depends on the orientation of the $\mathbf{x}_{\hat{c}_k}$-vectors that lie in the parting surface and depend on the orientation of the coordinate system $form$. The $\mathbf{x}_{\hat{c}_k}$-vectors are oriented parallel to the $\mathbf{x}_{form}\mathbf{z}_{form}$-plane and normal to the $\mathbf{y}_{form}$-direction. Therefore, the curvature of the parting surface can be reduced by minimizing

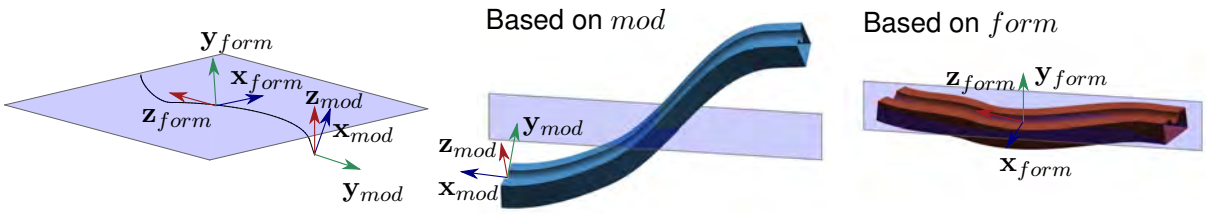

Figure 66 A coordinate system $form$ with appropriate orientation of the basis vectors ${}^{mod}\mathbf{x}_{form}$, ${}^{mod}\mathbf{y}_{form}$ and ${}^{mod}\mathbf{z}_{form}$ is defined along the principal axes of the centerline points for the construction of the bending form. In order to facilitate the opening of the lid, the deviation of the centerline in $\mathbf{y}_{form}$-direction should be minimized (left). An extrusion of the cross-sections in the coordinate system mod using the original transformation matrices ${}^{mod}\mathbf{T}_{c_k}$ does not give favorable results (middle). The use of the coordinate system $form$ with the axes aligned with the main directions of extent of the centerline results in a bending form shape with less curvature of the opening surface (right).

the deviation of the catheter centerline in $\mathbf{y}_{form}$-direction. This can be realized by aligning the coordinate system $form$ with the main directions of extent of the catheter centerline.

A principal component analysis (PCA) is performed to find the main directions of extent of the catheter centerline and therefore the plane that has the least summarized distance to the centerline points. The coordinate system $form$ with its three basis vectors is defined so that the direction with least extent points along the $\mathbf{y}_{form}$-direction and the two main axes of the centerline lie in the $\mathbf{x}_{form}\mathbf{z}_{form}$-plane. The $\mathbf{z}_{form}$-vector of the transformation matrix is aligned with the main axis that was identified by the PCA, the $\mathbf{x}_{form}$-vector is defined as the second axis and the $\mathbf{y}_{form}$-vector lies perpendicular to the two main axes. The directions of the basis vectors are chosen so that the $\mathbf{y}_{form}$-vector and the vector from the centroid of the centerline points to the end point of the bending form point into opposite directions and build an angle of more than 90°. Thereby, it is ensured that the lid tends to have a convex rather than a concave shape what facilitates its opening, as the vector $\mathbf{y}_{form}$ points from the center of the cross-section towards the lid. The origin of the coordinate system $form$ is positioned at the centroid of the centerline points.

Segments of the Bending Form. The lid of the bending form is separated into several segments to enable easier insertion of the catheter, as it has to be manually bended before being inserted into the form while kinking of the catheter has to be avoided.

The principal idea is to define a separate lid segment for every curved section of the catheter shape. If available, each curved section is combined with the following straight section into one lid segment. If there is an additional straight section at the tip of the catheter, it is defined as a separate segment. Therefore, as additional information to the centerline points and the transformation matrices, every point on the centerline is assigned to a curved or straight segment. At the end of the last curved section, the straight proximal part of the catheter sheath begins. A straight segment of fixed length is used to cover its beginning. The combined length of the curved and the straight part of the each lid segment is determined. If the length is not sufficient to add a hinge that connects the lid to the bottom part, it has to be joined with the following segment to a longer one.

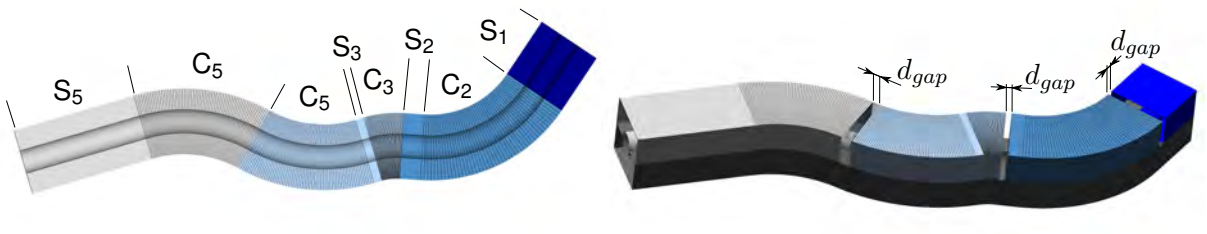

Figure 67 The lid of the bending form is separated into several segments to facilitate the insertion of the catheter (left). Generally, every curved segment ('C') forms a lid segment together with the following straight segment ('S'). However, if the length of the segment is too short to allow the attachment of a hinge, it has to be joined with the following segment, as can be seen for segment C_3. Segment S_1 only has a straight segment whereas segment C_4 only consists of a curved segment. A minimum gap width d_{gap} has to be respected between the lid segments to enable monolithic additive manufacturing and the opening of the lids (right).

Between the lid segments, a gap with minimum width d_{gap} has to exist in order to avoid fusion of the lid segments during the manufacturing process and to enable the opening of the lids without collisions. Each lid segment is shortened at the end to respect the minimum gap width between the lids. Depending on the geometry of the catheter shape, the gap width may need to be manually increased in order to allow complete opening of the lid. To realize the gaps, the cross-sections of the lid in the region of the gap are not interconnected. Therefore, in the straight segments, additional points are added to the centerline in a distance of the gap width from the end of the segment. At these points, the interconnection of the cross-sections ends. If the gap is added at the curved segment due to the lack of a straight segment, the minimum gap width has to be respected over the whole width of the bending form. Therefore, the distances between the points of two neighboring cross-sections are calculated at both sides of the bending form. No additional points have to be added but the number of cross-section in the curved segment that are not interconnected on the lid's side to comply with the gap width has to be determined. Figure 67 shows an example of a bending form with several segments and the gaps between the segments.

6.10.2 Hinges and Snap Hooks

Shape of the Hinges and Snap Hooks. Hinges connect the bottom part and the lid at one side of the bending form while snap hooks are used to close the lid on the opposite side. The hinges consist of a bolt that is attached to the bottom part by two supports and a sleeve on the lid. The width of the hinge is composed of the width of the two support segments $d_{support}$, the gap width between supports and the sleeve d_{gap} and the width of the sleeve d_{sleeve} as shown in Figure 68. A minimum gap width has to be respected between the support structures and the sleeve as well as between the radii of the bolt r_{bolt} and the hole in the sleeve r_{sleeve} to avoid fusion of the parts during the monolithic manufacturing process. Furthermore, minimum wall thicknesses are necessary to gain enough strength in case of the supports and the sleeve.

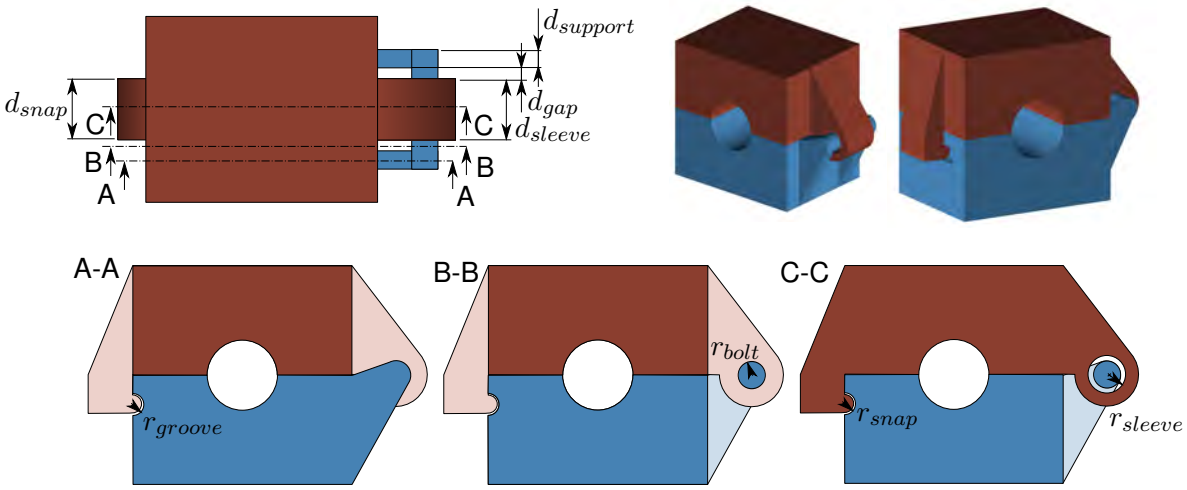

Figure 68 To close the bending form, it has a snap hook on the lid, which snaps into a groove at the bottom part. On the opposite side, a hinge consisting of a bolt and a sleeve allows the opening of the lid. The cross-sections of the hinge at three positions and the important dimensions for the construction are shown.

The snap hook is a part of the lid segment and it is located on the opposite side of the bending form than the hinge. On the bottom segment, a groove is added, which serves as the seat for the snap hook. The groove as well as the snap hook are shaped as semicircles with the radius of the snap hook r_{snap} being smaller than that of the groove r_{groove}.

On the hinge side, three different cross-sections of the hinge structure can be distinguished. On the side of the snap hook only two different cross-sections are necessary with the bottom part and the lid having one structure each. The cross-sections of the hinges and snap hooks are arranged symmetrically to the central point.

Position of the Hinges. Each segment of the lid is connected to the bottom part by either one or two hinges. The number of hinges per segment depends on the length of the segment. If the segment has a straight part that is longer than the width of two hinge elements, two hinges are chosen and positioned at the ends of the straight segment. Otherwise, one hinge is positioned in the center of the straight segment. If the straight part is not long enough for one hinge or the segment does not contain a straight part, the hinge is positioned in the middle of the bended segment. None of the lid segments is shorter than the hinge structure, as in this case they are combined with the following section. Figure 69 shows the arrangement of the hinges for one exemplary bending form shape.

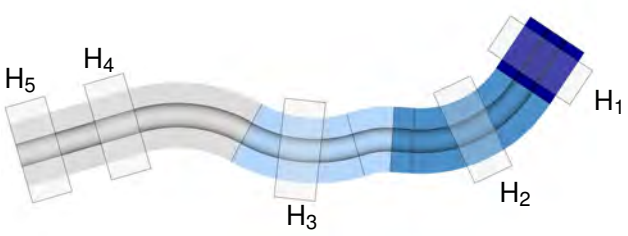

Figure 69 The number and position of the hinges depends on the length of the straight and curved part in each lid segment. If possible, one or two hinges are positioned in the straight segment. If the straight segment is too short or not existing, one hinge is positioned in the curved part. The gray rectangles mark the hinge positions in the four segments.

To enable the opening of the lids and avoid the collision of the opened segments, the hinge is positioned on the outer, convex side of the bend. While in bends with constant bending radius, this side is easy to identify, it is more difficult for complex shapes such as three-dimensional spline shapes. To identify the suitable side of the hinge for each segment, the centroid $\mathbf{p}_o$ of all points on the centerline of the curved segment are calculated and the central point $\mathbf{p}_m$ of the curved segment is identified. The hinges are positioned on the side of the bending form to which the vector from the centroid of the curved segment to the central point of the curved segment that is projected into the xz-plane points in the coordinate system $form$ (see Figure 70).

Construction of the Hinges. In the straight segment, at the corresponding distances to the central point of the hinge, six points are added to the centerline and the cross-sections of the hinges are transformed according to the transformation matrices of these centerline points.

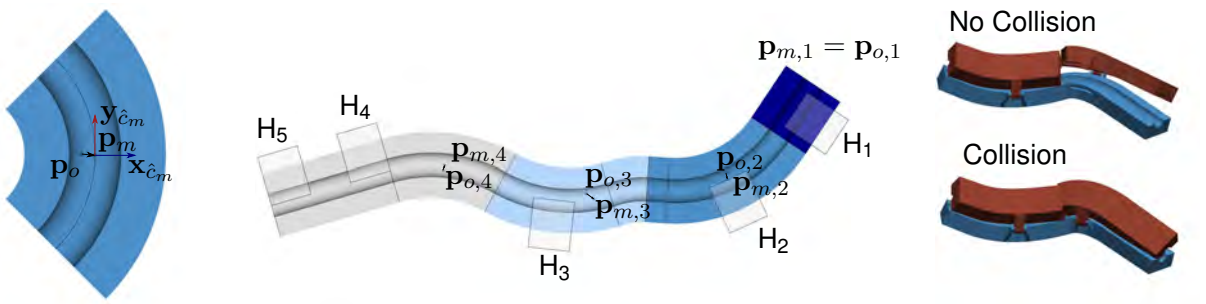

Figure 70 The lid of the bending form has to be positioned at the outer side of the bend to enable its opening without collisions. The vector from the centroid of the centerline points of the segment to the central point of the segment is calculated. The hinge should be positioned at the side that the vector points to (left). The image in the middle shows an example of the positioning of the hinges with the gray rectangles marking the hinge positions. The images on the right illustrate the collision problems occurring with inappropriate choice of the hinge side.

While the construction is easy for straight segments, attention has to be paid in curved line segments, as the bolt of the hinge has to be straight to form an appropriate axis for the rotation to open the lid. Furthermore, the area of the snap hook and the groove should be linearized. Therefore, a simple transformation of the cross-sections of the snap hook and the hinge in the curved segments is not possible, as this would lead to a curved shape of the hinges. Furthermore, multiple centerline points are available in the hinge segment, which are necessary for the smooth construction of the catheter seat. Therefore, existing points on the centerline are used for the construction of the hinges. However, different points are used at the hinge and the groove side, as the distances between the points vary due to the curvature of the bending form. The distances of each point at both sides of the curved segment to the corresponding point on the central cross-section of the curved segment are calculated. The cross-sections of the bending form with points that match the desired distances best are chosen and the cross-sections of the hinge components are transformed to all centerline points lying in the relevant region. Then all relevant points on the cross-sections that are the points on the hinge, the snap hook and the groove but also the points on the outsides of the separation surface are moved onto a straight line pointing along the vector $\mathbf{z}_{c_k}$ of the coordinate system of the central point in the curved segment (see Figure 71).

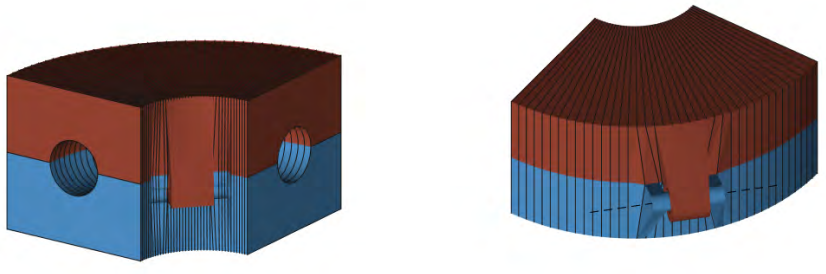

Figure 71 The hinges have to be straight to enable the opening of the lid. Therefore, after the transformation of the cross-sections into the centerline points, the points on the hinge and in the relevant curved area of the bending form are shifted onto a straight line.

Opening of the Lid. The bending forms cannot be manufactured in the closed state, as the parts would fuse during the production process. However, only in the closed state, all cross-sections are perpendicular to the normal vector of the catheter centerline. Therefore, the cross-sections are constructed and extruded along the centerline in the closed state and the lids of the virtual models are opened afterwards as illustrated in Figure 72. Therefore, all points belonging to one of the lid segments have to be rotated around the axis of the bolt of the hinge connecting the bottom part and the lid segment. The rotation angle has to be big enough to ensure the minimum gap width for monolithic additive manufacturing between all parts of the bottom segment and the lid.

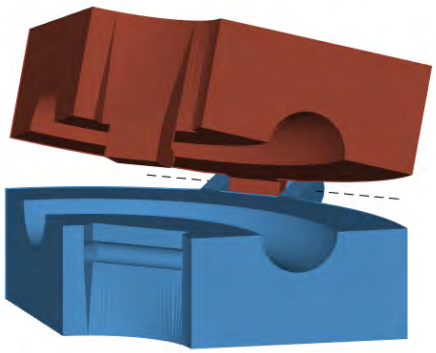

Figure 72 The points belonging to the lid segments have to be rotated around the axis of the corresponding hinge to open the lid in order to allow monolithic additive manufacturing of the bending form that needs minimum gap widths between parts that should not merge.

6.10.3 Approaches to Improve Bending Results

Compensation of the Spring-Back. The shape of the catheter that was produced using the bending form does not correspond to the shape of the bending form exactly, as the catheter bends back to a certain degree after removal from the form (see Figure 73). This is a common problem in bending processes and it can be addressed by overbending. Experiments showed that the deviation from the desired angle of the catheter depends on the duration of the heating and cooling phases in the bending form during the shaping process. Furthermore, the amount of spring-back is also dependent on the bending angle and the bending radius.

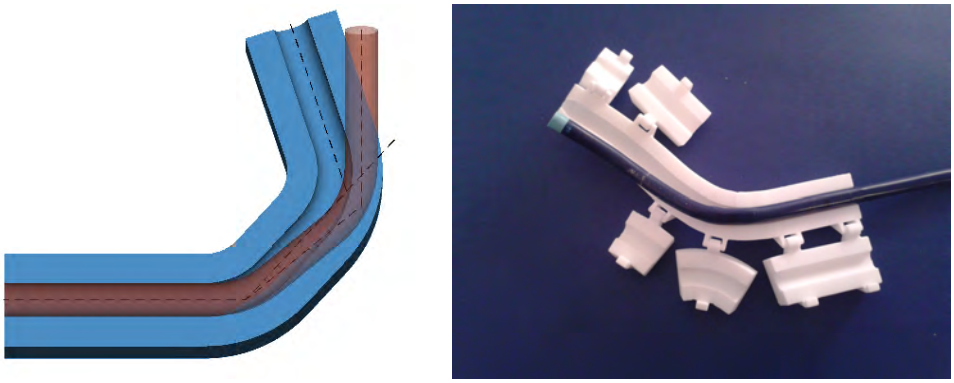

Figure 73 After removing the catheter from the bending form, it forms back again in a certain degree depending on the bending parameters and the geometry of the bend. The spring-back can be compensated by overbending the catheter.

For catheters with constant bending radii, the spring-back can be compensated by deforming the catheter more than the desired bending angle. A formula or look up table is necessary to describe the relation between the bending angles of the bending form and the resulting bending angle after the bending process. To find this correlation, a bending process and its parameters have to be defined and measurements of the resulting bending angles for defined angles of the bending form are carried out. This allows to determine which bending angle has to be used to overbend the catheter enough to get the desired bending angle.

Step-wise Bending. Sharp bends are difficult to produce, as the catheter sheath is prone to kink during the insertion of the catheter into the bending form. In order to facilitate the production of sharp bends, the bending can be performed step-wise. Thereby, several bending forms are produced that gradually approach the final bending form. In each bending form, the curvature is incrementally increased while respecting the angles and distances of the bends relative to each other.

To enable the gradual approach independent of the calculation method used, it has to be based on an alteration of the catheter centerline. Thereby, the distances of the points of the centerline to the main axis of the catheter shape are decreased. The following calculations are done in the coordinate system $form$ and the indices are left out to improve the readability. As the main extension of the centerline is oriented along the $\mathbf{z}_{form}$-component and the centroids of all centerline points are chosen as the origins of the respective coordinate systems, the $x_{p_{\hat{c}_k}}$- and $y_{p_{\hat{c}_k}}$-components of the positions of the points correspond to the distances from the main axis in $\mathbf{x}_{form}$- and $\mathbf{y}_{form}$-direction. A factor w_f that ranges between zero and one is used to decrease these distances (see Figure 74). Setting the factor w_f to zero leads to a straight line and increasing the factor to one results in a shape that is identical to the target catheter shape. In addition to the components in $\mathbf{x}_{form}$- and $\mathbf{y}_{form}$-direction, the value in $\mathbf{z}_{form}$-direction is adapted so that the distance $l_{\hat{c}_k}$ between two points is kept constant. By choosing the appropriate sign in the calculation of the $z_{p_{\hat{c}_k}}$-component, the extent in $\mathbf{z}_{form}$-direction is in the same direction as the original shape.

$$
\begin{aligned}
l_{\hat{c}_k} &= |\mathbf{p}_{c_k} - \mathbf{p}_{\hat{c}_{k-1}}|^2 \\
\mathbf{p}_{\hat{c}_k,w} &= \begin{pmatrix} w_f \cdot x_{p_{\hat{c}_k}} \\ w_f \cdot y_{p_{\hat{c}_k}} \\ z_{p_{\hat{c}_{k-1}}} + sgn(z_{p_{\hat{c}_k}} - z_{p_{\hat{c}_{k-1}}}) \sqrt{l_{\hat{c}_k} - w_f^2((x_{p_{\hat{c}_k}} - x_{p_{\hat{c}_{k-1}}})^2 + (y_{p_{\hat{c}_k}} - y_{p_{\hat{c}_{k-1}}})^2)} \end{pmatrix}
\end{aligned}
\tag{6.77}
$$

This adaptation is working as long as there is no change of direction of the $z_{p_{\hat{c}_k}}$-components of the points along the catheter shape.

The coordinate systems at the centerline have to be adapted as well. The normal vectors on the catheter cross-sections at every point are approximated as the normalized vectors between the two neighboring points.

$$
\mathbf{n}_{\hat{c}_k,w} = \frac{\mathbf{p}_{\hat{c}_{k+1},w} - \mathbf{p}_{\hat{c}_{k-1},w}}{|\mathbf{p}_{\hat{c}_{k+1},w} - \mathbf{p}_{\hat{c}_{k-1},w}|} \tag{6.78}
$$

Based on the normal vectors the transformation matrices are recalculated according to chapter 6.10.1.

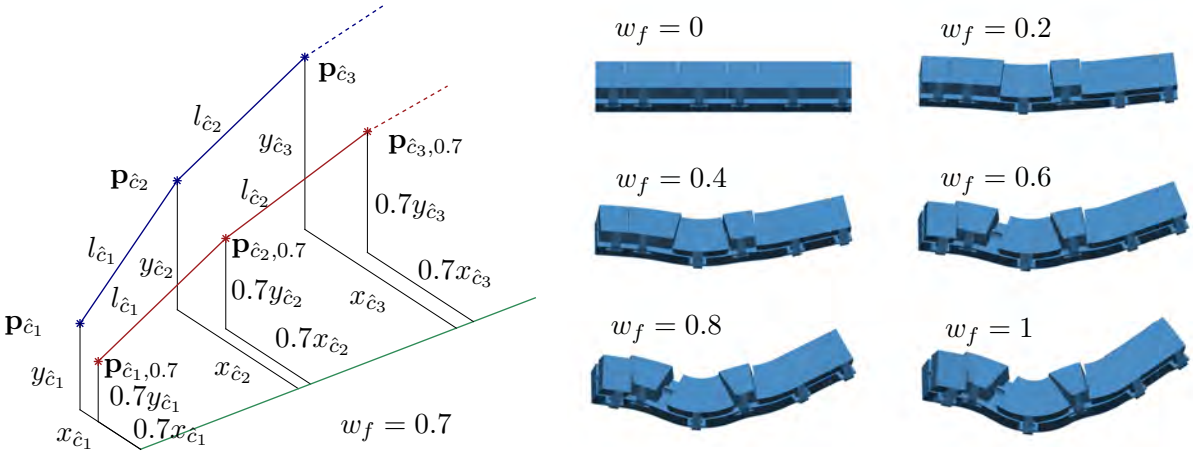

Figure 74 To enable the bending in several steps, the distances $x_{\hat{c}_k}$ and $y_{\hat{c}_k}$ of the points of the centerline $\mathbf{p}_{c_k}$ to the main axis of the catheter shape are altered using a factor w_f that is ranging between 0 and 1. The distances between the points $l_{\hat{c}_k}$ are kept constant. The blue line shows the original points $\mathbf{p}_{c_k}$ and the red line the altered points $\mathbf{p}_{\hat{c}_k,w}$. On the right side, bending forms resulting from different factors w_f are shown.

6.10.4 User Interaction During the Construction of the Bending Form

The bending form is automatically constructed by the program and displayed in a three-dimensional representation, which can be rotated interactively. The construction algorithm adjusts most of the settings that are necessary and adapts the bending form to the previously calculated catheter shape. The user can check the bending form in this stage and change some minor settings: he can increase or decrease the gap width between the parts of the lid or change the side of each hinge separately if this seems to be necessary in order to facilitate the opening of the lids. Furthermore, the user can decide to add a label on the bending form. If done so, the name of the patient and the date are added as relief text onto the last lid segment of the bending form.

6.10.5 Additive Manufacturing of the Bending Form by Selective Laser Sintering

Selective laser sintering is chosen as the manufacturing method for the production of the bending forms (see Figure 75). In selective laser sintering, a laser melts parts of a powder bed layer by layer. The machine EOS Formiga P100 (EOS GmbH, Krailing, Germany) is used with the thermoplastic powder PA2200. Parts made of PA2200 with sufficient thickness are able to withstand the temperatures that are necessary for the shaping of the catheter and the material is classified as biocompatible by the manufacturer (EOS, 2010). The minimum wall thickness that is required for the manufacturing of the anatomical models is 0.5 mm. Another important measure is the minimum gap width 0.3 mm. Table 2 lists the dimensions that were used for the production of the test parts.

Table 2 Dimensions for the construction of the hinges targeted towards manufacturing by selective laser sintering.

Radii [mm]		Widths [mm]	
r_{snap}	0.65	d_{snap}	4
r_{groove}	0.75	$d_{support}$	1.5
r_{bolt}	1	d_{gap}	0.3
r_{sleeve}	1.3	d_{sleeve}	4

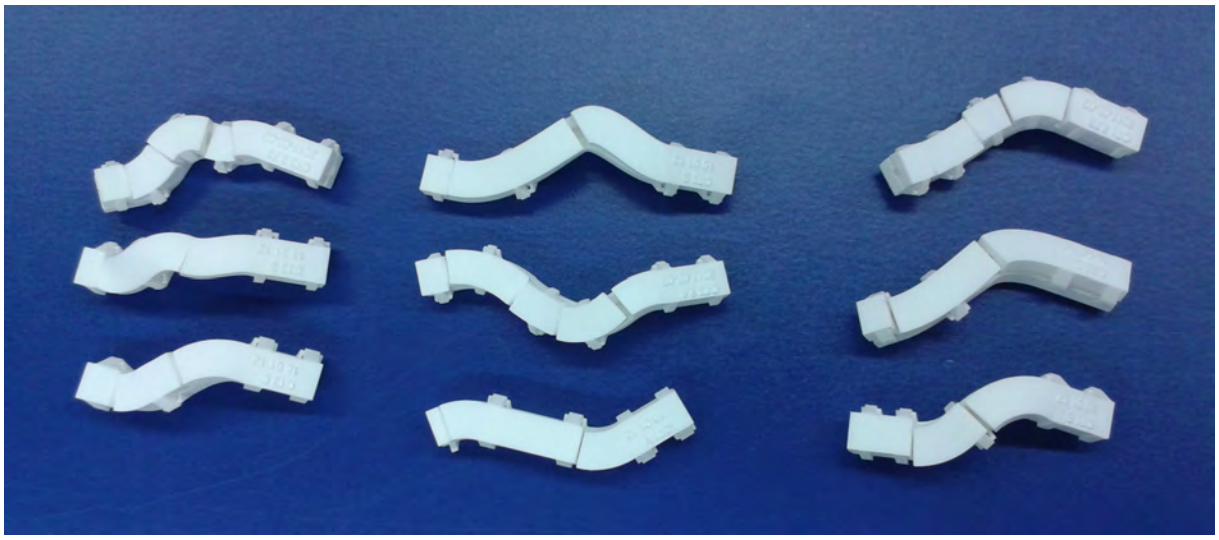

Figure 75 The bending forms are realized by additive manufacturing using the selective laser sintering technique. The shapes of the bending forms of different data sets but also of different calculation methods vary widely. Each column shows bending forms based on one data set that were calculated with different methods.

6.11 Heart Models for the Evaluation

In order to test and verity the developed calculation methods and the catheters, heart models with differences in anatomical details were produced that represent the patient-specific anatomy. The models were produced based on three-dimensional CT image data sets of the patients, as the images were also necessary for the testing of the approach of patient-individual catheter shaping based on the preoperative image data. Physical models were chosen over virtual models to be able to insert the real bended catheter and to evaluate the whole process from the planning, to the calculation and the shaping of the catheter. The production of different types of models is described. They can be a replica either of the whole heart or of only the relevant parts of it and they can be manufactured directly by additive manufacturing or by silicone molding. While direct additive manufacturing is easier, the molding of the models allows a wider choice of materials to replicate the imaging properties of the heart. To extract the information about the anatomy of the heart from the image data, segmentation is necessary.

6.11.1 Segmentation for the Model Production

For the segmentation of the image data an interactive program was written in MATLAB (see Figure 76). The left and right cavity of the heart as well as the heart walls are segmented separately. The user can activate one of the regions in random order and the subsequent segmentation actions are applied to this region. Different methods for the segmentation are available: threshold-based segmentation, a segmentation that selects connected regions and manual segmentation of the images. During the segmentation, three orthogonal image slices showing the original CT data with the segmented areas projected into it are displayed and the user can flip through the images.

For threshold-based segmentation, the user selects a lower and an upper segmentation threshold. Only the connected components between these two threshold values are chosen. The selected voxels are displayed and segmentation is applied only after user confirmation. For the segmentation that selects connected regions, the user clicks into the image and all connected voxels with similar gray value intensities that lie in a ROI with selectable width around the voxel value are marked. Furthermore, the user can choose a pen width and manually select or erase voxels by clicking into the image and dragging the cursor.

Boolean operations ensure that the segmented areas of the cavities and the heart walls do not overlap and that a minimum wall thickness is respected. Therefore, all voxels of the right cavity need to keep a minimum distance to the voxels of the left cavity. Overlapping voxels or those that are too close are erased from the segmented area of the right cavity. To ensure the compliance with the minimum thickness of the heart walls, all voxels surrounding the cavities with a distance of less than this thickness are considered part of the heart walls.

After segmentation of the image, the segmented voxel data set is transferred into a surface description by triangulation. The surface model is saved in STL format for additive manufacturing.

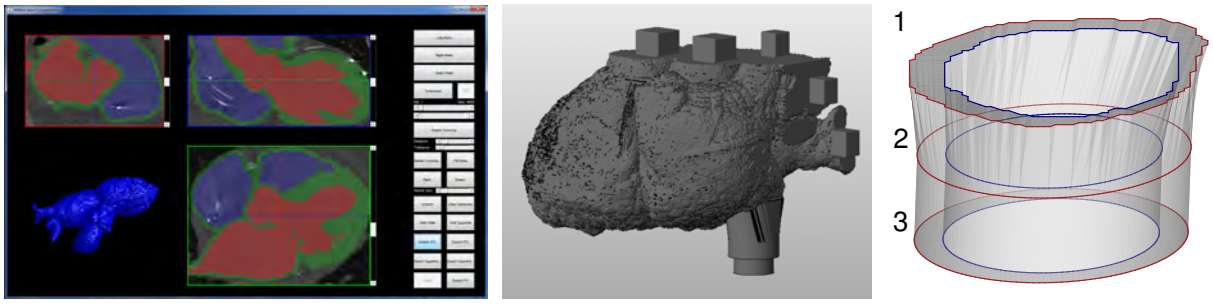

Figure 76 The heart walls and the two cavities of the heart are segmented separately in an interactive process using a graphical user interface (left). After triangulation, a surface model of the structures is available (middle). To control the insertion of the catheter, the outer (red) and inner (blue) border line of the last image of the inferior vena cava that is segmented in the image data (1) is elongated into a tube (2 and 3) (right).

Addition of the Inferior Vena Cava. In order to control the pathway of the insertion of the catheter into the model, the inferior vena cava is elongated and the shape is transferred to a circular cross-section at its end as shown in Figure 76, which allows the connection to a tube. The cross-section of the wall of the inferior vena cava in the last segmented slice is taken as a basis for the elongation. Two concentric circular cross-sections with the same amount of points as the inner and outer cross-section of the wall of the vessel are defined. They are positioned underneath the center point of the inferior vena cava and the circles are connected with the corresponding inner or outer cross-section of the segmented vessel by triangulated walls. The circular tube is elongated to the required length.

6.11.2 Vacuum molding of Silicone Models

Molding Process. The walls of the heart model can be made of silicone by a molding process. In order to obtain the hollow cavities of the left and right heart, lost cores are used (see Figure 77). Therefore, a master form of the heart and the lost cores in the shape of the two cavities are produced

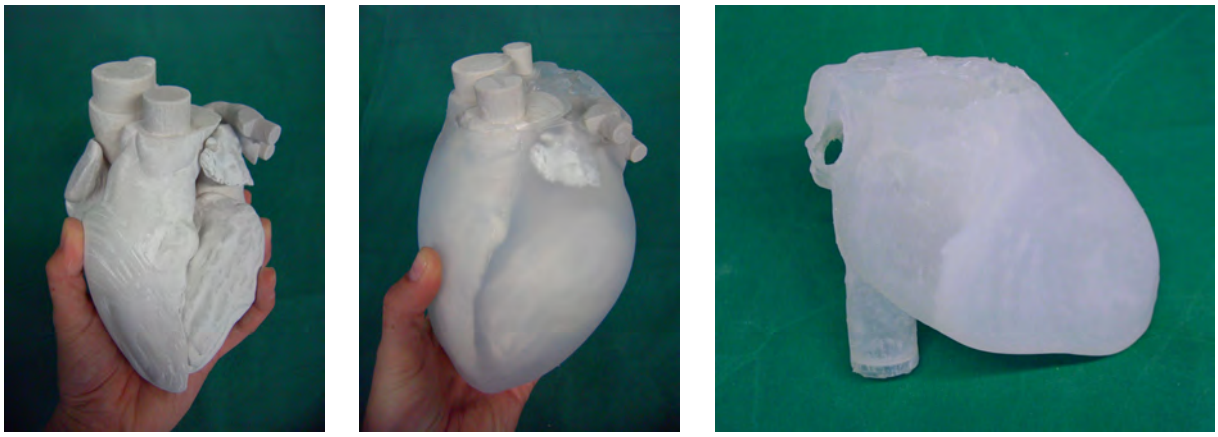

Figure 77 The heart model can be produced by a molding process with lost cores. The lost cores (left) are produced by additive manufacturing and they are covered by silicone in a vacuum molding process (middle, taken from Graf *et al.*, 2014, ©IEEE 2014). After shattering the cores, the hollow silicone model is available (right).

by additive manufacturing and the cores are shattered after the molding process. The process steps are displayed in Figure 78.

The master form displays the outer surface of the heart model. It is entirely embedded in silicone in a cubic form. By opening the silicone cube and removing the master form, a negative silicone mold form in several parts is produced. The lost cores are also produced by additive manufacturing on a ZCorp Spectrum Z510 printer (3D Systems, Rock Hill, SC, USA) on gypsum basis. The cores are positioned in the mold form and a sprue is cut into the mold. The heart model is produced by vacuum casting of silicone into the mold form. The model is removed from the mold and the cores are shattered to obtain the hollow model.

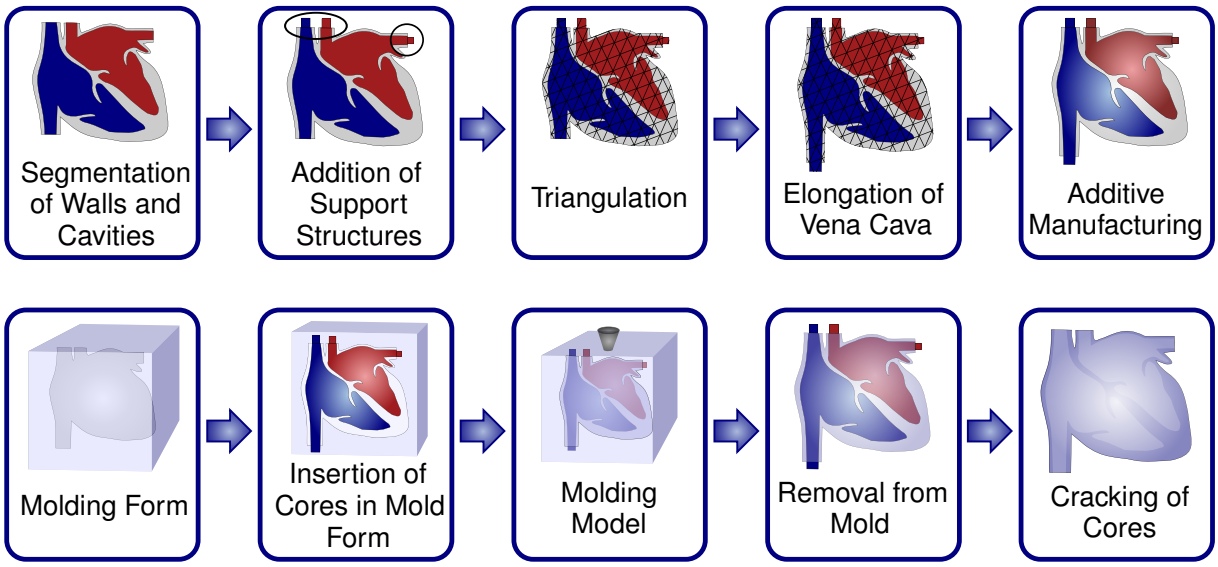

Figure 78 Process description of the production of anatomical heart models by silicone molding. A master shape and lost cores are produced by additive manufacturing based on the segmentation of the image data of the patient and the heart model is fabricated by silicone molding with lost cores.

Addition of Fixation Structures. In order to position the cores in the mold, fixation structures are needed. These are part of both the cores and the master form and they anchor the cores at the predefined position in the mold form. They are added in form of cubes or cylinders at the openings of arteries and veins of the heart, as at these regions no silicone layer covers the cores. To add them to the virtual model, a cubic region at user-defined positions is added to the segmented image data set before triangulation or alternatively, the cylindrical parts are added after triangulation.

Material Selection. Pure silicone can be used for the production of the models. The models are visible in fluoroscopy images as well as in ultrasound images. However, as the material is very homogenous, in the ultrasound images, only the boundaries between the surrounding material and the silicone are visible whereas inside the silicone layer no contrast is available. This leads to good results in three-dimensional representations but does not resemble the real human tissue in two-dimensional views. Therefore, filler materials can be added to the silicone before molding so that the filler particles are distributed throughout the heart wall. The ultrasound waves are reflected and scattered at these particles resulting in a contrast that makes the silicone layer visible. However, the addition of filler material has the disadvantages that the molding process is more difficult due to the deteriorated flow properties and that the ultrasound waves are attenuated and cannot advance so deep into the material anymore. In fluoroscopic images, the material of the heart model is clearly visible and has a higher contrast than natural human tissue (see Figure 79).

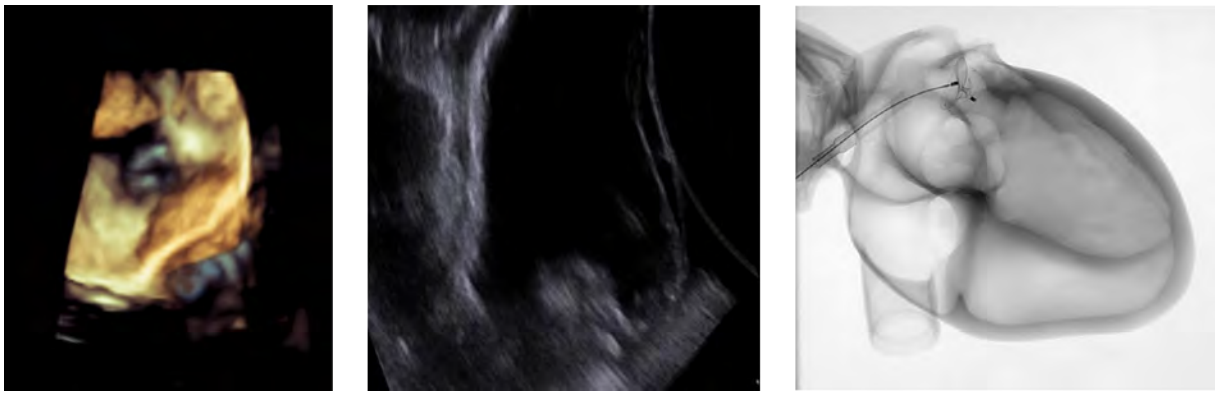

Figure 79 The silicone heart model is visible in ultrasound and in fluoroscopic images. The three-dimensional ultrasound images are realistic (left) whereas in two-dimensional images the lack of contrast in the heart walls leads to images that do not resemble the real human tissue (middle). The visibility of the model and the implant is good in fluoroscopic images (right) (All images taken from Graf *et al.*, 2014, ©IEEE 2014).

Integration into a Torso Model. To enable ultrasound imaging, the hollow heart model has to be filled with a fluid that transmits the ultrasound waves in its cavities. Transmitting fluid also needs to be present between the ultrasound probe and the visualized structures. Therefore, a torso model is developed that serves as a surrounding structure for the heart model. The heart model is placed in a water-filled box and the catheter and ultrasound probe can be introduced through tubes. Figure 80 shows the torso model.

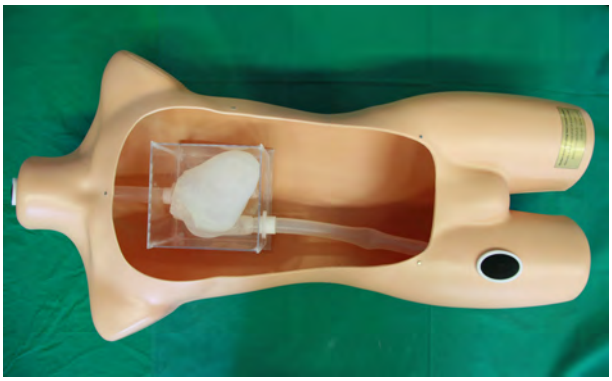

Figure 80 The heart model is placed in a box that can be filled with water in a torso model to ensure the transmission of the ultrasound waves from the transducer to the model and inside the model's cavities (taken from Graf *et al.*, 2014, ©IEEE 2014).

6.11.3 Additive Manufacturing of the Models

Alternatively, the models can be produced by direct additive manufacturing of the heart walls. Different additive manufacturing machines and materials are available depending on the required properties of the models. For hard, rigid materials, a hole at the position of the puncture location has to be added into the heart wall, as puncturing the wall with the medical equipment is not be possible in this case. Furthermore, this manufacturing technique allows the marking of the planned implant position in the model. Figure 81 shows the resulting models and Figure 82 describes the process.

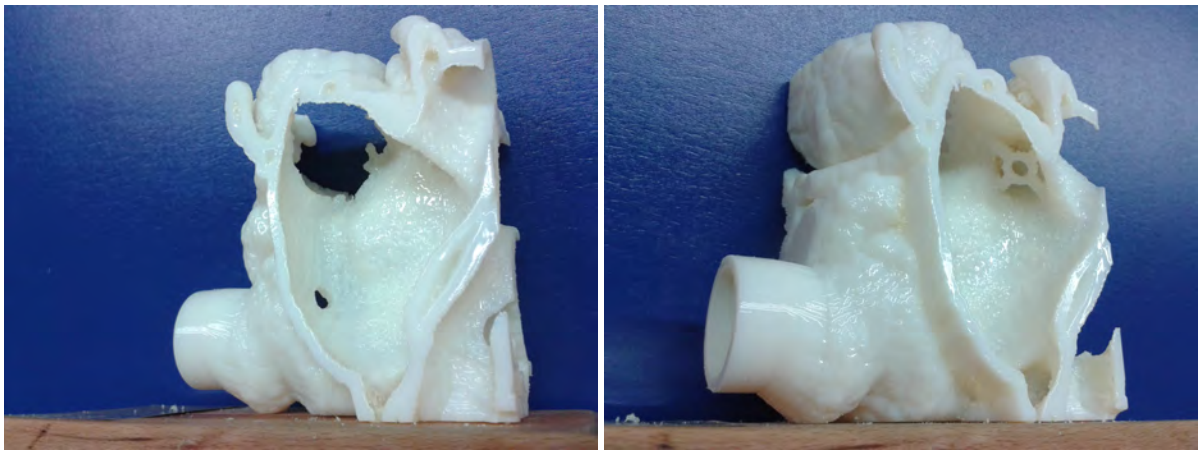

Figure 81 In the additively manufactured models, a hole can be added at the transseptal puncture, as it cannot be produced with the catheter equipment (left). Furthermore, the planned implant position can be marked in the model with a target marked (right).

Puncture Location. The hole in the interatrial septum is added before the triangulation in the segmented voxel data set. All voxels around the planned puncture position in the segmented area of the heart walls are erased. The distance of the each voxel to the planned puncture location is determined. If this distance remains below the desired diameter of the hole, the voxel value is set to zero. The diameter of the puncture hole is chosen slightly bigger than the catheter diameter to allow movements of the catheter.

Marker for the Implant Position. Markers can be added at the implant position to indicate the planned position and orientation of the implant. Therefore, a target circle is positioned at the implant position and connected to the heart model by support structures. After the triangulation, the marker structure is transformed into the implant plane at the planned position.

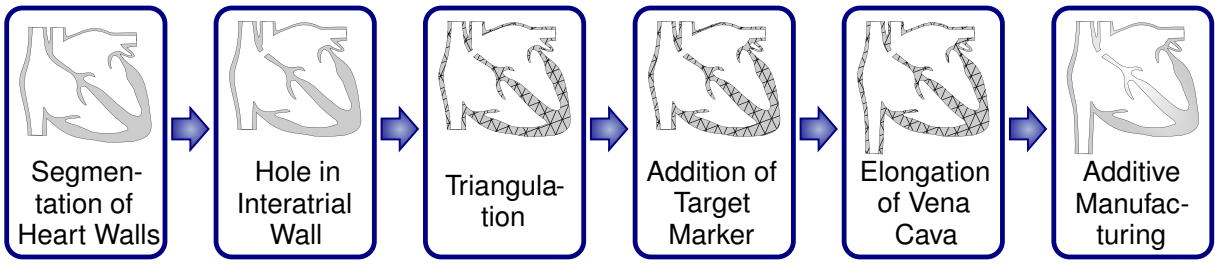

Figure 82 Process description for the direct additive manufacturing of the heart models. A hole at the puncture location and a target marker can be added to the model before and after the triangulation, respectively.

7 Experimental Evaluation

The patient-individual catheter shaping was evaluated in experiments on heart models, which are described in chapter 6.11. In a preliminary experiment the double bended catheter (see chapter 6.8.1) and the catheter with variable curvature (see chapter 6.8.3) was compared to the standard catheter and in the final evaluation the catheter with four bends (see chapter 6.8.4) was tested against the standard catheter.

7.1 Preliminary Comparison: Standard catheter, Double Bended Catheter and Catheter with Variable Curvature

In a preliminary experiment, the standard catheter was compared to the double bended catheter and the catheter with variable curvature to get a hint if the patient-individual shaping of the catheters seems to be favorable. Physicians tested the different catheters in heart models of the appropriate patient and rated the catheters to find the catheter type that is best suited. Furthermore, advantages and disadvantages of the calculation methods are detected.

7.1.1 Experimental Setup

Participants. Four cardiologists of the German Heart Center in Munich performed the preliminary experiment. One of the cardiologist had already performed more than 100 LAA occlusion procedures whereas the other three were not so familiar with the procedure and stated that they had performed less than 100 of these procedures.

Heart Model. Additively manufactured models as described in section 6.11.3 were used for the evaluation of the catheters. Rigid models of the anatomy of six different patients were used. The models were produced by additive manufacturing using the machine Objet30 (Stratasys, Eden Prairie, MN, USA). With four physicians testing six models each a total of 24 trials were performed. The models showed the relevant area of the heart consisting of the inferior vena cava, the interatrial septum and the left atrial appendage with parts of the left and right atrium. As the rigid models cannot be visualized by ultrasound imaging, they had an open design and the catheter was positioned under open sight. At the planned puncture location, a hole was left in the interatrial septum to be able to pass it with the catheter. The beginning of the inferior vena cava was simulated by a straight tube and the target point at the implant position in the left atrial appendage was marked by a ring.

Catheters. In every model, the standard catheter, the catheter with variable curvature and at least one double bended catheter were tested. In four of the six CT data sets, an exact solution of the double bended catheter with compliance to the boundary values was not possible due to the geometric situation. In these cases the optimization process for the calculation of a double bended catheter with additional tolerances was performed. A patient-specific catheter shape was calculated for a tolerance at each of the three available boundary conditions: implant orientation, puncture

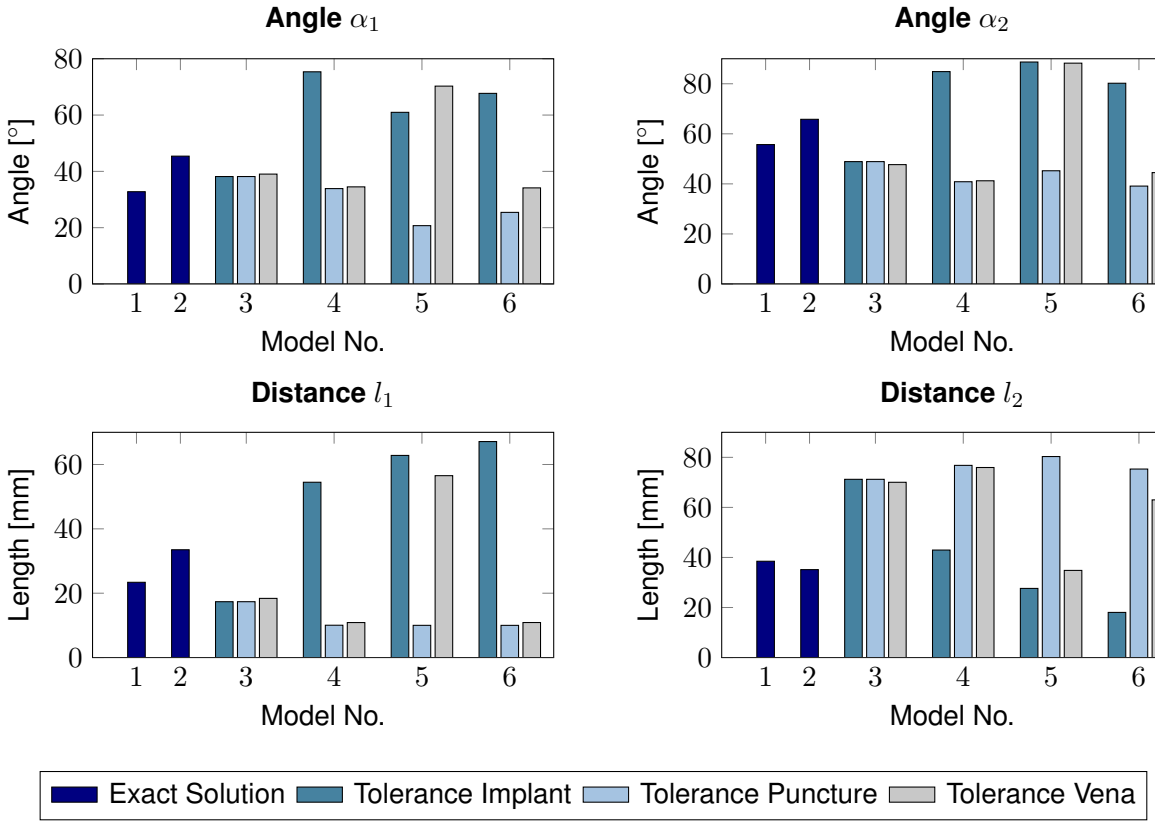

Figure 83 The calculated double bended catheters showed differences concerning bending angles and lengths of the segments in the tested image data sets. Whereas in some data sets the different optimization approaches for the double bended catheters led to similar results (for example model 4), they differed a lot in other data sets (for example model 6).

location and orientation of the inferior vena cava as described in chapter 6.8.2. After comparison of the solution of the optimization processes, in two cases not all of the catheters were produced and tested, as their resulting shapes were almost similar. In other cases the results between the optimized catheters differed a lot (see Figure 83). Therefore, the number of patient-specific catheters that was tested in one model differed between two and four. In total, each physician tested 17 patient-specific catheters in the six models. In general, the catheters for the different patients showed a great variability in shapes. No compensation of the spring-back was regarded during the calculation of the catheter bending form for this experiment.

As a reference for the patient-individually shaped catheters, the standard catheter that is used with the Amplatzer implants, the AMPLATZER TorqVue 45x45 catheter (St. Jude Medical, St. Paul, MN, USA), was tested. The suitability of the standard catheter was evaluated in the planning program by evaluating the distance and deviation of the virtually inserted standard catheter to the target position. The results showed that the standard catheter was clearly better suited in two cases than in the other four cases. These two models were the ones where the calculation of the double bended catheter led to an exact solution. Figure 84 shows the resulting distances and deviations between the calculated tip of the reference catheter and the planned implant position. The heart models in the following evaluation are sorted by increasing distance of the standard catheter from the planned implant position in the corresponding image data sets.

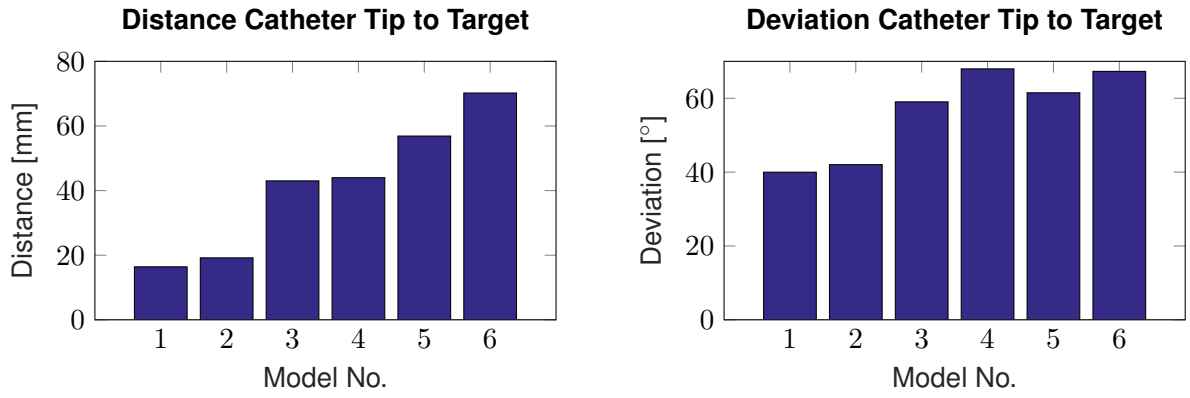

Figure 84 The distance and deviation of the virtually inserted standard catheter to the planned target was calculated for each of the models. The catheter was clearly better suited in two cases (models 1 and 2).

Questionnaire. Each physician answered a questionnaire with in total 60 questions. Each of the questions could be rated on a scale from 100 to 0 with 100 meaning total accordance with the statement and 0 complete denial.

For each of the six models, the questionnaire contained printed screenshots of the planning program showing the orthogonal images with the defined puncture location and the three image slices defining the implant plane with the marked orifice of the LAA.

For every model, the suitability of the puncture location and the target position in the screenshots and the additively manufactured model was rated. Furthermore, the statement 'The individually shaped catheters were advantageous compared to the standard catheter' was assessed for every model. For each of the tested catheters in the model, the statement 'The left atrial appendage was easily accessible with the catheter' was rated.

Seven general statements were provided in the questionnaire and assessed by the participants:

- The comparison of the catheters is possible with the models.
- The location of the puncture point can be rated using the image slices.
- The location of the puncture point can be rated using the model.
- The target position of the catheter can be rated using the image slices.
- The target position of the catheter can be rated using the model.
- An adaptation of the catheter to the anatomy is useful.
- I would use the adapted catheters again.

Furthermore, the number of minimally invasive closure procedures that the participant had already performed was asked with the available categories 'Below 100', 'Above 100', 'Above 250', 'Above 500' and 'Above 1000' interventions. The questionnaires were signed by the participants.

Experiment Procedure. The physicians tested the catheters in pairs taking terms in testing each catheter. The order of the models was constant for all participants, however, the corresponding catheters were in random order.

To test each catheter, it was introduced through the inferior vena cava and the transseptal puncture into the model. Starting from this position, the physicians tried to position the catheter tip at the target under direct view while only touching the catheter outside the model. Two of the physicians decided to define the left atrial appendage structure as the target, the other two tried to reach the target marker. If it seemed to be impossible to position the catheter at the respective target, the participants could decide to abort the trial.

Prior to starting the testing with every model, the physicians rated the suitability of the puncture location and the target position in the questionnaire. They evaluated each catheter after testing it and answered the question concerning the advantages of the patient-specific catheter after completing the tests on each model. The general questions were answered at the end of the experiment.

Parameters. In addition to the ratings of the statements in the questionnaire by the participants, the time that was necessary until successful positioning of the catheter could be achieved was recorded. Time measurement started after passing the interatrial septum and it was taken with a stopwatch. Furthermore, it was recorded if the target could be reached with the corresponding catheter or if the trial had to be aborted.

7.1.2 Results

Reaching the Target. The target could be reached with all of the patient-individually shaped catheters in all of the models. For the standard catheter, which served as a reference, this was not possible in seven cases. One of the physicians could reach the left atrial appendage with the standard catheter in all of the models whereas the other three physicians aborted at least one trial. One of them aborted one trial and the other two aborted three trials. The seven trials that were aborted occurred in three different models.

Rating of the Catheters. The ratings of the physicians for the catheters can be seen in Figure 85. The catheters are sorted by decreasing suitability of the standard catheter. In model two, the standard catheter was rated very well with values ranging from 90 to 100 whereas the other two catheters reached a wider range of ratings between 40 and 100. In model one, the rating of the standard catheter was a bit worse than in model one with values between 60 and 100. The double bended catheter received ratings in the same range. All user rated the catheter with varying curvature with values between 90 and 95. The median ratings for models one and two can be seen on the left side of Figure 86. With a value of 92.5, the standard catheter had the highest median rating value. In these two models, the rating of the standard catheter was better than at least one of the other catheter in eight of ten cases and in only three cases another catheter was rated better than the standard catheter.

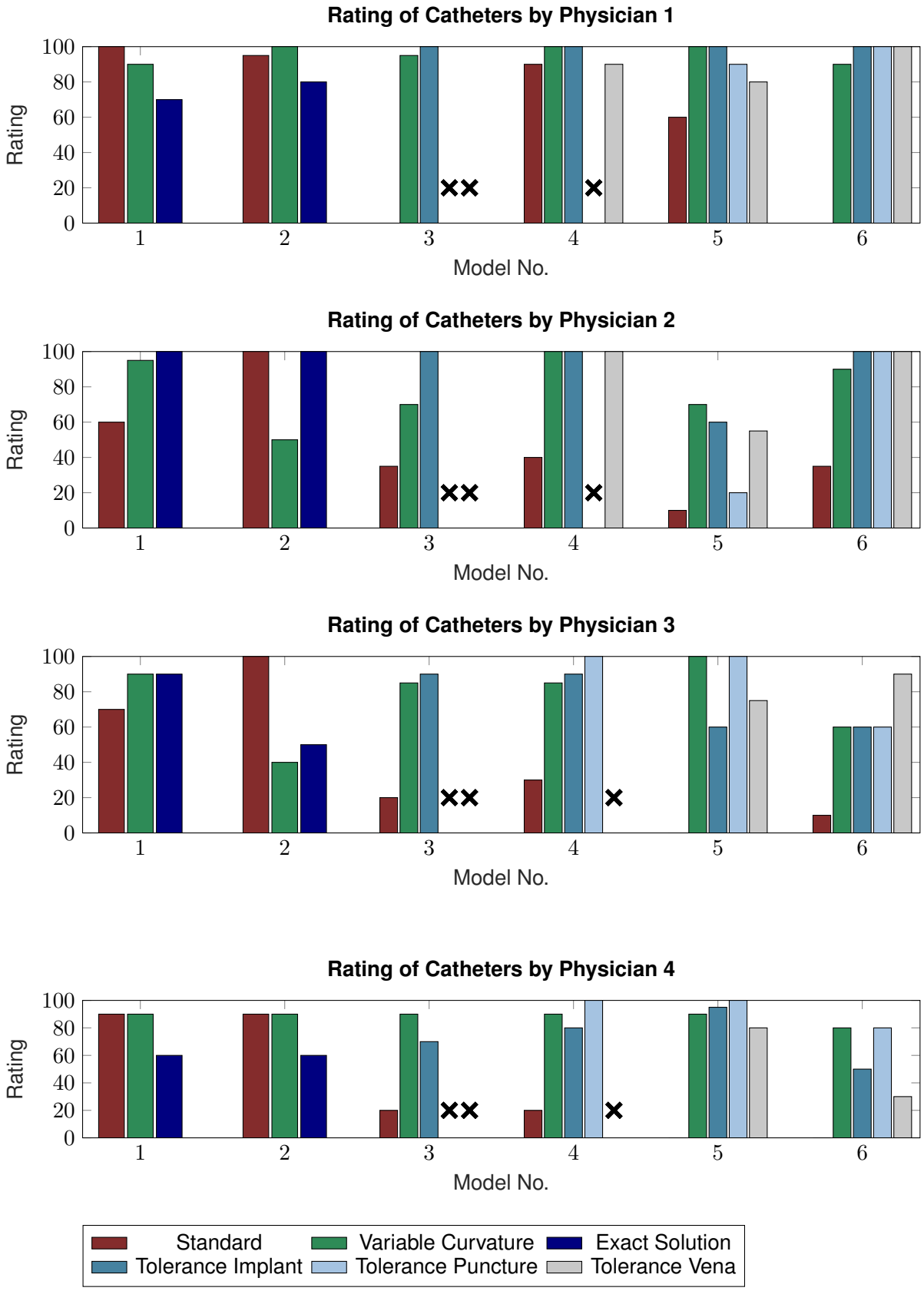

Figure 85 The suitability of each catheter was rated by the physicians. The different colors identify the types of the catheter and an 'X' stands for a missing value because the catheter was not tested.

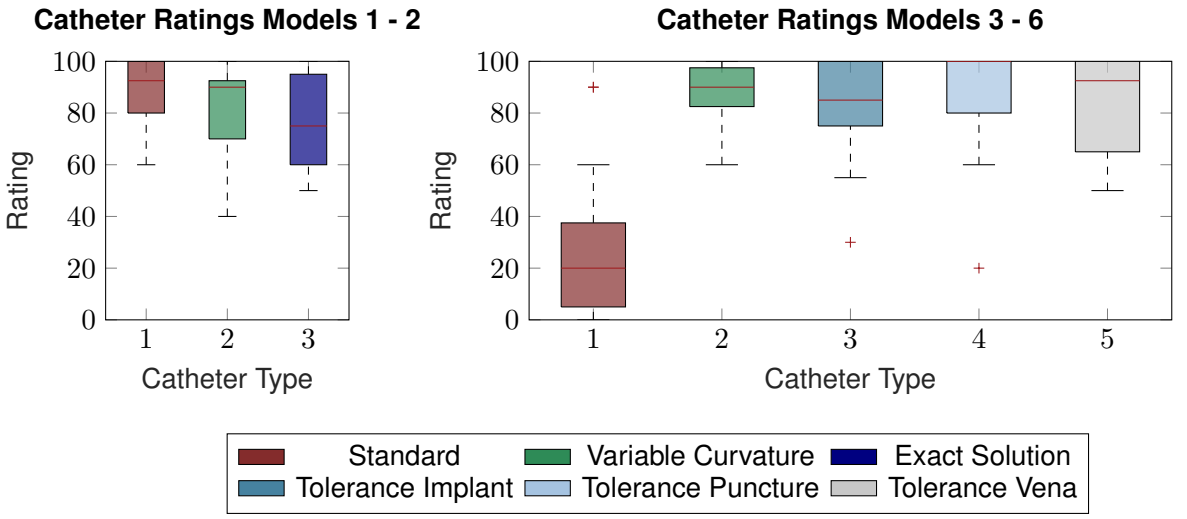

Figure 86 The median value of the rating of the standard catheter was above the patient-specific catheter with a value of 92.5 compared to 90 and 75 for the models where the standard catheter showed good suitability. However, in the less suited models, the rating of the patient-specific catheters (85 to 100) was well above the rating for the standard catheter, which had a value of 20.

In the other four models that required optimization for the calculation of the double bended catheter, the median value (20) of the standard catheter was well below the other catheter types, which reached median values between 85 and 100. In 9 of 16 cases, the standard catheter received a rating of 20 or below and in only three cases above 50. The standard catheter was rated worse than all of the patient-individual catheters in 14 cases, but did not receive a better rating than any of the patient-individual catheters. Comparing the patient-individual catheters, no clear favorite shape could be identified.

Time to Reach the Target. The physicians needed between 3 and 55 seconds to reach the target position. Some physicians were in general a bit faster than others with sample mean values of the necessary time between 9 and 25 seconds. The physicians tended to rate catheters better when they needed less time for the accomplishment of the task as shown in Figure 87.

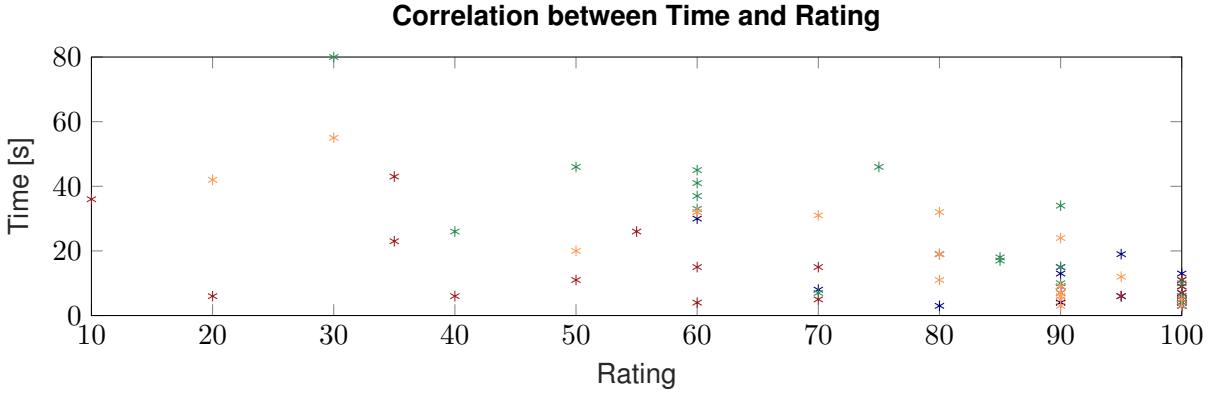

Figure 87 There was a tendency that the physician's rated trials worse if they needed longer to accomplish the task. The colors of the markers identify the four physicians.

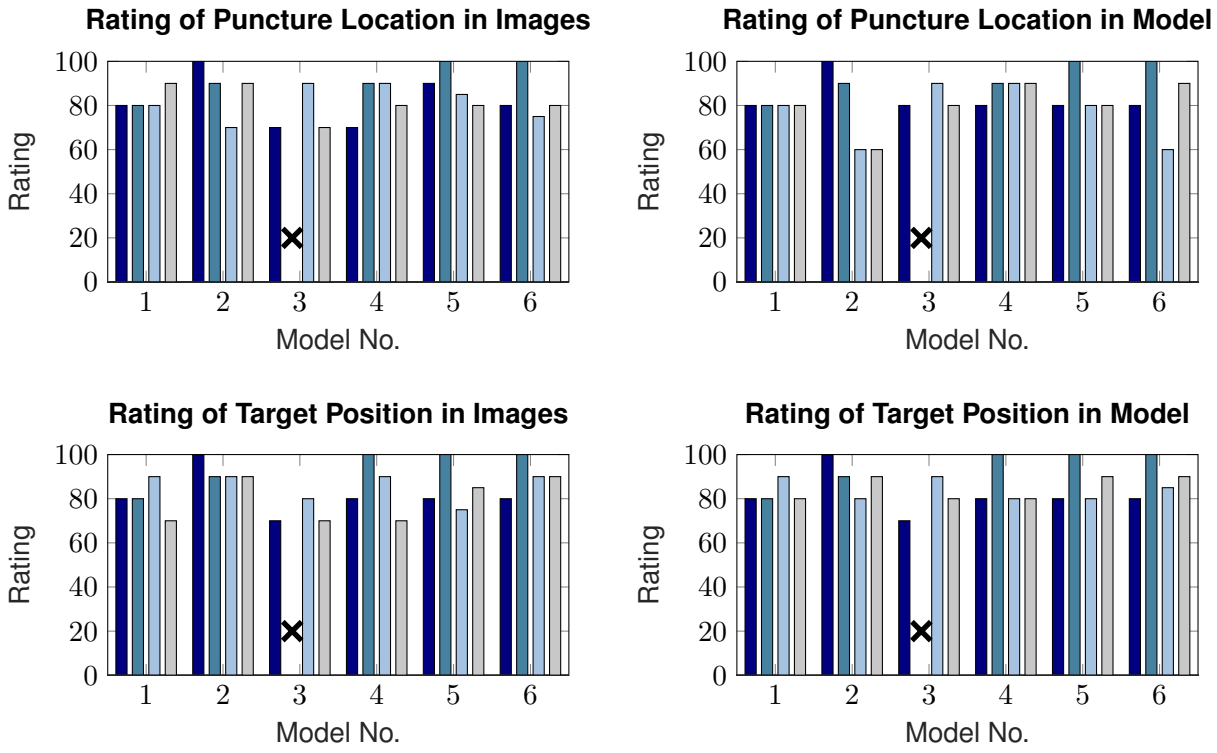

Figure 88 The planned puncture locations and target positions were rated by the physicians in the image data slices and in the model with 100 meaning that the position is suitable and 0 that the position is not suitable. A cross implicates a missing value and each color stands for a physician.

Rating of the Implant Position and Puncture Location. The physicians rated the suitability of the puncture location and the implant position. With a lowest value of 60 all of these questions were answered positively as shown in Figure 88.

Rating of the Patient-Individual Catheter Shaping. The four physicians rated for each of the six models if they considered the patient-individual shaping of the catheter as advantageous. The result showed that they generally rated the patient-individual shaping to be advantageous (see Figure 89).

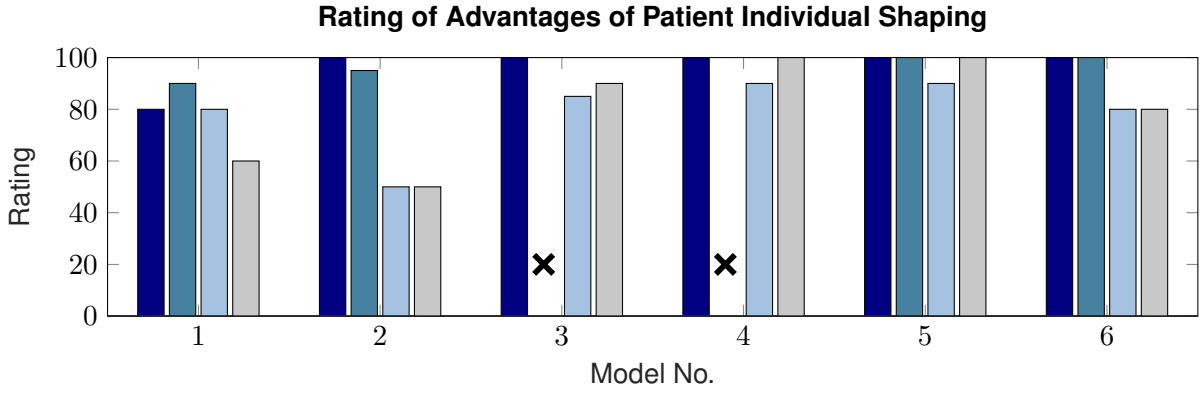

Figure 89 The advantages of the patient-specific shaping of the catheters were rated by the physicians for every model. While the results for the models one and two were not overall positive in the other models all ratings lay between values of 80 and 100. The colors indicate the different physicians and the crosses mark missing values.

The lowest values were given for the model two with twice a rating of 50, and model one with ratings between 60 and 90. The rating of the advantages of the use of the patient-specific shaping reached values equal to or above 80.

Overall rating. The overall rating whether the catheters can be compared using the heart models and whether the adaptation of the catheters to the anatomy is useful were generally positive. The results are shown in Figure 90. One of the physicians rated the possibility to evaluate the position of the transseptal puncture in the image data with a value of 40. All of the other ratings had a value of 60 or above. The feasibility to evaluate the catheters with the given models were given marks between 60 and 100. The question if the patient-specific catheters are advantageous and if they would be used again received ratings between 80 and 100.

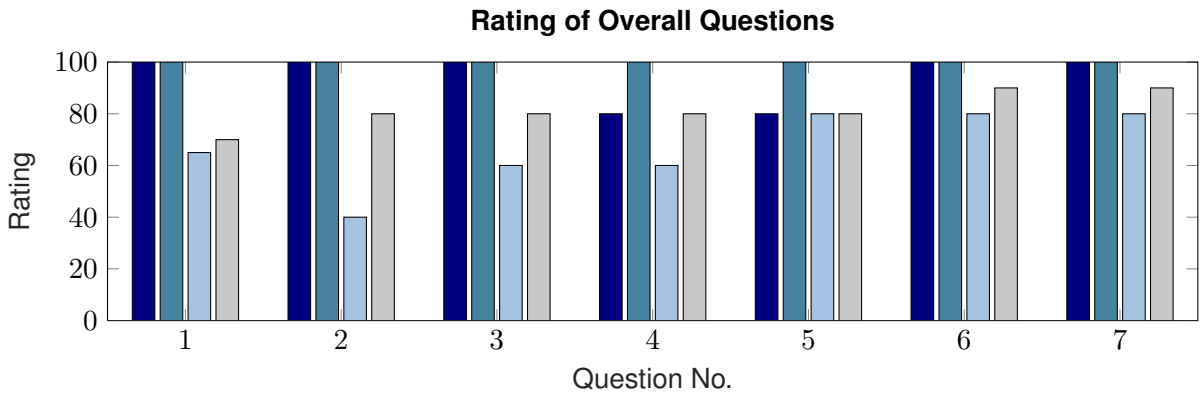

Figure 90 The following seven general questions were answered by the physicians:

1. The comparison of the catheters is possible with the models.
2. The location of the puncture point can be rated using the image slices.
3. The location of the puncture point can be rated using the model.
4. The target position of the catheter can be rated using the image slices.
5. The target position of the catheter can be rated using the model.
6. An adaptation of the catheter to the anatomy is useful.
7. I would use the adapted catheters again.

A rating of 0 stands for total disagreement with the statement and 100 for agreement. Bars of different colors indicate different physicians.

7.1.3 Discussion

The physicians stated that the comparison of the catheters using the presented models was possible and most of them answered the questions whether the puncture position and target position could be compared with the models and screen shots positively. This means that they considered the experiment feasible to test the catheters even so the models do not replicate all conditions in the catheter laboratory realistically as the imaging is different, the model is not flexible, not the whole access path is replicated and the puncture position is predefined in the model.

Due to the low number of participants and models, no statistical significant statement can be made. The overall opinion of the physicians indicates that they considered patient-individual shaping of the catheters generally advantageous. However, it is not considered advantageous for all cases of patient anatomy. If the standard catheter is well suited and the LAA is easy to reach, patient-individual shaping does not provide advantages. The suitability of the standard catheter that was

calculated with the planning program resembled the results of the experiments. When comparing the different calculation methods for the patient-individual shaping no clear favorite could be identified. In this experimental setup, the deviation from the direction vector in the vena cava should not be of importance as it can be easily compensated in the model. The deviations of the orientation in the implant position was also not weighty, as the participants did not consider the coaxial placement of catheter and LAA.

The reason for the negative ratings of the patient-individual catheters can be explained by deviations from the calculated shape to the resulting catheter shape as no spring-back compensation was employed and the catheters did not stay very long in the bending form as they were produced during the experiment. Furthermore, kinking of the catheters occurred. The catheters were prone to kink if their shape contained sharp bends, which means that high bending angles with small bending radii occurred. As a consequence, the optimization process to minimize the bending radii was implemented in order to avoid this problem.

7.2 Evaluation of the Catheter with Four Bends

In the final experiment, which is taken from Graf *et al.* (2018), the patient-individual catheters with four bends were compared to the standard catheter. Therefore, physicians tested both catheters on heart models and rated their suitability.

7.2.1 Experimental Setup

Question. The goal of this experiment was to evaluate if the rating of the patient-individually shaped catheter was better than that of the standard catheter. This question was not answered generally but separately for every model depending on the anatomical conditions.

Participants. Seven physicians working in the cardiology sector at the German Heart Center in Munich performed the experiment. One participant was experienced in the performance of the LAA occlusion procedure whereas the other six participants were novices in this procedure.

Heart Model. The rigid heart models as described in the preliminary experiment were used again for the comparison. The target marker was removed and therefore the LAA was available to allow the insertion of the implant. As the identical models were utilized, the same CT data sets as in the previous experiment were used and the planning points were not altered.

Catheters. Patient-individually shaped Amplatzer Torqvue catheters (St. Jude Medical, USA) were used and compared to the standard Amplatzer Torqvue 45x45 catheter. The patient-individual catheters with four bends and maximization of the bending radii were calculated with the planning program. The standard setting of the weighting factor was m_f = 0.1. However, if one of the bending radii was below 25 mm, the value was decreased to 0.05 or 0.025. Table 3 shows the resulting bending angles and bending radii for the six models and in Figure 91, the setup and the bending forms are displayed.

Table 3 Bending angles and radii of the resulting catheter shapes with four bends.

CT Data Set	α_1	α_2	α_3	α_4	r_1	r_2	r_3	r_4
	[°]				[mm]			
1	40	43	15	17	28	32	28	60
2	33	22	31	13	44	47	47	37
3	53	22	19	55	36	41	42	31
4	54	30	21	20	39	47	43	47
5	45	28	21	48	55	42	51	28
6	54	41	46	32	34	39	36	29

The catheters were shaped by inserting them into the bending form and placing it in the autoclave during a standard sterilization cycle with 121°C.

Figure 91 The catheters are introduced into the additively manufactured models and the implant is deployed in the LAA (left). The image on the right shows the six bending forms for the catheter shape with four bends.

Questionnaire. Each physician answered a questionnaire after performing the experiment. For every heart model, he rated the suitability of the standard catheter and of the patient-individual catheter on a scale between 100 (well suited) and 0 (not suited). Furthermore, he evaluated if the patient-individual catheter was advantageous compared to the standard catheter for the respective model on a scale between 100 (advantageous) and 0 (not advantageous). The physicians were asked to consider only the positioning of the catheter and not the introduction of the catheter through the transseptal puncture.

Experiment Procedure. The preshaped catheters and the standard catheter were provided. Every physician tested the standard catheter and the patient-individual catheter in each heart model. He inserted the catheter through the transseptal puncture and into the left atrial appendage. After positioning the catheter in the LAA, the occluder was deployed. If the position of the occluder was not satisfactory, it was retreated into the catheter and repositioned. The participant answered the questionnaire after the test of each model.

7.2.2 Results

The median ratings of the physicians for the standard catheter and the patient-individual catheter for every model are displayed in Figure 93. The ratings for the standard catheter ranged between 0 and 100 whereas the lowest rating for a patient-specific catheter was 50. While 86% of the ratings for patient-specific catheters had a value of 80 or above, this was true for only 52% of the standard catheters. The median values of the ratings for the patient-specific catheter was between 80 and 100. The median value for the standard catheter in the two data sets that were well suited for it according to the virtual insertion of the catheter reached a value of 80 and 100. In the other four data sets, it was ranging between 40 and 70.

For the first two data sets, the median value rating of the improvement that was achieved with the patient-specific catheter was 60 and 20 with a wide distribution of the physicians' single rating values. The improvements in the other four data sets was evaluated higher with a median value between 80 and 100.

This also correlated with the differences between the ratings of the standard catheter q_{std} and the patient-specific catheter q_{ps} as shown in Figure 92. In the first two models, no clear tendency whether the standard catheter or the patient-individual catheter was rated better could be identified. However, in the other four models the majority of the physicians rated the patient-specific catheter better. None of the physicians rated the standard catheter better in the models four and six and in model three, the patient-specific catheter received a better rating than the standard catheter from all participants.

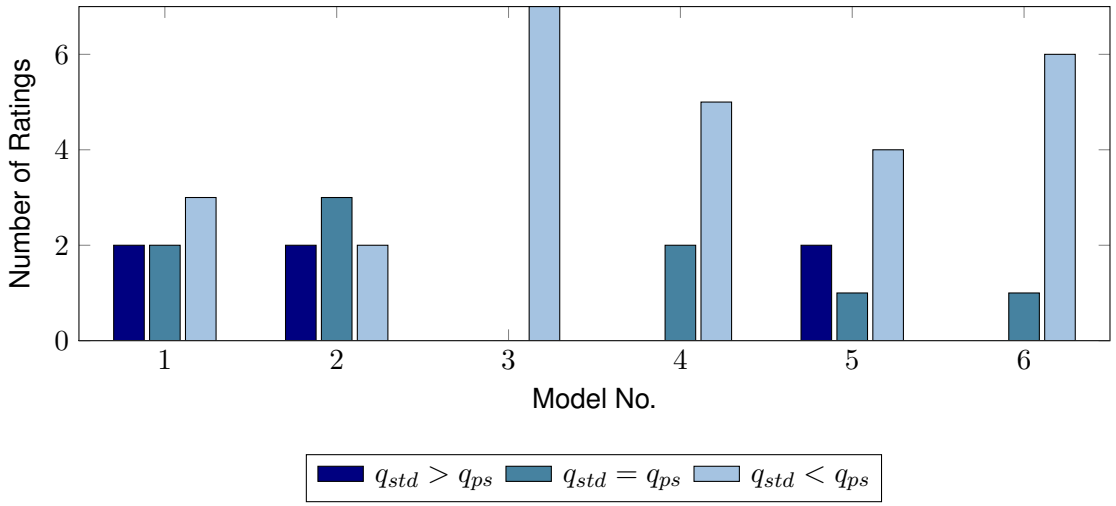

Figure 92 The differences between the ratings for the standard catheter q_{std} and the patient-specific catheter q_{ps} was calculated for every physician and each model. They were categorized according to the sign of the difference and the number of ratings per category was counted.

7.2.3 Discussion

As with the preliminary experiment, this experiment showed promising results in some but not all of the data sets. In anatomies that were well suited for the standard catheter, the patient-individual shaping of the catheters did not offer additional advantages. In contrast, in those that were difficult to access with the standard catheter, the patient-individual shaping seemed to be a good alternative,

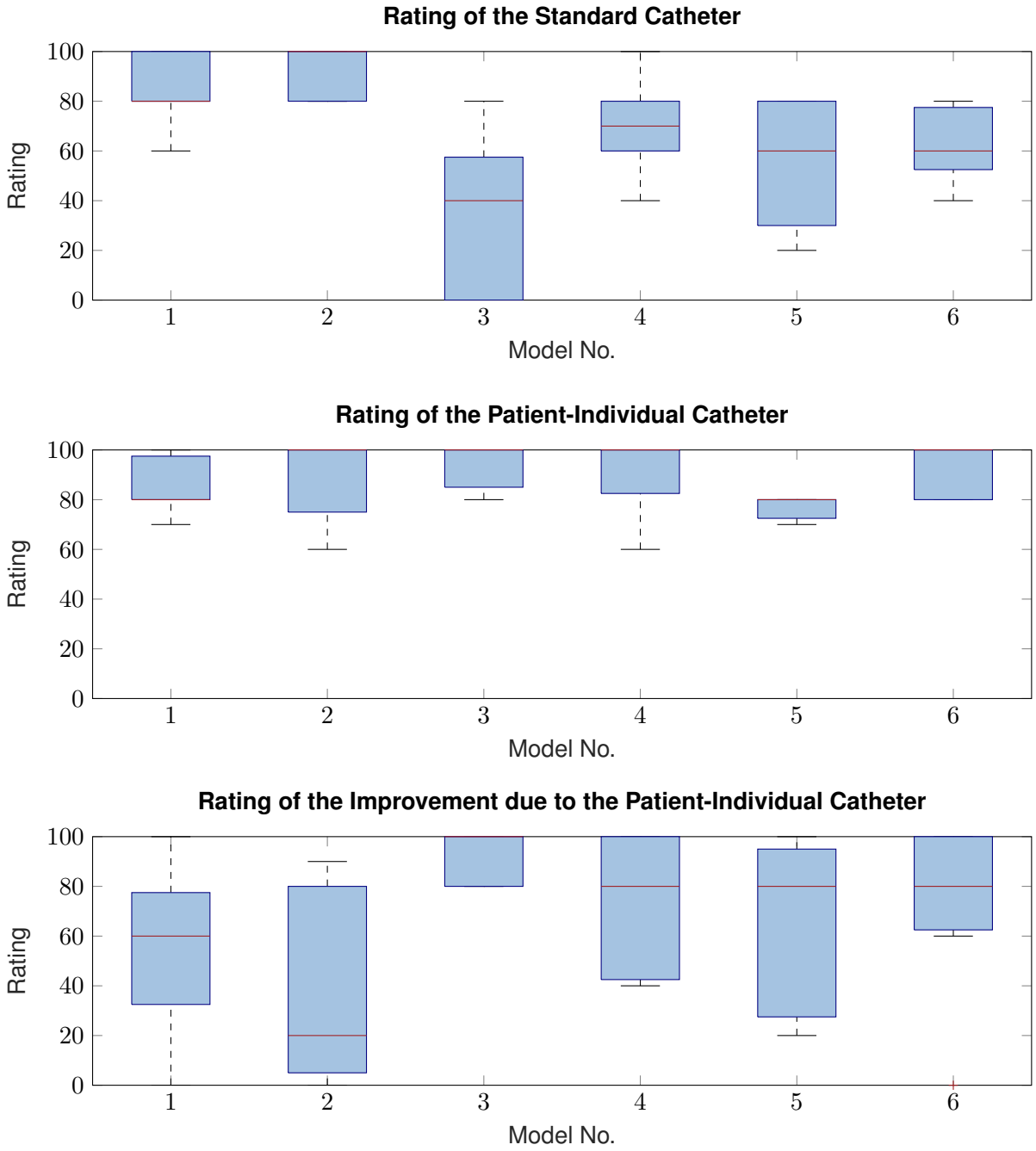

Figure 93 The graphs show boxplots of the ratings of the physicians for the standard catheter and the patient-specific catheters between 100 (suitable) and 0 (not suitable) as well as a rating of the advantages of the patient-specific shaping for the six different models.

as most of the physicians rated the patient-specific catheters better than the standard catheter. Although the models used in this experiment differed in some details from the conditions during the procedure, the experiment is a first confirmation that the patient-specific shaping seems to be advantageous for some patients with unfavorable anatomy.

8 Conclusion and Outlook

In this project an interactive planning system for the preoperative planning of the minimally invasive closure of the left atrial appendage was developed. A concept of the program was developed, the program was implemented and it was evaluated by physicians using patient-specific, additively manufactured heart models.

Motivation. Through the minimally invasive closure of the left atrial appendage with an occlusion device, strokes that are caused by thrombi originating in the LAA are prevented. The occlusion device is inserted into the left atrium of the heart through a catheter. The standard equipment is a non-steerable catheter sheath that is curved in three dimensions. With the long access paths and the use of non-steerable catheters, the maneuverability of the catheter in the heart is limited. In patients with unfavorable anatomy, this can lead to difficult if not impossible access to the implantation site. The successful choice of a suitable implant size depends on the imaging data and is challenging.

Concept and Realization. The developed planning program focuses on three major functionalities. The program enables the generation of a planning model for the implant size, the evaluation of the suitability of the standard catheter for the particular patient and the improved accessibility of the planned implant position by patient-specific shaping of the catheter.

In order to facilitate the planning of the implant size, the implant position is displayed in the image data and the compression of the implant can be evaluated. Additionally, anatomical models of the left atrial appendage can be produced based on the preoperative image data of the patient by additive manufacturing. The necessary files are directly generated in the planning program.

To obtain an estimation of the suitability of the standard catheter, its shape is displayed relative to the patient's image data after planning the boundary points of the procedure. The distance and the deviation of the catheter tip from the planned implant position provide an indication of the suitability of the standard catheter. Moreover, the pathway of the standard catheter is displayed in the image data.

In order to reach the implant position if the standard catheter is not well-suited, patient-individual catheter shapes can be determined with different calculation methods. Three different calculation methods were implemented: a double bended catheter, a catheter with varying curvature and a catheter with four bends and maximized bending radii in order to facilitate the shaping of the catheter. However, the structure of the planning program allows an easy exchange of the calculation method. The resulting catheter shape is displayed relative to the image data and if it seems to be suitable, a bending form can be generated. This form is used to shape the catheter adequately and it is automatically adapted to the catheter shape. An STL file is generated in the program by automated construction and the bending form is realized by additive manufacturing using selective laser sintering.

The planning program was realized in MATLAB R2014b and is available as a MATLAB library. It is designed as an interactive program with a graphical user interface. It works based on preoperative three-dimensional image data of the patient and requires user input through the selection of several points to plan the procedure. Based on this planning, the three functionalities can be performed independent of each other.

Results. The planning program was evaluated using additively manufactured heart models of the anatomy of six different patients. Physicians tested the standard catheters in comparison to the patient-individually shaped catheters and rated their suitability. The experiments showed promising results for the use of the patient-individual catheters. In cases were the standard catheter was not well suited, the use of a patient-individual catheter seemed to facilitate the positioning of the catheter tip in the left atrial appendage of the models.

Outlook. Future developments based on this works could include the following topics:

- **Safety of the Bending Process and Clinical Evaluation**
  The first evaluation on additively manufactured heart models showed promising results. In order to allow a clinical evaluation of the system, the safety of the bending process of the applied catheters would need to be proved. The bending behavior of the catheter including the spring-back would need to be tested and the parameters adapted. Additionally, the appropriate calculation method and its constraints have to be chosen for the particular catheter.
- **Definition of Difficult Anatomical Conditions**
  The experiments showed that the use of patient-specific catheters seems to be favorable for difficult anatomical conditions and not for all patients. In a next step, a larger number of data sets would need to be investigated to find the boundary values for the distance and deviation of the standard catheter from the planned implant position above which the anatomy is considered as difficult and a patient-specific shaping is advantageous.
- **Planning and Display of the Puncture Location**
  The evaluation of the suitability of the standard catheter can be used for an evaluation of different puncture locations to find the one that allows best access to the implantation site. As the planned puncture location has to be met during the operation, an intraoperative display of the planned puncture location would secure the success of the intervention.
- **Simulation of the Implant, Catheter and LAA Behavior**
  The presented program offers a rough estimation of the compression that the implant receives at the chosen implant position. The integration of a simulation of the implant and the LAA during the implant deployment would refine the estimation and provide information of the final implant shape after the release at a given catheter pose. As the standard catheter is usually deformed to reach the implantation site, a simulation of the bending behavior of the catheter would improve the suitability evaluation.

- **Adaptation to Other Interventional Procedures in Cardiology**
  The system can be adapted to other procedures in interventional cardiology, which would also benefit from patient-specific calculation of the catheter shape. As the display of the catheter and the calculation of the bending form works based on the centerline of the catheter and independent of the calculation method, it could be easily adapted for other procedures. The planning algorithms for the inferior vena cava and the puncture locations would be applicable for other transseptal procedures in the left atrium and the planning of the target plane would not need to be altered. This would allow the patient-specific adaptation of catheters, which could facilitate procedures especially during the treatment of patients with difficult anatomical conditions.

9 Appendix

9.1 Mathematical Conventions

In the following, the mathematical conventions that are used in this thesis are described. Generally, matrices and vectors are printed in bold whereas scalars are written in italics. Capital letters indicate matrices.

${}^1\mathbf{p}_a$	$3x1$ vector with the components x,y and z that describes a point with the name a, which is given in the coordinate system 1.
${}^1\mathbf{v}_b$	$3x1$ vector with the components x,y and z that describes a unit vector with length 1 and the name b, which is given in the coordinate system 1.
$\|\mathbf{v}\|$	Euclidean norm of the vector $\mathbf{v}$: $\|\mathbf{v}\| = \sqrt{x^2+y^2+z^2}$.
$\|a\|$	Absolute value of the scalar a.
${}^2\mathbf{T}_1$	Transformation matrix from the coordinate system 1 (index bottom right) to coordinate system 2 (index top left). It is a $4x4$ matrix of the form $${}^2\mathbf{T}_1 = \begin{pmatrix} {}^2\mathbf{R}_1 & {}^2\mathbf{t}_1 \\ \mathbf{0} & 1 \end{pmatrix}$$ consisting of a rotational part ${}^2\mathbf{R}_1$ and a translational part ${}^2\mathbf{t}_1$.
${}^2\mathbf{R}_1$	Rotational part of the transformation matrix consisting of the basis vectors of the coordinate system 1 given in coordinates of system 2: ${}^2\mathbf{R}_1 = \begin{pmatrix} {}^2\mathbf{x}_1 & {}^2\mathbf{y}_1 & {}^2\mathbf{z}_1 \end{pmatrix}$.
${}^2\mathbf{t}_1$	Translational part of the transformation matrix describing the position of the origin of the coordinate system 1 in coordinates of system 2: ${}^2\mathbf{t}_1 = {}^2\mathbf{p}_{0_1}$
$\mathbf{x_1}$, $\mathbf{y_1}$, $\mathbf{z_1}$	Basis vectors of the coordinate system 1 that are unit vectors with length 1.
∇f	Gradient of the function f: $\nabla f(k_1, k_2, ..., k_m) = \begin{pmatrix} \frac{\partial f}{\partial k_1} & \frac{\partial f}{\partial k_2} & ... & \frac{\partial f}{\partial k_m} \end{pmatrix}^T$
$\mathbf{H}_f$	Hessian matrix of f: $\mathbf{H}_f(\mathbf{k}) = \begin{pmatrix} \frac{\partial^2 f}{\partial k_1 \partial k_1} & \frac{\partial^2 f}{\partial k_1 \partial k_2} & \cdots & \frac{\partial^2 f}{\partial k_1 \partial k_m} \\ \frac{\partial^2 f}{\partial k_2 \partial k_1} & \frac{\partial^2 f}{\partial k_2 \partial k_2} & \cdots & \frac{\partial^2 f}{\partial k_2 \partial k_m} \\ \vdots & \vdots & \ddots & \vdots \\ \frac{\partial^2 f}{\partial k_m \partial k_1} & \frac{\partial^2 f}{\partial k_m \partial k_2} & \cdots & \frac{\partial^2 f}{\partial k_m \partial k_m} \end{pmatrix}$, with $\mathbf{k} = (k_1, k_2, ..., k_m)^T$.

9.2 Coordinate Systems and Variables

This chapter provides an overview of the variables that are used in the thesis.

Coordinate Systems. Every coordinate system is defined by its basis vectors $\mathbf{x}$, $\mathbf{y}$, $\mathbf{z}$ and the origin $\mathbf{p}_0$ of the coordinate system. Based on this information a transformation matrix $\mathbf{T}$ is calculated.

mod	Model of the patient
roi	Region of interest around the left atrial appendage, aligned with the implant axis
$form$	Coordinate system for the construction of the bending form, oriented along the main extents of the centerline points
img_1	Axial image for the selection of a cross-section of the left atrial appendage
img_2	Vertical image for the determination of the inclination of the implant
img_3	Oblique image that lies in the implant plane
c_k	Coordinate system at every point on the catheter centerline, basis vectors calculated based on the coordinate system mod
$\hat{c}_k$	Coordinate system at every point on the catheter centerline, basis vectors calculated based on the coordinate system $form$

Variables. The variables that are used in this thesis are listed below.

[h!] a	Distance from the boundaries at which the penalty function has the value b
α_1 to α_4	Bending angles of the catheter shape
$\alpha_{b,j}$	Bending angle at every point in a bended segment of the catheter shape
a	Value of the penalty function at a distance a from the boundaries
b_x, b_y, b_z	Spacing of the voxels in the image data set
b_{roi}	Spacing of the voxels in the ROI around the implant position
β	Angle between the two bending planes of a double bended catheter
β_2	Angle between the normal vector of the first bending plane and the direction vector of the third segment of a double bended catheter
c	Estimated compression of the implant
d_b	Distance of the points on the catheter centerline in the curved segment
d_{gap}	Gap width that is necessary to avoid the fusion of parts during additive manufacturing
d_{max}	Maximum diameter of the orifice of the LAA in the image slice
d_{min}	Minimum diameter of the orifice of the LAA in the image slice
d_p	Distance of the second segment of the double bended catheter from the planned puncture location

$d_{support}$	Width of the support structures of the bending form
d_{sleeve}	Width of the sleeve of the bending form
d_{snap}	Width of the snap hook of the bending form
d_{std}	Distance from the calculated catheter tip of the standard catheter to the implant position
d_{wall}	Wall thickness of the anatomical model
δ_i	Deviation of the direction vector at the tip of the calculated double bended catheter to the planned implant orientation
δ_j, $\delta_{j,min}$	Deviation of the implant axis between two iterations calculating automatic alignment of the implant axis with the LAA and boundary value of the deviation
δ_{std}	Deviation from the calculated catheter tip of the standard catheter to the implant orientation
δ_v	Deviation of the direction vector at the third segment of the calculated double bended catheter to the planned orientation of the inferior vena cava
δ_{v_p}	Deviation of the direction vector at the puncture location in the catheter shape with four bends from the planned vector orthogonal to the surface of the left atrium
ϵ_g	Boundary value for the difference between two iterations during the optimization
ϵ_g	Boundary value for the gradient of the target function during the optimization
f	Target function of the optimization
f_{right},f_{left}	Target function of the optimization, evaluated separately for the catheter segments in the right and left atrium
f_i, f_p, f_v	Target functions for the optimization of the double bended catheter with a tolerance at the planned implant, puncture or vena position or orientation
g	Factor of the penalty function controlling the steepness of the step
h	Factor of the penalty function controlling the value outside the boundaries
i, i_{max}	Number of iterations for the line search during the optimization and maximum number
$\mathbf{I}$	Matrix containing the gray value intensities of a two-dimensional image
j, j_{max}	Number of iterations for the Newton-Raphson-Method during the optimization and maximum number
k_1 to k_4, k_m	Variable parameters for the catheter shape optimization describing the lengths of the segments, the superscript counts the iterations
$\mathbf{k}$	Vector containing the variable parameters for the optimization, the superscript counts the iterations and a tilde means that only integer values are considered
κ	Curvature of the catheter shape

l_1 to l_3	Lengths of the segments of the double bended catheter
n_b	Number of points on the catheter centerline in the curved segment
n_{comp}	Number of segmented voxels in the data set of the compressed implant
n_l	Number of points on the outline of the orifice of the LAA
n_r	Exponent for the approximation of the maximum function
$\mathbf{n}_1$, $\mathbf{n}_2$	Normal vectors on the bending planes of the double bended catheter
n_{uncomp}	Number of segmented voxels in the data set of the uncompressed implant
$\mathbf{n}_{b,j}$	Normal vectors on the catheter cross-sections in the curved segment
$\mathbf{n}_{c_k}$	Normal vectors on the catheter cross-sections along the catheter centerline
$\mathbf{n}_{\hat{c}_k,w}$	Altered normal vectors on the catheter cross-sections along the catheter centerline for stepwise construction of the bending form
m_f	Weighting factor for the deviation from the vector at the puncture location in the target function of the optimization
p	Penalty function for the optimization, penalizing the non-compliance with boundary values, can refer to specific parameters and their maximum and minimum values as described in the index
p_{right}, p_{left}	Sum of the penalty functions that are relevant for the catheter shape in the right and left atrium
$\mathbf{p}_1$	Point on the first catheter segment
$\mathbf{p}_2$	Point on the second catheter segment
$\mathbf{p}_3$	Point on the third catheter segment
$\mathbf{p}_{b_1}$ to $\mathbf{p}_{b_4}$	Bending points of the catheter shape
$\mathbf{p}_{b,j}$	Points on the catheter centerline in the curved segment
$\mathbf{p}_{b,s}$, $\mathbf{p}_{b,e}$	Start and end point of a bended segment of the catheter shape
$\mathbf{p}_{b,o}$	Center point of the circle segment describing the bend of the catheter shape
$\mathbf{p}_{c_k}$	Points on the catheter centerline with the components $x_{p_{\hat{c}_k}}$, $y_{p_{\hat{c}_k}}$ and $z_{p_{\hat{c}_k}}$
$\mathbf{p}_{\hat{c}_k,w}$	Altered points on the catheter centerline for stepwise construction of the bending form
$\mathbf{p}_f$	Point on the second segment of the double bended catheter with least distance to the planned puncture location
$\mathbf{p}_i$	Planned implant position
$\mathbf{p}_{i_1}$ to $\mathbf{p}_{i_3}$	Three points that define the implant plane and that are selected by the user
$\mathbf{p}_{i_{1,2}}$	Central point of the connecting line between the points $\mathbf{p}_{i_1}$ and $\mathbf{p}_{i_2}$
$\mathbf{p}_{i,j}$, $\mathbf{p}_{i,j+1}$	Planned implant position before and after alignment with the LAA
$\mathbf{p}_l$	Points on the outline of the orifice of the LAA
$\mathbf{p}_m$	Central point on the catheter centerline in a segment of the bending form
$\mathbf{p}_o$	Centroid of the centerline points in a segment of the bending form

$\mathbf{p}_p$	Planned puncture position
$\mathbf{p}_{q,x_1}$, $\mathbf{p}_{q,x_2}$, $\mathbf{p}_{q,y_1}$, $\mathbf{p}_{q,y_2}$	Intersection points of the basis vectors in x- and y-direction with the borders of the image data set
$\mathbf{p}_{s0}$, $\mathbf{p}_{s1}$	Boundary points for the calculation of the spline segment
$\mathbf{p}_v$	Planned position of the inferior vena cava
$\mathbf{p}_{v1}$	Upper selected point of the inferior vena cava
$\mathbf{p}_{v2}$	Lower selected point of the inferior vena cava
q_{ps}	Rating of the standard catheter
q_{ps}	Rating of the patient-specific catheter
r_1 to r_6	Boundary radii of the catheter shape with four bends
r_{b1} to r_{b_4}	Bending radii of the catheter shape
r_{bolt}	Radius of the bolt of the bending form
r_{groove}	Radius of the groove of the bending form
r_{snap}	Radius of the snap hook of the bending form
r_{sleeve}	Radius of the hole in the sleeve of the bending form
s_1 to s_4	Lengths of the straight segments of the catheter shape with four bends at the boundary points
$\mathbf{u}_b$, $\mathbf{v}_b$	Vectors in the bending plane of a circular bend
$\mathbf{v}_1$	Direction vector of the first catheter segment
$\mathbf{v}_2$	Direction vector of the second catheter segment
$\mathbf{v}_3$	Direction vector of the third catheter segment
$\mathbf{V}$, $\mathbf{v}$	Voxel data set containing the image data and one point of the voxel data set
$\mathbf{v}_i$	Planned direction vector at the implant position
$\mathbf{v}_{i,j}$, $\mathbf{v}_{i,j+1}$	Planned direction vector at the implant position before and after alignment with the LAA
$\mathbf{v}_p$	Planned direction vector at the puncture location
$\mathbf{v}_{p,\delta}$	Direction vector at the puncture location with deviation from the planned vector normal to the surface of the left atrium
$\mathbf{v}_{s0}$, $\mathbf{v}_{s1}$	Direction vectors at the boundary points for the calculation of the spline segment
$\mathbf{v}_v$	Planned direction vector of the inferior vena cava
w_f	Factor for the reduction of the distances to the central axis for stepwise construction of the bending form
w_f	Damping parameter for the optimization, the superscript counts the iterations
γ_1, γ_2	Rotation angle of $\mathbf{v}_p$ about the x- and y-axis for the calculation of the catheter shape with four bends
z_{v1}, z_{v2}	z-component of the upper and lower point of the inferior vena cava

9.3 Glossary

This glossary provides an explanation of several terms that are used in this thesis.

Anterior	Anatomical direction: towards the front of the body (Patton & Thibodeau, 2014)
Anticoagluatant	Substance that prevents the clotting of blood (Mosby's, 2013, p. 110)
Arrhythmia	Cardiac rhythm differing from the normal sinus rhythm (Bayés de Luna, 2011, p. 3)
Atrial appendage	Pouch-like extensions hanging off the atria (Weinhaus, 2015, p. 63)
Appendectomy	Surgical amputation of the left atrial appendage (Hanif & Whitlock, 2015, p. 68)
Orifice	Entrance of a cavity of the body (Mosby's, 2013, p. 1283)
Ostium	See Orifice
Atrial fibrillation	Cardiac arrhythmia with disorganized electrical activity in the atria (Mosby's, 2013, p. 156)
Atrial flutter	Atrial tachycardia with contraction rates between 230 and 380 /min (Mosby's, 2013, p. 156)
Atrioventricular Valve	Valves in the heart that are situated between the ventricles and the arteries that are leading away from the heart (Thiriet, 2014, p. 6)
Atrium	Chambers of the heart that collect the blood before it flows into the ventricles (Weinhaus, 2015, p. 67)
Auricle	See Atrial appendage
Axial plane	Plane that lies normal to the body's main axis and divides it into an upper and a lower part
Catheterization	Introduction of a catheter (Mosby's, 2013, p. 307)
Catheter	Flexible hollow tube that is inserted into a vessel (Mosby's, 2013, p. 307)
Chordae tendineae	Tendinous chords that are attached to the papillary muscles and the leaflets of the atrioventricular valves (Thiriet, 2014, p. 7)
Coronal plane	Plane that runs in the body from side to side and divides it into an anterior and a posterior part (Patton & Thibodeau, 2014, p. 12)
Diastole	Filling phase of the heart (Mosby's, 2013, p. 530)
Distal	Anatomical direction: away from the trunk or point of attachment (Patton & Thibodeau, 2014)
Dyspnea	Breathlessness (Mosby's, 2013, p. 576)
Echocardiography	Studying the structure and motion of the heart using ultrasound (Mosby's, 2013, p. 582)

Endocardial	From within the heart
Endovascular	Inside the blood vessels
Epicardial	On the outside of the heart
Excision	Removal of the LAA (Hanif & Whitlock, 2015, p. 65)
Excitation	Nerve or muscle action as a consequence of impulse propagation (Mosby's, 2013, p. 655)
Exclusion	Isolation of the LAA from the circulation (Hanif & Whitlock, 2015, p. 65)
Extravascular	Outside the blood vessels
Fatigue	Exhaustion (Mosby's, 2013, p. 679)
Femoral vein	Large vein in the thigh (Mosby's, 2013, p. 686)
Fluoroscopy	Examination of the body by the continuous display of radiographic images (Mosby's, 2013, p. 712)
Fossa Ovalis	Oval depression of the right atrium, remnant of the foramen ovale in the fetus (Thiriet, 2014, p. 16)
Heart Failure	Condition in which the heart cannot pump enough blood (Mosby's, 2013, p. 812)
Hypotension	Condition with inadequate blood pressure for normal perfusion and oxygenation (Mosby's, 2013, p. 886)
Inferior	Anatomical direction: towards the bottom of the body (Patton & Thibodeau, 2014)
Interatrial septum	Wall separating the atria of the heart
Intracardiac echocardiography	Echocardiographic imaging of the heart using an ultrasound probe that is mounted on a cardiac catheter (Berti *et al.*, 2015, p. 102)
Mitral valve	Heart valve situated between the left atrium and the left ventricle (Weinhaus, 2015, p. 75)
Left Atrial Appendage	Muscular pouch situated at the left atrium
Occlusion	Closure (Mosby's, 2013, p. 1257)
Orifice	Entrance of a cavity of the body (Mosby's, 2013, p. 1283)
Ostium	See Orifice
Palpitations	Pounding or racing of the heart (Mosby's, 2013, p. 1319)
Papillary Muscles	Muscles situated inside the ventricles that help to open and close the atrioventricular vales (Mosby's, 2013, p. 1325)
Patent Foramen Ovale	Opening in the interatrial septum between left and right atrium, closes in most people after birth (Bass, 2015, p. 7)
Pigtail catheter	Cardiac catheter with a curled tip
Posterior	Anatomical direction: towards the back of the body (Patton & Thibodeau, 2014)
Proximal	Anatomical direction: towards the trunk (Patton & Thibodeau, 2014)

Pulmonary trunk	Vessel that carries the blood away from the right ventricle towards the lungs (Weinhaus, 2015, p. 67)
Pulmonary valve	Heart valve situated between the right ventricle and the pulmonary trunk (Weinhaus, 2015, p. 72)
Pulmonary vein	Vessels that enter the heart in the left atrium, arranged as two pairs, carrying the oxygenated blood from the lungs into the heart (Weinhaus, 2015, p. 73)
Sagittal plane	Plane running through the body from the front to the back and dividing the body into left and right (Patton & Thibodeau, 2014, p. 12)
Sinoatrial node	'Pacemaker' of the conduction system of the heart, situated in the right atrium (Weinhaus, 2015, p. 70)
Sinus rhythm	Cardiac rhythm that is stimulated by the sinus node with a frequency of 60 to 100/min (Mosby's, 2013, p. 1646)
Stroke	Condition with decreased blood supply in the brain due to the occlusion of a vessel or a bleeding (Weinhaus, 2015, p. 327)
Superior	Anatomical direction: towards the front of the body (Patton & Thibodeau, 2014)
Supraventricular tachycardia	Heart rate exceeding 100/min that originates in the sinus node, the atria or the atrioventricular bundle (Mosby's, 2013, p. 1720)
Syncope	Brief loss of consciousness (Mosby's, 2013, p. 1729)
Systole	Contraction phase of the heart (Mosby's, 2013, p. 1736)
Tachyarrhythmia	Abnormal cardiac rhythm with increased heart rate (Mosby's, 2013, p. 1737)
Thrombus	Blood clot (Mosby's, 2013, p. 1771)
Transesophageal echocardiography	Echocardiographic imaging of the heart using an ultrasound probe that is placed in the patient's esophagus (Berti *et al.*, 2015, p. 102)
Transthoratic echocardiography	Echocardiographic imaging of the heart using an ultrasound probe that is placed on the patient's chest
Tricuspid valve	Heart valve situated between the right atrium and the right ventricle (Weinhaus, 2015, p. 70)
Vena cava	Superior and inferior vena cava, large veins that lead oxygen-poor blood into the right atrium coming from above or below the heart (Weinhaus, 2015, p. 67)
Ventricles	Chambers of the heart that are pumping the blood away from the heart (Weinhaus, 2015, p. 67)

9.4 List of Abbreviations

ACP	Amplatzer Cardiac Plug
BREP	Boundary Representation
CCTA	Cardiac computed angiography
CT	Computed tomography
DICOM	Digital Imaging and Communications in Medicine
DOF	Degree of Freedom
Fr	French
HU	Hounsfield Unit
ICE	Intracardiac echocardiography
LAA	Left atrial appendage
LA	Left atrium
LV	Left ventricle
MDCT	Multidetector computerized tomography
MIP	Maximum-intensity projection
MPR	Multiplanar reconstructions
MRI	Magnetic resonance imaging
PCA	Principal Component Analysis
PLAATO	Percutaneous Left Atrial Appendage Transcatheter Occlusion
PTFE	Polytetrafluoroethylene
PVA	Polyvinyl acetate
RA	Right atrium
RV	Right ventricle
ROI	Region of Interest
STL	Stereolithography or Standard Tessellation Language
TAVI	Transcatheter aortic valve implantation
TEE	Transesophageal echocardiography
TTE	Transthoracic echocardiography
US	Ultrasound
2D	Two-dimensional
3D	Three-dimensional

9.5 Questionnaires

In the following chapter, the questions that were asked in the questionnaires of the two experiments are listed.

9.5.1 Experiment 1

The physicians answered general questions after completion of the whole experiment and a list of questions, which were asked for every CT data set and model separately. In both cases the physicians were asked to rate their agreement with statements. The ratings ranged from 0 (Complete denial, *Trifft nicht zu*) to 100 (Total accordance, *Trifft voll zu*).

General Questions

1. *Ein Vergleich der Katheter anhand der Modelle ist möglich.*
   The comparison of the catheters is possible with the models.
2. *Die Lage der Punktionsstelle kann anhand der Schnittbilder gut beurteilt werden.*
   The location of the puncture point can be rated using the image slices.
3. *Die Lage der Punktionsstelle kann anhand des Modells gut beurteilt werden.*
   The location of the puncture point can be rated using the model.
4. *Die Zielposition des Katheters kann anhand der Bilddaten gut beurteilt werden.*
   The target position of the catheter can be rated using the image slices.
5. *Die Zielposition des Katheters kann anhand des Modells gut beurteilt werden.*
   The target position of the catheter can be rated using the model.
6. *Ein Anpassen des Katheters an die Anatomie is sinnvoll.*
   An adaptation of the catheter to the anatomy is useful.
7. *Ich würde die angepassten Katheter wieder benutzen.*
   I would use the adapted catheters again.

Questions Depending on the CT Data Set.

These questions were asked for every CT data set separately. The fifth question regarding the accessibility of the left atrial appendage with the catheter was asked repeatedly depending on the number of catheters that were used with the corresponding model.

1. *Die gewählte Punktionsstelle erscheint in den Schnittbildern geeignet.*
   The planned puncture location seems to be suitable in the image slices.
2. *Die gewählte Punktionsstelle erscheint am Modell geeignet.*
   The planned puncture location seems to be suitable in the model.

3. *Die gewählte Implantatposition erscheint in den Schnittbildern geeignet.*
   The planned implant position seems to be suitable in the image slices.

4. *Die gewählte Implantatposition erscheint am Modell geeignet.*
   The planned implant position seems to be suitable in the model.

5. *Das Vorhofohr war mit dem Katheter 'X' gut zu erreichen.*
   The left atrial appendage was easily accessible with the catheter 'X'.

6. *Die individuell geformten Katheter haben gegenüber dem Standardkatheter Vorteile gebracht.*
   The individually shaped catheters were advantageous compared to the standard catheter.

9.5.2 Experiment 2

For every model, the physicians answered the following three questions rating the suitability in a range from 0 (Not suited, *Nicht geeignet*) to 100 (Well suited, *Gut geeignet*).

1. *Ist der Standardkatheter gut geeignet?*
   Is the standard catheter well suited?

2. *Ist der patientenindividuelle Katheter gut geeignet?*
   Is the patient-specific catheter well suited?

3. *Ist der patientenindividuelle Katheter besser geeignet als der Standardkatheter?*
   Is the patient-specific catheter better suited than the standard catheter?

9.6 Experimental Results.

The following tables list the results of the questionnaires as well as the time that was necessary for accomplishment of the task in the first experiment. The following abbreviations are used:

R Reference catheter (standard catheter)
S Catheter with variable curvature calculated using the spline interpolation
E Double bended catheter with exact solution of the intersection problem
I Double bended catheter with tolerance at the implant position
P Double bended catheter with tolerance at the puncture location
V Double bended catheter with tolerance at the orientation of the inferior vena cava

Suitability of the Standard Catheter.

CT Data Set	Distance d_{std} [mm]	Deviation δ_{std} [°]
CT 1	16.4	40.0
CT 2	19.2	42.0
CT 3	43.0	59.0
CT 4	44.0	68.0
CT 5	56.9	61.5
CT 6	70.2	67.3

9.6.1 Results of Experiment 1

Patient-Individual Double Bended Catheter Shapes.

CT Data Set	Catheter Type	Angle α_1 [°]	Angle α_2 [°]	Dist. k_1 [mm]	Dist. k_2 [mm]
CT 1	E	32.8	55.7	23.4	38.5
CT 2	E	45.4	65.8	33.5	35.1
CT 3	I	38.2	48.9	17.4	71.2
	P	38.2	48.9	17.4	71.2
	V	39.0	47.7	18.4	70.0
CT 4	I	75.4	84.9	54.5	43.0
	P	33.9	40.9	10.0	76.8
	V	34.5	41.2	10.9	75.9
CT 5	I	61.0	88.7	62.8	27.6
	P	20.7	45.2	10.0	80.3
	V	70.3	88.2	56.5	34.8
CT 6	I	67.7	80.2	67.1	18.0
	P	25.4	39.1	10.0	75.3
	V	34.1	44.5	10.9	63.0

Answers on General Questions.

	Quest. 1	Quest. 2	Quest. 3	Quest. 4	Quest. 5	Quest. 6	Quest. 7
Physician 1	100	100	100	80	80	100	100
Physician 2	100	100	100	100	100	100	100
Physician 3	65	40	60	60	80	80	80
Physician 4	70	80	80	80	80	90	90

Questions Depending on CT Dat Set.

		Question 1	Question 2	Question 3	Question 4	Question 6
CT 1	Physician 1	80	80	80	80	80
	Physician 2	80	80	80	80	90
	Physician 3	80	80	90	90	80
	Physician 4	90	80	70	80	60
CT 2	Physician 1	100	100	100	100	100
	Physician 2	90	90	90	90	95
	Physician 3	70	60	90	80	50
	Physician 4	90	60	90	90	50
CT 3	Physician 1	70	80	70	70	100
	Physician 2	X	X	X	X	X
	Physician 3	90	90	80	90	85
	Physician 4	70	80	70	80	90
CT 4	Physician 1	70	80	80	80	100
	Physician 2	90	90	100	100	X
	Physician 3	90	90	90	80	90
	Physician 4	80	90	70	80	100
CT 5	Physician 1	90	80	80	80	100
	Physician 2	100	100	100	100	100
	Physician 3	85	80	75	80	90
	Physician 4	80	80	85	90	100
CT 6	Physician 1	80	80	80	80	100
	Physician 2	100	100	100	100	100
	Physician 3	75	60	90	85	80
	Physician 4	80	90	90	90	80

Ratings of Catheters in Experiment 1.

	Catheter	Physician 1		Physician 2		Physician 3		Physician 4	
	Type	Rating	Time	Rating	Time	Rating	Time	Rating	Time
CT 1	R	100	3	60	4	70	7	90	9
	S	90	4	95	6	90	9	90	6
	E	70	8	100	5	90	34	60	32
CT 2	R	100	6	100	6	100	6	90	7
	S	95	13	50	11	40	26	90	24
	E	80	3	100	11	50	46	60	32
CT 3	R	0	X	35	23	20	X	20	X
	S	95	19	70	15	85	18	90	5
	V	100	5	100	5	90	15	70	31
CT 4	R	90	9	40	6	30	80	20	42
	S	100	4	100	9	85	17	90	3
	I	90	15	100	11	X	X	X	X
	P	X	X	X	X	100	4	100	3
	V	100	5	100	7	90	9	80	11
CT 5	R	60	30	10	36	0	X	0	X
	S	100	5	70	5	100	10	90	9
	I	80	19	55	26	75	46	80	32
	P	90	9	20	6	100	4	100	5
	V	100	4	60	15	60	45	95	12
CT 6	R	90	4	35	43	10	X	0	X
	S	90	13	90	7	60	41	80	19
	I	100	7	100	4	90	10	30	55
	P	100	3	100	5	60	33	80	19
	V	100	5	100	9	60	37	50	20

9.6.2 Results of Experiment 2

Ratings of Catheters in Experiment 2.

		Phys. 1	Phys. 2	Phys. 3	Phys. 4	Phys. 5	Phys. 6	Phys. 7
CT 1	Question 1	80	100	100	60	80	100	80
	Question 2	90	80	100	80	80	70	100
	Question 3	60	70	80	40	0	30	100
CT 2	Question 1	80	80	100	100	80	100	100
	Question 2	90	60	100	100	100	70	100
	Question 3	80	20	80	0	90	20	0
CT 3	Question 1	50	0	60	0	40	80	0
	Question 2	80	100	100	80	100	100	100
	Question 3	80	100	100	80	100	80	100
CT 4	Question 1	60	100	60	40	80	80	70
	Question 2	90	100	100	60	100	80	100
	Question 3	80	100	100	40	40	50	100
CT 5	Question 1	20	80	60	20	80	80	60
	Question 2	100	50	80	80	80	70	80
	Question 3	100	50	80	100	20	20	80
CT 6	Question 1	50	80	60	40	80	60	70
	Question 2	80	100	100	80	80	100	100
	Question 3	70	100	100	60	0	80	100

9.7 Student Research Projects

In the course of the project, several students were involved that were supervised by the author. Some of their results influenced the listed chapters of the thesis.

- **Julian Bernard** Master Thesis, 2015
  Entwicklung einer Biegemaschine für das patientenindividuelle Formen eines Katheters
- **Christoph Kugler** Bachelor Thesis, 2015
  Konzept und Realisierung einer handgehaltenen mechanischen Entfaltungsvorrichtung für den minimalinvasiven Vorhofohrverschluss
- **Sebastian Pammer** Term Paper, 2016
  Planung einer optimierten Punktionsstelle für den minimal-invasiven Vorhofohrverschluss
- **Julian Praceus** Diploma Thesis, 2015
  Interaktive bilddatenbasierte Planung einer optimierten Katheterform für den minimalinvasiven Verschluss des linken Vorhofohrs des Herzens
  Influenced chapters 6.2, 6.3.1, 6.6, 6.8.1, 6.8.2 and 6.9
- **Sandro Süß** Bachelor Thesis, 2017
  Untersuchung von Herstellungsparametern und Rückformungseigenschaften für die Konstruktion patientenindividuell angepasster Biegeformen für Katheter
  Influenced chapter 6.10.3
- **Franziska Zhu** Bachelor Thesis, 2016
  Optimierung eines Phantoms für die Simulation des minimalinvasiven Verschlusses des linken Vorhofohrs
  Influenced chapter 6.11.2

Bibliography

Agarwal, S.; Tuzcu, E.M.; Krishnaswamy, A.; Schoenhagen, P.; Stewart, W.J.; Svensson, L.G. & Kapadia, S.R. (2015): 'Transcatheter aortic valve replacement: current perspectives and future implications.' *Heart (British Cardiac Society)*, **101**(3): pp. 169–177, ISSN 1468-201X, doi:10.1136/heartjnl-2014-306254.

Ageno, W.; Gallus, A.S.; Wittkowsky, A.; Crowther, M.; Hylek, E.M. & Palareti, G. (2012): 'Oral anticoagulant therapy: Antithrombotic Therapy and Prevention of Thrombosis, 9th ed: American College of Chest Physicians Evidence-Based Clinical Practice Guidelines.' *Chest*, **141**(2 Suppl): pp. e44S–e88S, ISSN 1931-3543, doi:10.1378/chest.11-2292.

Ailawadi, G.; Gerdisch, M.W.; Harvey, R.L.; Hooker, R.L.; Damiano, R.J.; Salamon, T. & Mack, M.J. (2011): 'Exclusion of the left atrial appendage with a novel device: early results of a multicenter trial.' *The Journal of Thoracic and Cardiovascular Surgery*, **142**(5): pp. 1002–9, 1009.e1, ISSN 1097-685X, doi:10.1016/j.jtcvs.2011.07.052.

Al-Saady, N.M.; Obel, O.A. & Camm, A.J. (1999): 'Left atrial appendage: Structure, function, and role in thromboembolism.' *Heart*, **82**(5): pp. 547–554, ISSN 1355-6037, doi:10.1136/hrt.82.5.547.

Ali, A.; Plettenburg, D.H. & Breedveld, P. (2016): 'Steerable Catheters in Cardiology: Classifying Steerability and Assessing Future Challenges.' *IEEE Transactions on Biomedical Engineering*, **63**(4): pp. 679–693, doi:10.1109/TBME.2016.2525785.

Ayvali, E.; Liang, C.P.; Ho, M.; Chen, Y. & Desai, J.P. (2012): 'Towards A Discretely Actuated Steerable Cannula for Diagnostic and Therapeutic Procedures.' *The International Journal of Robotics Research*, **31**(5): pp. 588–603, ISSN 0278-3649, doi:10.1177/0278364912442429.

Bass, J.L. (2015): 'Embryology, Neonatal Circulation and Anatomy of PFO.' In: Z. Amin; J.M. Tobis; H. Sievert & J.D. Carroll (Eds.), *Patent Foramen Ovale*, Springer London, London, pp. 7–14, ISBN 978-1-4471-4986-6, doi:10.1007/978-1-4471-4987-3_2.

Bayés de Luna, A. (2011): *Clinical Arrhythmology*. John Wiley & Sons Ltd, Hoboken, ISBN 978-0-470-65636-5.

Bellmann, B.; Schnupp, S.; Kühnlein, P.; Javernik, C.; Kleinecke, C.; Rillig, A.; Landmesser, U.; Brachmann, J. & Park, J.W. (2017): 'Left Atrial Appendage Closure With the New Occlutech® Device: First in Man Experience and Neurological Outcome.' *Journal of Cardiovascular Electrophysiology*, **28**(3): pp. 315–320, ISSN 10453873, doi:10.1111/jce.13141.

Bergmann, M.W. & Landmesser, U. (2014): 'Left atrial appendage closure for stroke prevention in non-valvular atrial fibrillation: rationale, devices in clinical development and insights into implantation techniques.' *EuroIntervention*, **10**(4): pp. 497–504, ISSN 1969-6213, doi:10.4244/EIJV10I4A86.

Bergmann, M.W.; Tzikas, A. & Wunderlich, N.C. (2017): *Clinical Cases in LAA Occlusion: Indication, Techniques, Devices, Implantation*. Springer International Publishing, Cham, ISBN 978-3-319-51429-1.

Berti, S.; Paradossi, U. & Santoro, G. (2015): 'The Use of Intracardiac Echocardiography (ICE) to Guide LAA Closure.' In: J. Saw; S. Kar & M.J. Price (Eds.), *Left Atrial Appendage Closure*, Springer International Publishing, Cham, Contemporary Cardiology, pp. 101–116, ISBN 978-3-319-16279-9.

Blackshear, J.L. & Odell, J.A. (1996): 'Appendage obliteration to reduce stroke in cardiac surgical patients with atrial fibrillation.' *The Annals of Thoracic Surgery*, **61**(2): pp. 755–759, ISSN 0003-4975, doi:10.1016/0003-4975(95)00887-X.

Budoff, M.J. (2016): 'Computed Tomography.' In: M.J. Budoff & J.S. Shinbane (Eds.), *Cardiac CT imaging*, Springer, Cham, pp. 3–24, ISBN 978-3-319-28217-6.

Cairns, J.A. (2015): 'Efficiacy and Limitations of Warfarin and Novel Oral Anticoagulants with Atrial Fibrillation.' In: J. Saw; S. Kar & M.J. Price (Eds.), *Left Atrial Appendage Closure*, Springer International Publishing, Cham, Contemporary Cardiology, pp. 17–36, ISBN 978-3-319-16279-9.

Caliskan, E.; Cox, J.L.; Holmes, D.R.; Meier, B.; Lakkireddy, D.R.; Falk, V.; Salzberg, S.P. & Emmert, M.Y. (2017): 'Interventional and surgical occlusion of the left atrial appendage.' *Nature reviews. Cardiology*, ISSN 1759-5010, doi:10.1038/nrcardio.2017.107.

Camm, A.J.; Lip, G.Y.H.; de Caterina, R.; Savelieva, I.; Atar, D.; Hohnloser, S.H.; Hindricks, G. & Kirchhof, P. (2012): '2012 focused update of the ESC Guidelines for the management of atrial fibrillation: an update of the 2010 ESC Guidelines for the management of atrial fibrillation. Developed with the special contribution of the European Heart Rhythm Association.' *European Heart Journal*, **33**(21): pp. 2719–2747, ISSN 0195-668X, doi:10.1093/eurheartj/ehs253.

Chugh, S.S.; Havmoeller, R.; Narayanan, K.; Singh, D.; Rienstra, M.; Benjamin, E.J.; Gillum, R.F.; Kim, Y.H.; McAnulty, J.H.; Zheng, Z.J.; Forouzanfar, M.H.; Naghavi, M.; Mensah, G.A.; Ezzati, M. & Murray, C.J.L. (2014): 'Worldwide epidemiology of atrial fibrillation: a Global Burden of Disease 2010 Study.' *Circulation*, **129**(8): pp. 837–847, ISSN 1524-4539, doi:10.1161/CIRCULATIONAHA.113.005119.

Dave, A.S. & Valderrábano, M. (2017): 'Approaches to Left Atrial Appendage Closure: Device Design, Performance, and Limitations.' *Methodist DeBakey Cardiovascular Journal*, **13**(3).

de Jaegere, P.; de Santis, G.; Rodriguez-Olivares, R.; Bosmans, J.; Bruining, N.; Dezutter, T.; Rahhab, Z.; El Faquir, N.; Collas, V.; Bosmans, B.; Verhegghe, B.; Ren, C.; Geleinse, M.; Schultz, C.; van Mieghem, N.; de Beule, M. & Mortier, P. (2016): 'Patient-Specific Computer Modeling to Predict Aortic Regurgitation After Transcatheter Aortic Valve Replacement.' *JACC: Cardiovascular Interventions*, **9**(5): pp. 508–512, ISSN 1876-7605, doi:10.1016/j.jcin.2016.01.003.

Di Biase, L.; Santangeli, P.; Anselmino, M.; Mohanty, P.; Salvetti, I.; Gili, S.; Horton, R.; Sanchez, J.E.; Bai, R.; Mohanty, S.; Pump, A.; Cereceda Brantes, M.; Gallinghouse, G.J.; Burkhardt, J.D.; Cesarani, F.; Scaglione, M.; Natale, A. & Gaita, F. (2012): 'Does the left atrial appendage morphology correlate with the risk of stroke in patients with atrial fibrillation? Results from a multicenter study.' *Journal of the American College of Cardiology*, **60**(6): pp. 531–538, ISSN 07351097, doi: 10.1016/j.jacc.2012.04.032.

Don, C.W.; Cook, A.C. & Reisman, M. (2015): 'LAA Anatomy.' In: J. Saw; S. Kar & M.J. Price (Eds.), *Left Atrial Appendage Closure*, Springer International Publishing, Cham, Contemporary Cardiology, pp. 45–57, ISBN 978-3-319-16279-9.

EOS (2010): 'Materialdatenblatt PA 2200 Performance 1.0.'

Ernst, S.; Ouyang, F.; Linder, C.; Hertting, K.; Stahl, F.; Chun, J.; Hachiya, H.; Bänsch, D.; Antz, M. & Kuck, K.H. (2004): 'Initial experience with remote catheter ablation using a novel magnetic navigation system: magnetic remote catheter ablation.' *Circulation*, **109**(12): pp. 1472–1475, ISSN 1524-4539, doi:10.1161/01.CIR.0000125126.83579.1B.

Fan, Y.; Kwok, K.W.; Zhang, Y.; Cheung, G.S.H.; Chan, A.K.Y. & Lee, A.P.W. (2016): 'Three-Dimensional Printing for Planning Occlusion Procedure for a Double-Lobed Left Atrial Appendage.' *Circulation: Cardiovascular Interventions*, **9**(3): p. e003561, ISSN 1941-7640, doi: 10.1161/CIRCINTERVENTIONS.116.003561.

Fang, B.K.; Ju, M.S. & Lin, C.C.K. (2007): 'A new approach to develop ionic polymer–metal composites (IPMC) actuator: Fabrication and control for active catheter systems.' *Sensors and Actuators A: Physical*, **137**(2): pp. 321–329, ISSN 09244247, doi:10.1016/j.sna.2007.03.024.

Feldman, T.; Wasserman, H.S.; Herrmann, H.C.; Gray, W.; Block, P.C.; Whitlow, P.; St Goar, F.; Rodriguez, L.; Silvestry, F.; Schwartz, A.; Sanborn, T.A.; Condado, J.A. & Foster, E. (2005): 'Percutaneous mitral valve repair using the edge-to-edge technique: six-month results of the EVEREST Phase I Clinical Trial.' *Journal of the American College of Cardiology*, **46**(11): pp. 2134–2140, ISSN 07351097, doi:10.1016/j.jacc.2005.07.065.

Forssmann, W. (1929): 'Die Sondierung des Rechten Herzens.' *Klinische Wochenschrift*, **8**(45): pp. 2085–2087, ISSN 0023-2173, doi:10.1007/BF01875120.

Fu, Y.; Liu, H.; Huang, W.; Wang, S. & Liang, Z. (2009): 'Steerable catheters in minimally invasive vascular surgery.' *The International Journal of Medical Robotics and Computer Assisted Surgery*, **5**(4): pp. 381–391, ISSN 1478-596X, doi:10.1002/rcs.282.

Gaemperli, O. & Lüscher, T.F. (2013): 'Historical Account: Interventional Cardiology.' In: P. Lanzer (Ed.), *Catheter-Based Cardiovascular Interventions*, Springer Berlin Heidelberg, Berlin, Heidelberg, pp. 3–14, ISBN 978-3-642-27675-0.

Gafoor, S.; Heuer, L.; Franke, J.; Reinartz, M.; Bertog, S.; Vaskelyte, L.; Hofmann, I. & Sievert, H. (2015a): 'Novel Percutaneous LAA Closure Devices in Clinical or Preclinical Trials.' In: J. Saw; S. Kar & M.J. Price (Eds.), *Left Atrial Appendage Closure*, Springer International Publishing, Cham, Contemporary Cardiology, pp. 234–243, ISBN 978-3-319-16279-9.

Gafoor, S.; Heuer, L.; Schulz, P.; Matic, P.; Franke, J.; Bertog, S.; Reinartz, M.; Vaskelyte, L.; Hofmann, I. & Sievert, H. (2015b): '"A bend in time": Shaping the sheath facilitates left atrial appendage closure.' *Catheterization and Cardiovascular Interventions*, **86**(5): pp. E224–E228, ISSN 15221946, doi:10.1002/ccd.25996.

Gessat, M.; Merk, D.R.; Falk, V.; Walther, T.; Jacobs, S.; Nöttling, A. & Burgert, O. (2009): 'A planning system for transapical aortic valve implantation.' p. 72611E, doi:10.1117/12.810270.

Graf, E.C.; Ott, I.; Praceus, J.; Bourier, F. & Lüth, T.C. (2018): 'Patient-Specific Catheter Shaping for the Minimally Invasive Closure of the Left Atrial Appendage.' *International Journal of Computer Assisted Radiology and Surgery*, **13**(6): pp. 837–846, doi:10.1007/s11548-018-1752-4.

Graf, E.C.; Roppenecker, D.B.; Tiemann, K.; Samper, V.D. & Lüth, T.C. (2014): 'Development of an anatomic heart model for the minimally-invasive closure of the left atrial appendage.' *IEEE International Conference on Robotics and Biomimetics (ROBIO)*, pp. 607–612, doi:10.1109/ROBIO.2014.7090397.

Graf, E.C.; Tiemann, K.; Praceus, J. & Lüth, T.C. (2016): 'A planning system of the implant size and position for minimally-invasive closure of the left atrial appendage.' *6th IEEE International Conference on Biomedical Robotics and Biomechatronics (BioRob)*, **2016**: pp. 293–298, doi:10.1109/BIOROB.2016.7523641.

Guo, S.; Fukuda, T.; Kosuge, K.; Arai, F.; Oguro, K. & Negoro, M. (1995): 'Micro catheter system with active guide wire.' In: *IEEE International Conference on Robotics and Automation*, pp. 79–84, doi:10.1109/ROBOT.1995.525267.

Haga, Y.; Mineta, T. & Esashi, M. (2000): 'Multi-functional Active Catheter.' *Sensors Update*, **8**(1): pp. 147–186, ISSN 1432-2404, doi:10.1002/1616-8984(200011)8:1<147::AID-SEUP147>3.0.CO;2-Y.

Hagen, P.T.; Scholz, D.G. & Edwards, W.D. (1984): 'Incidence and Size of Patent Foramen Ovale During the First 10 Decades of Life: An Autopsy Study of 965 Normal Hearts.' *Mayo Clinic Proceedings*, **59**(1): pp. 17–20, ISSN 00256196, doi:10.1016/S0025-6196(12)60336-X.

Hanif, H. & Whitlock, R. (2015): 'Conventional Surgery for LAA Closure.' In: J. Saw; S. Kar & M.J. Price (Eds.), *Left Atrial Appendage Closure*, Springer International Publishing, Cham, Contemporary Cardiology, pp. 61–80, ISBN 978-3-319-16279-9.

Hart, R.G.; Pearce, L.A. & Aguilar, M.I. (2007): 'Meta-analysis: Antithrombotic Therapy to Prevent Stroke in Patients Who Have Nonvalvular Atrial Fibrillation.' *Annals of Internal Medicine*, **146**(12): p. 857, ISSN 0003-4819, doi:10.7326/0003-4819-146-12-200706190-00007.

Heeringa, J.; van der Kuip, Deirdre A M; Hofman, A.; Kors, J.A.; van Herpen, G.; Stricker, B.H.C.; Stijnen, T.; Lip, G.Y.H. & Witteman, J.C.M. (2006): 'Prevalence, incidence and lifetime risk of atrial fibrillation: the Rotterdam study.' *European Heart Journal*, **27**(8): pp. 949–953, ISSN 0195-668X, doi:10.1093/eurheartj/ehi825.

Holmes, D.R.; Reddy, V.Y.; Turi, Z.G.; Doshi, S.K.; Sievert, H.; Buchbinder, M.; Mullin, C.M. & Sick, P. (2009): 'Percutaneous closure of the left atrial appendage versus warfarin therapy for prevention of stroke in patients with atrial fibrillation: A randomised non-inferiority trial.' *The Lancet*, **374**(9689): pp. 534–542, ISSN 01406736, doi:10.1016/S0140-6736(09)61343-X.

Hoppe, U.C. (2009): 'Rhythmusstörungen des Herzens.' In: E. Erdmann (Ed.), *Klinische Kardiologie*, Springer Berlin Heidelberg, Berlin, Heidelberg, pp. 73–110, doi:10.1007/978-3-540-79011-2_3.

Humphries, J.A. (2015): 'The Use of Transoesophageal Echocardiography to Guide Percutaneous LAA Closure.' In: J. Saw; S. Kar & M.J. Price (Eds.), *Left Atrial Appendage Closure*, Springer International Publishing, Cham, Contemporary Cardiology, pp. 83–100, ISBN 978-3-319-16279-9.

Ikuta, K.; Matsuda, Y.; Yajima, D. & Ota, Y. (2012): 'Pressure Pulse Drive: A Control Method for the Precise Bending of Hydraulic Active Catheters.' *IEEE/ASME Transactions on Mechatronics*, **17**(5): pp. 876–883, ISSN 1083-4435, doi:10.1109/TMECH.2011.2138711.

January, C.T.; Wann, L.S.; Alpert, J.S.; Calkins, H.; Cigarroa, J.E.; Cleveland, JR, J.C.; Conti, J.B.; Ellinor, P.T.; Ezekowitz, M.D.; Field, M.E.; Murray, K.T.; Sacco, R.L.; Stevenson, W.G.; Tchou, P.J.; Tracy, C.M. & Yancy, C.W. (2014): '2014 AHA/ACC/HRS guideline for the management of patients with atrial fibrillation: a report of the American College of Cardiology/American Heart Association Task Force on practice guidelines and the Heart Rhythm Society.' *Circulation*, **130**(23): pp. e199–267, ISSN 1524-4539, doi:10.1161/CIR.0000000000000041.

Jayender, J.; Patel, R.V.; Michaud, G.F. & Hata, N. (2011): 'Optimal transseptal puncture location for robot-assisted left atrial catheter ablation.' *The International Journal of Medical Robotics and Computer Assisted Surgery*, **7**(2): pp. 193–201, ISSN 1478-596X, doi:10.1002/rcs.388.

Joy, S.; Bertog, S.; Betts, T.; Wilson, N.; Myerson, S. & Sievert, H. (2017): 'Left Atrial Appendage Morphology in Patients with Non-Valvular Atrial Fibrillation.' *Journal of Structural Heart Disease*, **3**(1): pp. 8–14, ISSN 2326-4004, doi:10.12945/j.jshd.2016.003.16.

Kanagaratnam, P.; Koa-Wing, M.; Wallace, D.T.; Goldenberg, A.S.; Peters, N.S. & Davies, D.W. (2008): 'Experience of robotic catheter ablation in humans using a novel remotely steerable catheter sheath.' *Journal of Interventional Cardiac Electrophysiology*, **21**(1): pp. 19–26, ISSN 1572-8595, doi:10.1007/s10840-007-9184-z.

Kanderian, A.S.; Gillinov, A.M.; Pettersson, G.B.; Blackstone, E. & Klein, A.L. (2008): 'Success of surgical left atrial appendage closure: assessment by transesophageal echocardiography.' *Journal of the American College of Cardiology*, **52**(11): pp. 924–929, ISSN 07351097, doi:10.1016/j.jacc.2008.03.067.

Kanmanthareddy, A.; Gunda, S.; Badhwar Nitish; Lee, R.J. & Lakkireddy, D. (2015): 'LARIAT: The Endo-Epicardial Technique for Left Atrial Appendage Exclusion.' In: J. Saw; S. Kar & M.J. Price (Eds.), *Left Atrial Appendage Closure*, Springer International Publishing, Cham, Contemporary Cardiology, pp. 205–223, ISBN 978-3-319-16279-9.

Kirchhof, P.; Benussi, S.; Kotecha, D.; Ahlsson, A.; Atar, D.; Casadei, B.; Castella, M.; Diener, H.C.; Heidbuchel, H.; Hendriks, J.; Hindricks, G.; Manolis, A.S.; Oldgren, J.; Popescu, B.A.; Schotten, U.; van Putte, B.; Vardas, P.; Agewall, S.; Camm, J.; Baron Esquivias, G.; Budts, W.; Carerj, S.; Casselman, F.; Coca, A.; de Caterina, R.; Deftereos, S.; Dobrev, D.; Ferro, J.M.; Filippatos, G.; Fitzsimons, D.; Gorenek, B.; Guenoun, M.; Hohnloser, S.H.; Kolh, P.; Lip, G.Y.H.; Manolis, A.; McMurray, J.; Ponikowski, P.; Rosenhek, R.; Ruschitzka, F.; Savelieva, I.; Sharma, S.; Suwalski, P.; Tamargo, J.L.; Taylor, C.J.; van Gelder, I.C.; Voors, A.A.; Windecker, S.; Zamorano, J.L. & Zeppenfeld, K. (2016): '2016 ESC Guidelines for the management of atrial fibrillation developed in collaboration with EACTS.' *European Heart Journal*, **37**(38): pp. 2893–2962, ISSN 0195-668X, doi:10.1093/eurheartj/ehw210.

Krieger, Y.S.; Roppenecker, D.B.; Kuru, I. & Lueth, T.C. (2017): 'Multi-arm snake-like robot.' *IEEE International Conference on Robotics and Automation (ICRA)*, **2017**: pp. 2490–2495, doi:10.1109/ICRA.2017.7989290.

Krijthe, B.P.; Kunst, A.; Benjamin, E.J.; Lip, G.Y.H.; Franco, O.H.; Hofman, A.; Witteman, J.C.M.; Stricker, B.H. & Heeringa, J. (2013): 'Projections on the number of individuals with atrial fibrillation in the European Union, from 2000 to 2060.' *European Heart Journal*, **34**(35): pp. 2746–2751, ISSN 0195-668X, doi:10.1093/eurheartj/eht280.

Lam, Y.Y. (2013): 'A new left atrial appendage occluder (Lifetech LAmbre Device) for stroke prevention in atrial fibrillation.' *Cardiovascular Revascularization Medicine*, **14**(3): pp. 134–136, ISSN 1878-0938, doi:10.1016/j.carrev.2013.04.003.

Lange, M.; Bültel, H.; Weglage, H.; Löffeld, P. & Wichter, T. (2016): 'Using a steerable guiding sheath to implant an AMPLATZER^{TM}Amulet^{TM} Left Atrial Appendage Occluder for prevention of thromboembolic stroke.' *International Journal of Cardiology*, **221**: pp. 466–467, ISSN 1874-1754, doi:10.1016/j.ijcard.2016.06.270.

Laske, T.G.; Shrivastav, M. & Iaizzo, P.A. (2015): 'The Cardiac Conduction System.' In: P.A. Iaizzo (Ed.), *Handbook of Cardiac Anatomy, Physiology, and Devices*, Springer International Publishing, Cham, pp. 215–233, ISBN 978-3-319-19463-9.

Lee, R.J. (2015): 'PLAATO Device.' In: J. Saw; S. Kar & M.J. Price (Eds.), *Left Atrial Appendage Closure*, Springer International Publishing, Cham, Contemporary Cardiology, pp. 135–142, ISBN 978-3-319-16279-9.

Lewalter, T.; Ibrahim, R.; Albers, B. & Camm, A.J. (2013): 'An update and current expert opinions on percutaneous left atrial appendage occlusion for stroke prevention in atrial fibrillation.' *Europace*, **15**(5): pp. 652–656, ISSN 1099-5129, doi:10.1093/europace/eut043.

Li, Z.; Chui, C.K.; Cai, Y.; Anderson, J.H. & Nowinski, W.L. (2001): 'Interactive Catheter Shape Modeling in Interventional Radiology Simulation.' In: G. Goos; J. Hartmanis; J. van Leeuwen; W.J. Niessen & M.A. Viergever (Eds.), *Medical Image Computing and Computer-Assisted Intervention – MICCAI 2001*, Springer Berlin Heidelberg, Berlin, Heidelberg, volume 2208 of *Lecture Notes in Computer Science*, pp. 457–464, ISBN 978-3-540-42697-4, doi:10.1007/3-540-45468-3_55.

López-Mínguez, J.R.; González-Fernández, R.; Fernández-Vegas, C.; Millán-Nuñez, V.; Fuentes-Cañamero, M.E.; Nogales-Asensio, J.M.; Doncel-Vecino, J.; Elduayen-Gragera, J.; Ho, S.Y. & Sánchez-Quintana, D. (2014): 'Anatomical classification of left atrial appendages in specimens applicable to CT imaging techniques for implantation of amplatzer cardiac plug.' *Journal of Cardiovascular Electrophysiology*, **25**(9): pp. 976–984, ISSN 10453873, doi:10.1111/jce.12429.

Lüth, T.C. (2014): 'Bild- und computergestützte Interventionen.' In: M. Kraft & U. Morgenstern (Eds.), *Faszination, Einführung, Überblick*, De Gruyter, Berlin, Biomedizinische Technik, pp. 329–369, ISBN 311025218X.

Lüth, T.C. (2015): 'SG-Library: Entwicklung einer grundlegenden MATLAB-Toolbox zu räumlichen Modellierung von Körper, Gelenken und Getrieben.' *11. Getriebekolloquium, Garching, Tagungsband*, pp. 183–203, doi:10.14459/2015md1276136.

Lüth, T.C. (2017): 'Lecture Notes 'Automatisierungstechnik in der Medizin': 'Mathematische Grundlagen'.' Department of Mechanical Engineering, Technical University of Munich.

Lüth, T.C. & Irlinger, F. (2013): 'Berechnete Erzeugung von dreidimensionalen Oberflächenmodellen im STL-Format aus der Beschreibung planarer Mechanismen für die Generative Fertigung durch selektives Lasersintern.' *10. Getriebekolloquium, Illmenau, Tagungsband*, pp. 267–284.

Madden, J.L. (1949): 'Resection of the Left Auricular Appendix.' *Journal of the American Medical Association*, **140**(9): p. 769, ISSN 0002-9955, doi:10.1001/jama.1949.02900440011003.

Meier, B.; Blaauw, Y.; Khattab, A.A.; Lewalter, T.; Sievert, H.; Tondo, C.; Glikson, M.; Document Reviewers; Lip, G.Y.H.; Lopez-Minguez, J.; Roffi, M.; Israel, C.; Dudek, D. & Savelieva, I. (2014): 'EHRA/EAPCI expert consensus statement on catheter-based left atrial appendage occlusion.' *Europace*, **16**(10): pp. 1397–1416, ISSN 1099-5129, doi:10.1093/europace/euu174.

Meier, B.; Palacios, I.; Windecker, S.; Rotter, M.; Cao, Q.L.; Keane, D.; Ruiz, C.E. & Hijazi, Z.M. (2003): 'Transcatheter left atrial appendage occlusion with Amplatzer devices to obviate anticoagulation in patients with atrial fibrillation.' *Catheterization and Cardiovascular Interventions*, **60**(3): pp. 417–422, ISSN 1522-1946, doi:10.1002/ccd.10660.

'Mosby's medical dictionary.' (2013): Elsevier/Mosby, St. Louis, Mo., 9th edition, ISBN 0323112587.

Nakajima, H.; Seo, Y.; Ishizu, T.; Yamamoto, M.; Machino, T.; Harimura, Y.; Kawamura, R.; Sekiguchi, Y.; Tada, H. & Aonuma, K. (2010): 'Analysis of the left atrial appendage by three-dimensional transesophageal echocardiography.' *The American journal of cardiology*, **106**(6): pp. 885–892, ISSN 1879-1913, doi:10.1016/j.amjcard.2010.05.014.

Okerlund, D.R.; Sra, J.S.; Vass, M.L. & Reddy, S.B. (2010): 'Cardiac CT system and method for planning left atrial appendage isolation.', US 7747047 B2.

Otton, J.M.; Spina, R.; Sulas, R.; Subbiah, R.N.; Jacobs, N.; Muller, D.W. & Gunalingam, B. (2015): 'Left Atrial Appendage Closure Guided by Personalized 3D-Printed Cardiac Reconstruction.' *JACC: Cardiovascular Interventions*, **8**(7): pp. 1004–1006, ISSN 19368798, doi:10.1016/j.jcin.2015.03.015.

Panikker, S.; Lord, J.; Jarman, J.W.E.; Armstrong, S.; Jones, D.G.; Haldar, S.; Butcher, C.; Khan, H.; Mantziari, L.; Nicol, E.; Hussain, W.; Clague, J.R.; Foran, J.P.; Markides, V. & Wong, T. (2016): 'Outcomes and costs of left atrial appendage closure from randomized controlled trial and real-world experience relative to oral anticoagulation.' *European Heart Journal*, **37**(46): pp. 3470–3482, ISSN 0195-668X, doi:10.1093/eurheartj/ehw048.

Park, J.W.; Bethencourt, A.; Sievert, H.; Santoro, G.; Meier, B.; Walsh, K.; Lopez-Minquez, J.R.; Meerkin, D.; Valdés, M.; Ormerod, O. & Leithäuser, B. (2011): 'Left atrial appendage closure with amplatzer cardiac plug in atrial fibrillation: Initial european experience.' *Catheterization and Cardiovascular Interventions*, **77**(5): pp. 700–706, ISSN 15221946, doi:10.1002/ccd.22764.

Patton, K.T. & Thibodeau, G.A. (2014): *Mosby's Handbook of Anatomy & Physiology*. Elsevier, St. Louis, Missouri, ISBN 978-0-323-22605-9.

Pellegrino, P.L.; Fassini, G.; Di Biase, M. & Tondo, C. (2016): 'Left Atrial Appendage Closure Guided by 3D Printed Cardiac Reconstruction: Emerging Directions and Future Trends.' *Journal of Cardiovascular Electrophysiology*, **27**(6): pp. 768–771, ISSN 10453873, doi:10.1111/jce.12960.

Phillips, K.P. & Kar, S. (2015): 'WATCHMAN Device.' In: J. Saw; S. Kar & M.J. Price (Eds.), *Left Atrial Appendage Closure*, Springer International Publishing, Cham, Contemporary Cardiology, pp. 143–168, ISBN 978-3-319-16279-9.

Piorkowski, C.; Eitel, C.; Rolf, S.; Bode, K.; Sommer, P.; Gaspar, T.; Kircher, S.; Wetzel, U.; Parwani, A.S.; Boldt, L.H.; Mende, M.; Bollmann, A.; Husser, D.; Dagres, N.; Esato, M.; Arya, A.; Haverkamp, W. & Hindricks, G. (2011): 'Steerable versus nonsteerable sheath technology in atrial fibrillation ablation: a prospective, randomized study.' *Circulation. Arrhythmia and Electrophysiology*, **4**(2): pp. 157–165, ISSN 1941-3084, doi:10.1161/CIRCEP.110.957761.

Pison, L.; Potpara, T.S.; Chen, J.; Larsen, T.B.; Bongiorni, M.G.; Blomstrom-Lundqvist, C.; Scientific Initiative Committee, E.; Proclemer, A.; Dagres, N.; Estner, H.; Hernandez-Madrid, A.; Hocini, M.; Potpara, T.; Sciaraffia, E.; Todd, D. & Savelieva, I. (2015): 'Left atrial appendage closure-indications, techniques, and outcomes: Results of the European Heart Rhythm Association Survey.' *Europace*, **17**(4): pp. 642–646, ISSN 1099-5129, doi:10.1093/europace/euv069.

Rafii-Tari, H.; Payne, C.J. & Yang, G.Z. (2014): 'Current and emerging robot-assisted endovascular catheterization technologies: a review.' *Annals of Biomedical Engineering*, **42**(4): pp. 697–715, ISSN 1573-9686, doi:10.1007/s10439-013-0946-8.

Rahman, S.u.; Wesarg, S. & Völker, W. (2011): 'Patient specific optimal catheter selection for right coronary artery.' doi:10.1117/12.878111.

Rajappan, K.; Baker, V.; Richmond, L.; Kistler, P.M.; Thomas, G.; Redpath, C.; Sporton, S.C.; Earley, M.J.; Harris, S. & Schilling, R.J. (2009): 'A randomized trial to compare atrial fibrillation ablation using a steerable vs. a non-steerable sheath.' *Europace*, **11**(5): pp. 571–575, ISSN 1532-2092, doi:10.1093/europace/eup069.

Rajwani, A.; Nelson, A.J.; Shirazi, M.G.; Disney, P.J.S.; Teo, K.S.L.; Wong, D.T.L.; Young, G.D. & Worthley, S.G. (2016): 'CT sizing for left atrial appendage closure is associated with favourable outcomes for procedural safety.' *European Heart Journal - Cardiovascular Imaging*, ISSN 2047-2412, doi:10.1093/ehjci/jew212.

Reddy, V.Y.; Holmes, D.; Doshi, S.K.; Neuzil, P. & Kar, S. (2011): 'Safety of Percutaneous Left Atrial Appendage Closure: Results From the Watchman Left Atrial Appendage System for Embolic Protection in Patients With AF (PROTECT AF) Clinical Trial and the Continued Access Registry.' *Circulation*, **123**(4): pp. 417–424, ISSN 1524-4539, doi:10.1161/CIRCULATIONAHA.110.976449.

Regueiro, A.; Bernier, M.; O'Hara, G.; O'Connor, K.; Paradis, J.M.; Beaudoin, J.; Rodriguez-Gabella, T.; Champagne, J. & Rodés-Cabau, J. (2016): 'Left atrial appendage closure: Initial experience with the ultraseal device.' *Catheterization and Cardiovascular Interventions*, ISSN 1522-1946, doi:10.1002/ccd.26870.

Riga, C.V.; Bicknell, C.D.; Sidhu, R.; Cochennec, F.; Normahani, P.; Chadha, P.; Kashef, E.; Hamady, M. & Cheshire, N.J.W. (2011): 'Advanced catheter technology: is this the answer to overcoming the long learning curve in complex endovascular procedures.' *European Journal of Vascular and Endovascular Surgery*, **42**(4): pp. 531–538, ISSN 1532-2165, doi:10.1016/j.ejvs.2011.02.004.

Rogers, G.W. (2012): 'Piezoelectric ultrasonic micro-motor system for minimally invasive surgery - the Intellimotor.' *International Congress on Ultrasonics*, pp. 705–708, doi:10.1063/1.3703280.

Roy, A.K.; Horvilleur, J.; Cormier, B.; Cazalas, M.; Fernandez, L.; Patane, M.; Neylon, A.; Spaziano, M.; Sawaya, F.J.; Arai, T.; Bouvier, E.; Hovasse, T.; Lefèvre, T.; Chevalier, B. & Garot, P. (2017): 'Novel integrated 3D multidetector computed tomography and fluoroscopy fusion for left atrial appendage occlusion procedures.' *Catheterization and Cardiovascular Interventions*, ISSN 1522-1946, doi:10.1002/ccd.26998.

Saw, J. (2015): 'Amplatzer Cardiac Plug and Amulet.' In: J. Saw; S. Kar & M.J. Price (Eds.), *Left Atrial Appendage Closure*, Springer International Publishing, Cham, Contemporary Cardiology, pp. 181–193, ISBN 978-3-319-16279-9.

Saw, J.; Kar, S. & Price, M.J. (Eds.) (2015a): *Left Atrial Appendage Closure: Mechanical Approaches to Stroke Prevention in Atrial Fibrillation*. Contemporary Cardiology, Springer International Publishing, Cham, ISBN 978-3-319-16279-9.

Saw, J.; Lopes, J.P.; Reisman, M. & Bezerra, H.G. (2015b): 'CT Imaging for Percutaneous LAA Closure.' In: J. Saw; S. Kar & M.J. Price (Eds.), *Left Atrial Appendage Closure*, Springer International Publishing, Cham, Contemporary Cardiology, pp. 117–132, ISBN 978-3-319-16279-9.

Sears, P. & Dupont, P. (2006): 'A Steerable Needle Technology Using Curved Concentric Tubes.' *IEEE/RSJ International Conference on Intelligent Robots and Systems*, pp. 2850–2856, doi:10.1109/IROS.2006.282072.

Sievert, H. (2002): 'Percutaneous Left Atrial Appendage Transcatheter Occlusion to Prevent Stroke in High-Risk Patients With Atrial Fibrillation: Early Clinical Experience.' *Circulation*, **105**(16): pp. 1887–1889, ISSN 1524-4539, doi:10.1161/01.CIR.0000015698.54752.6D.

Silbernagl, S. & Despopoulos, A. (2012): *Taschenatlas Physiologie*. Georg Thieme Verlag, Stuttgart, ISBN 9783135677088, doi:10.1055/b-002-50992.

Slater, A.D.; Tatooles, A.J.; Coffey, A.; Pappas, P.S.; Bresticker, M.; Greason, K. & Slaughter, M.S. (2012): 'Prospective clinical study of a novel left atrial appendage occlusion device.' *The Annals of Thoracic Surgery*, **93**(6): pp. 2035–8; discussion 2038–40, ISSN 0003-4975, doi:10.1016/j.athoracsur.2011.12.077.

Statistisches Bundesamt (2014): *Fallpauschalenbezogene Krankenhausstatistik (DRG-Statistik): Operationen und Prozeduren der vollstationären Patientinnen und Patienten in Krankenhäusern bis zum kodierbaren Endpunkt*. Statistisches Bundesamt, Wiesbaden.

Statistisches Bundesamt (2016): *Fallpauschalenbezogene Krankenhausstatisik (DRG-Statistik): Operationen und Prozeduren der vollstationären Patientinnen und Patienten in Krankenhäusern bis zum kodierbaren Endpunkt*. Statistisches Bundesamt, Wiesbaden.

Su, P.; McCarthy, K.P. & Ho, S.Y. (2008): 'Occluding the left atrial appendage: Anatomical considerations.' *Heart*, **94**(9): pp. 1166–1170, ISSN 1355-6037, doi:10.1136/hrt.2006.111989.

Suzumori, K.; Iikura, S. & Tanaka, H. (1991): 'Development of flexible microactuator and its applications to robotic mechanisms.' In: *IEEE International Conference on Robotics and Automation*, pp. 1622–1627, doi:10.1109/ROBOT.1991.131850.

Thiriet, M. (2014): *Anatomy and physiology of the circulatory and ventilatory systems*, volume 6 of *Biomathematical and biomechanical modeling of the circulatory and ventilatory systems*. Springer, New York, NY and Heidelberg and Dordrecht and London, ISBN 1461494699, doi:10.1007/978-1-4614-9469-0.

Toumanides, S.; Sideris, E.B.; Agricola, T. & Moulopoulos, S. (2011): 'Transcatheter patch occlusion of the left atrial appendage using surgical adhesives in high-risk patients with atrial fibrillation.' *Journal of the American College of Cardiology*, **58**(21): pp. 2236–2240, ISSN 07351097, doi:10.1016/j.jacc.2011.08.036.

Träger, M.F.; Krohmer, E.; Krieger, Y.S. & Lüth, T.C. (2015): 'Automatisierte Konstruktion von Zahnradgetrieben für die Herstellung mittels Rapid-Prototyping-Verfahren.' *11. Kolloquium Getriebetechnik*, pp. 235–254, doi:10.14459/2015md1276149.

Veinot, J.P.; Harrity, P.J.; Gentile, F.; Khandheria, B.K.; Bailey, K.R.; Eickholt, J.T.; Seward, J.B.; Tajik, A.J. & Edwards, W.D. (1997): 'Anatomy of the Normal Left Atrial Appendage: A Quantitative Study of Age-Related Changes in 500 Autopsy Hearts: Implications for Echocardiographic Examination.' *Circulation*, **96**(9): pp. 3112–3115, ISSN 1524-4539, doi:10.1161/01.CIR.96.9.3112.

Ventosa-Fernandez, G.; Quintana, E.; Castellá, M. & Pereda, D. (2015): 'Exclusion of the left atrial appendage with the TigerPaw II system: a word of caution.' *Interactive Cardiovascular and Thoracic Surgery*, **21**(6): pp. 803–804, ISSN 1569-9285, doi:10.1093/icvts/ivv256.

von Knobelsdorff-Brenkenhoff, F.; Dieringer, M.A.; Greiser, A. & Schulz-Menger, J. (2011): 'In vitro assessment of heart valve bioprostheses by cardiovascular magnetic resonance: four-dimensional mapping of flow patterns and orifice area planimetry.' *European Journal of Cardio-Thoracic Surgery*, **40**(3): pp. 736–742, ISSN 1873-734X, doi:10.1016/j.ejcts.2010.12.040.

Wang, Y.; Di Biase, L.; Horton, R.P.; Nguyen, T.; Morhanty, P. & Natale, A. (2010): 'Left Atrial Appendage Studied by Computed Tomography to Help Planning for Appendage Closure Device Placement.' *Journal of Cardiovascular Electrophysiology*, **21**(9): pp. 973–982, ISSN 10453873, doi:10.1111/j.1540-8167.2010.01814.x.

Webster, R.; Okamura, A. & Cowan, N. (2006): 'Toward Active Cannulas: Miniature Snake-Like Surgical Robots.' *IEEE/RSJ International Conference on Intelligent Robots and Systems*, pp. 2857–2863, doi:10.1109/IROS.2006.282073.

Weinhaus, A.J. (2015): 'Anatomy of the Human Heart.' In: P.A. Iaizzo (Ed.), *Handbook of Cardiac Anatomy, Physiology, and Devices*, Springer International Publishing, Cham, pp. 61–88, ISBN 978-3-319-19463-9.

Whitlock, R.; Healey, J.; Vincent, J.; Brady, K.; Teoh, K.; Royse, A.; Shah, P.; Guo, Y.; Alings, M.; Folkeringa, R.J.; Paparella, D.; Colli, A.; Meyer, S.R.; Legare, J.F.; Lamontagne, F.; Reents, W.; Böning, A. & Connolly, S. (2014): 'Rationale and design of the Left Atrial Appendage Occlusion Study (LAAOS) III.' *Annals of Cardiothoracic Surgery*, **3**(1): pp. 45–54, ISSN 2225-319X, doi:10.3978/j.issn.2225-319X.2013.12.06.

Wolf, P.A.; Abbott, R.D. & Kannel, W.B. (1991): 'Atrial fibrillation as an independent risk factor for stroke: the Framingham Study.' *Stroke*, **22**(8): pp. 983–988, ISSN 0039-2499.